



UNIVERSITÀ
DEGLI STUDI
DI PADOVA

Head Office: Università degli Studi di Padova

Department
GEOSCIENZE

Ph.D. COURSE IN: Geosciences
XXXV SERIES

INNOVATIVE SOLUTIONS FOR METAL GROUND HEAT EXCHANGERS

Coordinator: Prof. Claudia Agnini

Supervisor: Prof. Antonio Galgaro

Co-Supervisors: Dr. Adriana Bernardi, Dr. Giorgia Dalla Santa

Ph.D. student: Gianluca Cadelano

1 Abstract

Buildings are responsible for 40% of global energy consumption and about 30% of greenhouse gas emissions. In fact, ensuring that new and existing buildings are sustainable and energy efficient is the main goal of European Commission efforts to challenge climate change¹. Shallow geothermal energy is a constant, reliable and renewable energy source available almost everywhere, and geothermal heat pump systems have proven to be effective in limiting energy consumption for the heating and cooling needs of buildings. However, the need for research and improvement is mandatory because there are technical barriers that limit the spread of these systems, which need further development to be made more efficient, cheaper and safer.

This thesis describes the research and innovations obtained in the frame of Horizon 2020 GEO4CIVHIC project focused on improving one of the crucial components of shallow geothermal systems: the ground heat exchanger, focusing on the metal ones.

Ground heat exchangers (GHE) are tubes inserted into the ground inside which a fluid flows that allows heat to be transferred to the ground. Their effectiveness depends mainly on the local geological context such as stratigraphy and hydrological conditions and on the materials and technology used to build the GHEs.

This thesis, after an introductory part, describes traditional and innovative methods and procedures aimed at determining the thermophysical properties of different types of metallic GHEs. The proposed methods are then applied to study the interaction between GHEs and the environment, that is the underground which also includes its water content due to groundwater and its characterizing chemophysical properties. The study focuses on the effects of these interactions on heat transfer performance and, in the long term, on corrosion and pipe life. Workable solutions and measures to make metal ground heat exchangers more efficient, cost effective and safer have been identified and applied on a real case study. These include the development and implementation of an experimental type of GHE and the proposal of non-destructive inspection methods based on infrared thermography.

¹ DIRECTIVE (EU) 2018/844 OF THE EUROPEAN PARLIAMENT AND OF THE COUNCIL of 30 May 2018 amending Directive 2010/31/EU on the energy performance of buildings and Directive 2012/27/EU on energy efficiency

2 Sommario

Gli edifici sono responsabili del 40% del consumo energetico globale e di circa il 30% delle emissioni di gas serra. Per questo motivo, garantire che gli edifici nuovi ed esistenti siano sostenibili ed efficienti dal punto di vista energetico è l'obiettivo principale degli sforzi della Commissione europea per contrastare il cambiamento climatico². L'energia geotermica a bassa entalpia è una fonte di energia costante, affidabile e rinnovabile disponibile quasi ovunque. I sistemi geotermici a pompa di calore si sono dimostrati efficaci nel limitare il consumo di energia per le esigenze di riscaldamento e raffrescamento degli edifici. Tuttavia, è necessario continuare la ricerca in questo campo, perché esistono barriere tecniche che limitano la diffusione di questi sistemi, che vanno pertanto ulteriormente sviluppati e resi più efficienti, più economici e più sicuri.

Questa tesi descrive la ricerca e le innovazioni ottenute nell'ambito del progetto Horizon 2020 GEO4CIVHIC incentrate sul miglioramento di uno dei componenti cruciali dei sistemi geotermici superficiali: lo scambiatore di calore a terreno, nello specifico quelli in metallo.

Gli scambiatori di calore a terreno (GHE) sono tubi inseriti nel terreno all'interno dei quali scorre un fluido che consente il trasferimento di calore con il terreno stesso. La loro efficacia dipende principalmente dal contesto geologico locale, che implica stratigrafia e condizioni idrologiche, nonché dai materiali e dalla tecnologia utilizzati per costruire i GHE.

Questa tesi, dopo una parte introduttiva, descrive metodi e procedure tradizionali e innovativi volti a determinare le proprietà termofisiche di diversi tipi di GHE metallici. I metodi proposti vengono poi applicati per studiare l'interazione tra il GHE e l'ambiente circostante, ovvero il sottosuolo, che comprende anche il suo contenuto idrico dovuto alle falde acquifere e le sue stesse proprietà chimico-fisiche. Lo studio si è concentrato sugli effetti di queste interazioni sulle prestazioni di trasferimento del calore e, a lungo termine, sulla corrosione e sulla durata dei tubi. Soluzioni e misure preventive praticabili per rendere gli scambiatori di calore metallici efficienti, convenienti e più sicuri sono state identificate e applicate su un caso studio reale. Queste includono lo sviluppo e l'implementazione di un modello sperimentale di GHE e la proposta di metodi di ispezione non distruttivi basati sulla termografia a infrarossi.

² DIRETTIVA (UE) 2018/844 DEL PARLAMENTO EUROPEO E DEL CONSIGLIO del 30 maggio 2018 che modifica la direttiva 2010/31/UE sulla prestazione energetica nell'edilizia e la direttiva 2012/27/UE sull'efficienza energetica

3 Table of contents

1	Abstract	I
2	Sommario	III
3	Table of contents	V
4	List of terms and acronyms	IX
5	Introduction	1
5.1	Context of the thesis	1
5.1.1	The GEO4CIVHIC project.....	1
5.1.2	Thesis outlines	3
5.1.3	Aims of the study.....	4
5.1.4	References	6
5.2	State of the art on closed loop shallow geothermal systems	8
5.2.1	Heat-transfer fluids in closed-loop systems	10
5.2.2	Vertical Ground Heat Exchangers classification	11
5.2.3	References	30
5.3	Corrosion of metal ground heat exchangers and ancillary metal components 34	
5.3.1	Chemical risks due to leaks of heat transfer fluid	34
5.3.2	Corrosion of metal components	36
5.3.3	Types of corrosion.....	40
5.3.4	Corrosion in ground environment	49
5.3.5	An overview of the main corrosion mechanisms in buried Fe-alloys pipes 49	
5.3.6	References	66
6	Anti-corrosion measures	69
6.1.1	Passive and active anti-corrosion measures for buried steel pipes	69
6.1.2	Active protection	72
6.1.3	Selection of specific regulation on cathodic protection	74
6.1.4	Advantages and drawbacks of anti-corrosion measures applied to GHEs 76	

6.1.5	Overview of the state of the art of standard methods for corrosion monitoring and verification procedures for buried steel pipes	77
6.1.6	References	81
7	Materials and methods	85
7.1.1	Numerical corrosivity scale and evaluation methods.....	85
7.1.2	Ground pH	90
7.1.3	Ground electrical resistivity	91
7.1.4	On-site thermal performance of GHEs: Thermal Response Test.....	97
7.1.5	Thermophysical properties of GHEs materials	103
7.1.6	Finite element method	108
7.1.7	Non-destructive evaluation of corrosion and joint tightness by active infrared thermography.....	108
7.1.8	Evaluating the corrosive attack on carbon steel GHEs in ground.....	113
7.1.9	References	114
8	Themed topic chapter: Design of innovative coaxial heat exchangers for shallow geothermal	117
8.1	Innovative Coaxial Heat Exchangers for shallow geothermal	119
8.1.1	Abstract.....	119
8.1.2	Introduction	120
8.1.3	Rotating and vibrating machine head for penetrometers	122
8.1.4	New inner and outer coaxial GSHE tube material	124
8.1.5	Demonstration sites and costs and heat extraction rates comparison	128
8.1.6	Conclusions and further developments	130
8.1.7	References	132
8.2	Adapted well point technique and subsequent field evaluation for the installation	133
8.2.1	Abstract.....	133
8.2.2	Introduction	134
8.2.3	Investigation survey about the use of the well point across Europe	139
8.2.4	The pilot site	140
8.2.5	The modelling analysis.....	143
8.2.6	Heat exchanger materials	145

8.2.7	Well point heat exchangers installation method at Padova Pilot site	151
8.2.8	Conclusions	164
9	Themed topic chapter: Evaluation of the thermal performance of metal GHEs	165
9.1	Evaluation of the Effect of Anti-Corrosion Coatings on the Thermal Resistance of Ground Heat Exchangers for Shallow Geothermal Applications ...	167
9.1.1	Abstract.....	167
9.1.2	Introduction	167
9.1.3	Materials and Methods	169
9.1.4	Results	178
9.1.5	Discussion.....	181
9.1.6	References	182
9.2	FEM evaluation of heat exchange efficiency variability under transient conditions for different coaxial ground heat exchangers materials and subsoil contexts.....	186
9.2.1	Abstract.....	186
9.2.2	Introduction	186
9.2.3	Materials and methods.....	188
9.2.4	Results	190
9.2.5	Conclusions	194
9.2.6	References	195
10	Themed topic chapter: Evaluation of the durability of metallic GHEs and the effectiveness of passive anti-corrosion measures	197
10.1	Laboratory assessment of carbon steel corrosion rate of grout-less ground heat exchangers	198
10.1.1	Abstract	198
10.1.2	Introduction	198
10.1.3	Materials and methods	200
10.1.4	Results	203
10.1.5	Conclusions	205
10.1.6	References	207
10.2	Evaluation of different metal anti-corrosion countermeasures on coaxial ground loop heat exchangers for shallow geothermal applications.....	209

10.2.1	Abstract	209
10.2.2	Introduction	209
10.2.3	Materials and methods	211
10.2.4	Results	216
10.2.5	Conclusions	221
10.2.6	References	222
11	Themed topic chapter: Non-destructive control method for the inspection of metal GHEs based on infrared thermography	225
11.1	Internal corrosion and joint failure detection for the inspection of vertical geothermal heat exchangers by infrared thermography	226
11.1.1	Abstract	226
11.1.2	Introduction	226
11.1.3	Internal corrosion	227
11.1.4	Results	232
11.1.5	Joint fittings	234
11.1.6	Results	236
11.1.7	Conclusions	236
11.1.8	References	237
12	Conclusions	239
12.1.1	Future research developments	246

4 List of terms and acronyms

3LPE:	Three-Layers PolyEthylene
3LPP:	Three-Layers PolyPropylene
4DCT:	Four-Dimensional Computed Tomography
AC:	Alternating Current
AISI:	American Iron and Steel Institute
ARPAV:	Regional Agency for the Protection of the Environment of Veneto
AS:	Australian Standards
ASHRAE:	American Society of Heating, Refrigerating and Air-Conditioning Engineers
ASTM:	ASTM International, American Society for Testing and Materials
AWWA:	American Water Works Association
BHE:	Borehole Heat Exchanger
BP:	PolyButylene
BS:	British Standards
BSPP:	British Standard Pipe Parrallel (fitting type)
CEN:	Comité Européen de Normalisation (European Committee for Standardization)
Cheap-GSHPs:	CHEAP and efficient application of reliable Ground Source Heat exchangers and PumpS (H2020 research project)
CLSCC:	Chloride promoted stress corrosion cracking
CNR:	Consiglio Nazionale delle Ricerche (National Research Council of Italy)
COP:	Coefficient Of Performance
COR-TEN:	CORrosion resistant, TENsile strength (commercial steel grade trademark)
CR:	Corrosion Rate
CS:	Carbon Steel
CT:	Correlated contrast Thermography
DC:	Direct Current

DFT:	Discrete Fourier Transform
DHW:	Domestic Hot Water
DIN:	Deutsches Institut für Normung
Double-U:	Geometry type for GHEs
DSC:	Differential Scanning Calorimetry
EC:	European Commission
EED:	Earth Energy Designer software
ERT:	Electrical Resistivity Tomography
EU:	European Union
Euronorm:	European Standard, an international technical standard applicable in the European Union. It has been prepared by CEN member states
FBE:	Fusion Bonded Epoxy coating
FDM:	Finite Difference Method
FEA:	Finite Element Analysis
FEM:	Finite Element Method
FFT:	Fast Fourier Transform
FP6:	Framework Programme 6 (European Union scientific research initiative 2002-2006)
g.l.:	ground level
GEO4CIVHIC:	Most Easy, Efficient and Low Cost Geothermal Systems for Retrofitting Civil and Historical Buildings (H2020 research project)
GHE:	Ground Heat Exchanger
GROUNDHIT:	Ground coupled heat pumps of high technology (FP6 research project)
GRT:	Ground Response Test
GSHE:	Ground Source Heat Exchanger
GSHE:	Ground Source Heat Exchanger
GSHP:	Ground Source Heat Pump
H2020:	Horizon 2020 (European Union scientific research initiative 2014-2020)
HDPE:	High Density PolyEthylene
HVAC:	Heating, Ventilation, and Air Conditioning

Hydra-Red:	Hydra srl-RED srl. GHE installation method named after the main companies involved in its development.
ICCP:	Impressed Current Cathodic Protection
IRT:	InfraRed Thermography
ISO:	International Organization for Standardization
LFM:	Laser Flash Method
MC:	Moisture Content
MIC:	Microbiologically Influenced Corrosion
MMO:	Mixed Metal Oxide
mmy:	millimetres per year (unit for Corrosion Rate)
MPY:	thousandths of an inch per year (unit for Corrosion Rate)
MSA:	Multiple Average Sum filter
NACE:	National Association of Corrosion Engineers (Unites States of America)
Nd:YAG laser:	Solid-state laser device that uses a neodymium-doped yttrium aluminum garnet crystal
NDT&E:	Non-Destructive Testing and Evaluation
NDT:	Non-Destructive Testing
NZEB:	Near Zero Energy Building
OD:	Outside Diameter
PCA:	Principal Components Analysis
PCT:	Principal Components Analysis applied to Thermography
PE:	PolyEthylene
PE80, PE100, PE100RC:	designations of PE based on the long-term strength, known as the minimum required strength in accordance with ISO 12162.
PEX:	Cross-linked PolyEthylene
pH:	potential of Hydrogen" (or power of Hydrogen)
PLST:	Partial Least Squares Thermography
ppm:	parts per million
PREN:	Pitting Resistance Equivalent Number

REFPROF:	US NIST Reference Fluid Thermodynamic and Transport Properties Database
SCC:	Stress corrosion cracking
SMC:	Saturation Moisture Content
SRB:	Sulphate Reducing Bacteria
SST:	Stainless Steel
SVD:	Singular Value Decomposition
TRL:	Technological Readiness Level (i.e. maturity of technology innovation according to scale proposed by EC in Part 19 - Commission Decision C(2014)4995)
UNI:	Ente Nazionale Italiano di Unificazione
US NIST:	United States of America National Institute of Standards and Technology
UT:	Ultrasound Testing
U-tube:	Geometry type for GHEs
XRD:	X-Ray Diffractometry
XRF:	X-Ray Fluorescence

5 Introduction

5.1 Context of the thesis

5.1.1 *The GEO4CIVHIC project*

The work here presented is focused on the study of metallic ground heat exchangers (GHEs), but it has been unfolded in the frame of a larger and holistic endeavour aimed at innovating the shallow geothermal energy systems. The European Commission (EC) strongly supports research and development in geothermal technologies, funding projects on both the use of extracted heat to generate electricity and direct use of heat (such as in shallow geothermal). EC support also focuses on reducing costs in geothermal plants design, materials and drilling, because geothermal installations have high capital costs.

Shallow geothermal energy systems greatly contribute to the decarbonization of new constructions. However, for widespread use in existing buildings that need to be energetically retrofitted (Bertonea et al., 2016), especially historic buildings, the technology needs to be further developed (Sanner et al., 2013) and new ideas need to be tested before their market introduction. GEO4CIVHIC (acronym for Most Easy, Efficient and Low Cost Geothermal Systems for Retrofiting Civil and Historical Buildings) project, funded under Horizon 2020 European Research and Innovation programme aims at facilitating the application of shallow geothermal in the built environment, that is not enough developed. The main barriers today are:

- higher initial investments compared to other conventional solutions such as condensing gas boilers for heating and expansion systems for refrigeration;
- lack of cost-effective and environmentally friendly drilling to overcome difficulties that are commonly found in the built environment (outdoor space restrictions, regulatory limitation in allowed depth, etc.)
- need to change the heating and cooling terminals for proper performance of heat pumps, especially in historical buildings (Bamigbetan et al., 2017; Yang et al., 2017);
- low level of awareness, reluctance to risk and/or lack of experience between designer and operators (architects, installers, building owners) in the ultra-conservative construction industry;

- restrictions due to architectural constraints, which can make it difficult to have a suitable place for the geothermal field (e.g. outdoor space limitation) or room sufficient to house the geothermal heat pumps (no presence of a dedicated room for technical systems). Often only the architectural-aesthetic constraints can be avoided (typical of some types of buildings, such as listed historical ones) because most of the systems are underground and therefore not visible.

To overcome the above barriers, the total investment cost of geothermal systems must decrease compared to the alternative solutions. The high cost of drilling needs to be addressed. Drilling with large and very efficient but heavy drilling machines is difficult and often impossible in the built environment.

Increasing the thermal efficiency of ground source heat exchangers is another way to reduce the overall length of GHEs to install (Jalaluddin and Myiara, 2012) and the number of drillings needed to cover the energy demand of the served building. Development and improvements of GHEs are strictly linked to drilling and installation methodologies, that have to be compatible and synergistic. During GEO4CIVHIC and previous Horizon 2020 Cheap-GSHPs (acronym for CHEAP and efficient application of reliable Ground Source Heat exchangers and PumpS) projects, drilling methodologies and drilling machine components have been developed in such way to reduce cost and space limitation (Tsagarakis et al., 2020) and ultimately to permit the installation of novel types of GHEs, also developed within the projects. Moreover in GEOCOND H2020 project (acronym for Advanced materials and processes to improve performance and cost-efficiency of Shallow Geothermal systems and Underground Thermal Storage) pipe materials have been explored aimed at further increasing efficiency and decreasing operating costs of GSHP solutions.

Drilling and GHE innovations

One of the most promising methodologies is the rotary, vibration piling of enlarged steel co-axial ground source heat exchangers at depths between 50–80 m using a sacrificial drill bit in combination with small quantities of water. Good drilling speed is achieved using small machines with a moderate torque that relies on a caseless drilling design where the momentum is transferred to the drill bit by an internal rotating shaft. The GHE is attached to the drill bit through a bearing balls system and is dragged down during the drilling.

All of these combined developments significantly reduce installation time and costs in unconsolidated undergrounds, especially when borehole stabilization measures are required. Since this novel installation method requires much less energy, the drill rig

remains small and compact. These are crucial enabling factors for allowing the implementation of shallow geothermal systems in retrofitted buildings in built environments and historical districts, where space and manoeuvrability are limited. As mentioned earlier, an efficient GHE makes it possible to reduce the total area occupied by the geothermal exchange field. This goes in the same direction by allowing the geothermal system in a built environment where only a garden or a small area is available. Another key feature of this drilling technique is the capability to use metal pipes, which can be installed without the need to pre-drill the borehole. Therefore, it is not necessary to fill the annular space between the pipe and the hole with grouting, thus the pipe is in direct contact with the ground, resulting in a further improvement in thermal performance, which would lead to a reduced length of the GHE. This is strategic because it would make possible to overcome the problem of drilling depth limits that some sites may have.

One of the goals of GEO4CIVHIC was to demonstrate the practical feasibility of development and solutions. We used several demonstration cases to validate on the field the improved drilling methods and mechanical components. In one of them, improved metal GHEs were specifically tested, including a new coaxial type of concept based on the adaptation of wellpoint technology for drainage.

5.1.2 Thesis outlines

After the introductory sections including critical comments on the technical background of reference, the core part of this thesis is structured in 7 different papers, which are presented and redacted in themed chapters 8 to 11. These papers have been published (or are currently under editorial process by the journals), released as congress proceedings or as GEO4CIVHIC project deliverables. The four thematic chapters of this thesis are briefly introduced below, while the individual papers are detailed in the forewords of each thematic chapter.

Themed topic chapter: Design of innovative coaxial heat exchangers for shallow geothermal. Based on two manuscripts:

- “Innovative coaxial heat exchangers for shallow geothermal”;
- “Adapted well point technique and subsequent field evaluation for the installation”.

Themed topic chapter: Evaluation of thermal performance of metallic GHEs. Based on two manuscripts:

- “Evaluation of the effect of anti-corrosion coatings on the thermal resistance of ground heat exchangers for shallow geothermal applications”;
- “FEM evaluation of heat exchange efficiency variability under transient conditions for different coaxial ground heat exchangers materials and subsoil contexts”.

Themed topic chapter: Evaluation of the durability of metallic GHEs and the effectiveness of passive anti-corrosion measures. Based on two manuscripts:

- “Laboratory assessment of carbon steel corrosion rate of grout-less ground heat exchangers”;
- “Evaluation of different metal anti-corrosion countermeasures on coaxial ground loop heat exchangers for shallow geothermal applications”.

Themed topic chapter: Non-destructive control method for the inspection of metal GHEs based on infrared thermography. Based on one manuscript:

- “Internal corrosion and joint failure detection for the inspection of vertical geothermal heat exchangers by infrared thermography”.

5.1.3 Aims of the study

The research aimed to identify the most suitable materials for GHEs and the safest protection systems to improve durability and safety of metallic tubes.

The final aim has been to reach a technological solution reducing the cost of geothermal systems, increasing efficiency, safety and durability of GHEs, adaptable to geological and hydrogeological contexts as varied as possible.

The environmental aspect has been paramount: research aimed at preventing problems of leaks of fluid (e.g. glycol mixtures often with anticorrosive/antialgal additives) thanks to the study of degradation processes of metal GHEs. This has been a core topic recurring over the study. The research wanted to establish a step forward in the following strategic aspects related to shallow geothermal energy systems:

- Exploring the use of carbon steel as the main material for GHEs. Together with new installation methodologies developed within the EU Cheap-GSHPs and GEO4CIVHIC projects, it can contribute to reduce the cost of ownership of shallow geothermal systems. This is critical because the cost of ownership is one of the main factors limiting the spread of this promising green energy source,

and therefore is part of the struggle to transition to more environmentally sustainable energy sources.

- Increasing in the field of applicability of low enthalpy geothermal. The better comprehension of limits and advantages of metal GHE solutions would help to expand this energy source to contexts in which the geological conditions do not make it possible or limit the current state of the art.
- Aiming at using geothermal energy without limitations or performance compromises even in areas with aggressive soil conditions through the guided section of the most suitable materials. Currently it is only possible with low conductivity plastic/stainless steel tubes which have lower thermal performance than other metal GHE solutions (i.e. the ones based on carbon steel).
- Exceeding the limits on drilling depth. Thanks to the use of materials with high thermal conductivity, a shorter length of pipes would be required, which would allow the installation of geothermal systems even in the presence of aquifers or other conditions that limit their application.
- A major purpose of this research has been to evaluate if corrosion-protected metal GHE solutions can compete or even overtake the current more traditional systems based on stainless steel/plastic exchangers in terms of in heat exchange performance in transient and steady state.
- Improving reliability and life expectancy of geothermal systems thanks to enhanced quality of joints and corrosion prevention that would significantly extend life expectancy. This would be achieved through the use of inspection methodologies that can be actually applicable on site, as the ones based on active infrared thermography.

The activities necessary to achieve the aforementioned outcomes were carried out in the three-year doctorate covering these aspects:

- Information gathering and bibliographic research, aimed at the screening of the materials used in shallow geothermal systems, their interaction with the grounds and the methods already used to prevent or limit corrosion.
- Laboratory testing aimed to investigate the long-term durability of the proposed metal solutions. Selected ground conditions that could be found in real cases have been replicated in laboratory, assessing the corrosion rate and evaluating the resulting effects on the materials with a quantitative evaluation method.
- Mathematical modelling was applied to evaluate the heat exchange performance of different GHE solutions by analytical and FEM methods, after measuring in laboratory the thermophysical properties of GHE materials.

- Field experimental activity that included an on-site campaign for the evaluation of shallow geothermal systems in a demonstration case in the frame of the GEO4CIVHIC EU project. The activities on the field abroad initially provided were interrupted by Covid-19 pandemic, so that the research was refocused on a local case study, where all the planned research tasks were nevertheless completed. The site was selected at the CNR headquarters in Padua. It was therefore possible to analyse different types of GHEs: metallic (coaxial, well-point) and several anti-corrosion measures. Each GHE solution was designed, including the installation methodology and subsequently installed, as part of this research. During the last period it has been possible to verify the heat exchange performance using ground response test (GRT). Ground boundary conditions were assessed by electrical resistivity tomography (ERT) and chemophysical measurements.

5.1.4 References

- Bamigbetan O., Eikevik T.M., Nekså P., Bantle M. Review of vapour compression heat pumps for high temperature heating using natural working fluids, *International Journal of Refrigeration*, Volume 80, 2017, Pages 197-211, ISSN 0140-7007.
- Bertonea E., Sahin O., Stewart R.A., Zouc P., Alam M. Blair E. State-of-the-art review revealing a roadmap for public building water and energy efficiency retrofit projects. *International Journal of Sustainable Built Environment*, Volume 5, Issue 2, December 2016, Pages 526-548
- Horizon 2020 project Advanced materials and processes to improve performance and cost-efficiency of Shallow Geothermal systems and Underground Thermal Storage . <http://geocond-project.eu>
- Horizon 2020 project Cheap and efficient application of reliable ground source heat exchangers and pumps. <http://cheap-gshp.eu/>
- Horizon 2020 project Most Easy, Efficient and Low Cost Geothermal Systems for Retrofitting Civil and Historical Buildings . <http://www.geotech-project.eu/>
- Jalaluddin, Miyara A., Thermal performance investigation of several types of vertical ground heat exchangers with different operation mode, *Applied Thermal Engineering*, Volume 33, 2012, Pages 167-174, ISSN 1359-4311.

- Sanner B., Dumas P., Gavriiliuc R., Zeghici R. The use of geothermal energy for buildings refurbishment in Europe - technologies, success stories and perspectives. *Revista Română de Inginerie Civilă*, Volumul 4 (2013), Numărul 3. 2013.
- Tsagarakis, K. P.; Efthymiou, L.; Michopoulos, A.; Mavragani, A.; Anđelković, A. S.; Antolini, F.; Bacic, M.; Bajare, D.; Baralis, M.; Bogusz, W.; Burlon, S.; Figueira, J.; Genç, M. S.; Javed, S.; Jurelionis, A.; Koca, K.; Ryżyński, G.; Urchueguia, J. F.; Žlender, B. A Review of the Legal Framework in Shallow Geothermal Energy in Selected European Countries: Need for Guidelines. *Renew. Energy* 2020.
<https://doi.org/10.1016/j.renene.2018.10.007>.
- Yang W.W., Cao X.Q., He Y.L., Yan F.Y. Theoretical study of a high-temperature heat pump system composed of a CO₂ transcritical heat pump cycle and a R152a subcritical heat pump cycle, *Applied Thermal Engineering*, Volume 120, 2017, Pages 228-238, ISSN 1359-4311.

5.2 State of the art on closed loop shallow geothermal systems

Geothermal systems can be divided into low, medium and high enthalpy systems. In this case, the term "enthalpy" is closely associated to the system temperature. Since it is possible to obtain a low geothermal temperature at a relatively shallow depth, low enthalpy geothermal systems are also known as shallow geothermal systems (Banks, 2012). Low enthalpy geothermal energy is a technology that makes it possible to achieve the energy transition (Sharma et al., 2018) envisaged by the European Green Deal. Furthermore, by producing energy locally, it contributes to increasing the energy resilience of countries that import heavily energy, i.e. along the path that envisages fewer and fewer imports of natural gas from outside EU. Shallow geothermal energy systems use the underground as a heat storage reservoir to efficiently provide heating and cooling in geothermal systems based on ground source heat pumps (also called geothermal heat pumps, GSHP). The basic principle of a GSHP system (figure 1) is to extract heat from the ground at a relatively low temperature, raise the temperature with a heat pump and refrigeration cycle and use it in buildings HVAC (heating, ventilation, and air conditioning) systems.

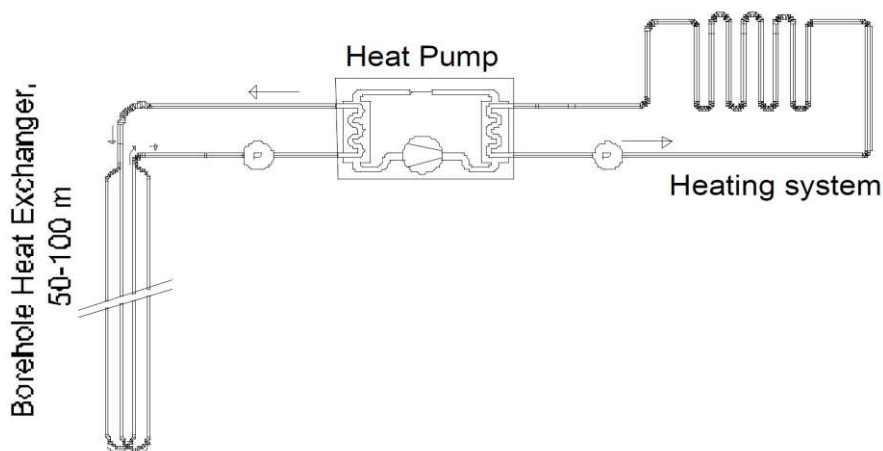


Figure 1: Schematic of a ground source heat pump system for heating. (source: Burkhard Sanner: Shallow geothermal energy)

In summer cooling, the system can be reversed to inject heat from the building, then further lower the temperature to meet the cooling needs of the building. The efficiency of a heat pump system is defined as the coefficient of performance (COP), which is the ratio between the production of heating or cooling and the energy introduced to operate the machine. A well-designed system achieves a COP of around 4 or higher throughout the year. The primary energy needed to operate the GSHPs is generally electricity. Depending on the energy mix of a country, electricity can come from fossil fuels, or it

can be obtained from green sources. Moreover, electricity can be produced locally when a photovoltaic plant is integrated into the system (Emmi et al., 2015 and 2016; Han et al., 2017; Liu et al., 2021). These characteristics of shallow geothermal systems for the conditioning of building spaces make them one of the most promising technologies because they are extremely energy efficient and sustainable from an environmental point of view (Casasso and Sethi, 2019). Replacing traditional heating and cooling systems with shallow geothermal systems can significantly reduce peak energy consumption and greenhouse gas emissions.

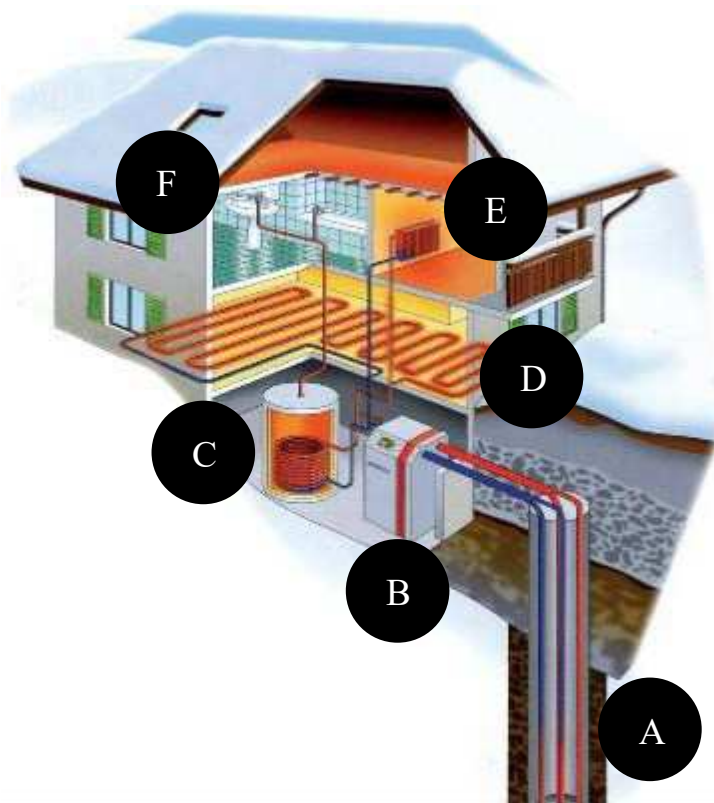


Figure 2: Shallow geothermal system, including (Sáez Blázquez et al., 2017) :vertical ground heat exchanger(A), ground source heat pump (B), storage water tank (C), low enthalpy (D, radiant floor) and high temperature terminals (E, radiators)and domestic hot water outlets (F). (image source:geo4civhic.eu)

As shown in figure 2, a shallow geothermal system can also provide domestic hot water (DHW). Shallow geothermal systems are conventionally classified into two main categories: open or closed-loop systems. Open loop systems use groundwater from a well (or spring, flooded mine, river or lake), as a means of transferring heat which is supplied directly to the heat pump. In closed-loop systems, heat transfer occurs between the heat-transfer fluid that flows inside pipes buried in the ground and the ground itself. The pipes can be embedded in trenches, boreholes, or other structures (such as foundation piles). The tubes in which the fluid flows act as heat exchangers

and are called geothermal (or ground) heat exchangers. These can be of different shape and length. GHEs can be installed in the ground in different ways (vertical, horizontal, diagonal) using different drilling methods that are designed to better match a particular underground stratigraphy (Qi et al., 2019). Usually, a borehole with a diameter of about 15 cm is drilled by a drilling machine and one single or two U- tubes are inserted. Then, the borehole is sealed with grout. Another pipe geometry is the coaxial configuration. In this case the tubes have different diameters and are inserted one into the other. The heat carrier fluid flows downwards in the annular space and upwards in the internal tube or vice versa. Coaxial GHEs can be installed in two ways: drilling of a borehole and subsequently inserting the external and internal tubes followed by grouting or by piling the external tube into the ground and inserting the internal tube afterwards. The wall of the borehole may be sustained temporarily, by a casing that is removed when the borehole is completed. There are several options for filling the annular gap. A common design is grout injection, that is, cementing the borehole. Cement is needed not only to ensure thermal contact between the pipe and the ground, but also for environmental reasons. The GHEs may be organized in groups of hydraulically connected pipes (in series, parallel or a combination of both) which together constitute a geothermal field serving a building. The spacing, spatial distribution and total length of the GHEs in the field may vary, depending on the local climatic context, the energy performance characteristics of the building itself, the local geological/hydrogeological conditions and the heat exchange performance of the GHEs.

5.2.1 Heat-transfer fluids in closed-loop systems

The most noticeable type of heat transfer fluid in a closed loop system is water. However, pure water is not suitable for systems where the transfer fluid reaches temperatures close to or below 0 °C (e.g. central and northern Europe). In this case, some form of anti-icing agent is added to the water (Bartolini et al., 2020). Antifreezes are solutions of inorganic salts (sodium chloride, magnesium chloride, calcium chloride, or potassium carbonate), organic salts (potassium acetate), or alcohols or glycols (methanol, ethanol, ethylene glycol, or glycol propylene).

5.2.2 Vertical Ground Heat Exchangers classification

Heat exchangers are devices that efficiently transfer heat between two physical bodies or fluids. The car radiator, an elephant's ear and the grill on the back of a refrigerator are heat exchangers. In an efficient heat exchanger the heat exchange surface will be as large as possible to maximize the heat transfer by conduction, and on the other hand the thermal resistance will be as small as possible to maximize the heat flow (Gordon et al., 2017). The main task of a ground heat exchanger is to facilitate the exchange of heat from the ground to the heat transfer fluid flowing inside the pipes and vice versa with the lowest possible thermal resistance (Raymond et al., 2015). There are several factors that affect this heat exchange, such as pipe material, wall thickness, pipe surface properties, fluid flow rate, GHE geometry, hole diameter, grouting, etc. (Sanner et al. 2003 and 2010; Boban et al., 2021). Exploring the design improvement of vertical ground heat exchangers requires considering several aspects:

- Geometry and materials;
- Corrosion mechanisms and anti corrosion measures;
- Evaluation of performance and safety.

Geometry

For vertical GHEs, all geometries can be grouped into two basic schemes: U-tube and coaxial, with the latter further divided into simple coaxial, complex coaxial and helical. The main difference between the groups is that the U-tube always shows a mirror symmetry, while the coaxial GHEs are radially symmetrical.

U-tube geometries

Single-U-tube

Although the U-tube geometry (figure 3) is first mentioned in the United States in the 1940s, the first traces in European documents are seen around 1980 and the first patent applications were filed in 1984. However, the design of the U-tube and its derivatives, is still largely dominant today. Most of the patents granted concern only GHE U-tube

parts, such as pins (elbows), spacers, centerers, etc. In U-tube GHEs, two tubes coupled to the lower loop with a U-bend are inserted into the borehole and grouted to improve performance and provide protection.

The advantages of a single U-tube GHE are its simplicity and low material and manufacturing costs. Another positive fact is that the limited cross-sectional area of the flow channel makes it easier to achieve turbulence in the tube. The disadvantage is that efficiency is limited compared to other geometries. For boreholes deeper than 100 m, pipes with an outer diameter of 40 mm or 45 mm are often used. In areas where drilling costs are relatively low and therefore reducing drilling meters is not a priority, a single U-tube GHE is the recommended solution on the market.

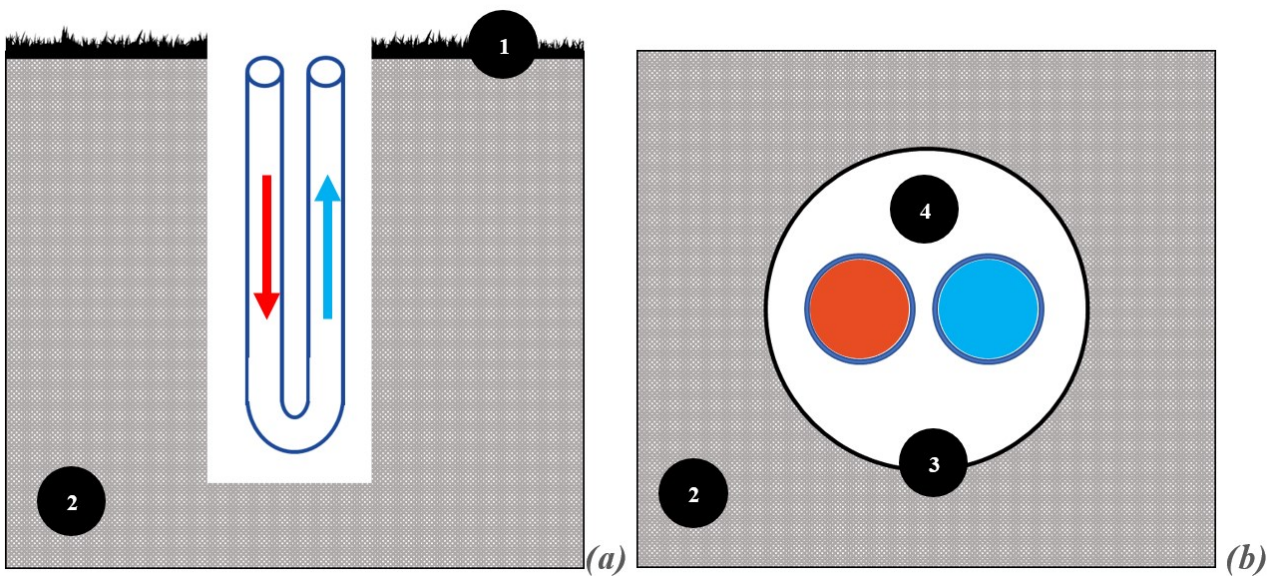


Figure 3: Schemes of single U-tube geometry, general view (a) and section (b). 1)-surface area; 2)-ground mass 3)-wall of the hole; 4)-filling the hole. Red and blue represent different flow directions (e.g. inlet and outlet of the hydraulic circuit).

Double-U-tube

By inserting two U-tubes (figure 4) into a borehole, you can achieve higher efficiency than GHE using a single U-tube. To accommodate additional tubes, you should generally choose a slightly larger hole diameter. Of course, the efficiency is not doubled, but the thermal resistance of the well is usually reduced by about 30%.

Doubling the number of tubes also increases the total cross-sectional area of the flow channel, requiring more total flow to achieve turbulence than a single U-tube GHE. Generally, tubes with an outside diameter of more than 32mm are used for boreholes

more than 120 m deep. The double U-tube GHE is economically significant in areas with relatively high drilling costs because it can reduce the overall length required; this option dominates markets such as Austria, Germany and Switzerland.

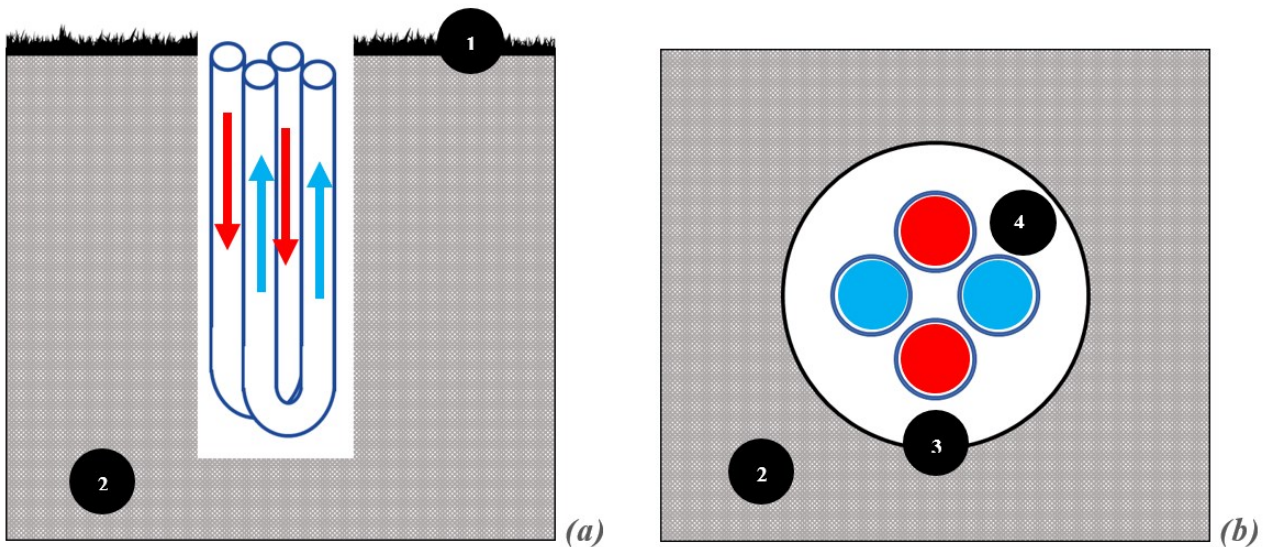


Figure 4: Schemes of double U-tube geometry, general view (a) and section (b). 1)-surface area; 2)-ground mass 3)-wall of the hole; 4)-filling the hole. Red and blue represent different flow directions (e.g. inlet and outlet of the hydraulic circuit).

Multi-U-tube

Again, adding further U-tubes in the boreholes augment the heat transfer efficiency, but in most cases requires a larger diameter of the borehole to accommodate them. Depending on the scenario, the reduction in thermal borehole resistance can range from less than 10% to about 20% for triple U-tubes compared to double-U tubes. Each additional set of U-tubes increases the overall cross-sectional area of the flow channel and reduces the likelihood of turbulence in the tube.

Multiple U-tube shapes have the real advantage only in large diameter holes that can be aligned with the wall of the hole. This is typical of heat exchanger piles where pipes are connected to the rebar cages of cast concrete foundation poles. For traditional GHE in boreholes drilled solely for geothermal purposes, multi-U-tube GHEs can be overlooked from a market perspective.

Coaxial geometries

Simple coaxial

In the coaxial GHE geometry (figure 5), the hydraulic circuit consists of two separate pipes that share a common axis, so that the GHE section is concentric.

The coaxial design offers a variety of alternatives for handling downflow and upflow channels differently and for isolating downflow and upflow from each other. Since the coaxial construction is basically a tube in another tube, it complexly tends to exhibit a larger outside diameter. This generally makes the coaxial GHE stiffer than the tubes used for the U-tube GHE and is therefore more difficult to handle.

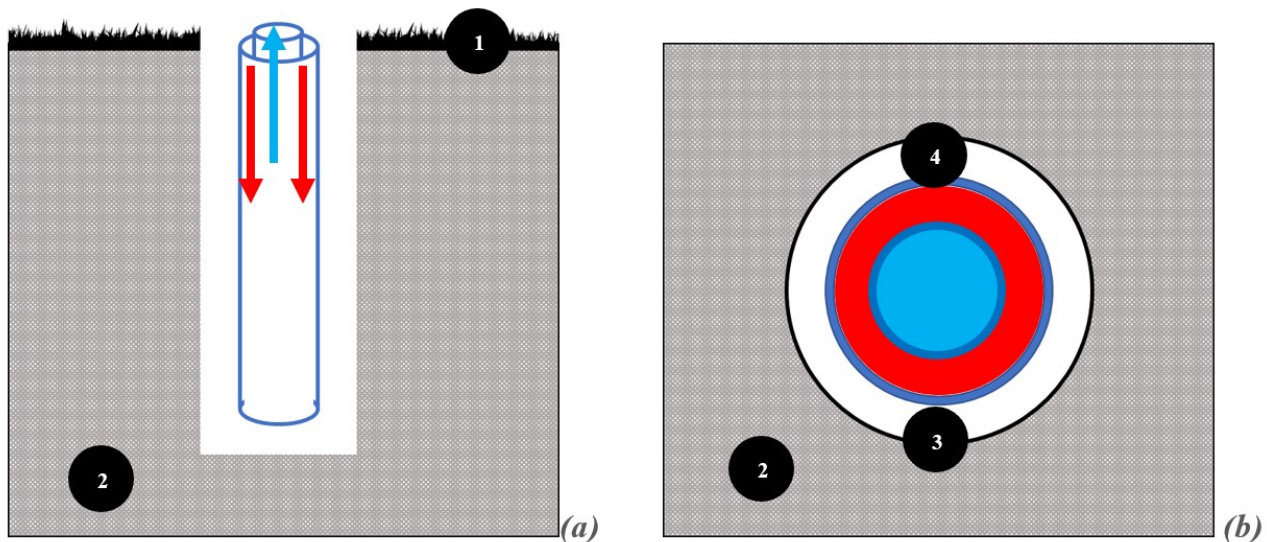


Figure 5: Schemes of coaxial geometry, general view (a) and section (b). 1)-surface area; 2)-ground mass 3)-wall of the hole; 4)-filling the hole (optional on unconsolidated ground). Red and blue represent different flow directions (e.g. inlet and outlet of the hydraulic circuit).

The coaxial GHEs allow direct installation on loose ground which can be carried out by pushing or piling. This installation methodology was used only with steel pipes. The contingent problems linked to corrosion problems have largely reduced the diffusion of this methodology, which seems to have completely disappeared from the market. This concept was reintroduced with stainless steel pipes in Northern Italy in 2007 using a penetrometer as an installation tool (figure 6). Direct installation of coaxial GHEs in this way can handle depths of up to about 20 meters.



Figure 6: Direct installation of a 50 mm diameter coaxial GHE in SS304-SS304L stainless steel using a penetrometer (methodology patented by Tecnopenta srl – RED srl).

New developments in drilling platform technology over the last few years allow for continuous improvement of the methodology. The Hydra Vibrasond 500 drilling rig (2008) allowed to overcome depth limitation and to reach 50-100 m in loose grounds. This methodology has proved successful in several applications: Venice Lagoon (2008), Mons in Belgium (2012), Batibouw in Belgium (2014). The rotation movement has been added to the drilling capacity to allow the penetration of compact clayey soils (experimented in Boom - Yper, Belgium). To date, more than 25,000 m of GHE pipes have been installed, reaching the highest level with the EU Cheap GSHPs project where an even more sophisticated drilling configuration has been approved. Interestingly, patent applications for coaxial GHEs can be traced back to 1955 in Europe and 1933 in the USA, although in the latter case not for use with a heat pump, but for direct cooling of the water. Coaxial GHE may have superior thermal properties to U-tube GHE. Custom manufacturing is required, while mass-produced plastic tubing can be used for U-tube GHE. In the FP6-funded GROUNDHIT project (acronym for Ground coupled heat pumps of high technology), an attempt was made to design a simple coaxial GHE from only commercially available standard tubes and fittings. This GHE was tested on demonstration sites as part of this project around 2005/06 and also for commercial use, but failed to succeed in the market against the dominance of the U-tube GHE. The diameter of the outer tube is limited by the fact that the GHE must be delivered to the drilling site. For spools, the minimum diameter of the reel depends on the ductility of the material and the diameter of the spool. In most European countries, trucks are typically 2.55 m wide and 4.0 m high, with special regulations for wide loads when exceeding this. If the coil for a coaxial GHE cannot be mounted on a standard truck, special equipment and permits are required. An alternative is to use rigid sections of pipe of the maximum suitable truck length (about 16 m or more on special trucks)

and weld the segments together during installation. This spot welding adds cost and time and is discouraged by most standards and regulations due to the harsh environment on the job site. However, some installers have done and still do this type of transport and installation. Single coaxial GHE can be manufactured with a variety of outside and inside pipe diameters. The choice of pipe diameter is usually limited to the standard material available on the market and the diameter of the borehole cannot be less than approximately 80 mm. A practical limit to increase the diameter of a single coaxial GHE seems to exist at an OD of about 125 mm; for larger diameter bores, a coaxial or twisted compound GHE snails provide alternatives. Stainless steel GHEs with outside diameters up to 80 mm are assembled by butt-welding in place, from 3 or 6 m lengths of pipe. Pressure resistance greater than 200 bar, a single value for GHE, and coefficient of thermal expansion of $15 \mu\text{m}/(\text{m}\cdot\text{K})$, about 10 to 14 times less than PE grades. The inner tube is made of plastic, with a choice of material depending on the maximum operating temperature and possibly foam insulation.

Complex coaxial

Complex coaxial designs use multiple tubes for external flow channels. This can be achieved by extruding a tube with an outer wall consisting of an external circuit with multiple chambers or by arranging multiple tubes around a central tube. The advantage of these complex coaxial geometries is the highest possible thermal efficiency. In fact, by choosing the right ratio of inner and outer channel diameters, it is possible to obtain turbulent flow in the outer tube (which increases heat exchange) and laminar flow in the inner tube. Nevertheless, they are pushed into a market niche due to their higher manufacturing cost and more complex installation compared to other simpler geometries.

Helicoidal

Helicoidal GHEs (figure 7) use spring-bent and small-diameter pipes as float channel. This kind of GHE can essentially be assumed as a variant of the geometry of the coaxial GHE, considering that one flow channel (commonly the downward one) surrounds the other. The upward channel is usually straight and may be placed both within the middle or in an eccentric position. The benefit of the helical GHE is the huge feasible

diameter of the borehole and the large contact area with the surrounding ground, ensuing in better thermal efficiency.

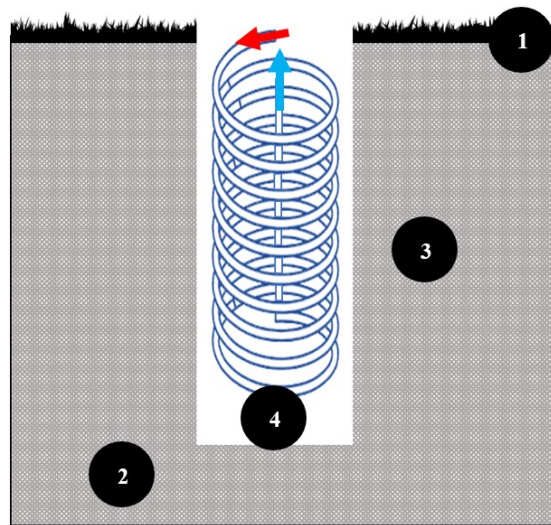


Figure 7: Scheme of helical geometry. 1)-surface area; 2)-ground mass 3)-wall of the hole; 4)-filling the hole. Red and blue represent different flow directions (e.g. inlet and outlet of the hydraulic circuit).

However, the depth of the GHE spiral is limited to approximately 10 m due to excavation and installation constraints. Helical GHE is therefore ideal for sites where there are geological or hydrogeological limitations on the drilling depth. Helical GHE is available in metal and plastic, the latter more largely present on the market.

Materials

Despite the specific geometry and hydraulic configuration, geothermal systems are most often permanently installed in the underground. Subsequent changes or deletions of the tubes are usually not possible. Therefore, the materials used must meet specific quality and safety requirements. In recent years, guidelines and standards have been developed for the quality assurance, construction and operation of geothermal systems in almost all EU Member States (Badenes et al., 2020). Based on compatibility with geometry and installation methodology, GHEs can be made from a variety of materials, which can be mainly classified into plastics and metals. A recent review of GHE's pipe materials was provided by Mendrinós et al. (2016 and 2017), which came to the conclusion that HDPE (High Density Polyethylene) is the most competitive option due to its low price and its moderate thermal conductivity. Metal pipes with a plastic

coating have also been tried in the past but were soon discontinued for cost reasons. Nowadays, HDPE pipes dominate the European market, while other plastic materials and metals are pushed into smaller niches.

Metal

Steel grades and other metal alloys with structural potential and tensile strength can be considered as pipe materials. Metals have a much higher thermal conductivity than thermoplastics, but they are more susceptible to corrosion. In fact, metal pipes for GHEs have long been proposed and have been widely used due to their high thermal performance. However, the problem of corrosion is considered an obstacle, and for non-corrosive metals such as stainless steel, the unit price can impact the economical sustainability of the system. Corrosion can affect the service life of GHE depending on the aggressiveness of the corrosive environment and the coupling between the pipe material and the subsoil. In addition, internal corrosion of pipes can also adversely affect the life of other system components, including circulation pump and heat pump evaporator. In fact, these will fail when injected by solid particles (rusty flakes or other corrosion products) that can be present in the heat transfer fluid. The first vertical GHE detected in Europe dates back to 1974 in southwestern Germany. In this early implementation the GHE was coaxial, with a rigid steel pipe measuring 60 x 5 mm. The outer pipe construction was bolted through a joint and a plastic pipe was used as inner circuit. Glycol-water mixture was used as the heat transfer fluid. The GHE was not grouted. In 2005, after about 30 years of operation, one of the installed GHEs leaked, probably due to corrosion. Steel GHEs were sold primarily in France until 2000s, but they had to be discontinued because it was more difficult to install and less price competitive than the PE-GHEs.

Stainless-steel grades with anti-corrosive action used for piping

Stainless steel (SST) is an alloy of Fe, Cr and C. Occasionally it has other complementary elements, the most common being Ni. Cr gives resistance to corrosion. In oxidizing environment, Cr produces a very dense and thin passivating layer which insulates the material from any corrosive action as long as it is kept intact. SSTs are classified according to the amount of the elements in their composition i.e. martensitic, ferritic, and austenitic. Austenitic stainless steels (table 1) are iron-based alloys that

contain nominally 19% chromium and 9% nickel. As the name suggests, austenite is the predominant microstructural phase at room temperature in austenitic stainless steels. The chemical composition can be varied, for example by lowering the carbon content and adding titanium, niobium or tantalum to prevent carbide formation, or by adding molybdenum to increase localized corrosion resistance. The high corrosion resistance of austenitic stainless steels in most atmospheric and aqueous environments is due the presence of a thin (~2nm) layer of chromium oxide (passivating layer). Wet and humid environments containing chloride ions can cause pitting corrosion and crevice corrosion of austenitic stainless steel components (Ma, 2012). Austenitic is the group with the greatest advantages in manufacturing, as well as in service performance such as easy welding and great corrosion resistance. AISI 304 contains 18% Cr and 8% Ni. For more severe conditions of higher chloride level, lower pH and/or higher temperatures, the alloys are added with Mo (molybdenum), which helps to resist to corrosion from chlorides in seawater and marine environments. In such context AISI 316 should be considered, which contains 16% Cr, 10% Ni and 2% Mo. The Mo-containing alloys 316 and Alloy 316L may handle waters with up to about 2000 ppm of chloride. Other austenitic stainless steels used for pipework are listed below.

Table 1: Austenitic steel grades used for manufacturing pipes.

AISI	Description
304	The general-purpose grade, widely used where good formability and corrosion resistance are required.
304L	As 304 but with lower carbon content to minimise carbide precipitation during welding.
301 and 302	Higher strength versions of 304 that are often cold worked to give higher strength.
303 and 303Se	General purpose grades with sulphur or selenium added to improve machinability.
321	As 304 with an addition of titanium to prevent carbide precipitation during welding. The resistance of the stabilized Alloys 321 to pitting and crevice corrosion in the presence of chloride ion is similar to that of Alloy 304 or 304L stainless steels because of similar chromium content. And therefore 100 ppm chloride in aqueous environments is considered to be the limit for the stabilized alloys, particularly if crevices are present.

347	As 304 with addition of niobium and or tantalum to prevent carbide precipitation during welding.
316	As 304 but with molybdenum added to increase resistance to localised corrosion in marine and chemical environments.
316L	As 316 but with lower carbon content to minimise carbide precipitation during welding.

AISI 304

AISI 304 (table 2) is the most common stainless steel. The steel contains both chromium (between 18% and 20%) and nickel (between 8% and 10.5%) metals as the main non-iron constituents. It is an austenitic stainless steel. It is less electrically and thermally conductive than carbon steel and is essentially magnetic, although less than carbon steel. It has a higher corrosion resistance than regular steel and is widely used because of the ease in which it is formed into various shapes. The composition was developed by W. H. Hatfield at Firth-Vickers in 1924 and was marketed under the trade name "Staybrite 18/8". Other names for the same material are 1.4301 (Euronorm), X5CrNi18-10 (DIN), 304S31 (BS).

Table 2: Stainless steel AISI 304 chemical composition

AISI 304 chemical composition (excl. iron) by weight (%)						
% Cr	% Ni	% C	% Mn	% Si	% P	% S
18–20	8–11	0.08	2	1	0.045	0.03

AISI 304 stainless steel has excellent resistance to a wide range of atmospheric environments and many corrosive agents. It is subject to pitting and crevice corrosion in warm chloride environments and to stress corrosion cracking above about 60 °C. It is considered resistant to pitting corrosion in water with up to about 400 mg/l chlorides at ambient temperatures, reducing to about 150 mg/l at 60 °C. AISI 304 is corrosion resistant in fresh waters containing low levels of chloride ion of up to 100 ppm. This level of chloride is considered to be the limit for the 18-8 alloys, particularly if crevices are present. Higher levels of chloride might cause crevice corrosion and pitting. The 18-8 alloys are not recommended for exposure to marine environments which have much higher levels of chloride. AISI 304 stainless steel is also very sensitive at room temperature to the thiosulfate anions released by the oxidation of pyrite (as encountered

in acid mine drainage) and can undergo severe pitting corrosion problems when in close contact with pyrite- or sulphide-rich clay materials exposed to oxidation.

For more severe corrosion conditions, when 304 stainless steel is too sensitive to pitting or crevice corrosion by chlorides or general corrosion in acidic applications, it is commonly replaced by 316 stainless steel.

AISI 316

Marine grade stainless alloys typically contain molybdenum to resist the corrosive effects of NaCl in seawater. Concentrations of salt in seawater can vary, and splash zones can cause concentrations to increase dramatically from the spray and evaporation. AISI 316 stainless steel (table 3) is a molybdenum-alloyed steel and is the second most common austenitic stainless steel (after AISI 304 grade). It is the preferred steel for use in marine environments because of its greater resistance to pitting corrosion than other grades of steel without molybdenum. The fact that it is negligibly responsive to magnetic fields means that it can be used in applications where a non-magnetic metal is required. Other names for the same material are 1.4401 (Euronorm), X5CrNiMo17-12-2 (DIN), 316S31 (BS).

Table 3: Marine grade Stainless steel AISI 316 chemical composition

AISI 316 chemical composition (excl. iron) by weight (%)								
% Cr	% Ni	% C	% Mn	% Si	% P	% S	% N	% Mo
16–18	10–14	0.08	2	0.75	0.045	0.03	0.10	2.0–3.0

In GHE applications, the internal wall of the pipe is protected from corrosion by the presence of heat transfer fluid, that contains dissolved oxygen. For the same reason, constant presence of groundwater should allow the regeneration of the passivating layer on the outer wall of the pipe. Nonetheless, as described in the following section devoted to corrosion mechanism, other underground characteristics can lead to corrosion of stainless steel, as the presence of chlorides, sulphide, anoxic environments or microorganisms. Despite the interesting capability of resisting corrosion in selected environments, stainless steel costs three times more than the carbon steel (table 4), and has lower thermal conductivity (table 5).

*Table 4: Thermal conductivity of reference materials**

Material	W/mK
HDPE	0.5
Mild/low-Carbon Steel AISI 1018	51.9
Stainless Steel AISI 304	14.4
Stainless Steel AISI 316	16.2

*Source: US NIST, matweb.com, engineeringtoolbox.com

*Table 5: Market price of reference materials***

Material	€/ton
HDPE	1080
Mild/low-Carbon Steel	900
Stainless Steel AISI 304	2900
Stainless Steel AISI 316	3480

**Source: Milano Finanza/Camera di Commercio di Milano 2019. Average market price from the producer/importer to the industry, VAT excluded

Aluminium and Copper

Aluminium (Al) and copper (Cu) do not corrode in the atmosphere, since the corrosion products form a protective oxide layer that covers the entire surface of the metal, which self regenerates when damaged by subsequent reaction with the Oxygen. Its resistance to corrosion in the underground environment depends on the formation of the passivation layer, therefore it is strictly dependent on the presence of dissolved oxygen in the underground. In GHE applications, copper and its alloys are expected to exhibit exceptional corrosion resistance in most underground conditions. In aggressive geological environments like aquifers with a high concentration of chlorides, sulphates, ammonia and/or sulphides, characterized by a low resistivity of less than 5 Ωm , copper and its alloys are subject to general or localized corrosion. In this case, cathodic protection is required. The resistivity of 5 Ωm corresponds to 900 ppm of chlorides or 1400 ppm of sulphates dissolved in groundwater. The use of copper is also not recommended in the event of the presence of traces of dissolved hydrogen sulphide or ammonia in the aquifers. Copper and Aluminium offer both excellent thermal conductivities values (Cu: 398 $\text{W m}^{-1} \text{K}^{-1}$, Al: 239 $\text{W m}^{-1} \text{K}^{-1}$). Ranging from 3k (Al) to 10k (Cu) euros per tonne (bulk metal, not machined), the cost of building GHE would be much higher compared to other materials such as plastic or carbon steel, which makes these metals an unfavourable choice for cost-effective applications.

Weathering steel

Weathering resistant steel are commonly referred to by the generic trademark COR-TEN steel. US Steel company owns the trademark on the COR-TEN name, which refers to two distinctive properties of this steel: corrosion resistance and tensile strength.

COR-TEN steel is a group of steel alloys developed to eliminate the need for protective paint and sport a rust-like appearance that stabilizes after years of exposure to the weather. COR-TEN originally received the standard designation A242 (COR-TEN A) from the ASTM (table 6). The new ASTM grades are A588 (COR-TEN B, table 7) and A606 for thin plates. Weathering refers to the chemical composition of these steels, allowing them to exhibit increased resistance to atmospheric corrosion compared to other steels. This is because the steel forms a protective layer on its surface under the influence of the weather.

Table 6: Corten ASTM A242 chemical composition

ASTM A242 chemical composition (excl. iron) by weight (%)								
%C	%Si	%Mn	%P	%S	%Cr	%Cu	%V	%Ni
0.12	0.25– 0.75	0.20– 0.50	0.01– 0.20	0.030	0.50– 1.25	0.25– 0.55	-	0.65

Table 7: Corten ASTM A588 chemical composition

ASTM A588 chemical composition (excl. iron) by weight (%)								
%C	%Si	%Mn	%P	%S	%Cr	%Cu	%V	%Ni
0.16	0.30– 0.50	0.80– 1.25	0.030	0.030	0.40– 0.65	0.25– 0.40	0.02– 0.10	0.40

The corrosion-retarding effect of the protective layer is produced by the particular distribution and concentration of alloying elements in it. The layer protecting the surface develops and regenerates continuously when subjected to the influence of the weather. In other words, the steel is allowed to rust in order to form the protective

coating. For GHE, it presents various advantages, primarily due to its good thermal properties (thermal conductivity: $25 \text{ W m}^{-1} \text{ K}^{-1}$). Its protective oxide patina acts as passivating layer similarly as stainless steel. Ultimately, due to its tensile mechanic properties, it can be machined into pipes. Its use for GHE is nonetheless impracticable because of major disadvantages. Corten requires special welding techniques and tools. Moreover, weathering steel is not rust-proof in any condition. If water is allowed to accumulate on the surface of the steel, it will experience a higher corrosion rate, so provision for drainage must be made. Weathering steel is sensitive to humid subtropical climates, and in such environments it is possible that the protective patina may not stabilize but instead continues to corrode. Furthermore, the weathering of the material can lead to discolorations, known as "bleeding" or "runoff", dispersing oxidization products in the surrounding environment. Ultimately, its bulk cost is similar to the stainless steel, thus price cannot be considered a competitive advantage against other more viable metals.

Titanium

Titanium and its alloys are among the most corrosion resistant materials currently known. For this reason, they are commonly used in many applications. Titanium superior corrosion resistance results from the formation of a stable outer protective layer of titanium oxides, composed primarily of TiO_2 . Unlike stainless steel, aluminium, and copper, TiO_2 is formed from the reaction of titanium with traces of oxygen or water. The resulting crevice corrosion immunity is at temperatures up to 300°C , much higher than any other metals and alloys mentioned in this document, making it also suitable for geothermal applications other than shallow ones. With respect to both carbon and stainless steels, Titanium has a much lower thermal conductivity ($17 \text{ W m}^{-1} \text{ K}^{-1}$).

Plastic

Plastic materials are vastly used in the manufacture of geothermal hydraulic components. Reasons for this include high flexibility, corrosion resistance, and low cost. The first modern GHE made from PE pipes was installed in 1980 in Switzerland. Austria soon followed. High-density polyethylene (HDPE) has been the most utilized material for decades after the early experiments on various metal and plastic materials.

The introduction of factory-manufactured GHE coils dates back to the late 1980s. The main advantages were cost, ease of use including welding, and durability. Development moved from PE80 to PE100 and PE100RC, and then to cross-linked polyethylene (PEX). Materials other than PE were used only when required at high temperatures.

Hard Rock

GHEs have also been used to store thermal energy underground by accessing hard rock through boreholes. One of the first large test sites was built in 1982/83. In such applications, the drilled hard rock represents the outer wall of the coaxial GHE. At this time, hard rock channels acting as GHE are not used in the field of shallow geothermal but represent a promising fringe technology for the high temperature geothermal energy sector.

Joints and connections

In case of plastic pipe, it is usually unfolded into the borehole from a continuous coil. For steel pipes, measures can be implemented to significantly reduce the occurrence of corrosion, as discussed in detail in subsequent chapters. With the proper precautions, the corrosion phenomena in the wall pipe may not constitute a major issue for such material, but the risk of potential failure is not negligible on the joints which occur between adjacent sections of a vertical ground heat exchanger.

Depending on the drilling rig and the length of the heat exchangers, between ca. 15-30 joints are needed for each one. Such joints on metal pipes are usually welded on site, sometimes under unfavourable conditions such as dirt environments and presence of moisture. During this process, no inspection on welded joints is taken as a praxis, so the risk of leakage during the operational phase of the geothermal system is not precluded.

Furthermore, welded joints on vertical geothermal heat exchangers are subjected to creep fatigue during the installation due to the mechanical action of the torque of the rotating drilling rig while pushing the pipe deep into the ground.

According to non-geothermal-specific regulation on pipelines, the junction of the steel pipes is usually welded and can be:

- A) socket for overlap welding (compliant with the requirements of Appendix C of the UNI EN 10224 standard): in this case one end of the pipe is socket-shaped.
- B) butt welding (according to point 7.10 of the UNI EN 10224 standard): in this case the two ends of the pipe are not shaped but must be suitably prepared as follows according to the thickness of the pipes:
- with straight edges for thicknesses ≤ 3.2 mm;
 - with bevelled edges at 30° for thicknesses > 3.2 mm.

In the first case there are two types of socket joint:

- cylindrical socket that is used for pipes up to and including 125 mm. This type of joint is characterized by the advantage of achieving perfect centering between the various contiguous pipes and the disadvantage of not allowing any deviation due to the minimum play between the ends to be joined;
- with spherical cup for diameters from 150 mm up to 900 mm. This type of joint makes it possible to create angular deviations without resorting to special pieces (curves). Not common in standard vertical ground heat exchangers for shallow applications.

The welding process may result in metallurgical changes in both fusion zone and heat affected zone. In most alloy systems some degradation in pitting and crevice corrosion resistance occurs in welding, but these effects can be minimized if proper materials and practices are used (Moore et al., 2015). Proper materials usually involve over-alloyed consumables and practices includes proper heat sources. It is important that correct information are sought from suppliers. Again, looking at the extremely high pitting resistant alloys it has been found that the high molybdenum alloys are particularly susceptible to micro-segregation in fusion zone, leading to lowered pitting resistance. Alloys such as 4565S which achieve their pitting resistance by high nitrogen rather than very high molybdenum levels have been found to be less affected by weld segregation.

Threaded joints for metal GHEs developed in Cheap-GSHPs and GEO4CIVHIC

The external tubes of the GHEs installed by means of Hydra-Red method (patent request n.102018000011157) developed in the frame of Cheap-GSHPs project, and further developed during GEO4CIVHIC, were 88.9 mm external diameter, 2 mm thick tubes connected with threaded fittings, which components are shown table 8. Both

male and female components were machined starting from a $\Phi 88.9 \times 11.13$ mm tube. O-rings (item 2-234 in figure 8) assure sealing.

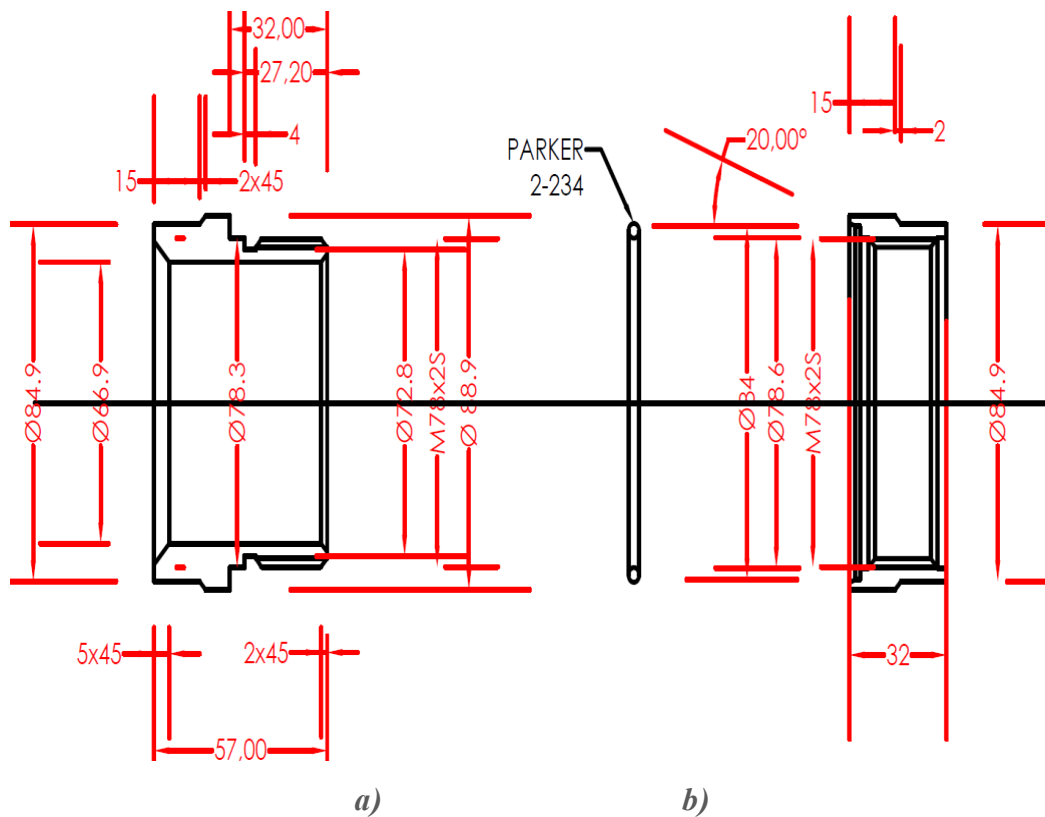


Figure 8: Threaded fittings for Hydra-Red method: male (a) and female (b). (image courtesy of RED srl).

The following figure 9 shows a drawing of the transition components from the GHE external tube to the head. Such transition piece is female threaded at one end. The first component (left) was machined starting from a $\Phi 88.9 \times 11.13$ mm, whereas the other (in violet) from a $\Phi 73 \times 9.53$ mm tube. A $\Phi 63.5 \times 2$ tube segment of suitable length (about 1.5 m) was welded to the transition piece in such a way to fit with the probe head (figure 10).

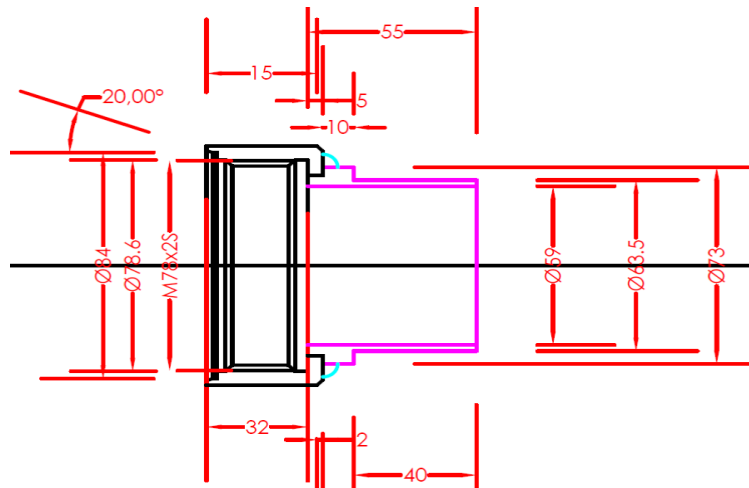


Figure 9: Connection piece (female threaded) from external tube to head. (image courtesy of Hydra srl).

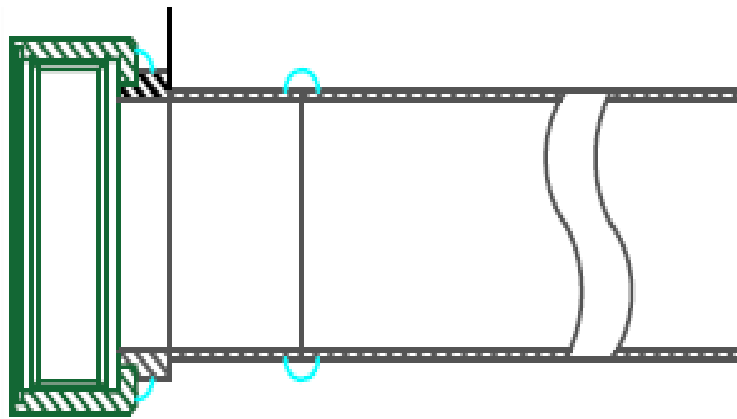
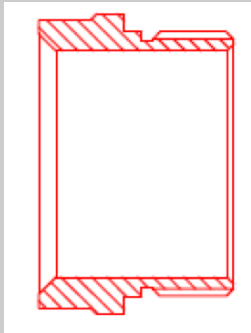

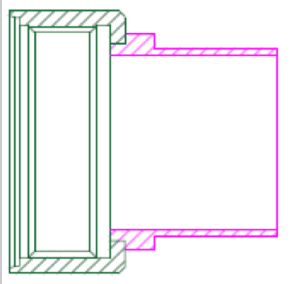


Figure 10: $\phi 63.5 \times 2$ tube segment welded to the transition piece – Hydra-Red method. (image courtesy of RED srl).

Table 8: Overview of the threaded fittings with ID code - Hydra-Red.

ITEM	ID	ROUGH TUBE	DRAWING
Male threaded fitting devoted to $\Phi 88.9 \times 2$ pipes	G.F.M. 88.9	88.9X11.13	
Female threaded fitting devoted to $\Phi 88.9 \times 2$ pipes	G.F.F. 88.9	88.9X11.13	
Transition piece between $\Phi 88.9 \times 2$ pipe and connection head	G.T. 88.9	88.9X11.13	

A female threaded coupling was welded to the drill bit in workshop. An 88.9 pipe with two male fittings at both ends will be screwed to the drill bit.

The components of the GHE external tube are shown in the figure 11:

- 3m-long $\phi 88.9 \times 2$ pipe with two male threaded fittings welded to both ends. Such tube shall be screwed to the drill bit;
- 3m-long $\phi 88.9 \times 2$ pipe with a female fitting welded to one end and a male fitting welded to the other;
- a transition piece (female threaded) welded to a (approx.) 1.5 m-long $\phi 63.5 \times 2$ pipe that shall be connected to the probe head;
- the drill bit and a female fitting to be welded to the bit.

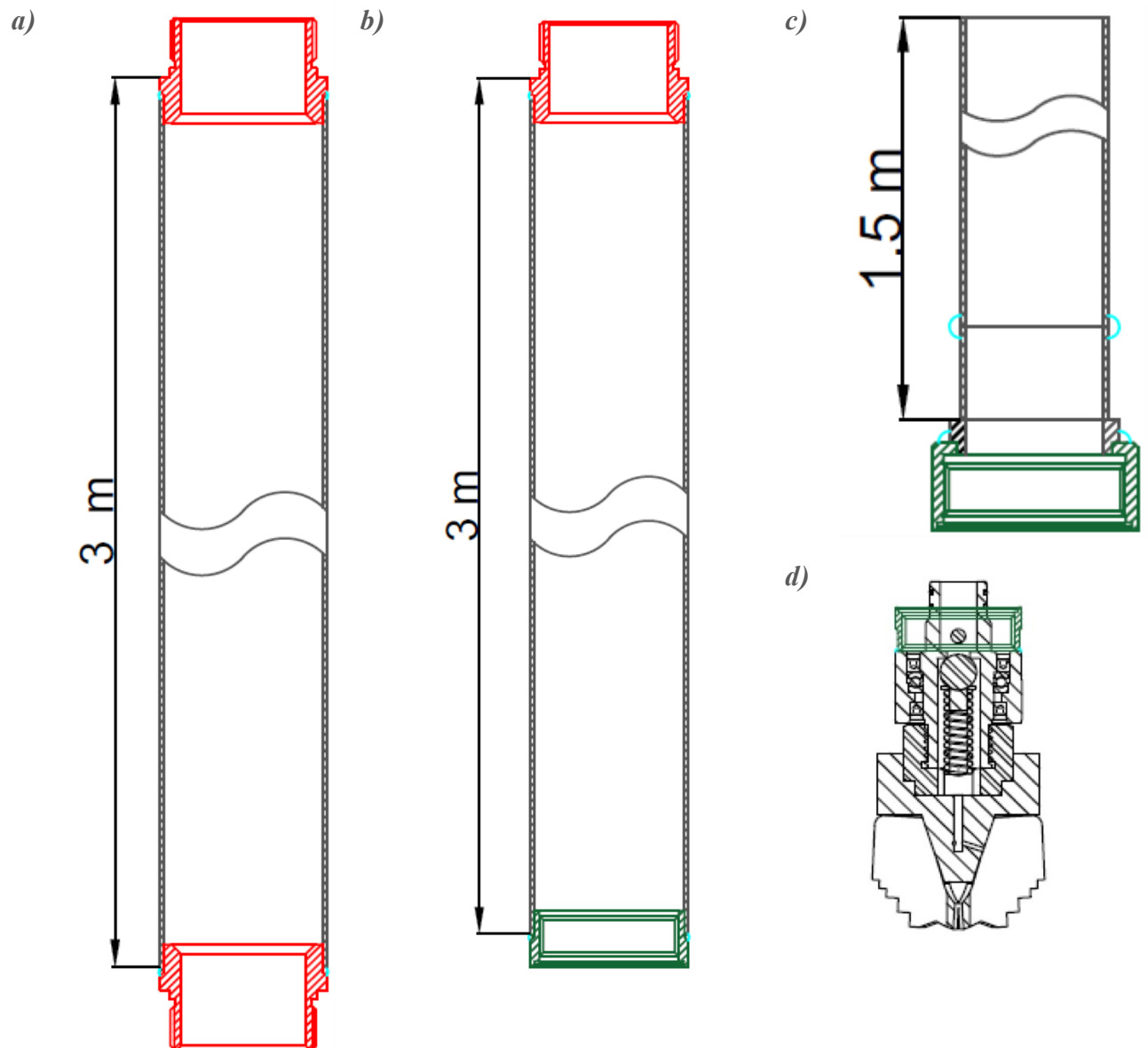


Figure 11: Sketch of the components of BHE external tube according to Hydra-Red method. (image courtesy of RED srl).

5.2.3 References

- Badenes, B.; Sanner, B.; Mateo Pla, M. Á.; Cuevas, J. M.; Bartoli, F.; Ciardelli, F.; González, R. M.; Ghafar, A. N.; Fontana, P.; Lemus Zuñiga, L.; Urchueguía, J. F. Development of Advanced Materials Guided by Numerical Simulations to Improve Performance and Cost-Efficiency of Borehole Heat Exchangers (BHEs). *Energy* 2020. <https://doi.org/10.1016/j.energy.2020.117628>.

- Banks, D. An Introduction to Thermogeology: Ground Source Heating and Cooling: Second Edition; 2012. <https://doi.org/10.1002/9781118447512>.
- Bartolini, N.; Casasso, A.; Bianco, C.; Sethi, R. Environmental and Economic Impact of the Antifreeze Agents in Geothermal Heat Exchangers. *Energies* 2020. <https://doi.org/10.3390/en13215653>.
- Boban, L.; Miše, D.; Herceg, S.; Soldo, V. Application and Design Aspects of Ground Heat Exchangers. *Energies*. 2021. <https://doi.org/10.3390/en14082134>.
- BS EN 17522. Design and construction of borehole heat exchangers.
- Casasso, A.; Sethi, R. Assessment and Minimization of Potential Environmental Impacts of Ground Source Heat Pump (GSHP) Systems. *Water (Switzerland)*. 2019. <https://doi.org/10.3390/w11081573>.
- Decisione della Commissione del 9 novembre 2007 che stabilisce i criteri ecologici per l'assegnazione del marchio comunitario di qualità ecologica alle pompe di calore elettriche, a gas o ad assorbimento funzionanti a gas.
- Decreto legislativo 11 febbraio 2010, n°22: Riassetto della normativa in materia di ricerca e coltivazione delle risorse geotermiche, a norma dell'articolo 27, comma 28, della legge 23 luglio 2009, n. 99.
- Decreto legislativo 3 aprile 2006, n°152: Norme in materia ambientale.
- Direttiva 2009/28/CE del Parlamento Europeo e del Consiglio sulla promozione dell'uso dell'energia da fonti rinnovabili, recante modifica e successiva abrogazione delle direttive 2001/77/CE e 2003/30/CE.
- Emmi G., Tisato C., Zarrella A., De Carli M. Multi-source Heat Pump Coupled With A Photovoltaic Thermal (pvt) Hybrid Solar Collectors Technology: A Case Study In Residential Application, *International Journal of Energy Production and Management*, Volume 1, Issue 4, 2015, Pages 382-392, ISSN 2056-3272., 2016.
- Emmi G., Zarrella A., De Carli M., Galgaro A. An analysis of solar assisted ground source heat pumps in cold climates, *Energy Conversion and Management*, Volume 106, 2015, Pages 660-675, ISSN 0196-8904.
- Gordon D., Bolisetti T., Ting D. S-K., Reitsma S. Experimental and Analytical Investigation on Pipe Sizes for a Coaxial Borehole Heat Exchanger, *Renewable Energy*, Available online 31 August 2017, ISSN 0960-1481.
- Han Z., Qu L., Ma X., Song X., Ma C. Simulation of a multi-source hybrid heat pump system with seasonal thermal storage in cold regions, *Applied Thermal Engineering*, Volume 116, 2017, Pages 292-302, ISSN 1359-4311.

- Legge 23 luglio 2009, n°99: Disposizioni per lo sviluppo e l'internazionalizzazione delle imprese, nonché in materia di energia.
- Liu, X.; Spitler, J. D.; Qu, M.; Shi, L. Recent Developments in the Design of Vertical Borehole Ground Heat Exchangers for Cost Reduction and Thermal Energy Storage. *J. Energy Resour. Technol. Trans. ASME* 2021. <https://doi.org/10.1115/1.4050418>.
- Ma, F.-Y. Corrosive Effects of Chlorides on Metals. In *Pitting Corrosion*; 2012. <https://doi.org/10.5772/32333>.
- Mendrinos, D.; Katsantonis, S.; Karytsas, C. Pipe Materials for Borehole Heat Exchangers. *Eur. Geotherm. Congr.* 2016 2016.
- Mendrinos, D.; Katsantonis, S.; Karytsas, C. Review of Alternative Pipe Materials for Exploiting Shallow Geothermal Energy. *Innov. Corros. Mater. Sci. (Formerly Recent Patents Corros. Sci.)* 2017. <https://doi.org/10.2174/2352094907666170327163227>.
- Moore, P.; Booth, G. Welding Problems and Defects. In *The Welding Engineer's Guide to Fracture and Fatigue*; 2015. <https://doi.org/10.1533/9781782423911.1.23>.
- Qi, D.; Pu, L.; Ma, Z.; Xia, L.; Li, Y. Effects of Ground Heat Exchangers with Different Connection Configurations on the Heating Performance of GSHP Systems. *Geothermics* 2019. <https://doi.org/10.1016/j.geothermics.2019.02.002>.
- Raymond, J.; Mercier, S.; Nguyen, L. Designing Coaxial Ground Heat Exchangers with a Thermally Enhanced Outer Pipe. *Geotherm. Energy* 2015. <https://doi.org/10.1186/s40517-015-0027-3>.
- Sáez Blázquez, C.; Farfán Martín, A.; Martín Nieto, I.; Carrasco García, P.; Sánchez Pérez, L. S.; González-Aguilera, D. Efficiency Analysis of the Main Components of a Vertical Closed-Loop System in a Borehole Heat Exchanger. *Energies* 2017. <https://doi.org/10.3390/en10020201>.
- Sanner, B.; Dumas, P.; Fernandez, I.; Regueiro, M. Geotrained - A New European Initiative for Training and Education of Planners, Drillers and Installers. In *Proceedings World Geothermal Congress 2010*; 2010.
- Sanner, B.; Karytsas, C.; Mendrinos, D.; Rybach, L. Current Status of Ground Source Heat Pumps and Underground Thermal Energy Storage in Europe. *Geothermics* 2003. [https://doi.org/10.1016/S0375-6505\(03\)00060-9](https://doi.org/10.1016/S0375-6505(03)00060-9).

- Sharma, A.; Shukla, A.; Aye, L. Preface. *Green Energy and Technology. Low Carbon Energy Supply* 2018.
- SIA 384/6: Sondes Géothermiques. 2009, Svizzera
- UNI EN 15450: Progettazione degli impianti di riscaldamento a pompa di calore. 2008.
- UNI EN ISO 14040: Valutazione del ciclo di vita. Principi e quadro di riferimento. 2006.
- UNI TS 11300 part 1: Determinazione del fabbisogno di energia termica dell'edificio per la climatizzazione estiva ed invernale. 2008.
- UNI TS 11300 part 2: Determinazione del fabbisogno di energia primaria e dei rendimenti per la climatizzazione invernale e per la produzione di acqua calda sanitaria. 2008.
- UNI TS 11300 part 3: Determinazione del fabbisogno di energia primaria e dei rendimenti per la climatizzazione estiva. 2010.
- VDI 4640 part 1: Thermal use of Underground: fundamentals, approvals, environmental aspects. Aggiornamento. 2010, Germany.
- VDI 4640 part 2: Thermal use of Underground: ground source heat pump systems. 2001, Germany.
- VDI 4640 part 3: Utilization of the subsurface for thermal purposes: underground thermal energy storage. 2001, Germany.
- VDI 4640 part 4: Thermal Use of underground: direct uses. 2004, Germany.

5.3 Corrosion of metal ground heat exchangers and ancillary metal components

The study presented in this thesis is dedicated to exploring the possibility of using metal tubes to form more efficient, safer and cheaper geothermal heat exchangers. Despite the many advantages that metals such as structural carbon steel can guarantee, the risk of corrosion is a major drawback, as it can lead to leakage of heat transfer fluid into the underground, and thus causing environmental hazard. The following section provides insights into corrosion as a chemical phenomenon. Corrosion affects not only buried metal pipes, but also all the other metal components present in the geothermal field. Amongst these components: threaded connections, hydraulic components, and GHE heads.

5.3.1 Chemical risks due to leaks of heat transfer fluid

The use of de-icing mixtures makes it essential to assess the environmental risks due to the consequences of leaks. As long as the closed-loops circuit is intact, it can be argued that no leaks or contamination will occur, but this makes the permitting process very problematic, and regulators usually require to cement the borehole with grouting for additional protection. Leaks in the closed-loop systems must be avoided by all means since they can cause serious environmental problems in the event of the outflow of contaminating liquids from inside the pipeline into the aquifers. This crucial aspect must be addressed by taking special precautions to minimize the risk. One measure relates to the design of the GHE, which should be built for optimum sealing and longevity of the outer tube (Miller, 1980). The latter is based on the choice of a heat transfer fluid that minimizes the consequences in case of failure, or that does not favour corrosion of the pipe from the internal side. These aspects are extensively discussed in the following chapters of this thesis and represent the main challenge faced in this study. As for the choice of the heat transfer fluid, useful information is given below to frame the topic. Generally speaking, all heat-transfer fluids are usually water and certain substances dissolved in variable amounts (about 20-30%), which reduce the freezing temperature (table 9).

Table 9: Freezing point of some water-based mixture used as heat transfer fluids. Source: EU Geotrained GSHP – Manual for designers (2011).

Name	Percentage	Freezing point
Monoethylenglycol	25 %	-14 °C
Monoethylenglycol	33 %	-21 °C
Monopropylenglycol	25 %	-10 °C
Monopropylenglycol	33 %	-17 °C
Ethanol	25 %	-15 °C
Salt (brines)		
Potassium carbonate	25 %	-13 °C
Potassium carbonate	33 %	-20 °C
Calcium chloride	20 %	-18 °C

The ideal liquid would be: non-toxic non-flammable, chemically stable, compatible with the materials of other components of the system, with low environmental impact, non-corrosive, economical, with excellent heat exchange characteristics, and with low viscosity. Apparently, no fluid can meet all of these properties at the same time, thus over the years, many solutions have been tried to find the best compromise. Toxicity is a much felt issue for regulators, who usually encourage the use of plain water over other solutions. The toxicity of antifreeze should always be considered when installing GHEs in sensitive aquatic environments such as: lakes, surface water, aquifers. Heinonen proposed a methodology to select antifreeze based on a number of reference aspects. An example is given in table 10, where different anti-freeze solutions are assessed using the following score-system: 1 indicates a potential problem, 2 is intermediate, and 3 indicates little or no risk.

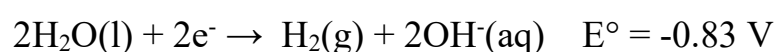
Table 10: Risk Factors for Antifreeze Assessment (Heinonen et al. , 1997), Ethylene Glycol Added by Basta and Minchio (2007)

	Methanol	Ethanol	propylene glycol	antifreeze potassium acetate	Calcium Magnesium Acetate	Urea	Ethylene glycol
Maintenance cost	3	3	2	2	2	2	3
Corrosion	2	2	3	2	2	1	3
Leakages	3	2	2	1	1	1	-
Health risks	1	2	3	3	3	3	2
Flammable	1	1	3	3	3	3	3
Environmental risks	2	2	3	2	2	3	2
Forbidden by regulations	1	2	3	2	2	2	2

It is worth noting that corrosion is considered a risk factor. It follows that the correct design of the GHE must take into account the possibility of internal corrosion caused by the heat transfer fluid, which is added to the corrosion on the external side of the pipe that is exposed to the underground environment.

5.3.2 Corrosion of metal components

The corrosion is the undesirable oxidation of a metal. Corrosion limits the lifetime of steel components. The replacement of corroded metal parts is indeed considered a major factor of cost in many industries (e.g. automotive, civil engineering, etc.). The corrosion is an electrochemical process, that can be recollect to the electrochemical series, which is also an indication for possible measures. The main factor in corrosion is the presence of water. This is the principal semi reaction involved:

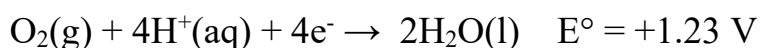


This standard E° is true for a concentration of OH^- equals to 1 mol L^{-1} , which corresponds to pH 14, i.e. an extremely alkaline solution.

When pH is equal to 7, Nernst's equation gives $E = -0.41 \text{ V}$. Therefore, every kind of metal with a standard potential minor than -0.41 V could reduce the water at $\text{pH} = 7$.

Since $E^\circ = -0.44 \text{ V}$ for $\text{Fe}^{2+}(\text{aq}) + 2\text{e}^- \rightarrow \text{Fe}(\text{s})$ at $\text{pH} = 7$, the Fe is not strongly affected by oxidation in water. That's the reason why is common to use such metal alloy to build pipes for water transportation, and many archaeological findings of iron have been preserved for centuries into anaerobic water environments.

But if iron is in an environment where water and oxygen are present at the same time, the semi reaction to be considered is the following:



At $\text{pH} = 7$, the potential of such reaction is $+0.82$, thus much higher than the one of the iron. In such conditions metal can reduce the oxygen of the watery solutions. In other words, when combined, water and oxygen can easily oxidate the Fe^{2+} .

As the reaction goes on, water and oxygen still oxidate the ions $\text{Fe}(\text{II})$ and $\text{Fe}(\text{III})$, because $\text{Fe}^{3+}(\text{aq}) + \text{e}^- \rightarrow \text{Fe}^{2+}(\text{aq})$ is $E^\circ = +0.77 \text{ V}$.

Information about the corrodibility of a metal in water solution can be retrieved by consulting the electrochemical series of standard potentials. The standard cell potential is the potential difference between the cathode and anode. The standard potentials are all measured at 298 K , 1 atm , and with 1 M solutions. When solving for the standard cell potential, the species oxidized and the species reduced must be identified. This can be done using an activity series. Table 11 shows the standard reduction potentials in decreasing order. The species at the top have a greater likelihood of being reduced while the ones at the bottom have a greater likelihood of being oxidized. Therefore, when a species at the top is coupled with a species at the bottom, the one at the top will become reduced while the one at the bottom will become oxidized.

Table 11: Standard reduction potentials

Reduction Half-Reaction	Standard Reduction Potential (V)
$\text{F}_2(\text{g}) + 2\text{e}^- \rightarrow 2\text{F}^-(\text{aq})$	+2.87
$\text{S}_2\text{O}_8^{2-}(\text{aq}) + 2\text{e}^- \rightarrow 2\text{SO}_4^{2-}(\text{aq})$	+2.01
$\text{O}_2(\text{g}) + 4\text{H}^+(\text{aq}) + 4\text{e}^- \rightarrow 2\text{H}_2\text{O}(\text{l})$	+1.23
$\text{Br}_2(\text{l}) + 2\text{e}^- \rightarrow 2\text{Br}^-(\text{aq})$	+1.09
$\text{Ag}^+(\text{aq}) + \text{e}^- \rightarrow \text{Ag}(\text{s})$	+0.80
$\text{Fe}^{3+}(\text{aq}) + \text{e}^- \rightarrow \text{Fe}^{2+}(\text{aq})$	+0.77
$\text{I}_2(\text{l}) + 2\text{e}^- \rightarrow 2\text{I}^-(\text{aq})$	+0.54
$\text{Cu}^{2+}(\text{aq}) + 2\text{e}^- \rightarrow \text{Cu}(\text{s})$	+0.34
$\text{Sn}^{4+}(\text{aq}) + 2\text{e}^- \rightarrow \text{Sn}^{2+}(\text{aq})$	+0.15
$\text{S}(\text{s}) + 2\text{H}^+(\text{aq}) + 2\text{e}^- \rightarrow \text{H}_2\text{S}(\text{g})$	+0.14
$2\text{H}^+(\text{aq}) + 2\text{e}^- \rightarrow \text{H}_2(\text{g})$	0.00
$\text{Sn}^{2+}(\text{aq}) + 2\text{e}^- \rightarrow \text{Sn}(\text{s})$	-0.14
$\text{V}^{3+}(\text{aq}) + \text{e}^- \rightarrow \text{V}^{2+}(\text{aq})$	-0.26
$\text{Fe}^{2+}(\text{aq}) + 2\text{e}^- \rightarrow \text{Fe}(\text{s})$	-0.44
$\text{Cr}^{3+}(\text{aq}) + 3\text{e}^- \rightarrow \text{Cr}(\text{s})$	-0.74
$\text{Zn}^{2+}(\text{aq}) + 2\text{e}^- \rightarrow \text{Zn}(\text{s})$	-0.76
$\text{Mn}^{2+}(\text{aq}) + 2\text{e}^- \rightarrow \text{Mn}(\text{s})$	-1.18
$\text{Na}^+(\text{aq}) + \text{e}^- \rightarrow \text{Na}(\text{s})$	-2.71
$\text{Li}^+(\text{aq}) + \text{e}^- \rightarrow \text{Li}(\text{s})$	-3.04

The most common corrosion mechanism of iron is shown in figure 12. When a water droplet is in contact with the surface of an iron component, it act as an electrolyte , thus generating a small electrochemical cell. On the edge of the droplet, the oxygen in solution oxidates the metal, according to the reaction previously described. Furthermore, the electrons which have been detached from the metal could be retrieved by a nearby part of the same metal, which is acting as a conductor. This typically happens beneath the central part of the droplet, where the oxygen is minimum. The atoms of Fe release their electrons, thus making ions Fe^{2+} , which are then dispersed into the surrounding water. This loss of ions generates small cavities on the surface of

the metal component. The Fe^{2+} is also oxidized to become Fe^{3+} , thanks to the oxygen in solution, and finally precipitates as Fe(III) hydrated. This $\text{Fe}_2\text{O}_3 \cdot \text{H}_2\text{O}$ is commonly known as “rust”.

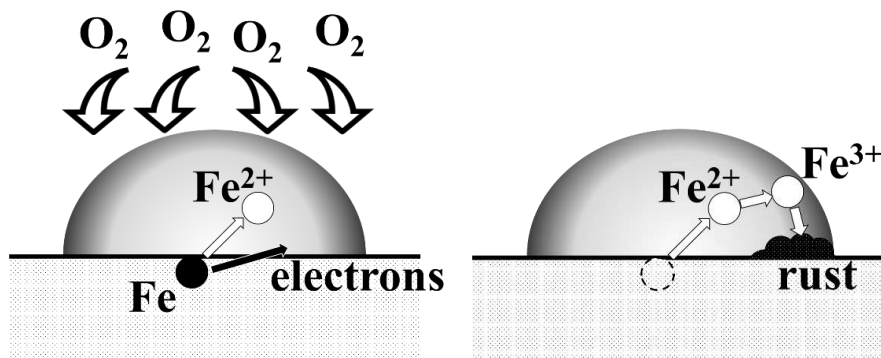


Figure 12: Corrosion mechanism of iron.

As the ions are formed, the water solution becomes even more conductive, thus accelerating the development of rust. A different form of corrosion occurs in absence of moisture at high temperatures when oxygen is present. This is known as “dry corrosion” and its general reaction is: $2\text{Me} + \text{O}_2 \rightarrow 2\text{MeO}$. Such phenomenon depends on the temperature and the kind of metal. It is not common at all for buried metal alloys, apart special situations such as fires or other thermal processes.

Passivating layer

Because of the boundary conditions such as the natural environments are complex and different from the ones used to calculate the standard potentials, and because are also generally changing in time (e.g. precipitating chemicals into the water solutions altering their concentrations, etc.), such tables have to be considered just indicative of the electrochemical behaviour of the metals. Moreover, such table does not take into account the formation of a passivating layer, which is an oxide film that can develop on the surface of some types of metals during the first stages of the corrosion process. This layer (0.3–5 nm thick) is homogeneous, unsolvable, and very adherent, thus making a barrier to further corrosive processes. The formation of the passivating layer occurs according to the following mechanism, which is depending on the kinetic of the reaction. During the oxidation, metal ions Me^{n+} are developed. If such process is fast enough, the concentration of ions on the surface of the metal component overcomes the process of solvation of a species of the metal scarcely solvable, such as an oxide or

a hydroxide, which precipitates cladding uniformly the surface and forming a passivating layer protecting the metal underneath. Metals who are easily corrodible, such as the ones with very negative E° , such as Cr, Ti, Al, are commonly found covered by this thick and uniform layer of oxide, thus sensibly improving the metals behaviours against corrosion in respect to the ones according to the electrochemical series. This is the basic principle that makes the galvanized steel (protected by Zinc oxide), the chromed steel (protected by cladded Cr) and stainless steels (Fe-alloy that contains Cr and other elements with very negative E°).

5.3.3 Types of corrosion

Corrosion that occurs on metal surfaces in contact with aggressive solutions can take many forms, depending on metallurgical and environmental factors.

Generalised

Generalised corrosion develops evenly on the whole metal surface exposed to corrosive conditions. This is the typical form of corrosion that affects metals in acid solutions, or not-passivated metals in natural environments such as open air, ground, and water.

Localised

Localised corrosion occurs on specific areas of the metal surface, often in the anodic areas where the metal dissolves, rather than the cathodic areas where the oxygen is reduced.

Pitting

Pitting corrosion is a very localized form of degradation, which can severely damage the stainless steel components in a short amount of time. It occurs on metals covered

by a passivating layer where aggressive ions such as chlorides interfere with the alloys ability to reform a passivating film. This corrosion proceeds at high pace after a slower start up phase where the aggressive ions attack the weaker spots on the passivating layer. Promoting factors are the concentration of ions, turbulent fluid flow, cavitation, pH, morphological unevenness on the surface such as fouling corrosion products, interstices, scratches, cracks, etc. One way to estimate the pitting resistance of stainless steels is through the Pitting Resistance Equivalent Number (PREN), which can be calculated from the chemical composition of the steel. The higher the value, the better the resistance. The formula used to calculate the PREN is not unique. Several multiplicative coefficients have been proposed. The most common form of the PREN formula is expressed as mass fractions (wt%):

$$\text{PREN}_{\text{wt}} = \text{Cr}_{\text{wt}\%} + 3.3 \cdot \text{Mo}_{\text{wt}\%} + 16 \cdot \text{N}_{\text{wt}\%}$$

There is no apparent influence of nickel for concentrations below 40%. PREN above 30 is supposed to be the bare minimum for resisting to marine pitting corrosion. (PREN of AISI 304 is in between 18 and 20, PREN of AISI 316 is in between 24.2 and 29.5). Very specific alloys such as Inconel® alloy 625 (PREN 46.4 – 56.0) or Hastelloy® alloy C-276 (PREN 64.0 – 73.8) or non-ferrous metals should be used in coastal environment but are not suitable for strictly cost-effective applications. On the right axis, in figure 13, the chlorine limit for a particular material is included to aid in the material selection decision. The scale is based on having a neutral pH, 35 °C flowing water (to prevent deposits from building up and cracking), which is common in many water treatment plants.

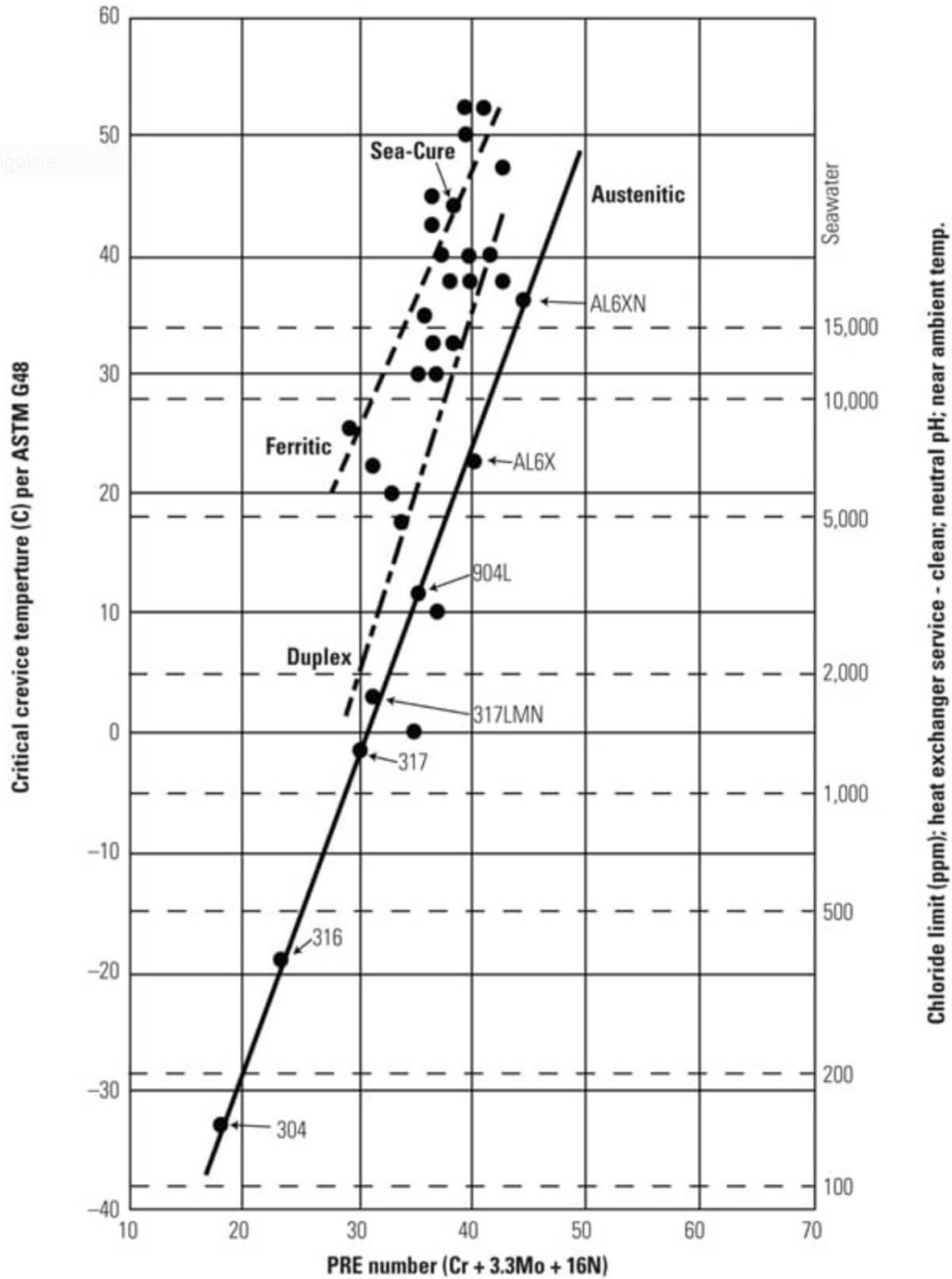


Figure 13. Critical crevice temperature and maximum chloride levels versus PREN of various stainless steels. Source: C.W. Kovach and J.D. Redmond, "Correlation Between the Critical Crevice Temperature 'Pre-Number' and Long-Term Crevice Corrosion Data for Stainless Steels," presented at the NACE Annual Conference Corrosion 93, New Orleans, La. (April 1993).

In GHE pipes, pitting corrosion is considered one of the most dangerous, due to the higher penetration rate that determines their end of life, as it causes pipe perforation locally and loss of heat transfer fluid in the environment.

Intergranular

Intergranular corrosion occurs on the edges of the grains of a metal alloy which has been sensitized as an effect of a thermal treatment. Such treatment can cause the precipitation of chemical phases on the edges of the grains, thus altering the properties of the alloy in these areas. This causes for instance that the centre of the grain is still passive, while its edges are in active condition.

Crevice

Crevice corrosion affects the areas of a component, which is covered by a passivating layer, where there is a very limited flow of electrolyte, for instance in the space gaps between two different surfaces. The metal surface area which is in contact with the part of the electrolyte with that has lack of oxygen acts as anodic, while the one in contact with the oxygenated part electrolyte acts as cathode. After a start up phase, the corrosion process proceeds fast in the interstitial area. Measures to reduce the crevice corrosion are: design and fabricate to avoid crevices, design and fabricate to avoid trapped and pooled liquids, weld with correct consumables and practices and inspect to check for inadvertent crevices, pickle to remove all weld scale.

Stress corrosion cracking

Stress corrosion cracking (SCC) can lead to the critical failure of a metal component and happens when there is a combined action of a mechanical stress and a corrosive environment, even if each of them would separately be not capable of causing any damage. Different metal alloys are differently susceptible to SCC depending on the specific chemical environment. For instance, copper-alloys suffer SCC in ammonia solutions; austenitic stainless steels in presence of chlorides (see chloride promoted stress corrosion cracking), ferritic steels in hydrogen sulphide. It happens that the combined action of the environment and the mechanical stress provokes a damage in the passivating layer covering the metal surface, thus forming a crack. The apex of the crack is more stressed and therefore it stays active, while the edges of the crack re-passivate again because they are not under mechanical stresses. When the temperature of the GHE tube fluctuates during heat pump operation over a 2-6°C for a few minutes

and up to 10-20°C when heat pump stops for about an hour, cyclic stress impacts GHE pipes, which can cause stress corrosion cracking.

Chloride promoted stress corrosion cracking

Chloride promoted stress corrosion cracking (CLSCC). It is a typical damage mechanism of the stainless steel component of the austenitic series that leads to the formation of cracks (Parrott and Pitts, 2011). It is a particularly insidious decay mechanism because the failure is usually not easily identifiable until the component is finally broken. CLSCC initiates from sites of localised pitting or crevice corrosion. CLSCC propagation occurs when cracks grow more quickly from the pit or crevice than the rate of corrosion. The initiation of CLSCC has been shown to involve a competition between localised corrosion, which is strongly dependent on chloride concentration but has a weak dependence on temperature, and crack growth which has a strong dependence on temperature but is relatively unaffected by chloride concentration and pH. Contributory factors include: the use of highly cold worked and/or free-machining grades, iron contamination of the surface, and the presence of a highly corrosive film containing chloride compounds.

Fatigue

Fatigue corrosion occurs when a cyclic stimulus is applied to the metal component and it generates a series of cracks which are normal to the direction of the applied force. This type of corrosion is unlikely to occur in geothermal ground heat exchangers as there are no moving parts during the operation, but can it arguably occur during pipe transportation or installation.

Galvanic

Galvanic corrosion happens when two metal of alloys of different nobility (i.e. different electrochemical potential) are in electrical connection by means of an electrolyte. This is called a galvanic couple: the less noble metal than acts as anode, and therefore the corrosion rate increases on its side. Meanwhile, the more noble metal

acts as cathode. There are factors influencing the galvanic corrosion, such as: the electrical conductivity, and the ratio between the connected areas (i.e. the anodic and the cathodic ones). The smaller the anodic area is, in comparison with the cathodic one, the greater the corrosive action will be, because it is concentrated in a relatively small area.

Selective

Selective corrosion is typical of polyphase alloys with remarkable differences in the chemical composition amongst each one of the phases. It happens that the corrosion affects the less noble phases, and the attack is corroborated by the galvanic coupling with the surrounding more noble phases.

Wear

Wear corrosion originates where two surfaces (no matter if they are made of the same metal or the same alloy, they can differ) are in contact under a load in an aggressive environment (Dalmau et al., 2018). It happens that the rate of corrosion increases, with respect to the same configuration under static conditions, due to the wearing out of the passivating layers from the metal surfaces. As for fatigue, wear corrosion is unlikely to occur in geothermal heat exchangers during operation.

Microbiologically Influenced Corrosion

Microbiologically Influenced Corrosion (MIC) can occur as an independent corrosion mechanism or in conjunction with other corrosion mechanisms. These characteristics present challenges to implementing effective corrosion management of systems in which MIC is an applicable threat. About a dozen of bacteria are known to cause microbiologically influenced corrosion of carbon steels and stainless steels in waters and grounds with pH between 4 and 9 and temperature ranged from 10 to 50°C. These bacteria can be generally classified as aerobic (requires oxygen to become active) or anaerobic (oxygen is toxic to the bacteria, or at least it reduces their activity as for *Desulfovibrio vulgaris*). Sulphate reducing bacteria (SRB, e.g. *Desulfovibrio*

caledoniens, *Geobacter sulfurreducens*, etc.) are anaerobic and are responsible for most instances of accelerated corrosion damages (Muyzer and Stams, 2008; Anandkumar et al., 2016; Guan et al., 2016) to steel structures in marine environments. Logical mechanism for corrosion caused by sulphate reducers was first provided by the classical theory of von Wolzogen Kuhr (1961), which proposed the following sequence of reactions as the mechanism of anaerobic bacterial:

Anodic reaction: $4\text{Fe} \rightarrow 4\text{Fe}^{2+} + 8\text{e}^{-}$

Dissociation/ionization of water: $8\text{H}_2\text{O} \rightarrow 8\text{H}^{+} + \text{OH}^{-}$

Cathodic reaction: $8\text{H}^{+} + 8\text{e}^{-} \rightarrow 8\text{H}$

Cathodic depolarization by SRB: $\text{SO}_4^{2-} + 8\text{H} \rightarrow \text{S}^{2-} + 4\text{H}_2\text{O}$

Corrosion products: $\text{Fe}^{2+} + \text{S}^{2-} \rightarrow \text{FeS}$; $3\text{Fe}^{2+} + 6\text{OH}^{-} \rightarrow 3\text{Fe}(\text{OH})_2$

Iron and manganese oxidizing bacteria are aerobic and are frequently associated with accelerated pitting attacks on stainless steels at welds. In underground pipeline industry MIC typically happens in water-saturated clay-type grounds of near-neutral pH with decaying organic matter and a source of SRB. Sea water is a primary source of sulphate reducing bacteria. The biological activities modify the local chemistry and making it more acid, thus corrosive to the steels.

Graphitization

Graphitization is a degradation of cast iron, and of some low carbon alloy steels. While in steel the iron dissolves in the electrolyte, leaving visible craters on the surface of the metal, in cast irons the ferrite corrosion products do not move away and remain mixed with graphite. Graphitized tubes often retain the look of those intact and an indication on the extent of the attack can be obtained only after the removal of the products of corrosion. These pipes make a dull sound when struck and can be easily engraved with a metal tip. In this situation the pipe can suddenly break even a low pressures, as a result of stresses such as, for example, road traffic or vibrations.

Stray currents

The stray currents constitute a phenomenon of dispersion of the electric current from metal-type conductors that normally carry current (typically the train tracks, as

represented in figure 14) but also electrochemical plants or cathodic protection facilities) to the ground.

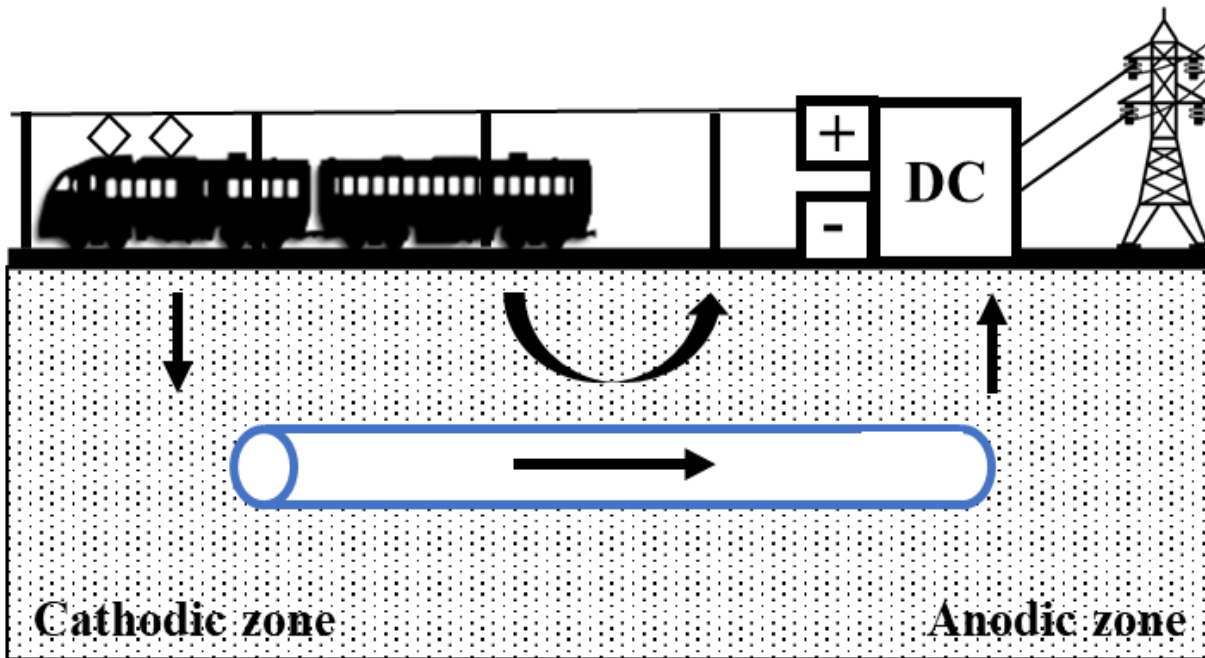


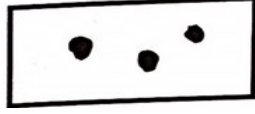
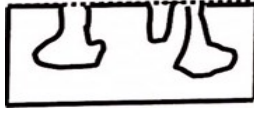
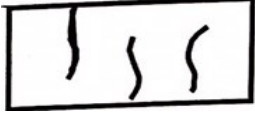



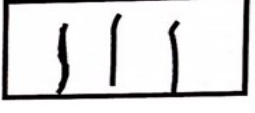

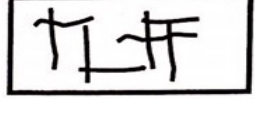

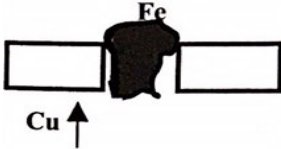
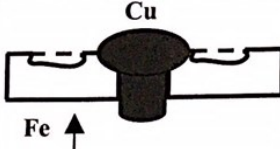
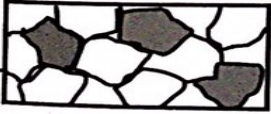
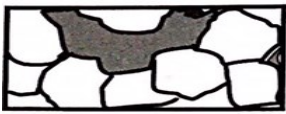
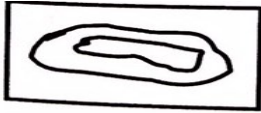



Figure 14: Stray current as effect of DC powered rail roads.

Electrolytic corrosion in the ground can be caused by stray currents of different origin such as fault currents which instead of returning to the negative of the battery or generator through the appropriate cables, re-enter with different paths or are dispersed in the ground through metal items. The currents involved can be high and the effects of corrosion are in that case faster and devastating. It should be remarked that only direct currents (DC) cause corrosion as they have direction through the electrolyte, from the anode to the cathode. Conversely, alternating currents (AC) cause no corrosion because they do not have an electronic constant direction. The latter is the reason why corrosion due to stray currents is not common (except for particular instances as the vicinity to a rail line). The common idea that unearthed AC electrical systems of buildings are related to corrosion due to stray currents is without foundation. Different types of corrosion have characteristic patterns (table 12) that allow them to be identified and, if necessary, to take appropriate measures.

Table 12: Common shapes of corrosion of metal components (M. Cavallini and R. Montanari 2003).

Corrosion type	Plan view	Section view
Generalised		
Pitting		
Intergranular		
Crevice		
SCC		
Fatigue		
Galvanic		
Selective		
Wear		

5.3.4 Corrosion in ground environment

Corrosion in ground depends on many factors because it represents a complex and mutating environment. Main factors are the content of solvated salts, humidity, dissolved gases, organic matter, microorganisms, and temperature. In particular, the content of water is extremely varying near the surface (due to evaporation, absorption by plants, rainfalls, etc.). Furthermore, underneath the water table, whose level changes due to meteorological, geological and hydrogeological factors, the pores are filled with water. Above such level, water can still be present due to capillary rise. Regarding the presence of oxygen, its diffusion in depth is limited and slow, such as that corrosion gradually decreases its impact with depth. Near the surface, where the oxygen is more abundant, it can happen that corrosion is still slowed by the lack of electrolytes, specially in case of grounds with high seepage. In general, the most favourable conditions for the corrosion are in the underground layers just above the phreatic zone, where all the required conditions for the corrosion are present. Ground management, due to agricultural activities such as plowing and harrowing, increases the ground aeration. Vice versa, the ground compaction after the passage of heavy machinery has a negative effect on the aeration. Two areas of the same ground with different content of oxygen could actually generate micro piles, thus developing the conditions for corrosion for different aeration. In grounds with scarce oxygenation the risk is represented by the sulphates because, if sulphur reducing bacteria are present, they can be transformed into hydrogen sulphide, which is highly aggressive. Furthermore, pH values of ground have an impact on corrosion, because the stable products of corrosion can act as protection only at certain pH values. A ground is commonly considered as aggressive when its pH is lower than 4 and above 8.5. The pH can change due to anthropic activities or other natural factors such as the plants metabolism.

5.3.5 An overview of the main corrosion mechanisms in buried Fe-alloys pipes

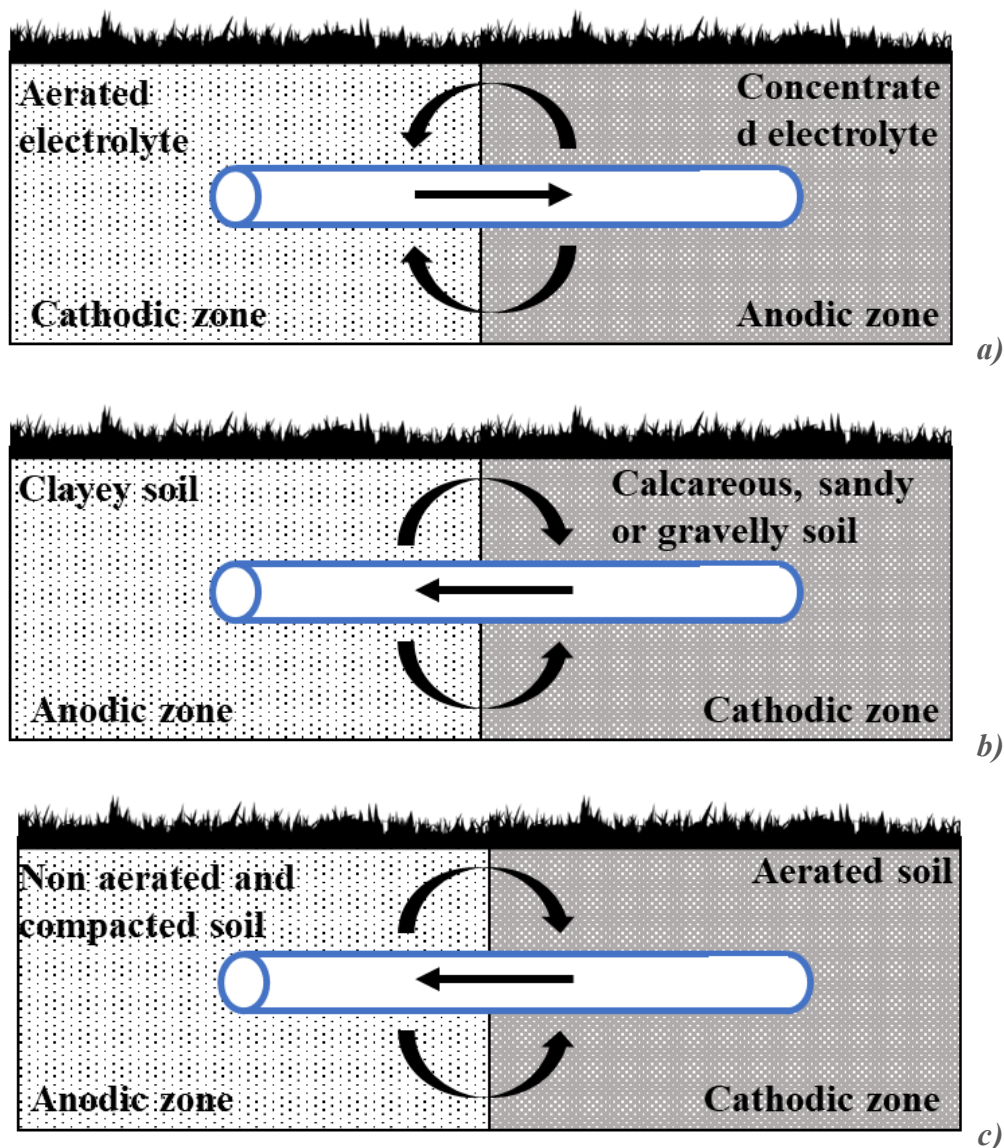
There are many factors concurring to determinate the corrosion rate of a buried metal component. The ground parameters which are directly or indirectly involved with this phenomenon will be discussed more in depth in the following chapter.

Evaluation of ground corrosibility

Oxidation of metal parts when buried in the ground is a serious problem in many areas, especially in underground tanks, pipes, or any activity that requires structural parts such as foundations and piles (Airapetov, 1986). Over time, many of the best design methods and techniques for assessing ground corrosiveness based on geology or chemistry have been proposed to avoid corrosive situations in metal structures (Beauregard and Mah, 2021). These are both qualitative and quantitative (Bonds et al., 2005). At the design stage of underground structures, it is important to understand ground behaviour related to corrosion potentials. Even if none of the proposed methods can predict the corrosion rate in detail, appropriate anticorrosion measures can provide valuable information for design decisions. On the other hand, the quantitative assessment of the corrosion process is still unreliable at the current state of the art, as the interaction of related factors is not always easy and therefore the overall system of components, ground and boundary conditions is very dynamic. This makes it very difficult to assess predictable interactions over time, especially given that the desired lifespan of such components and equipment is typically 30 years or more (Hähnlein, 2013). In short, while quantitative methods can explain the *de facto* situation fairly completely, unpredictable behaviour of the system over time can lead to very serious design errors. It can happen that the same metallic component corrodes in a very different way if it is exposed to different grounds at the same time, especially if the component is very large or extends over a long period of time or in the same direction, such as a pipeline. Therefore, sometimes no particular design can take into account all the different positive contexts faced by a component during its lifetime. Of the many existing standards, dealing with corrosion affecting buried steel components, the one proposed by US NIST is perhaps the most comprehensive. It was originally published in 1957 and includes an extensive database of metallic behaviours in ground. It is based on a quantitative and multivariable approach, so it is possible to optimize the design of buried metal components with a model that provides a quantitative approximation of the corrosion they will cause when passed in the ground. Ground is one of the most complex media and its physicochemical properties also make it one of the most corrosive media. Therefore, when a metal is buried in the ground, it must be considered that it will be exposed to corrosive environments, ranging from low to severe levels depending on the many parameters involved. One of the combined factors that complicates the process of ground corrosion is its inherent instability due to the constant development of the underground environment. The main factors affecting the corrosion rate and degradation mechanism of buried steel are electrochemical and depend on the properties of the underlying ground (Arriba-Rogriguez et al., 2018). These are presented in the following sections.

Texture of the ground

The grain size distribution, shape and mineral composition of the particles are the parameters that determine the texture of the ground. Essentially, ground can be described as a mixture of particles classified according to their size. The higher grade is clay (grain diameter <0.002 mm), followed by silt (particle diameter 0.0002 to 0.5 mm), and the coarsest sand (grain diameter > 0.05 mm). Other classifications subdivide each into heavy, medium, and fine. Most grounds can be described on the basis of these class/subclass relationships. In terms of corrosivity, the texture of the ground plays a role (figure 15), which is indirectly related to the water-binding capacity through the specific surface area of the grain. Therefore, the best structures are the most corrosive to buried steel components. In addition, the mineral composition has an effect on the final water content, in fact clay minerals can readily absorb water.



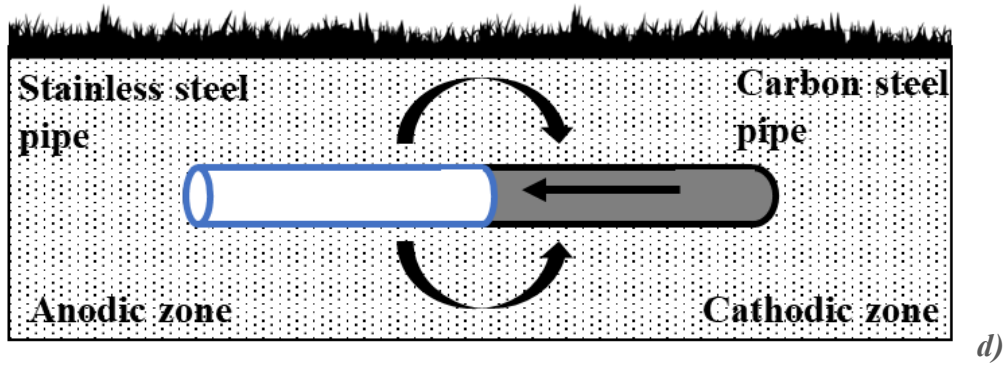


Figure 15: Corrosion of metal pipes in underground environments: electrolyte concentration discontinuity (a), ground texture inhomogeneity (b), differentiated aeration (c), metal couplings (d).

Presence of water

The presence of water is paramount in evaluating the corrosivity of the ground, because it is one of the necessary conditions that are required for developing the corrosion process. In fact, the mobility of ions and electrons from the anodic to the cathodic areas is possible only by means of an electrolyte. Actually, there is a direct correlation between the mass loss in steel tubes and the moisture content of grounds. Further studies showed the influence of water in determining the corrosion rate. Hence, all the parameters that are connected with water do have a crucial impact on the corrosivity of the ground. Parameters such as ground moisture, water holding capacity, groundwater level and its change over time and the transport of large volumes of water through the ground all have an indirect impact on corrosivity.

Aeration of the ground

Oxygen is a dominant factor in determining the corrosion in neutral or alkaline grounds. The concentration of dissolved oxygen in the underground waters, its concentration gradient and the gas permeability have a major impact on the rate of corrosion because of its participation in the cathodic reaction. Additionally, the drilling process, which varies depending of the installation method used to insert the GHEs into the ground, can oxygenate the otherwise undisturbed ground. For the same reasons, also excavation works can substantially increase the ground aeration and

subsequently they make it possible to introduce atmospheric oxygen into the ground. It is generally accepted that corrosion rate in disturbed grounds is significantly higher than that in grounds that have not been drilled or excavated. It should be noted that corrosion can also occur in the absence of oxygen, e.g. in the presence of certain bacteria that have a strong corrosive effect even under anaerobic conditions.

The oxygen diffusion in the ground

The transport of oxygen in undisturbed ground occurs mainly by diffusion, a process that depends on the physical properties of the ground such as texture, structure, porosity and water content (Neira, 2015). These factors affect the transport of oxygen in the most superficial layers (i.e., at a depth of about one meter above ground level) and O₂ is mainly due to the gas transfer mechanism with the atmosphere, not so much from other sources in the ground (e.g. roots and plants metabolism) (Wigham, 1973; Rose and Long, 1988). In the field of geothermal, this could affect the corrosion phenomenon of some components such as metal parts of the horizontal hydraulic connections, and as regards the vertical heat exchanger itself, the GHE head and metal joints. Molecular gas diffusion in grounds is controlled by the concentration gradient and the diffusion coefficient (Marshall and Holmes, 1980). Mathematically, the passage of any gas in the ground under steady state conditions occurs according to the following differential equation, which is Fick's first law:

$$J = \frac{Q}{At} = D_p \frac{\partial c}{\partial x}$$

where J is the flux of a given gas, Q is the mass (g), A is the area (m²), t is time, D_p is the diffusion coefficient of the gas in the ground, c is the concentration of the gas (g m⁻³) and x is the distance. The processes occurring in the ground are more complex than those modelled in Fick's First Law, as the flow of a gas in the ground changes over time; that is, no gas transport occurs under steady-state conditions. More complex models have been proposed to describe the movement of oxygen in the ground, applicable to transient conditions which also considers oxygen sources and sinks (e.g. plants and microorganisms):

$$\frac{\partial c}{\partial t} = D_p \frac{\partial^2 c}{\partial x^2} - S_g(Sx, t)$$

where c is gas concentration, t is time, x is distance and S_g represents the consumption and/or releases of oxygen due to different sources (microorganisms, roots, oxidation-reduction processes) and depends upon time and distance.

The ground gas diffusion coefficient D_p incorporates the effects of ground tortuosity and porosity; it is usually estimated by the following equation:

$$D_p = D_0 \tau \varepsilon$$

where D_0 is the diffusion coefficient of the gas in air ($\text{m}^2 \text{s}^{-1}$), ε is the ground air-filled porosity ($\text{m}^3 \text{air m}^{-3} \text{ground}$) and τ is the tortuosity of the ground. The ground porosity filled with air (ε) is a factor essentially controlled by the water-filled porosity and the total porosity, which is mainly dependent on the texture and structure of the ground.

Dissolved gases in underground waters and oxygen below the water table

The most abundant dissolved gases in underground waters are oxygen (O_2), carbon dioxide (CO_2), hydrogen sulphide (H_2S), hydrogen (H_2), methane (CH_4), heavy hydrocarbons, nitrogen (N_2) and noble gases (Klimentov, 1980). The gases present in underground waters are found either in solution or in the free state. Declining pressure may lead to the transformation of a dissolved gas into a free gas. The solubilities of gases in underground waters are also controlled by temperature. Usually, this parameter decreases with rising temperature. Oxygen is predominantly of atmospheric origin; an additional source is the photosynthesis in aquatic plants. Oxygen is present in underground waters in the form of dissolved molecules, whose concentrations range from 0 to 15 mg/l. Oxygen is mainly contained in the water found in the zone of aeration, groundwater, and relatively shallow water of artesian aquifers. However, in the recharge areas of artesian aquifer systems, as well as along the tectonic fractures in the piedmont and folded mountain regions, the oxygen contained in meteoric water percolates down to the great depths of hundreds of metres (Winograd and Robertson, 1982).

Carbon dioxide found in water as the carbonic acid gas is called free carbon dioxide. Similar to oxygen, it is absorbed by underground waters from the atmospheric air. In addition, it is generated by the biochemical and chemical processes taking place within the rocks composing the earth's crust, and also by volcanic activity and metamorphism. Underground water containing an over-equilibrium amount of free carbon dioxide is aggressive towards carbonate rocks, it is capable of leaching out rocks, concrete, and reinforced concrete, and hence of breaking them. Hydrogen sulphide in underground waters may be represented by the dissolved H_2S gas, hydrosulphide (HS^-), or sulphide ion (S^{2-}). Hydrogen sulphide accumulation in underground waters results mainly from the sulphate reduction produced by hydrocarbons in the course of anaerobic sulphate-reducing bacterial activity, or under high temperatures and pressures (thermometamorphism). The hydrogen sulphide contents of underground waters are usually less than 50 mg/l; it is only in the water from certain oil-and-gas fields that the hydrogen sulphide concentrations are as high as 1000-2000 mg/l. Hydrogen accumulates in underground water in the form of ions as a result of water dissociation, the decay of organic matter, and hydrolysis of heavy metal salts (iron, copper, aluminium sulphates and other sulphates) within the oxidized zones of sulphide ore deposits. In addition, free hydrogen is originated in areas of active volcanism. The hydrogen-ion concentrations vary within a wide range from 10^{-4} up to 10^{-9} . Methane and heavy hydrocarbons present in underground waters (Lundegard, 1964) are generated by the biochemical decay of organic matter taking place basically in prolific areas and coal basins, as well as in areas of swamps and peat lakes. The CH_4 content of underground waters can be as high as 50 cm^3/l . Nitrogen and noble gases (helium, neon, argon, krypton, and xenon) are inert. These gases, found in underground waters, may be of atmospheric, biogenic, or radiogenic origin. The O_2 has often been assumed to be absent below the water table because there is no interface with the atmosphere. There may be instead CO_2 which comes from the carbon cycle. The oxygen could come from the photosynthesis if the water contains algae, but this is unlikely. Instead this is true if we are considering water from an aquifer. If we considered water from an open well, there will be dissolved oxygen at the surface layer because of the interface with the atmosphere. The bottom layer may not have dissolved oxygen. That is why at the bottom of such water bodies, reduction processes prevail. Field and lab meters (e.g. by titration or electrode methods) to measure dissolved oxygen have been around for a long time. Modern meters are small and highly electronic. They still use a probe, which is located at the end of the cable. Dissolved oxygen is dependent on temperature (an inverse relation), so the meter must be calibrated properly before each use. Variable water vadose zone and/or disturbed ground due to drilling can produce respectively the H_2O and the O_2 (coming from the opening of the borehole) thus making possible the corrosion process at some extent.

Redox potential

Redox potential is basically an indicator of the degree of aeration of the ground, where a high redox potential implies a high level of O₂. The value of ground redox potential changes on the base of the amount of dissolved oxygen in the pore water. It also gives some indication on the conditions in which the reducing bacteria of the ground could produce sulphate. Vice versa, low and negative values of redox potential may suggest that such environment is proper for developing anaerobic bacteriological activity.

pH of the ground

In geoengineering, the pH of the ground is very important, since it has been observed that corrosion commonly occurs in acidic grounds, and it is common practice to state that such a substrate is at risk of much higher corrosion for buried steel structures (Karafyllias, 2016). In addition, alkaline grounds tend to have high concentrations of magnesium and calcium, often forming deposits on the subsurface with protective properties against corrosion. Even so, studies have confirmed that corrosion of buried steel occurs at any pH value. However, it seems that it is only at the limit (whether low or high value) that pH has a direct impact on the corrosion process. This means that between pH 4 and 8.5, this parameter is less relevant. This selective behaviour makes the assessment of ground pH very important for corrosivity information.

Electrical Resistivity

Corrosion is primarily an electrochemical process in which electrons and ions mobility is the main mechanism at the atomic level. Since this is actually the current flowing between the cathode and the anode, the electrical properties of the medium directly affect the entire process.

In particular, conductivity is directly proportional to the progress of corrosion. For this reason its reciprocal, resistivity has always been considered the most important variable to assess in the field of ground corrosiveness.

The electrical resistivity is the electrical resistance per unit length and per unit of cross-sectional area at a specified temperature. The SI unit of electrical resistivity is the ohm·metre ($\Omega\cdot\text{m}$, or more commonly $\Omega\cdot\text{cm}$ in the field of ground measurement) and it describes how difficult it is to make electrical current flow through a material. The higher is the electrical resistivity of the ground, the more difficult is the flow of ions and electrons participating to the corrosion reaction. As a result, grounds with low electrical resistance are more aggressive than grounds with low values, the latter being more suppressive. Electrical resistance is a function of water content and ion concentration. However, while this electrical property of the ground alone is not sufficient to determine the occurrence of corrosion in the ground, it does provide information on its kinetics.

Ions Content

Chlorides and sulphates are amongst the chemical species most linked to corrosion. Chloride ions participate directly in the reactions of anodic dissolution of metals. Chloride stress corrosion cracking (CLSCC) is one of the most common reasons why austenitic stainless steel pipework deteriorate in the petrochemical industries or in specific environments where such chemical is abundant.

In order to avoid the formation of biological grow in the geothermal systems, algacide containing Cl, such as Chloramine-T (N-Chloro 4-methylbenzenesulfonamide) are added to the heat transfer fluid flowing into the GHEs. The factor to consider is the amount of free Chlorine (Cl_2) which is a very effective oxidizer and therefore high levels of Chlorine may accelerate chloride corrosion of stainless steels.

The process starts within localized pits on the surface of metals coated with the passivating layer. Anodic reaction inside the pit is: $\text{Fe} \rightarrow \text{Fe}^{2+} + 2\text{e}^-$ (dissolution of iron). The electrons given up by the anode flow to the cathode where they are discharged in the cathodic reaction: $1/2\text{O}_2 + \text{H}_2\text{O} + 2\text{e}^- \rightarrow 2(\text{OH}^-)$. As a result of these reactions the electrolyte enclosed in the pit gains positive electrical charge in contrast to the electrolyte surrounding the pit, which becomes negatively charged. The positively charged pit attracts negative ions of chlorine Cl^- increasing acidity of the electrolyte according to the reaction: $\text{FeCl}_2 + 2\text{H}_2\text{O} \rightarrow \text{Fe}(\text{OH})_2 + 2\text{HCl}$. The pH of the electrolyte inside the pit drops from 6 to 2-3, which causes further acceleration of corrosion process. Large ratio between the anode and cathode areas favours the increase of the corrosion rate. Corrosion products $\text{Fe}(\text{OH})_3$ form around the pit resulting in further separation of its electrolyte.

Steel grades AISI 304 and 304L, 321 SST may be used for water applications with up to 2 ppm chlorine, while 316 and 316L alloys may withstand up to 4 ppm. Therefore, as a source of possible CLSCC, the susceptible stainless steel grades AISI 304 and AISI 316 should be avoided if such additives are used.

Furthermore, the presence of chloride ions tends to decrease the resistivity of the ground. Chlorides can be found in grounds naturally or they can come from external sources, such as sprinkling road salt in winter. The concentration of chloride ions is subject to significant variations depending on the degree of ground moisture. Although the corrosive effect produced by sulphate ions on metals is lower than that of chlorides, its risk increases with the possibility that sulphates become highly corrosive sulphides due to the activity of anaerobic bacteria which can lead to sulphate reduction.

Bacteria

Corrosion can occur also due to microbial activity. The properties of organic matter and the carbonate content that the ground exhibits are important in the corrosion of steel. This can occur in humus-rich clays, which are very cohesive and inhibit the formation of an anti-corrosion passivation layer on the surface of metal components. There have been cases of extremely fast rates of corrosion due to microbial activity, and it is increasingly clear that most steel alloys are susceptible to this type of corrosion. Some studies have shown that microbiological corrosion is one of the causes of failure of underground pipelines. Quantitatively, more than 20% of tube failures are related to microorganisms. Due to the importance of microorganisms in corrosion, the term inoculated corrosion (referring to MIC) has emerged, which refers to corrosion that is initiated and or increased by microbial activities. The first case of MIC was identified in 1934, in which sulphate-reducing bacteria collapsed cast iron pipes buried in anaerobic ground. There is no certain test or accepted standardized methodology that can be applied to directly relate the MIC as a probable cause, it is usually determined by a process of factual inference and other mechanisms are excluded.

Organic matters and microorganisms in underground waters

The studies of organic compounds and microorganisms present in underground waters have always been connected with the quality evaluations of fresh water used to provide water supplies, as well as with the chemical analyses of groundwater associating with

oil and gas fields (El-Sherik, 2017). At present, the following groundwater constituents are under examination: humic acids, bitumen, phenols, fatty acids, naphthenates, as well as the concentrations of organic carbon, organic nitrogen and other species.

The sources of organic matter contained in underground waters are the precipitation, surface waters, ground, sea waters and sea ooze, rocks, and accumulations of oil, coal, and peat. Organic matter present in underground waters usually comes from external sources, but it may also originate within the earth's crust itself. The total amount of organic matter in water is determined either from oxidability values or from the total organic carbon (in non-volatile, volatile neutral, and volatile basic components, and volatile acids). Oxidability is an amount of oxygen required to oxidize the organic matter. One mg of oxygen is assumed to be equivalent to 21 mg of organic matter. In areas where the infiltration (atmospheric, river) of water from the surface is taking place, the organic compounds of animal origin are commonly found together with the products of decay of meadow and forest vegetation. Microorganisms found in underground waters are represented by various bacteria, usually unicellular, but sometimes multicellular as well. The probable limit for their distribution within the under-exceeding 100°C. Generally, this depth is 4 to 5 km below the earth's surface.

Other natural environments

There are components not closely related to buried pipes, but that are still ancillary parts of GHEs or accessories in the geothermal field. For instance, metal thread connections, manifold parts, valves, GHE heads. Although such parts are not buried, they are metal, and therefore are prone to corrosion when exposed to the atmosphere.

Atmosphere corrosion

Atmospheric corrosion is usually a generalized type of corrosion, even if under specific conditions it can cause local attacks. It starts when an electrolyte is in contact with a metal component exposed to the atmosphere. Typically the water is represented by rain or dew. The aggressivity of the atmosphere is increased by pollutants, such as sulphur oxides, that is relatable to urban areas; also solid particulate can compete for corrosion. The carbonaceous particles are accountable for dew phenomena and for SO₂ absorption. Even the hygroscopic salts can promote dew. For instance, chloride ions, which are very present in the costal areas, strongly increase the corrosion at high values of relative humidity (<70%). Concluding, the atmospheric corrosion is associated to (i)

factors related to the material (type of metal or alloy, structural conditions, type of products of corrosion), (ii) environmental factors (relative humidity, composition of the atmosphere, urban, marine, industrial, rural, etc.), (iii) factors related to the exposure of the component (indoor, outdoor, windy conditions, height from the ground, vertical, horizontal positions, placement in a niche, etc.).

Atmospheric corrosion always takes place with a lower intensity than the intensity it would have in case other corrosive phenomena developing on structures placed in the ground or immersed in waters; nevertheless, given the enormous spread of metal works exposed to the atmosphere, it assumes great economic importance both as regards industrial plants and for civil works (bridges, means of transport, metal poles, etc.). Of course, the essential condition for this corrosion to occur is that it forms on metal material a layer of moisture; this may be visible, but more often it is consisting of a very thin invisible film, while sometimes the humidity condenses in anfractuosity or pores and the liquid is therefore hidden from an external examination.

The European standard CEN 12500: 1998, entitled "Protection of metallic materials against corrosion - Probability of corrosion in ambient atmosphere - Classification, determination and estimation of the corrosivity of atmospheric environments", classifies environments according to four different categories with increasing corrosivity. Essentially they can be traced to the following types:

- Indoor environments: in these conditions of controlled temperature and humidity the metal is subjected to the minimum risk of corrosion; some metals can burnish or corrode after contact with frequently used detergents for glass or stone (acid muriatic acids or other weak acids), even if only in the form of fumes or vapours. Rural atmospheres: corrosion progresses quite slowly; some dangers can they come from the presence of fertilizers that settle on aggressive alkaline films.
- Arid climates: in dry, desert or semi-desert environments, as well as in climatic zones particularly rigid, corrosion cannot advance rapidly. If temperature is very high, the most likely form of degradation will be related to stresses resulting from differential thermal expansions. In case of frequent presence of strong wind, the transport of abrasive particles (sand) can cause serious erosion damage. An eroded surface, characterized by high roughness and therefore by high exposed surface, however, is more sensitive to corrosive attack (Allen et al., 1981).
- Coastal areas: in structures in direct contact with sea water, or in affected areas no matter how strong the presence of marine aerosols, the agent of greatest danger it is salt, and more particularly chloride ion. Salt, accumulated in pores and interstices and concentrated in the veil of moisture that covers the metal surface, causes severe localized attacks on all metals, that tend to protect themselves with the formation of a superficial patina. In this case the corroded

surface appears covered by small craters, more or less deep depending on the intensity of the attack. However, the strongly conductive solution contributes to create localized polarization phenomena on the metal surface, between the different grains of a metal or between the different constituents of an alloy, thus speeding up the process corrosive.

- Urban or industrial atmospheres: they constitute the potentially most dangerous exhibition to corrosive atmosphere. The most aggressive agent in highly urbanized environments or industrialized is sulphur dioxide (SO_2), which in the presence of oxygen and moisture is oxidized to sulfuric anhydride (SO_3) and partially transforms itself into sulfuric acid (H_2SO_4), which is very corrosive. Also chlorine, hydrochloric acid, hydrogen sulphide, and compounds can be so generated. Ammonia, can exert an aggressive action too.

Atmospheric corrosivity classes

For the purposes of ISO 12944, atmospheric environments are classified into six classes of atmospheric corrosivity:

- C1 very low
- C2 low
- C3 average
- C4 high
- C5-I very high (industrial)
- C5-M very high (marine)

Virtually, all oxides tend to limit the corrosive attack, but the extension of the phenomenon and especially the time in which the status of sufficient protection is reached are extremely variable. Also the same metal can behave very differently when exposed to environments with different conditions. Very important is also the exposure of the structures as well as the frequency of rains or sunny periods. Even in a moderately corrosive environment, it happens that if the electrolyte has had the possibility of stalling on the metal surface or because it is always in the shade or due to the fact that it is not subject to washing by rain, the action of aggressive agents can develop more and more vehemently. In environments subjected to contamination and in presence of humidity, the absorption of sulphur dioxide, which by the action of oxygen in the air causes the formation of sulfuric acid, very aggressive with many

metals. The sun has a beneficial effect since when drying the metallic surfaces it eliminates the electrolyte.

In an urban setting, the chosen period of the year is also an important factor when considering the installation of the material. The season, in fact, affects the protective property and it can therefore happen that the same metal, exposed for the first time in December or in June suffers attacks of considerably different intensity over time. This is due to the presence in the atmosphere during winter months of much larger amounts of pollutants, especially sulphur dioxide, deriving from combustion made for domestic heating. The use of methane has significantly reduced this risk.

In the marine environment, the presence of tiny droplets containing sodium chloride, blown into the air by winds, can greatly accelerate corrosive phenomena and cause pitting even in metals or alloys that are normally resistant to attack atmospheric corrosive.

Suspended particulate

The amount and type of solid particles found in the air influence noticeably atmospheric corrosion. If the city air can normally hold 2 mg/m^3 of dust, in an industrial environment it reaches up to 1 kg/m^3 and more of particles. The importance assumed by the presence of these particulate was highlighted by experimental tests carried out with steel specimens exposed freely to the atmosphere and with others in the same atmosphere but protected by a filter cloth cage; while the first have suffered considerable corrosion, the latter have been almost not affected. If the particles are hygroscopic, they have a doubly harmful function as they also facilitate the formation of the electrolyte; so in the urban environment, sulphate of ammonium in the industrial environment and sodium chloride in the marine atmosphere are the most common harmful particles (Dera, 1992).

Gas

Contrary to what was supposed in the past, carbon dioxide does not absolutely cause corrosion; due to its small concentration in the air. Sometimes gases work against corrosion, positively affecting the formation of protective compounds, for example for zinc. The most harmful gas in atmosphere is undoubtedly sulphur dioxide, which is

very widespread in industrial cities, especially in the winter months. Iron, zinc and cadmium are seriously attacked by the mentioned gas; lead, aluminium and copper are instead, slightly corroded.

Humidity

In theory, if there are absolutely no pollutants in the air below the 100% relative humidity, there should be no corrosion; in fact, even in very humid environments, as long as the air is clean, as in a tropical jungle, the attack is insignificant. However, the inevitable fluctuations in temperature and the presence of hygroscopic particles concur to ensure that this limit is lowered significantly. However, there is a relative humidity threshold, even in the presence of 0.01% sulphur dioxide, valid for ferrous materials, below which there is no appreciable corrosion.

Water

Corrosion in water mainly depends on temperature, pH, content of O₂, concentration of solvated ions (ions calcium, ions sulphate, ions chlorine, etc.) and presence of microorganisms. A particularly aggressive environment is sea water, because its high content of chlorides would promote pitting corrosion.

Internal corrosion

Metal pipes can corrode even on the inner side. However, due to the limited presence of oxygen, the inner wall of pipes is usually less corroded than on the outside. Nevertheless, corrosion can occur, which is mainly related to the chemistry of the heat transfer fluid. A known problem is the effect of chloride, which is rarely used as an antifungal agent. The following are suggested characteristics of the fluid that should minimize the occurrence of internal corrosion, and the related mitigating measures (tables 13 and 14).

Table 13: Requirements for the extracted water for open-loop systems (UNI EN 15450:2008)

Components	Value	Unit
Organic matters	Absent	-
pH value	6.5 – 9	-
Electrical conductivity	50 – 1000	$\mu\text{S}\cdot\text{cm}^{-1}$
Chloride	< 300	$\text{mg}\cdot\text{l}^{-1}$
Iron and Manganese	< 1	$\text{mg}\cdot\text{l}^{-1}$
Sulphate	< 2	$\text{mg}\cdot\text{l}^{-1}$
O₂ content	< 2	$\text{mg}\cdot\text{l}^{-1}$
Chlorine	0 – 5	$\text{mg}\cdot\text{l}^{-1}$
nitrate	0 - 100	$\text{mg}\cdot\text{l}^{-1}$

Table 14: Considerations on the chemical characteristics of water in open-loop systems (Basta e Minchio 2007; Rafferty 2001)

Parameter	Range	Interaction with materials	Mitigating measures
pH	5.5 - 8.5	Acid pH catalyse the corrosion of metals, alkaline pH promote fouling	Avoid to use open water basins, use compatible steels
Suspended solids	200 - 1000 ppm	increase the deposit possibility, especially if Magnesium, Calcium, carbonates, or solvates are present.	If concentration > 500 ppm perform analysis of ions, Mg, Ca, CO ₃ , SO ₄
Iron	0 – 5 ppm	Can indicate the presence of iron bacteria	Perform analysis

Ryznard index		Index describing the fouling/corrosion rate based on CaCO_3	pH > 7.5 prone to corrosion (use adequate materials); pH < 6.0 prone to fouling (reduce water flow)
Chlorine	6 – 20 ppm	Catalyse the corrosion of steel, produces micro cavities.	Use adequate materials
bicarbonate/ CO₂			If $\text{HCO}_3^- > 100$ ppm and pH > 8.0, keep the fluid pressure high to limit the chemical equilibrium
Hydrogen sulphide	< 0.5 ppm	Aggressive for Cu, Ni and their alloys	If $\text{H}_2\text{S} > 0.2$ ppm avoid components made of Cu and Ni
Oxygen	< 2.0 ppm	Accelerate the corrosion of steel	Degassing
Sand content	< 1 ppm for bore discharge, 5 – 10 for surface discharge	Abrasion of components, depletion of the aquifer causing possible subsidence	Size the filter correctly

Of course, taking the proper preventive measures does not rule out the possibility of corrosion or damage. Therefore, you need to make sure that this device is easy to connect and deploy for easy access for maintenance and replacement.

- Installing a removable filter in front of the exchanger can reduce chemical or biological deposits, by maintaining a high pressure inside the groundwater circuit to avoid CO_2 degassing inside the exchanger;
- preventing groundwater from coming in contact with atmospheric oxygen (for example by favouring the installation of closed systems);
- adding small quantities of biocidal chemicals or reducing chemical substances, to respectively prevent the formation of biofilm and the oxidation of iron;

- washing the ground heat exchanger with acid or with detergents or reagents to remove the accumulation of calcite and/or manganese and/or iron hydroxide deposits.

5.3.6 References

- Airapetov, D. Architectural Materials Science. Mir Publisher 1986.
- Allen, C.; Ball, A.; Protheroe, B. E. The Abrasive-Corrosive Wear of Stainless Steels. *Wear* 1981. [https://doi.org/10.1016/0043-1648\(81\)90169-1](https://doi.org/10.1016/0043-1648(81)90169-1).
- Anandkumar, B.; George, R. P.; Maruthamuthu, S.; Parvathavarthini, N.; Mudali, U. K. Corrosion Characteristics of Sulfate-Reducing Bacteria (SRB) and the Role of Molecular Biology in SRB Studies: An Overview. *Corrosion Reviews*. 2016. <https://doi.org/10.1515/correv-2015-0055>.
- Arriba-Rodriguez, L. De; Villanueva-Balsera, J.; Ortega-Fernandez, F.; Rodriguez-Perez, F. Methods to Evaluate Corrosion in Buried Steel Structures: A Review. *Metals*. 2018. <https://doi.org/10.3390/met8050334>.
- Basta S. & Minchio F. 2007. Geotermia e pompe di calore, Hoepli Italia.
- Beauregard, Y.; Mah, A. Assessing Soil Corrosivity for Buried Structural Steel. In Proceedings of the Biennial International Pipeline Conference, IPC; 2020. <https://doi.org/10.1115/IPC2020-9285>.
- Bonds, R. W.; Barnard, L. M.; Horton, A. M.; Oliver, G. L. Corrosion and Corrosion Control of Iron Pipe: 75 Years of Research. *J. / Am. Water Work. Assoc.* 2005. <https://doi.org/10.1002/j.1551-8833.2005.tb10915.x>.
- Cavallini R., Montanari M. La metallografia nei beni culturali. 2003. Collana tecnica AIM.
- Dalmau, A.; Richard, C.; Igual – Muñoz, A. Degradation Mechanisms in Martensitic Stainless Steels: Wear, Corrosion and Tribocorrosion Appraisal. *Tribol. Int.* 2018. <https://doi.org/10.1016/j.triboint.2018.01.036>.
- DeBerry, D. W.; Ellis, F. F.; Thomas, C. C. Materials Selection Guidelines for Geothermal Power Systems. First Edition. 1978.
- Dera, J. Marine Physics. *Mar. Phys.* 1992. [https://doi.org/10.1016/0377-0265\(94\)90009-4](https://doi.org/10.1016/0377-0265(94)90009-4).

- El-Sherik, A. M. Trends in Oil and Gas Corrosion Research and Technologies: Production and Transmission; 2017.
- Guan, F.; Zhai, X.; Duan, J.; Zhang, M.; Hou, B. Influence of Sulfate-Reducing Bacteria on the Corrosion Behavior of High Strength Steel Eq70 under Cathodic Polarization. PLoS One 2016. <https://doi.org/10.1371/journal.pone.0162315>.
- Hähnlein, S.; Bayer, P.; Ferguson, G.; Blum, P. Sustainability and Policy for the Thermal Use of Shallow Geothermal Energy. Energy Policy 2013. <https://doi.org/10.1016/j.enpol.2013.04.040>.
- ISO 12944-5:2018 - Protective paint systems.
- ISO 8044:2020. Corrosion of metals and alloys — Vocabulary.
- Karafyllias, G.; Galloway, A.; Humphries, E. The Effect of Low PH in Erosion-Corrosion Resistance of High Chromium Cast Irons and Stainless Steels. Wear 2019. <https://doi.org/10.1016/j.wear.2018.11.021>.
- Klimentov, P. P. General hydrogeology. 1983. Mir Publishers; Rev. from the 1980 Russian ed edition.
- Lundegard, P. D. Methane. In Environmental Forensics: Contaminant Specific Guide; 1964. <https://doi.org/10.1016/B978-012507751-4/50028-8>.
- Marshall, T. J.; Holmes, J. W. Soil Physics. Soil Phys. 1980.
- McCorry, M.; Jones, G. L. Geotrained Training Manual for Designers of Shallow Geothermal Systems; 2011.
- Miller, R. L. Corrosion and materials selection for geothermal systems. In Proceedings of the Intersociety Energy Conversion Engineering Conference; 1980.
- Muyzer, G.; Stams, A. J. M. The Ecology and Biotechnology of Sulphate-Reducing Bacteria. Nature Reviews Microbiology. 2008. <https://doi.org/10.1038/nrmicro1892>.
- Neira, J.; Ortiz, M.; Morales, L.; Acevedo, E. Oxygen Diffusion in Soils: Understanding the Factors and Processes Needed for Modeling. Chilean Journal of Agricultural Research. 2015. <https://doi.org/10.4067/S0718-58392015000300005>.
- Parrott, R.; Pitts, H. Chloride Stress Corrosion Cracking in Austenitic Stainless Steel. Crown 2011.

- Rafferty, K.D., 2001, Design aspects of commercial open-loop heat pump systems. *GHC Bulletin*, 22, 16–24
- Rose, S.; Long, A. Monitoring Dissolved Oxygen in Ground Water: Some Basic Considerations. *Groundw. Monit. Remediat.* 1988. <https://doi.org/10.1111/j.1745-6592.1988.tb00981.x>.
- Vallejo Vitaller, A.; Angst, U. M.; Elsener, B. Laboratory Tests Simulating Corrosion in Geothermal Power Plants: Influence of Service Conditions. *Geotherm. Energy* 2020. <https://doi.org/10.1186/s40517-020-00163-y>.
- von Wolzogen Kuhr, C. A. H. Unity of Anaerobic and Aerobic Iron Corrosion Process in the Soil. *Corrosion* 1961. <https://doi.org/10.5006/0010-9312-17.6.119>.
- Wigham, J. M.. *Soil Physics* . L. D. Baver . J. Geol. 4th ed.1973.
- Winograd, I. J.; Robertson, F. N. Deep Oxygenated Ground Water: Anomaly or Common Occurrence? *Science* (80-.). 1982. <https://doi.org/10.1126/science.216.4551.1227>.

6 Anti-corrosion measures

Since the research is aimed on focusing on steel pipes as principal materials for efficient and cost-effective ground heat exchangers, it is mandatory to guarantee the protection against corrosion to assure safety and cost effectiveness at the same time. The following section offers a critic overview of selected anti-corrosion measures that can be applied to GHEs. Most of them are already implemented in other fields such as piling or engineering of buried manufacts and have therefore been evaluated in relation to their application to shallow geothermal systems.

6.1.1 Passive and active anti-corrosion measures for buried steel pipes

In many fields, such as plumbing or the installation of electricity poles, there are methods and standards to limit the occurrence of corrosion in underground pipes or similar metal artifacts. These anti-corrosion measures include both active and passive solutions. Since reducing the overall costs of installing shallow geothermal is a major concern, the design choice has to take into account the running costs to keep the protection on during the provisioned life-time of the system.

Passive protection

Passive protection is used to mechanically insulate the metal surface of pipes from the surrounding environment by means of coatings. Measures of this type also include softening and degassing of the water. Such operations are made, respectively, to avoid corrosion due to differential ventilation of the encrusted support part with respect to the rest of metal surface (e.g. the inner surface of the steel pipes) and the causes of direct corrosion (i.e. the oxygen). In any case, it is possible to preserve the metal structures from external aggressions by means of protective coatings, as they can be both external and internal.

In order to avoid contact with the environment, which can cause corrosion, metal surfaces can be painted, covered with plastic sheeting, enamelled or clad with metals. In general, the most effective coatings have good properties of adhesion to the substrate, permeability, resistance to abrasion and chemical corrosion, toughness and flexibility. The paint can be spread with the brush or, more and more often, by spraying

it on. The metal surfaces had to be before cleaned mechanically or chemically. Mechanical cleaning consists of abrasion with steel brushes, rotating discs and by sandblasting mostly with quartz elements.

The chemical method, called pickling, is carried out after mechanical cleaning and is done with the use of chemical reagents, generally acidic, in order to remove oxide and salt deposits.

The enamels use mixtures of mineral type or obtained from synthetic resins.

The most commonly used external protective coatings are:

- three-layers polyethylene - 3LPE (according to UNI 9099) and cold-applied self-adhesive tapes (according to EN 12068);
- bitumen (according to UNI 5256) and polyurethane (according to UNI 10290);
- polypropylene in 3 layers - 3LPP (according to DIN 30678);
- fusion bonded epoxy coating (FBE) (according to DIN 30671);
- in the case of subsea pipelines, to avoid that the buoyancy thrust it is customary to weigh it down with the application of an external coating in meshed concrete, generally gunite (sprayed concrete) coating is utilised. The external gunning is applied to the others external coating of the pipes (bituminous, polyethylene coating, etc.).

Typical piping interior coatings consist of:

- epoxy paints or
- bituminous primer (for non drinkable water).

These protective films of polymeric/bituminous origin are applied over the entire length of the material or only in points subject to corrosion. Before applying the coatings, pipes have to be prepared. The preparation of the surface to be coated must include the removal, by sandblasting with a siliceous or metallic abrasive, of rust, calamine and other foreign and poorly adherent particles, until an almost white metal is obtained, i.e. until 95% of the surface is free from any visible residue (degree of sandblasting type Sa 2½ - according to ISO 8501-1: 2007).

Immediately after the preparation of the surface, the adhesion layer (primer) is applied according to the methods provided by the UNI ISO 5256 standard.

The average thickness of the primer layer must be such that complete coverage of the metal surface is ensured and that in no point of the surface itself there is a primer thickness lower than 500 µm.

Other passive anti-corrosion measures are:

- passivating layers, i.e. the oxidation products obtained e.g. by natural anodic oxidation of metals such as Al, Ni or Co. The oxides of these materials are very tough and adherent to the surface layer, insulating them from the environment;
- metals such as Cr or alumina could be applied by plating/cladding the pipes;
- the cementation of the annular space surrounding the GHE pipes makes it resistant to the appearance of corrosion as it mechanically isolates the metal from the underground environment. This solution is recommended or required at the regulatory level. However, grouting for corrosion protection may not be successful due to cracks or poor coverage. When installed, the GHE almost always does fit straight or is centred correctly along its full length. This puts the pipe in direct contact with the ground in some areas even when grout is used to fill the gaps in the borehole.

Protection by insulation between different metals

When two different metals, far apart in the galvanic series, are placed in direct contact in wet areas and their potential difference is greater than 200 mV, corrosion of the metal occurs on the less electronegative one.

A solution to this problem is to interpose a dielectric element between the two materials. The passage of charges and, consequently, corrosion is prevented by electrically isolating the metals from each other with flanges and washers of plastic or insulating fibre or by means of insulating pipe sections. This type of insulation can be found especially in steel hydraulic pipes, to insulate any copper components or accessories. It is important to keep metals dry and/or protected from ionic compounds (salts, acids and bases), e.g. by encapsulating them inside plastic shells or epoxy resin.

Protection by galvanic chain

An immediate way to predict if a material in contact with a certain substance is subject to corrosion consists in the use of "corrosion tables", which indicate some combinations material-electrolyte and for each of these combinations indicate whether the material is corrodible or not.

Tables can be used at an early stage of the design to choose the most suitable material for a specific application within a narrow selection of materials. If it is not possible to

avoid the use of a pair of metal materials that are compatible with each other, the galvanic chain can be extended by introducing a third metal, of intermediate nobility making up the couple.

Anodic coatings

Galvanizing generally refers to hot-dip galvanizing which is a way of coating steel with a layer of metallic zinc or tin. Galvanized coatings are quite durable in most environments because they combine the barrier properties of a coating with some of the benefits of cathodic protection. If the zinc coating is scratched or otherwise locally damaged and steel is exposed, the surrounding areas of zinc coating form a galvanic cell with the exposed steel and protect it from corrosion. This is a form of localized cathodic protection - the zinc acts as a sacrificial anode.

Galvanizing, while using the electrochemical principle of cathodic protection, is not actually a cathodic protection. Cathodic protection requires the anode to be separated from the metal surface to be protected, with an ionic connection through the electrolyte and an electron connection through a connecting cable, bolt or similar. This means that any area of the protected structure within the electrolyte can be protected, whereas in the case of galvanizing, only areas very close to the zinc are protected. Hence, a larger area of bare steel would only be protected around the edges. While the galvanized steel represents a good measure to limit the corrosion, there are drawbacks in terms of cost, which is about 60% higher than a bare carbon steel pipe. Moreover, galvanizing does not protect the pipe in the welded areas at the joints between the sections. Common practice is to cover the welded parts with a protective paint such as bitumen or an alkyd primer.

Metals with very negative E° , such as Zn could be applied by immersing the Fe-alloy in a galvanic bath of molten Zinc;

6.1.2 Active protection

Cathodic protection prevents corrosion by converting all of the anodic (active) sites on the metal surface to cathodic (passive) sites by supplying electrical current (or free electrons) from an alternate source. Cathodic protection consists in making the surface of a metal to be protected more electronegative than its redox potential in a given electrolyte. Of course, current must be provided by creating a circuit capable of

circulating the current in the electrolyte with ion exchange powered by an oxidation reaction. In other words, it will not be sufficient to have a direct electric current generator, but it will also be necessary to insert in the circuit an expendable element on which the oxidation reaction can take place.

- Sacrificial anode consists in attaching a bulk sacrificial anode made of Zinc or other (less noble than Fe, e.g. Mg, Al, etc.) alloy to the pipe in case of stray currents. Being Zn more reducing than Fe, oxidation proceeds on the Zn and the pipe remains protected until all the Zn has been consumed.

Usually this takes the form of galvanic anodes, which are more active than steel. This practice is also referred to as a sacrificial system, since the galvanic anodes sacrifice themselves to protect the structural steel or pipeline from corrosion.

In the case of Aluminium anodes, the reaction at the Aluminium surface is:



At the steel surface molecular oxygen is converted to ions which combine with water to form hydroxyl ions):



As long as the current (free electrons) arrives at the cathode (steel) faster than oxygen is arriving, no corrosion will occur.

- Other active methods consist in applying a contrary electromotive force where the pipe is connected to the negative pole of a direct current generator whose positive pole is in turn connected to an inert electrode. This system is called Impressed Current Cathodic Protection (ICCP). ICCP setup for a pipeline consists of a DC power source, (often an AC powered transformer rectifier) and an anode, or array of anodes buried in the ground (figure 16). Anodes for ICCP systems are available in a variety of shapes and sizes. Common anodes are tubular and solid rod shapes or continuous ribbons of various materials. These include high silicon cast iron, graphite, mixed metal oxide (MMO), platinum and niobium coated wire and other materials. The DC power source would typically have a DC output of up to 50 amperes at 50 volts, but this depends on several factors, such as the size of the pipeline and coating quality. The positive DC output terminal would be connected via cables to the anode array, while another cable would connect the negative terminal of the rectifier to the pipeline.

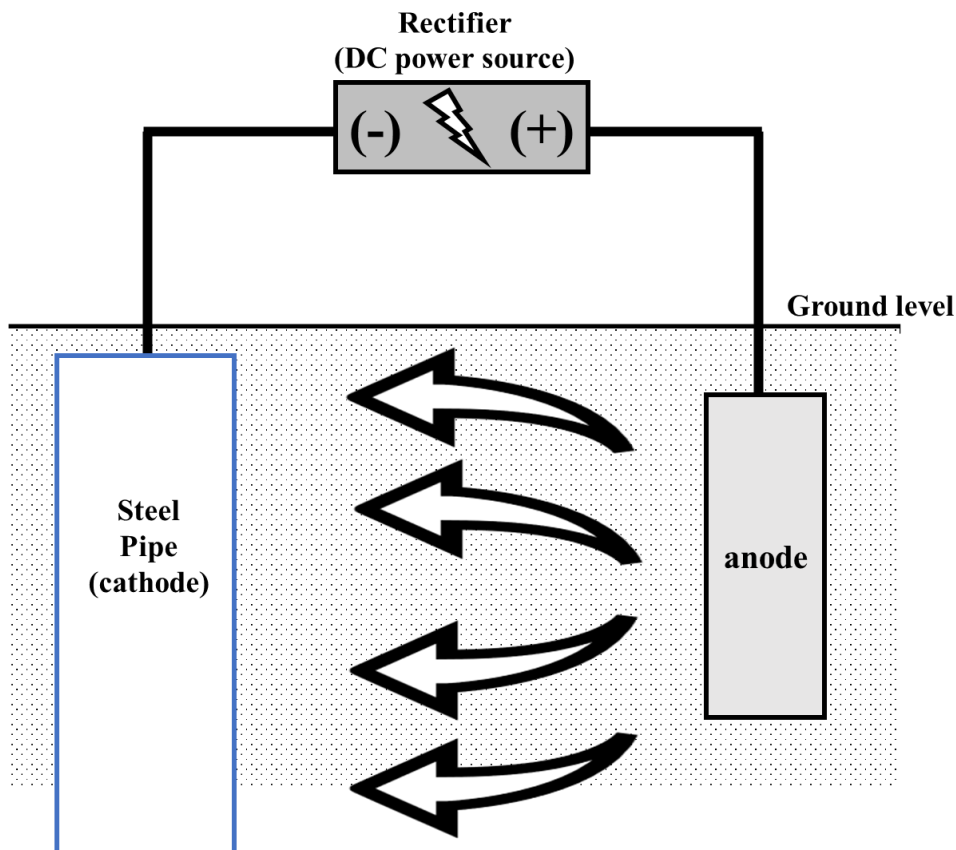


Figure 16: Working scheme of an Impressed Current Cathodic Protection system

For pipelines protection, anodes are arranged on several design and field condition factors including current distribution requirements. Common configurations consist of a vertical hole backfilled with conductive coke (a material that improves the performance and life of the anodes) or laid in a prepared trench, surrounded by conductive coke and backfilled.

6.1.3 Selection of specific regulation on cathodic protection

Cathodic protection is extensively contemplated within the following national and international technical standards:

- ISO 15589-1 Petroleum, petrochemical and natural gas industries Cathodic protection of pipeline systems;
- UNI EN 13509 Tecniche di misura per la protezione catodica;

- UNI EN 50162 Protezione contro la corrosione da correnti vaganti generate da sistemi eserciti in corrente continua;
- ISO 15257 Cathodic protection – Competence levels of cathodic protection persons
Basis for a certification scheme;
- AS 2832 - Australian Standards for Cathodic Protection;
- ASME B31Q 0001-0191;
- ASTM G 8, G 42 - Evaluating Cathodic Disbondment resistance of coatings;
- DNV-RP-B401 - Cathodic Protection Design - Det Norske Veritas;
- EN 12068 - Cathodic protection. External organic coatings for the corrosion protection of buried or immersed steel pipelines used in conjunction with cathodic protection. Tapes and shrinkable materials;
- EN 12473 - General principles of cathodic protection in sea water;
- EN 12474 - Cathodic protection for submarine pipelines;
- EN 12499 - Internal cathodic protection of metallic structures;
- EN 12696 - Cathodic protection of steel in concrete;
- EN 12954 - Cathodic protection of buried or immersed metallic structures. General principles and application for pipelines;
- EN 13636 - Cathodic protection of buried metallic tanks and related piping;
- EN 14505 - Cathodic protection of complex structures;
- EN 15280- Evaluation of a.c. corrosion likelihood of buried pipelines;
- EN 50162 - Protection against corrosion by stray current from direct current systems;
- BS 7361-1 - Cathodic Protection;
- NACE SP0169:2013 - Control of External Corrosion on Underground or Submerged Metallic Piping Systems;
- NACE TM 0497 - Measurement Techniques Related to Criteria for Cathodic Protection on Underground or Submerged Metallic Piping Systems.

6.1.4 Advantages and drawbacks of anti-corrosion measures applied to GHEs

Active methods have higher installation and maintenance costs than the aforementioned passive methods, and therefore is quite inconvenient for cost-effective/long-term applications such as GHEs. It is sometimes more economically viable to protect a pipeline using galvanic (sacrificial) anodes. This is often the case on smaller diameter pipelines of limited length.

The coatings represent an additional thermal resistance to the pipe. Indeed, it affects the overall borehole thermal resistance, because any layer between the heat transfer fluid and the undisturbed ground, as per definition, increases the resistance. In the case of metal pipes this is particularly relevant, since metal pipes have a relatively high thermal conductivity compared to the coating materials. This means that the coating can potentially negate the advantages of metal over plastic.

This issue was addressed in the thematic chapter on evaluations of the thermophysical properties and on-site performance of coated GHEs.

The same principle is applicable to loose oxidation products that may form on the surface of the pipe, they can be protective (a lot of cladding) or encrusting by reforming (rust). These incoherent substances act as low conductive layers that interpose themselves on the surfaces of the pipes, negatively affecting the thermal flow between the fluid and the undisturbed ground.

Passive coatings offer adequate protection to the steel pipes as long as they are intact, but they can indeed be damaged somehow. In fact, when using a surface coating for protection, there is still a risk of deterioration of the artifact. In fact, during handling, storage, transportation and installation of the components can cause permeability of the coatings, small cracks or detachments due to impacts, cuts, abrasions, etc. A small crack is sufficient to generate corrosion phenomena. Once corrosion has started, products are formed that are generally characterized of a higher volume and therefore support the oxidative process, undermining the protective coating and offering a new surface to progressive deterioration.

Grouting of GHEs theoretically should provide adequate external corrosion protection to the metal pipe, but in practice, no grouting job can be perfect due to possible swelling or protuberance of borehole walls locally. Furthermore, boreholes usually have a small inclination, which is sufficient to create a direct contact of internal pipe to the undisturbed underground to expose it to potential corrosion. Finally, the annular gap between the GHE and the borehole, even if filled with cements with adequate thermal conductivity, indeed represents an additional thermal resistance which limits the heat flux between the heat transfer fluid and the ground.

The sacrificial anode is inexpensive but can cause damage during its installation with bolt rivets that can puncture the pipe. As it protrudes from the pipe, it can also be damaged when inserting the GHE into the borehole.

Galvanized steel has negligible impact on the thermal resistance of the pipe, but leaves uncovered areas that can be attacked by corrosion such as weld joints, which must be manually protected with paint when installing the internal GHE, with negative effect on installation time (and consequently on installation costs) and increased complexity due to this additional process. Furthermore, the Zinc layer is usually extremely thin (e.g. 86 μm of zinc as for ASTM 929) that makes this measure very temporary having the effect of just extending the life time of the pipe.

In all passive methods, protection relies on the presence of a layer which mechanically insulate the metal. Nonetheless, during the installation phase, i.e. when the vertical GHE is inserted into the ground, such “shield” could be damaged by scratching against the sides of the borehole.

6.1.5 Overview of the state of the art of standard methods for corrosion monitoring and verification procedures for buried steel pipes

Inspection procedures for buried steel pipes are common in engineering fields such as poles oil and gas distribution. A failure to operate steel oil and gas pipelines can have devastating environmental, social and economic implications. In order to prevent or mitigate these adverse effects, a methodology is needed to predict the useful life of corroded steel pipes, which allows for preventative maintenance and repair. Other relevant fields of application of corrosion monitoring are piling for lightning or power distribution. According to common practice. the tests performed at each pole are:

Visual inspection

A detailed visual inspection of the mast's condition reveals any abnormalities (scratches, dents, holes, visible corrosion attacks, etc.) compared to its original condition and takes pictures of important parts. The visual inspection of the support must be carried out in compliance with the EN standard 970. Equipment must be used which, if necessary, will allow the operator to remove, cut, scrape to reach the pole surface. Visual inspection is hardly applicable to ground heat exchangers, because the vast majority of the pipes is not visually accessible. Nonetheless, the most superficial

sections, where the vertical pipe top opening is jointed with the head, is usually exposed. Moreover, due to material couplings and greater exposure to weather conditions makes this a crucial part of the GHE that can be easily attacked by corrosion, therefore it deserves special attention.

Measurement of spontaneous potential

The spontaneous potential (SP) determines the natural or spontaneous potential difference which can be generated during the corrosion phenomenon and which exists in the absence of any artificially applied current.

Also indicated as corrosion potential, it designates the tendency of metals to corrode, but it does not provide the corrosion rate, as other electrochemical methods do. In fact, the corrosion rate is proportional to the rate of electron (current) transferred between electrode and electrolyte.

Measurement of spontaneous potential consists of measuring the electrochemical potential with a precision multimeter between the metal pole and a reference electrode at the surrounding ground. The most commonly used reference electrodes for this type of measurement are: Saturated copper sulphate electrode (Cu/CuSO₄), or silver chloride electrode.

Measurement of corrosion rate

A quantitative measurement of the corrosion rate is performed using a corrosive meter that uses current dynamic electrochemical method with a system of three electrodes, the poles of which form the working electrode. The other two are an austenitic stainless steel (AISI 304) counter electrode and a reference electrode (figure 17). This equipment provides corrosion rate data directly in microns/year.

Considering that the corrosion process that occurs in a metallic material immersed in a watery environment, or electrically conductive medium, is the manifestation of the effect of galvanic cells, it is possible, on the basis of the electro-chemical theory, to estimate the speed of the corrosion by indirect means, stimulating the metal/electrolyte system with external electric excitation.

This methodology is based on the Stern-Geary equation. It makes it possible to deduce, after knowing the resistance of polarization, the current of corrosion. Given the current

of corrosion it is possible to calculate the corrosion rate. This consists of determining the voltage variations ΔE of the metal, in accordance with the passage of an external current Δi_{appl} between the metal component and a counter electrode, taking into account an area of the surface (A). The ratio $\Delta E/\Delta i_{appl}$ is the resistance of polarization (R_p) which is measured in $\Omega \cdot \text{cm}^2$.

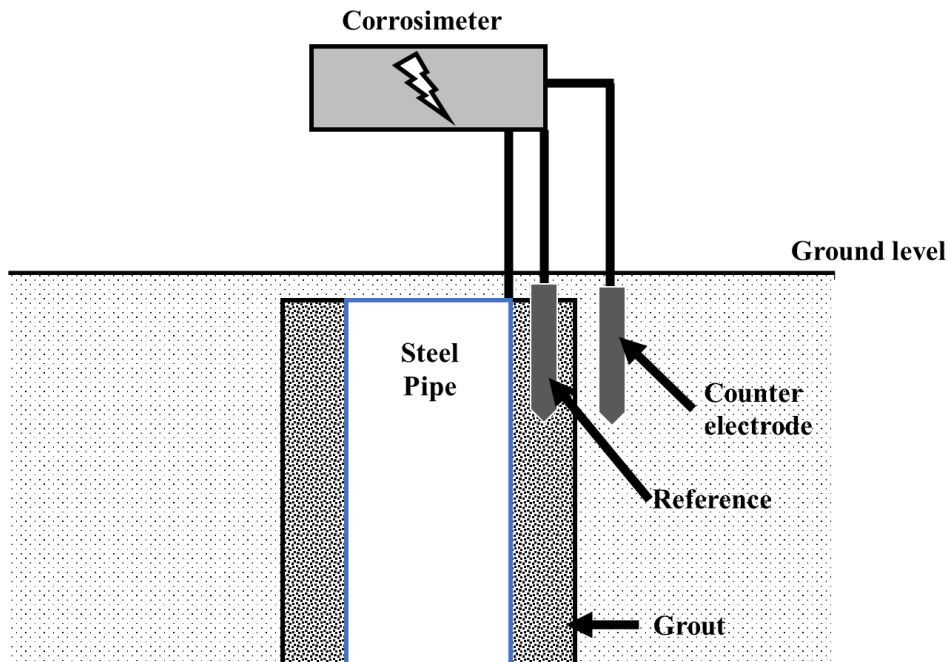


Figure 17: Scheme for determining the corrosion rate by means of electrochemical method.

For evaluating the density of the current of corrosion $i_{corr} \Delta A$ (cm^2) the equation of Stern-Geary is used, which is valid for $\Delta E < 20$ mV and $i_{corr} = B/R_p$ where B è is a constant value that in the case of the carbon steel is equal to 0.026 V. The corrosion rate can be obtained from the density of current using the Faraday law:

$$\text{Corrosionrate}(\text{mmy}) = 3270 \cdot i_{corr} \cdot A \cdot \frac{28}{d}$$

where d is the density of the metal in g/cm^3 .

Measure the residual thickness of the pole

A direct measurement of the amount of corroded metal is performed using an ultrasonic thickness gauge. Measurements are performed circumferentially according to four base

directions (north, south, east, west) and four half points. The thickness measurement is carried out with ultrasonic instrumentation. Ultrasound testing (UT) exploits the phenomena of propagation of elastic waves in solids, liquids or gases, i.e. compression and decompression waves of the matter, with a frequency higher than that of sounds audible to the human ear. More than any other NDT (non-destructive test), the UT requires a highly experienced, capable operator to correctly interpret every signal that appears on the monitor and to take full advantage from the possibilities that this technique offers. Misinterpretation of signals is not uncommon, already considered defects, which disappear by repeating the examination with a more suitable probe frequency, or with a different angle of propagation. The presence of progressive inhomogeneity of the material, of micro-defects, of very pronounced grain edges, or of segregations, can strongly attenuate the background echo, up to its total deletion. However, these defects are not always real discontinuities of the material, nor can they be objectively considered serious, or detrimental to the functionality or reliability of the examined component.

Industrial radiology

Industrial radiography is a modality of non-destructive testing that uses ionizing radiation to inspect materials and components with the objective of locating and quantifying defects and degradation in material properties that would lead to the failure of engineering structures. It plays an important role in the science and technology needed to ensure product quality and reliability. Industrial Radiography uses either X-rays, produced with X-ray generators, or gamma rays generated by the natural radioactivity of sealed radionuclide sources. After crossing the specimen, photons are captured by a detector, such as a silver halide film, a phosphor plate, flat panel detector or CdTe detector. The examination can be performed in static 2D (named radiography), in real time 2D, (fluoroscopy) or in 3D after image reconstruction (computed tomography). It is also possible to perform tomography nearly in real time (4-dimensional computed tomography or 4DCT). Particular techniques such as X-ray fluorescence (XRF), X-ray diffractometry (XRD), and several other ones complete the range of tools that can be used in industrial radiography.

6.1.6 References

-
- Aparicio, M.; Jitianu, A.; Rodriguez, G.; Degnah, A.; Al-Marzoki, K.; Mosa, J.; Klein, L. C. Corrosion Protection of AISI 304 Stainless Steel with Melting Gel Coatings. *Electrochim. Acta* 2016.
<https://doi.org/10.1016/j.electacta.2015.12.142>.
- ASTM A929/A929M-18. Standard Specification for Steel Sheet, Metallic-Coated by the Hot-Dip Process for Corrugated Steel Pipe.
- DIN 30671 : Thermoset plastic coatings for buried steel pipes.
- DIN 30678 : Polypropylene coatings on steel pipes and fittings.
- DIN EN 12068 1999. External organic coatings for the corrosion protection of buried or immersed steel pipelines used in conjunction with cathodic protection - Tapes and shrinkable materials.
- El-Wahab, H. A.; El-Hai, F. A.; El-Fattah, M. A.; Lin, L. Effect of Short Oil-Length Alkyd Additive on the Properties of Coal Tar Binder. *Pigment Resin Technol.* 2011. <https://doi.org/10.1108/03699421111176216>.
- EN 10216-5, Seamless steel tubes for pressure purposes - Technical delivery conditions - Part 5: Stainless steel tubes.
- EN 1057, Copper and copper alloys - Seamless, round copper tubes for water and gas in sanitary and heating applications.
- EN 12168, Copper and copper alloys - Hollow rod for free machining purposes.
- EN 12201-2:2011, Plastics piping systems for water supply, and for drainage and sewerage under pressure - Polyethylene (PE) - Part 2: Pipes.
- EN 12201-3:2011, Plastics piping systems for water supply, and for drainage and sewerage under pressure - Polyethylene (PE) - Part 3: Fittings.
- EN 12201-5:2011, Plastics piping systems for water supply, and for drainage and sewerage under pressure - Polyethylene (PE) - Part 5: Fitness for purpose of the system.
- EN 12449, Copper and copper alloys - Seamless, round tubes for general purposes.
- EN 1965-2, Structural adhesives - Corrosion - Part 2: Determination and classification of corrosion to a brass substrate.

- EN 970:1997 - Non-destructive examination of fusion welds.
- EN ISO 1127, Stainless steel tubes - Dimensions, tolerances and conventional masses per unit length.
- EN ISO 15494, Plastics piping systems for industrial applications - Polybutene (PB), polyethylene (PE), polyethylene of raised temperature resistance (PE-RT), crosslinked polyethylene (PE-X), polypropylene (PP) - Metric series for specifications for components and the system.
- EN ISO 15875-1:2003, Plastics piping systems for hot and cold water installations - Crosslinked polyethylene (PE-X) - Part 1: General.
- EN ISO 22391-1, Plastics piping systems for hot and cold water installations - Polyethylene of raised temperature resistance (PE-RT) - Part 1: General.
- Florida, G.; Blandini, F.; Iuculano, S.; Belfiore, G. M.; Viccaro, M. Innovative Solutions for Improving the Heat Exchange in Closed-Loop Shallow Geothermal Systems. *Energies* 2020. <https://doi.org/10.3390/en14010108>.
- Haehnlein, S.; Bayer, P.; Blum, P. International Legal Status of the Use of Shallow Geothermal Energy. *Renewable and Sustainable Energy Reviews*. 2010. <https://doi.org/10.1016/j.rser.2010.07.069>.
- Heinonen, E. W.; Beall, A. N.; Wildin, M. W.; Tapscott, R. E. Assessment of Antifreeze Solutions for Ground-Source Heat Pump Systems. In *ASHRAE Transactions*; 1997.
- ISO 8501-1:2007. Preparation of steel substrates before application of paints and related products — Visual assessment of surface cleanliness — Part 1: Rust grades and preparation grades of uncoated steel substrates and of steel substrates after overall removal of previous coatings.
- Pöhl, F.; Harges, C.; Theisen, W. Scratch Behavior of Soft Metallic Materials. *AIMS Mater. Sci.* 2016. <https://doi.org/10.3934/matersci.2016.2.390>.
- UNE EN 15450:2008 Heating systems in buildings - Design of heat pump heating systems, Category: 27.080 Heat pumps.
- UNI 9099 : 1989. Steel pipes for buried or submerged pipelines - external polyethylene coating applied by extrusion.
- UNI EN 10290:2003. Tubi e raccordi di acciaio per condotte terrestri e marine - Rivestimenti esterni in poliuretano e poliuretano- modificato applicato allo stato liquido.

- UNI ISO 5256:1987. Tubi ed accessori di acciaio impiegati per tubazioni interrate o immerse. Rivestimento esterno e interno a base di bitume o di catrame.
- Vasconcelos, D. C. L.; Carvalho, J. A. N.; Mantel, M.; Vasconcelos, W. L. Corrosion Resistance of Stainless Steel Coated with Sol-Gel Silica. *J. Non. Cryst. Solids* 2000. [https://doi.org/10.1016/S0022-3093\(00\)00155-1](https://doi.org/10.1016/S0022-3093(00)00155-1).

7 Materials and methods

The specific literature on the evaluation of the material properties of geothermal components is not extensive and therefore the bibliographic search has been extended to other fields. Aside from standard geotechnical procedures such as Thermal Response Testing and geoelectric techniques, the methods presented in this chapter have been selected from other fields so that they are applicable to components found in shallow geothermal systems and in some cases have been critically adapted to scope. Soil chemistry methods are mainly borrowed from the agricultural sector. As for the underground metal structures and the corrosion of the underground, the main sources are linked to the sector of the poles for the distribution of electricity. Other areas of origin are plumbing, water recirculation standards, water treatment and more generally the evaluation of buried metal engineering components. The following sections illustrate the main techniques, standards and methodologies applied during this study which can be found in a more concise form within the thematic chapters. These methods are divided into main categories:

- the ones related to ground characterization (scale and evaluation of corrosivity, pH, electrical resistivity, Thermal Response Test);
- and the ones dedicated to GHEs evaluation (thermophysical properties of materials and infrared thermography).

7.1.1 Numerical corrosivity scale and evaluation methods

Ground corrosivity assessment is a complex task due to the multifaceted nature of the ground itself. For this reason, the state of the art only allows qualitative methodologies, usually based on scoring systems, to evaluate the aggressiveness of a site. The American Water Works Association (AWWA) developed a numerical ground corrosivity scale, applicable to iron alloys. The severity ranking by assigning points for different variables (table 15). When the points total of a ground in the AWWA scale equals ten (or higher), corrosion protective measures are recommended for iron alloys.

Table 15: the scores system for predicting ground corrosivity according the AWWA C-105 Standard.

Ground Parameter	Assigned Points
Electrical resistivity (ohm cm)	
<700	10
700 - 1000	8
1000 - 1200	5
1200 - 1500	2
1500 - 2000	1
> 2000	0
pH	
0-2	5
2-4	3
4-6.5	0
6.5-7.5	0
7.5-8.5	0
>8.5	3
Redox potential (mV)	
>100	0
50-100	3.5
0-50	4

<0	5
Sulphides	
Positive	3.5
Trace	2
Negative	0
Moisture	
Poor drainage continuously wet	2
Fair drainage generally moist	1
Good drainage generally dry	0

The most modern approach in qualitative methods is to introduce a Design Decision Model, that is a qualitative model that converts the recommendations obtained in the AWWA point system into a risk matrix (table 16). In this way, it is possible to arrive at a new vision that relates the operational reliability and the difficulties that may exist, also affecting maintenance and repairs, and establishes the appropriate recommendation for corrosion mitigation.

Table 16: design decision model (x : likelihood and C : consequences)

Likelihood	Consequences	Proposed action
< 10	Any	Standard protection
10 – 20	< 30 $1035.7x^{-1.015} > C >$ $240.25x^{-0.7}$ $> 1035.7x^{-1.05}$	Standard protection, PE (polyethylene), PE+bonded joints
20 – 35	< 25 $1596.1x^{-1.08} > C >$ $1035.7x^{-1.05}$ $> 1596.1x^{-1.08}$	PE (polyethylene), PE+bonded joints, PE+bonded joints or Cathodic protection
35 – 40	< 30 $1177.8x^{-0.89} > C >$ $1596.1x^{-1.08}$ $> 1177.8x^{-0.89}$	PE+bonded joints, PE+bonded joints or Cathodic protection, Cathodic protection
40 – 45	$< 1177.8x^{-0.89}$ $> 1177.8x^{-0.89}$	PE+bonded joints or Cathodic protection, Cathodic protection
45 – 50	Any	Cathodic protection

The points system does not quantify, and was never designed to quantify, the corrosivity of a ground. It is a tool used to distinguish non-aggressive grounds from aggressive ones in relation to an iron pipe. Basically, grounds <10 points are considered non-aggressive to iron pipes, while grounds with 10 points are considered aggressive. Subsoils of 15 and 20 points respectively are considered aggressive for the iron pipe; however, due to the nature of the measured ground parameters, a 20-points ground may not necessarily be more aggressive than the 15-points one. The methods used to assess the severity of the corrosion attack are used in other fields of engineering, the most relevant being the lighting pole sector. Based on test procedures that can determine the corrosion rate or corrosion potential, a qualitative rating is provided as a severity scale. Corrosion level evaluation is provided for both ground coupled and concrete coupled steel poles. That is interesting because it allow to transfer this methodology to both geothermal probes in direct contact with the ground and to grouted ones. Correlation between corrosion rate and corrosion level for steel poles in direct contact with the ground is presented in tables 17, 18 and 19:

Table 17: Rif. APCE proceedings – electrochemical method for the evaluation of the degradation of metal materials used for lighting poles – Rome 1996.

Severity class	Corrosion rate [$\mu\text{m}/\text{year}$]	Corrosion level
I	<15	Negligible
II	15 - 35	Low
III	35 - 50	Moderate
IV	>50	High

Correlation between corrosion potential and corrosion level for steel poles in direct contact with concrete:

Table 18: Rif. ASTM.

Severity class	Corrosion potential E_{corr} [mV] CSE	Corrosion level
I	> -200	Negligible
II	-200 - -350	Possible
III	< -350	Intense

Correlation between corrosion rate and corrosion level for steel poles in direct contact with concrete:

Table 19: Rif. Cost 509 Corrosion and protection of metal in contact with concrete 1997.

Severity class	Corrosion rate [$\mu\text{m}/\text{year}$]	Corrosion level
I	<1	Negligible
II	1 - 5	Low
III	5 - 10	Moderate
IV	>10	High

7.1.2 Ground pH

Measurement of the pH of the ground

Ground pH is a measure of the acidity or alkalinity in the ground. It is also called ground reaction. Ground pH is one of several properties used as a general indicator of ground corrosivity. The most common classes of ground pH are presented in table 20.

Table 20: Qualitative ground corrosibility rate based on pH.

Ground reaction	Range of pH
Extremely acid	3.5 – 4.4
Very strongly acid	4.5 – 5.0
Strongly acid	5.1 – 5.5
Moderately acid	5.6 – 6.0
Slightly acid	6.1 – 6.5
Neutral	6.6 – 7.3
Slightly alkaline	7.4 – 7.8
Moderately alkaline	7.9 – 8.4
Strongly alkaline	8.5 – 9.0

Generally, grounds that are either highly alkaline or highly acid are likely to be corrosive to steel. Grounds that have pH of 5.5 or lower are likely to be highly corrosive to cements.

What influences the ground pH

The acidity or alkalinity in grounds have several different sources. In natural systems, the pH is affected by the lithology, climate, and weathering. Management of grounds often alters the natural pH because of acid-forming nitrogen fertilizers, or removal of bases (potassium, calcium, and magnesium). Grounds that have sulphur-forming minerals can produce very acid ground conditions when they are exposed to air. These

conditions often occur in tidal flats or near recent mining activity where the ground is drained. In agricultural contexts, the application of anhydrous ammonia as a nitrogen fertilizer contributes to lowering the ground pH. In cultivated areas, applications of ammonia lower the surface ground pH from ranges of 6.6 to 7.3 to below 5.6. Chemical substances that contain sulphur generally form an acid when introduced into the ground, which lowers the ground pH.

Ground pH can change during the year. It depends on temperature and moisture conditions, and can vary to as much as a whole pH unit during the growing season. Since pH is a measure of the hydrogen ion activity (H^+), many different chemical reactions can affect it.

Temperature

Temperature changes the chemical reactivity, so most measurements of pH include a temperature correction to a standard temperature of 25°C. The ground pH generally is recorded as a range in values for the ground depth selected.

Measurement of ground pH

A variety of kits and devices are available to determine the pH in the field. The methods include dyes, paper strips and glass electrodes. The latter is the base of the measurement procedure according to the American Society of Testing and Materials (ASTM). 1995. *Annual Book of ASTM Standards*, Designation D4972 - 95a: Standard Test Method for pH of Grounds. Measurement of ground pH is carried out using a potentiometer determines the degree of acidity or alkalinity in grounds suspended in water and in 0.01 Molar (M) calcium chloride solution. The potentiometer is calibrated with buffer solutions of known pH prior to the analysis of samples.

7.1.3 Ground electrical resistivity

Ground resistivity is a function of ground moisture and the concentrations of ionic soluble salts and it is considered to be most comprehensive indicator of a ground's corrosivity. Typically, the lower the resistivity, the higher will be the corrosivity as indicated in table 21.

Table 21: corrosivity ratings based on ground electrical resistivity.

Ground electrical resistivity [Ohm-cm]	Corrosivity rating
> 20000	Essentially non-corrosive
10000 - 20000	Mildly corrosive
5000 – 10000	Moderately corrosive
3000 – 5000	Corrosive
1000 – 3000	Highly corrosive
< 1000	Extremely corrosive

The geoelectric method

Ground resistivity is measured in ohm-cm and is achieved by various means. A long-standing practice uses the four-points Wenner method. The goal is to reconstruct subsurface resistivity models through a process of inversion of the data acquired *in situ*. This type of non-invasive tests are based on the principles that describe electrical conduction through a medium: the more a substance is allowed to pass through charge carriers, the more it is defined conductive; vice versa it is defined resistive. When electric charges are made to flow through a conductor it is possible to measure the passage in a time; it is therefore possible to define the concept of electric current (I):

$$\lim_{\Delta t \rightarrow 0} \frac{\Delta Q}{\Delta t} = I$$

In the presence of an ohmic conductor (An ohmic conductor is an electrical conductor for which Ohm's law is) the electric current encounters a resistance (R), measured in Ohm, which depends on the potential difference (V), measured in Volts, and the current (I) according to Ohm's Law. Resistivity is the attitude of a material to resist the passage of electrical charges. Since ionic current flow is associated with ground corrosion reactions, it can be argued that high ground resistivity will slow down corrosion reactions. Ground resistivity generally decreases with increasing water content and concentration of ionic species. Sandy grounds rank high on the resistivity scale and are

therefore considered the least corrosive. Clay grounds, especially those contaminated with salt water, are at the opposite end of the spectrum. Electrical resistivity tomography (ERT) is a well-established geophysical method that provides insights regarding an investigated domain based on its electrical properties. Surveys are performed with multi-electrodes device in order to retrieve the electrical properties distribution of the underground (figure 18). An array of dozens of electrodes is coupled with the substrate in order to ensure galvanic contact with the ground. The apparent resistivities ρ_a (Ωm) of the underground are retrieved by injecting the current I (A) in two of the electrodes (current electrodes) and by recording the potential difference ΔV (V) that arise at the potential ones. To carry out the resistivity measurements, two conductive electrodes are used (conventionally called A and B) which, in contact with the ground, allow the introduction of electric current. At a known distance, through two other electrodes (conventionally called M and N), the potential difference (V) is measured. This configuration is called a quadrupole. The measurements are performed along the entire electrodes array, retrieving a pseudo-section of apparent resistivities (Day-Lewis et al., 2008). Inversion process of the collected dataset finally obtains the real distribution of the electrical properties in the underground. This can be done by using codes which iteratively find the best underground model that minimize the misfit between the measured and the computed dataset (Binley and Kemna, 2005).

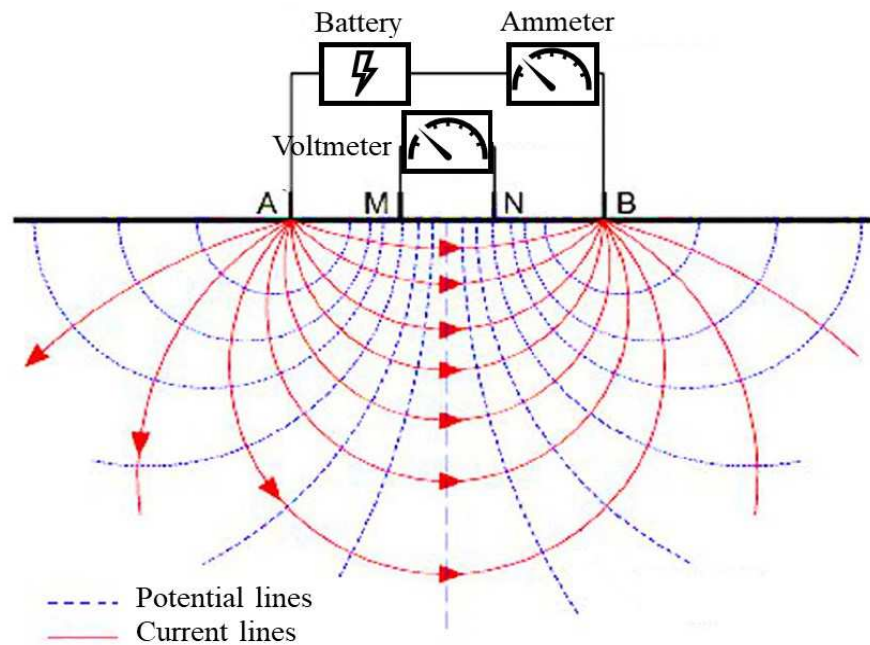


Figure 18: ERT measurement configuration scheme.

The resistivity of the underground depends on various factors such as porosity, presence of fluids, mineralogical composition, degree of fracturing, degree of

saturation as well as the presence of organic substances (hydrocarbons, solvents, etc.). In particular, the resistivity of the rocks is always greater than that of the water in the pores, it is minimum corresponding to the maximum degree of saturation and the lower is the greater the porosity. As is evident by observing the values reported in table 22, also for single classes of rocks or grounds, there is a great variability of the resistivity values (The resistivity values sometimes vary by one order of magnitude).

Table 22: Ground electrical resistivity for common ground types.

Ground type	Ground electrical resistivity [Ohm-cm]
Poor or slow drainage, costal areas	150 – 1200
Costal plains, low elevation	600 – 1500
Costal plains, satisfactory to good drainage	1200 – 1500
Farm and range lands	3500 – 10000
Desert plains, mountains	5000 – 25000
Excellent drainage, dry and arid	10000 - 25000

Unconsolidated sediments generally have a lower resistivity than sedimentary rocks. However, precisely because they are not well consolidated, it is difficult to estimate their resistivity value, which depends on the porosity and clay content. Clayey grounds commonly have lower resistivity values than sandy grounds. Finally, the water content plays an important role in determining the apparent resistivity of the ground, determining a lowering of the average resistivity (table 23).

Table 23: Resistivity ranges for some types of rocks and grounds commonly encountered during geoelectric surveys.

Material	Resistivity interval
Sandstone	60 – 10 ⁴ Ωm
Clay	1 – 120 Ωm
Sand	100 – 1000 Ωm
Silt	10 - 800 Ωm
Gravel	100-5000 Ωm
Limestone	100 – 5000 Ωm
Basalt	10 – 10 ⁵ Ωm
Basalt	100 – 10 ⁸ Ωm
Granite	100 – 10 ⁶ Ωm

At the CNR site located in Padua-Italy (which is the main case study addressed in this study), data were collected with a X612EM+ georesistivimeter (MAE Advanced Geophysics Instruments), along an investigation line of 47m with 48 stainless-steel electrodes spaced 1m apart and a Dipole-dipole skip-0 configuration.

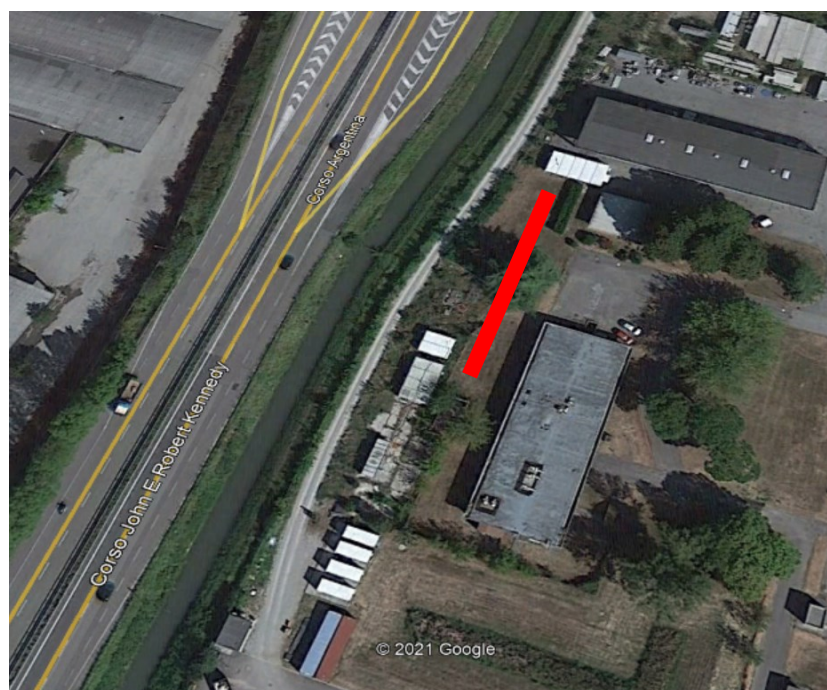


Figure 19: Survey area at CNR Padua site. Red line indicates the position of the ERT profile.

The inversion process of the acquired dataset has been realized in Python environment with the software ResIPy (Blanchy et al., 2020), based on the R2/R3t codes developed on Occam's inversion method (Binley, 2015). Before each survey, the contact resistances recorded by the georesistivimeter were checked in order to evaluate the reliability of the measurement. Furthermore, the dataset was acquired with reciprocal measurements (Cassiani et al., 2006), exchanging current and potentiometric electrodes for each measured quadrupole; this way it is possible to assess the quality of the recorded datasets and correctly define the expected data error for the inversion processes. Once defined an acceptable difference threshold of 20% between the reciprocal measurements, the quadrupoles exceeding that target were removed (Figure 20) and the dataset was inverted.

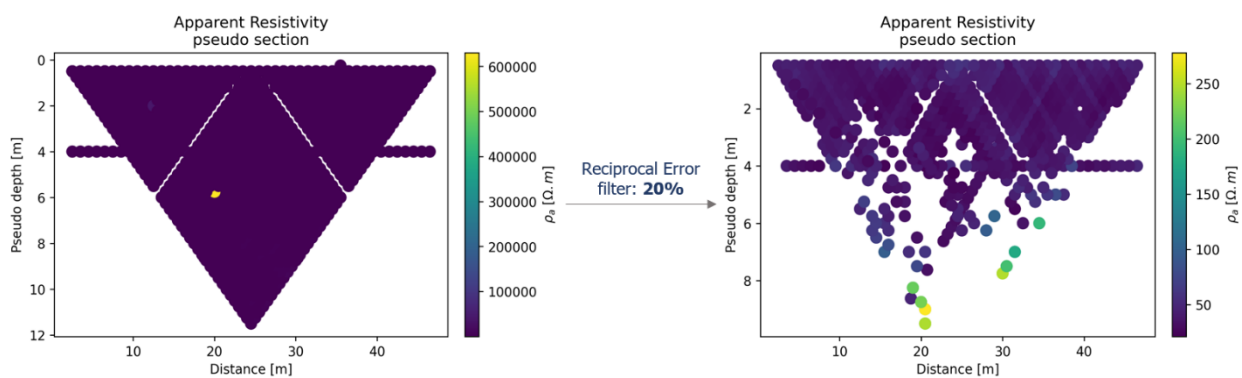


Figure 20: Apparent resistivity pseudosections before and after the processing.

The solution of the inversion process converged at the first iteration with a final RMS misfit of 1.02 and the result is shown Figure 21. The resistivity distribution across the whole profile appears consistently homogeneous, with values relatively stable on 45-50 Ωm (see histogram in Figure 2) until depths of approximately 7m from ground level. A very thin and shallow layer shows slightly higher resistances (around 65-75 Ωm), but its influence on the investigated volume is negligible given its cm-thick width. Therefore, it is reasonable to assume a constant value of c.a. 50 Ωm for the whole field which hosts the pilot site.

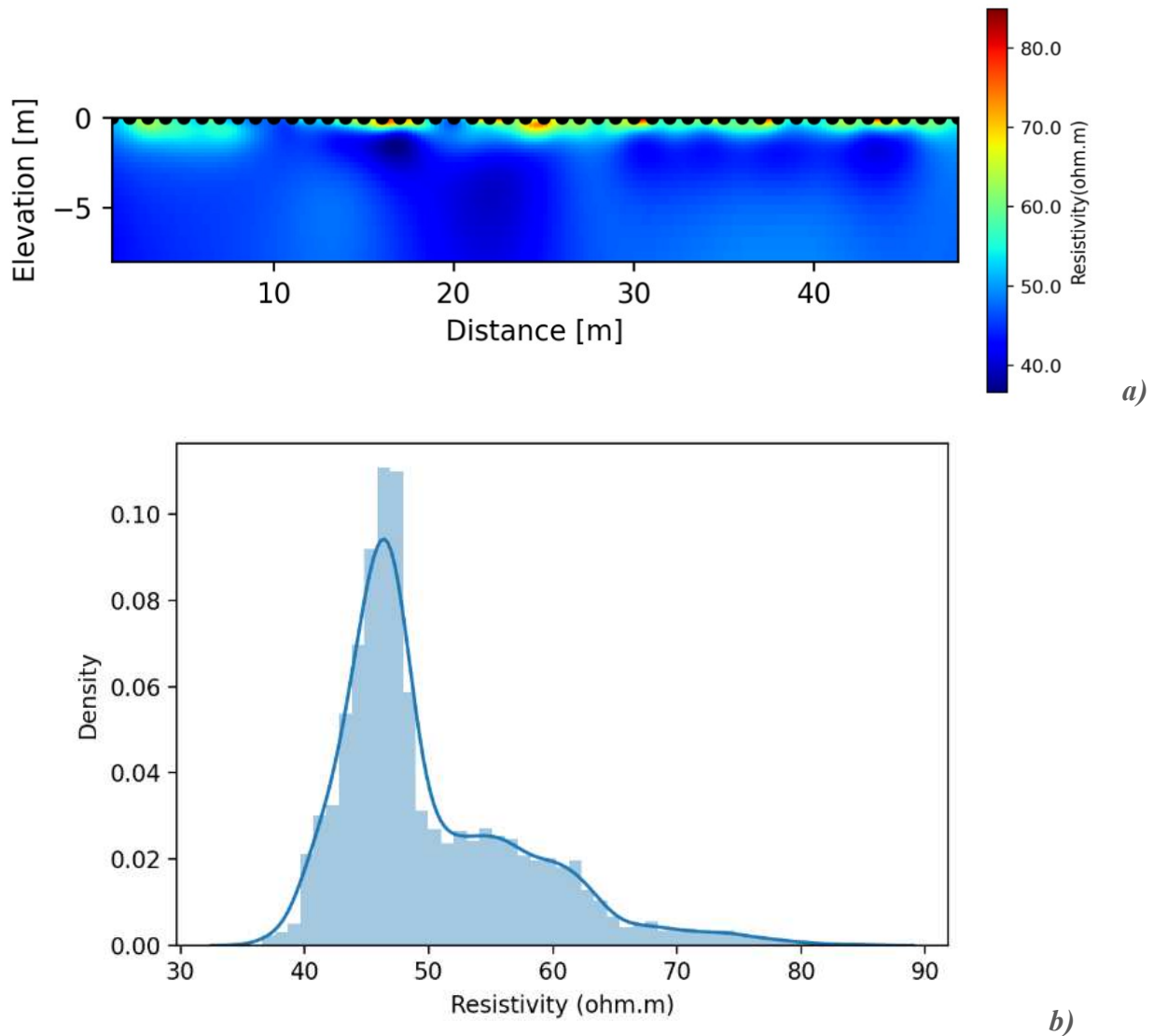


Figure 21: Resistivity model obtained from the inversion process (a) and statistical distribution of the obtained values (b).

7.1.4 On-site thermal performance of GHEs: Ground Response Test

The ground response test is, today, the in situ test for the characterization of the thermal properties of the ground with the highest degree of accuracy (Sanner et al., 2005). The GRT consists in the simulation of the operations of injection/extraction of heat at constant power inside a GHE (or a circuit of GHEs) for a limited time. By analysing the temperature variation of the heat transfer fluid, it is possible to estimate the thermal properties equivalents of the almost cylindrical ring of ground affected by the heat exchanger. The apparatus (figure 22) consists of a pipe system, circulation pump, a chiller or heater with constant power rate, and continuous logging of the inlet and outlet temperatures of the flow, and a flow meter. The equipment is normally contained

within a single unit for ease of transport and efficient use. The thermal response data (i.e. temperature development in the borehole at a certain energy injection/extraction) allows estimation of the effective thermal conductivity of the ground and the thermal resistance of the borehole.

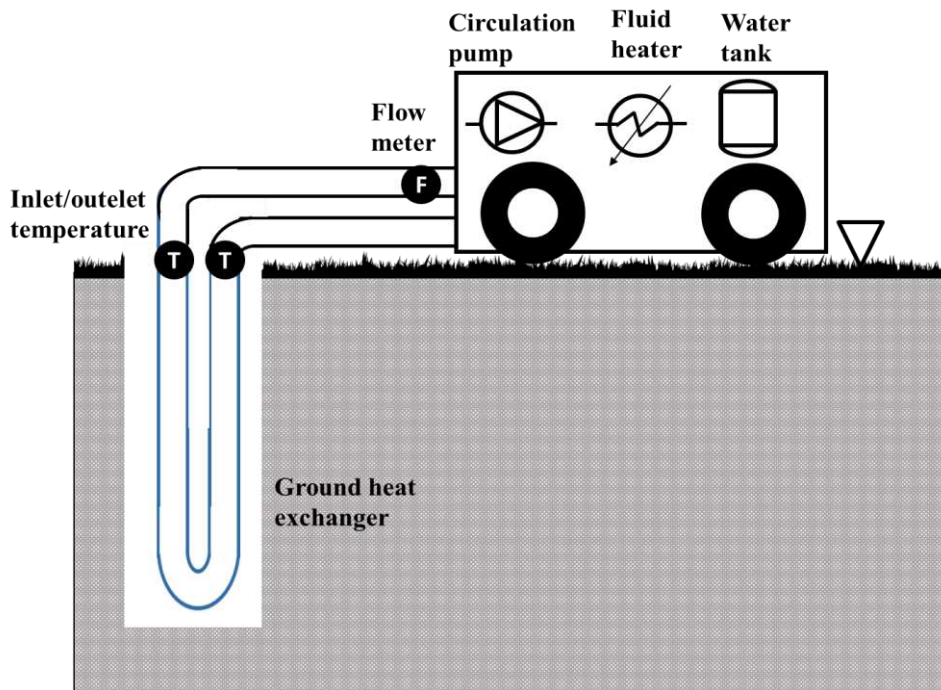


Figure 22: Ground Response Test rig schematics.

Undisturbed Ground Temperature

Most analysis procedures for estimating ground thermal conductivity from test data require good appraisals of the undisturbed ground temperature at the site. The undisturbed ground temperature must be determined before the response test begins. Undisturbed ground temperature can be calculated in two ways: downhole temperature log and/or flow temperature measurements.

Gehlin and Nordell made the temperature measurements using both methods. The conclusion of the analysis showed that the borehole temperature log is supposed to provide the correct undisturbed ground temperature profile. However, the circulation of the fluid also results in values that are in agreement with the previous method. Borehole temperature can be:

- 1) Temperature as a function of depth: The first method is to lower a thermocouple down the water-filled tube of the GHE. The water contained within the GHE must be in thermal equilibrium with its surroundings. Temperature is measured every few

meters along the GHE and the readings are used to calculate an arithmetic mean borehole temperature.

2) Temperature as a function of time: the second method is to circulate the heat transfer fluid from the wellbore heat exchangers through the wellbore until the inlet and return flow are in thermal equilibrium. The water contained within the GHE must be in thermal equilibrium with the ground. Although the heater does not inject heat, there will always be some heat gained in the system due to the work of the pump. The temperature is measured every second for about half an hour. The collected temperature data is used to estimate the average temperature of the well. Gehlin and Nordell suggest using the flow temperature after 20 minutes of circulation.

Thermal Conductivity of the Ground: preliminary calculations

The average temperature is calculated as the arithmetic average between the inlet and the outlet temperature for each measured step.

The thermal power exchanged between the fluid and the ground is calculated as:

$$Q = \dot{m} \cdot c_p \cdot \Delta T$$

where \dot{m} is the mass flow rate in [kg s^{-1}], c_p is the specific heat in [$\text{J kg}^{-1} \text{K}^{-1}$] and ΔT is the temperature difference between inlet and outlet temperatures.

The mass flow rate, the inlet temperature and the outlet temperature are measured during the test. The specific heat and the density can be obtained from REFPROP (NIST Reference Fluid Thermodynamic and Transport Properties Database) by imposing the atmospheric pressure and the mean temperature of the fluid for each step.

Simplified Infinite Line Source Approximation

The heat flux to or from the borehole can be represented as an infinite line source or sink in the ground with negligible effect of heat fluxes along the borehole axis. The most widespread and consistent method to date is the continuous line source model, based on a constant heat flux per unit of time. The evaluation of the equivalent thermal conductivity of the ground is possible using the average temperature of the fluid

between the inlet and the return. By plotting the average water temperature in the GHE against the natural logarithm of time, a linear relationship can be obtained (an example is given in figure 23).

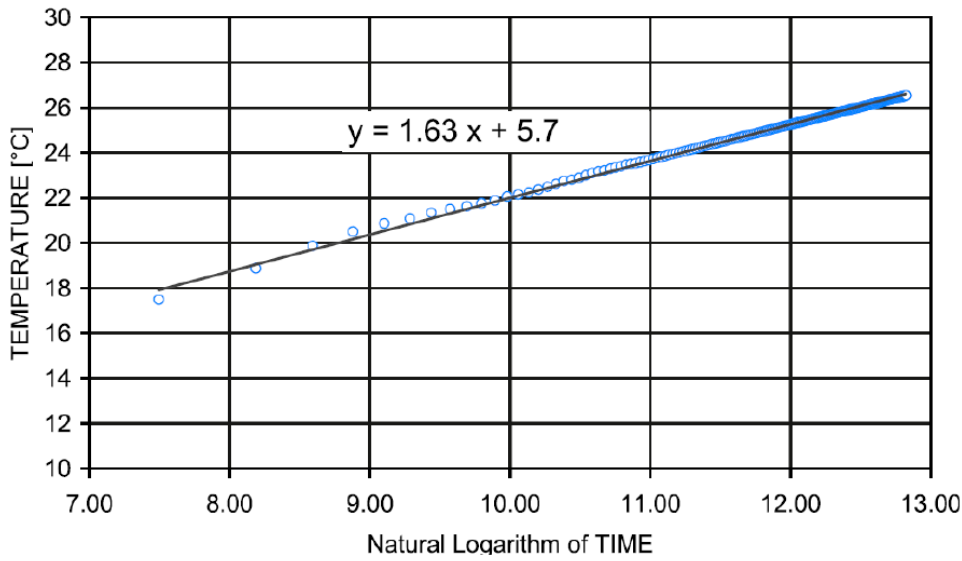


Figure 23: Example of average temperature trend against logarithm of time during GRT.

Analysis with the infinite line source method

Using the slope k of this linear equation and the constant power rate per unit length (q'), the thermal conductivity can be calculated by the following relationship:

$$k_{ground} = \frac{q'}{4\pi\lambda}$$

The GHE can be approximated by an infinite line source as proposed by Carslaw and Jaeger. The equation for the temperature as a function of time and radius around a line source with a constant rate of heat injection can be used as an approximation of the heat injection of a GHE:

$$T(r, t) = \frac{q}{4\pi\lambda} \int_{\frac{r_b^2}{4at}}^{\infty} \frac{e^{-u}}{u} du$$

Where: a thermal diffusivity [m^2s^{-1}], λ thermal conductivity [$\text{Wm}^{-1}\text{K}^{-1}$], r radius [m] and t time [s].

The fluid temperature is evaluated by replacing the unknown radius with the borehole radius r_b and adding the effect of the thermal resistance R_b between the fluid and the borehole wall:

$$T_{mean} = \frac{q}{4\pi\lambda} \int_{\frac{r_b^2}{4at}}^{\infty} \frac{e^{-u}}{u} du + qR_b + T_g$$

Conductivity is obtained by testing, using the ordinary least squares method. Whilst this method provides greater simplicity and less computational time, it neglects the axial heat transfer. This simplified approach can be used only for long boreholes with small diameters and to analyse long term thermal behaviour.

Cylinder Source Approximation

The cylindrical heat source method was first developed by Carslaw and Jaeger and can be used to consider a finite diameter. It represents an exact solution of an infinite cylindrical heat source placed in a homogenous domain representing the ground. The properties of the ground are assumed to be constant, the axial heat transfer is neglected and a perfect contact between the cylinder wall and the ground is assumed. The cylinder source model may be used by approximating the GHE as an infinite cylinder with a constant heat flux. The heat exchanger pipes are normally represented by an equal diameter cylinder. The cylindrical source solution for a constant heat flux is as follows:

$$T(r, t) = \frac{q}{k} G(z, p)$$

where:

$$z = \frac{at}{r^2}; p = \frac{r}{r_b}$$

The G function is defined through the Bessel functions of the first and second kind of order 0 and 1. The temperature on the borehole wall that is of interest as it is the representative temperature in the design of the GHEs, can be evaluated with this method. The fluid temperature is calculated by replacing the unknown radius with the borehole radius rb and adding the effect of the thermal resistance Rb between the fluid and the borehole wall:

$$T_{mean} = \frac{q}{k} G(z) + qR_b + T_g$$

The conductivity is obtained by trial, using the least squares method.

Numerical models

Numerical models can be used as an alternative to interpret the GRT. In these cases, all temperature values recorded during the GRT are compared to the trend of the calculated water temperature profile. An example of a possible result can be seen in figure 24 where a comparison between measurements and simulations has been made by comparing the return temperature (mass flow rate and outlet temperature are imposed).

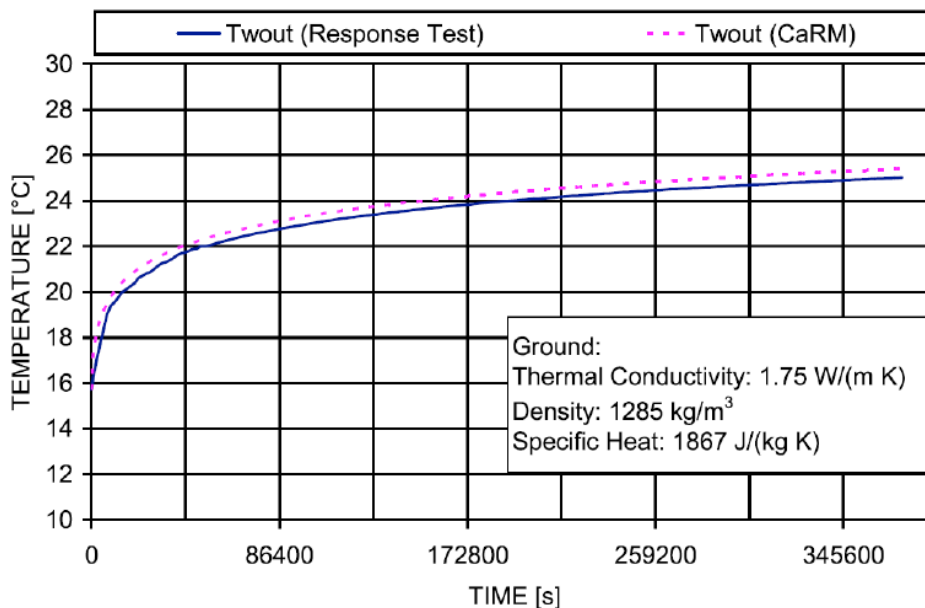


Figure 24: Example of analysis with a numerical method.

There are different processing methods: Finite Element Method (FEM), Finite Difference Method (FDM), or other numerical models. The first two calculation methods are very detailed but require a lot of calculation time. They are usually done in 2D to solve the problem with reasonable time consumption. When dealing with short probes, a 3D simulation is necessary due to the axial heat flow. Therefore, the calculation time increases considerably.

7.1.5 Thermophysical properties of GHEs materials

The thermophysical properties are parameters for the description of heat exchange phenomena based on Fourier's law. In the frame of this study, the ultimate purpose of the thermophysical properties of GHE materials is to evaluate and compare the thermal performance of different solutions and to allow advanced evaluations of the heat exchange mechanisms. The thermophysical properties of the material are normally measured in the laboratory with standard test methods. However, a specific setup such as a thin coating layer on bulk materials (e.g. the anti-corrosion coating applied on a carbon steel pipe) would require bespoke procedures. The main thermophysical properties that have been taken into consideration and then measured for the study of metal GHEs are thermal conductivity, specific heat, density and thermal diffusivity.

Specific heat measurement by Differential Scanning Calorimetry

The measurement of the specific heat was carried out using the Differential Scanning Calorimetry (DSC) technique. The DSC is an instrument consisting of two channels and a control and acquisition system. An apparatus (figure 25) provides a thermal stimulus to the two measurement channels, ranging between two extreme temperature values, at a constant speed and acquires the corresponding voltage signal, which is proportional to the difference in heat capacity between the two channels.



Figure 25: Differential scanning calorimeter with regulation and acquisition system.

The measurement procedure involves the execution of three distinct measurements: in the first measurement, defined as "baseline", the measurement channels remain empty: the corresponding signal is equal to:

$$S_e(T, v) = I(T) + k(T, v)\Delta C(T)$$

where:

T is the temperature in Kelvin;

v is the speed of the temperature ramp in K min^{-1} ;

$S(T, v)$ is the signal generated by the instrument in V ;

$I(T)$ is the signal due to the heat exchange between the measurement channels and the environment (V);

$k(T; v)$ is a conversion factor ($V K J^{-1}$);

ΔC is the difference in heat capacity between the two channels ($J K^{-1}$).

The second measurement involves the insertion, in one of the two measurement channels, of a known specific heat material, i.e. a synthetic sapphire. The latter constitutes the reference material for the measurement of specific heat according to the NIST (National Institute of Standard and Technology) standard. The generated signal is equal to:

$$S_s(T, v) = I(T) + k(T, v)(\Delta C(T) + m_s c_{p_s}(T))$$

where:

m_s is the mass of the a sapphire sample with known properties;

$c_{ps}(T)$ is its specific heat.

In the third measurement, the sample of material to be assessed is inserted into one of the two measurement channels; the corresponding signal is equal to:

$$S_x(T, v) = I(T) + k(T, v)(\Delta C(T) + m_x c_{px}(T))$$

where:

m_x is the mass of the unknown sample;

$c_{px}(T)$ is its specific heat.

Once the three measurements have been carried out, the specific heat of the specimen is given by the following relationship:

$$c_{px} = \frac{S_x - S_e}{S_s - S_e} \frac{m_s}{m_x} c_{ps}$$

Density

The density measurement was performed using the Archimedes principle, which states that "a body receives a thrust from the bottom up, equal to the weight of the displaced liquid volume".

In measurement procedure a scale was used, equipped with a device to measure the weight of a solid, both in air and immersed in water.

Density (ρ) is determined according to the following relationship:

$$\rho = \frac{m_a \rho_{fl}}{m_a - m_{fl}}$$

where:

- m_a it is the weight of the sample in air;
- m_f is the weight of the sample immersed in the fluid;
- ρ_f is the density of the fluid.

Thermal diffusivity

The thermal diffusivity α is the ability of a material to transfer the heat more or less quickly. The measurement of the thermal diffusivity can be done with different techniques. The method most commonly used is the so-called "flash method", as originally proposed by Parker et al.. Starting from the measurements of thermal diffusivity, specific heat and density, the thermal conductivity is obtained from the following relationship:

$$\lambda = \rho \alpha c_p$$

where:

- λ is the thermal conductivity;
- ρ is the density;
- α is the thermal diffusivity;

Laser flash method (Parker's method)

The measurement of thermal diffusivity along the thickness of the material was performed with the "Laser Flash" technique, according to the procedures provided for by the ASTM E-1461 standard. Thermal conductivity can be derived from thermal diffusivity. The mathematical model that describes the heat conduction problem of the Laser Flash Method (LFM) is well known for the case of a slab of thickness L . Choosing the LFM transmission setup, a heat flux is applied on the front face of the specimen and the temperature is measured on the back. The boundary conditions are a

pulsed heat flux of finite duration th on the front side of the specimen and a heat exchange with the environment, that is described by the Newton linear law (fixed heat exchange coefficient and reference ambient temperature), on the back side of the specimen. This method consists in heating the front surface of the sample with a very short laser pulse (2 ms); at the same time, an infrared detector acquires the temperature trend of the opposite surface. The sample consists of a disk with a diameter of 15 mm and a thickness of 1-2 mm. The temperature profile over time on the back face of the specimen is given by the following:

$$T(t) = \frac{Q}{h} \sum_{i=1}^{\infty} \frac{2 \sin \mu_i}{\mu_i + \sin \mu_i \cos \mu_i} \left[\exp \left(-\mu_i^2 \frac{\alpha}{L^2} (t - t_h) \right) - \exp \left(-\mu_i^2 \frac{\alpha}{L^2} t \right) \right]$$

where:

Q is the power of the thermal impulse released by the laser [W m^{-2}];

- h is the heat exchange coefficient [$\text{W m}^{-2} \text{K}^{-1}$];

- α is the thermal diffusivity [$\text{m}^2 \text{s}^{-1}$];

- L is the thickness of the specimen [m];

- t is the time [s];

- th is the duration of the impulse [s];

- μ_i is the solution of the transcendental equation $\mu_i \tan \mu_i = Bi$;

- $Bi = (h * L) / \lambda$ is the Biot number (dimensionless);

- λ is the thermal conductivity [$\text{W m}^{-1} \text{K}^{-1}$].

The model of equation above depends on some known parameters, such as acquisition time and pulse duration, and other unknown ones, expressed by the following vector P :

$$P = \{p_1, p_2, p_3\} = \left\{ \frac{Q}{h}, \frac{\alpha}{L^2}, Bi \right\}$$

The iterative procedure modifies the parameters of the P vector in order to minimize the difference between the experimental data and the model. Once this condition is reached, the parameter $p_2 = \alpha / L^2$ is determined. Consequently, once the thickness of the specimen is known, the thermal diffusivity α is obtained.

7.1.6 Finite element method

Measurements of thermophysical properties were also critical in providing reliable input data to power numerical modelling to understand the interaction between GHE material, GHE design, geological and hydrogeological context and their effect on heat exchange under different conditions. The Finite Element Method (FEM) is a standard method for numerically solving differential equations resulting from engineering and mathematical modelling. Typical fields of application include structural analysis, heat transfer, fluid flow, mass transport, and electromagnetic potential. To solve a problem, FEM breaks down a large system into smaller and simpler parts which are called finite elements. This is achieved through a particular discretization of the space in the dimensions of the space, implemented through the construction of a mesh of the object: the numerical domain of the solution, which has a finite number of points. Finally, the formulation of the finite element method of a boundary problem results in a system of algebraic equations. The simple equations that model these finite elements are then assembled into a larger system of equations that models the whole problem. The FEM then approximates a solution by minimizing an associated error function by calculating the variations. The study or analysis of a phenomenon with FEM is often referred to as finite element analysis (FEA). It is observed that these methods do not provide the analytical solutions of problems, but only the numerical values in the domains of the solution.

7.1.7 Non-destructive evaluation of corrosion and joint tightness by active infrared thermography

Infrared thermography basics

Today, infrared thermography (IRT) is a standard method for non-destructive testing and evaluation (NDT&E) of materials and structures (Maldague et al., 2001). The terms infrared thermography encompass the processes and equipment that enable the measurement of infrared radiation emitted by a body and its conversion into a temperature value. The term “thermography” emphasizes the fact that typical sensors

are cameras that can produce images (called thermograms) of the observed objects. A fairly complete and formal definition is as follows: IRT is a non-destructive, non-intrusive, and non-contact technique that allows the mapping of thermal patterns of a surface. Infrared thermography is a tool that has now become widely used for the non-destructive evaluation of hydraulic components. This is especially true for passive thermographic techniques, they can be easily applied on site thanks to their contactless and non-invasive nature. However, the information content is often lower than what could be obtained from the application of active techniques.

Active infrared thermography

Active thermography is an imaging procedure for non-destructive material testing. A heat flow is induced by an energetic excitation of the test object, which can be done in a transmissive or a reflective setup. The resulting heat flow is influenced by interior material layers and defects. These inhomogeneities can be captured on the object surface by high-precision thermographic cameras. The additional application of different evaluation algorithms improves the signal-to-noise-ratio, which allows for detection of smallest defects.

Signal processing algorithms for thermal images.

Infrared thermography is currently a standard method for the thermal inspection of industrial components with a wide range of applications, including metallic and composite materials with non-planar geometries such as pipes (Laaidi et al. 2010; Cadelano et al., 2016; Amer et al. 2020). The typical experiment layout consists in a thermal camera that records the temperature evolution of a specimen when a thermal stimulus (e.g. flash, sinusoidal heating) is applied on it. The results are sequences of thermal images (figure 26).

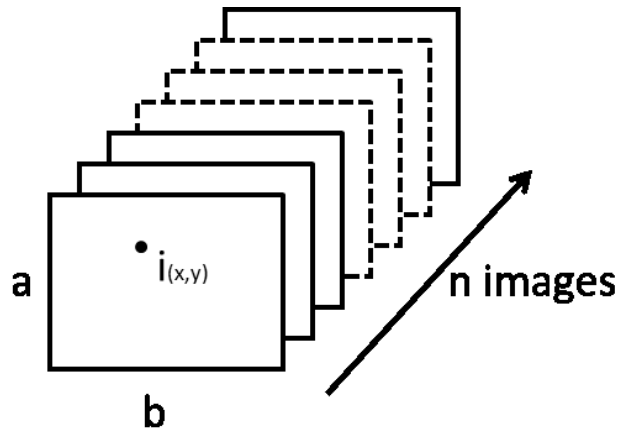


Figure 26: A sequence of thermal images represented as a three-dimensional matrix.

A thermal sequence of has size $a*b*n$ pixels, where $a*b$ pixels is the surface area under investigation and n is the number of images in time. The temperature profile of the i -th pixel, located in x,y coordinates, runs through the n images. The obtained sequences of temperature data are then analysed with different image processing algorithms, to help the operator discerning the defective areas from the sound ones. Relevant advances in the detectability of defects have been made in the recent times, thanks both to the improvement of the thermal sensors and to the introduction or refinement of data analysis methods. In the scientific literature, an extremely wide range of data processing algorithms is available and the thermographic operator should choose the most effective one for each kind of inspected specimen and testing procedure (Ibarra-Castanedo, 2005; Ferrarini et al., 2020; Tao et al., 2022). In this work, five algorithms have been applied to the acquired thermal sequences: correlated contrast (CT), principal component thermography (PCT), fast Fourier transform (FFT), the novel multiple sum average filter (MSA) and partial least squares thermography (PLST). All data have been imported in the Matlab environment where dedicated routines are available, such as IR view6 (Klein et al., 2008).

Correlated contrast

When dealing with thermal sequences of images, defects cannot always be observed directly on a single infrared image. For this reason some algorithms try to compress all the information into a single image, for example computing a correlation image. In Statistics correlation is interpreted as a relationship between two random variables such that to each value of the first corresponds with some regularity a value of the second one. Correlation should be applied very carefully, as it does not necessarily imply

causation. Experience has shown that it is nevertheless a powerful tool for the enhancement of small subsurface defects. As stated before, correlation needs a reference variable: for thermographic sequences the easiest solution is to choose the average of the temperature evolution of all the pixels, as this choice removes any human decision. The observed variables are the temperature values of each pixel in the sequence. The calculation of the correlation coefficients leads to a matrix with a wide range of values: to avoid this issue it is possible to compute the m^{th} root of the coefficients to lower the dynamic.

Principal Component Thermography

Principal component analysis (PCA) is a statistical procedure widely used for image processing. This technique uses orthogonal transformations to convert a set of observations of possibly correlated variables into observations of a set of linearly uncorrelated variables. The latter are called principal components and their number is less than or equal to the number of original variables. Principal component thermography (PCT) works like PCA and is based on the singular value decomposition (SVD), a method to extract spatial and temporal data from a matrix in a compact and simplified manner. The essence of SVD is to simultaneously provide the PCAs for both the row and column spaces. The singular value decomposition of a matrix $X \in \mathbb{R}^{p \times q}$, with $p > q$, is based on the equation:

$$X = USV^T$$

Fourier Transform

The data obtained from a thermographic experiment are temperature profiles in the time domain. Through the discrete Fourier transform (DFT) it is possible to analyse the data in the frequency domain:

$$F_n = \Delta t \sum_{k=0}^{N-1} T(k\Delta t) \exp\left(-\frac{i2\pi nk}{N}\right) = \text{Re}(F_n) + i\text{Im}(F_n)$$

where n is the frequency increment, Δt is the sampling interval and Re and Im are respectively the real and imaginary part of the transform. These are the basis for the estimation of the amplitude A and phase P :

$$A_n = \sqrt{\text{Re}(F_n)^2 + \text{Im}(F_n)^2} \quad P_n = \tan^{-1}\left(\frac{\text{Im}(F_n)}{\text{Re}(F_n)}\right)$$

The discrete Fourier transform is usually applied to a wide range of thermal testing and the analysis of the phase is of peculiar interest, as it is less influenced than the raw data by several parameters that could introduce undesired noise such as environmental reflections, emissivity variations, non-uniform stimulus.

Multiple Sum Average

The basic idea of the multiple sum average (MSA) algorithm is enhancing the temperature signal contained in the original thermal sequence, preserving the physical consistency. The first step is the creation of an averaged matrix M , where each pixel of each timed image is replaced with the average of its neighbouring pixels of the same timed image. After this it is possible to create a new image where each pixel is the sum, for every timed image, of the difference between the original temperature value and the average value, as shown by the following equation:

$$\text{MSA}_{i,j} = \sum_{t=1}^n X(t)_{i,j} - M(t)_{i,j}$$

where X is the original thermal sequence composed by n frames having width and height equal to a and b pixels. An advantage of this method is the possibility, as in correlation, to compress the information of a sequence into a single image.

Partial Least Squares Thermography

The partial least squares (PLS) method is a set of statistical procedures that have several areas of application, including chemistry, economics and neuroscience. The family of partial least squares methods include correlation, regression and path modelling techniques. From a thermographic standpoint, an interesting objective is performing a linear regression of the data matrix Y with a model matrix X. As in PCT, the original three dimensional thermal sequence must be reshaped into a two dimensional matrix, with a number of columns equal to the number of pixels of the image and a number of rows equal to the number of images of the sequence. In this way a B coefficient matrix could be obtained according to the least squares criterion, being E the residual matrix, as shown below:

$$[Y] = [X] * B + E$$

The choice of the model matrix X is related to the analysed experiment; in our thermographic application the proposed matrix is a polynomial of ninth order. The regression is performed in logarithmic scales, leading to the following equation:

$$\begin{bmatrix} \log(T_{1,1}) & \cdots & \log(T_{p,1}) \\ \vdots & \ddots & \vdots \\ \log(T_{1,n}) & \cdots & \log(T_{p,n}) \end{bmatrix} = \begin{bmatrix} 1 & \log(t_1) & \log^2(t_1) \cdots & \log^9(t_1) \\ \vdots & \vdots & \ddots & \vdots \\ 1 & \log(t_n) & \log^2(t_n) \cdots & \log^9(t_n) \end{bmatrix} * B + E$$

where $T_{h,k}$ is the temperature value at the image pixel $h(1..p)$ at time t_k .

7.1.8 Evaluating the corrosive attack on carbon steel GHEs in ground

Shallow geothermal systems are characterized by a substantial upfront cost for installation, so it is a fact that their diffusion and attractiveness on the market must leverage economic factors such as the payback time. The break-even point (i.e. when the ownership total cost and the total revenue as a result of saving on energy bills are equal) depends on the energy performance of the system. After reaching the break-

even point, it is critical to extend as much as possible the operative lifetime of the system in order to actually make profit of the investment. The expected lifetime of any geothermal system is limited and in most cases can be considered sustainable when it is over 30 years. When using carbon steel GHEs, the payback time is arguably reduced due to the thermal performance and low cost of raw materials, compared to stainless steel GHEs. Compared to plastic GHEs, the cost/performance trade-off should be considered on a case-by-case basis. However, the expected life of carbon steel GHEs may be limited by the occurrence of corrosion, so it is critical to evaluate this information as accurately as possible. At present, quantitative methods to evaluate the effect of corrosion on GHE are not common, since the state of the art is devoted to the qualitative evaluation of ground corrosivity on the basis of a number (variable according to each standard) of relevant parameters that describe the chemical-physical characteristics of the ground. In fact, none of them take into account the direct calculation of the penetration due corrosion rate per unit of time, for example millimetres per year, or loss of thickness or mass during the exposure period. Furtherly, none take in consideration the GHE materials, just limiting to the ground characteristics and geology.

Corrosion rate by gravimetric analysis

Despite the lack of specific methods for GHEs, there are standards for general engineering materials to quantitatively assess the corrosion rate associated to grounds in the laboratory (e.g. “ASTM G162-Standard Practice for Conducting and evaluating laboratory corrosion tests in grounds”) based on gravimetric analysis. This methodology has been applied and further improved to study the effect of some ground parameters on the corrosion rate of steel samples. The detailed presentation is given in “Themed topic chapter: Evaluation of the durability of metallic GHEs and the effectiveness of passive anti-corrosion measures”, subchapter: “Laboratory assessment of carbon steel corrosion rate of grout-less ground heat exchangers”.

7.1.9 References

- Amer, S.; Al Zarkani, H.; Sfarra, S.; Omar, M. Infrared Thermography Approach for Pipelines and Cylindrical Based Geometries. Polymers (Basel). 2020. <https://doi.org/10.3390/polym12071616>.

- American Society of Testing and Materials (ASTM). 1995. Annual Book of ASTM Standards, Designation D4972 - 95a: Standard Test Method for pH of Soils.
- AWWA C105 Standard for corrosion protection of Ductile Iron Pipe in aggressive environments.
- Binley, A., 2015. Tools and Techniques: Electrical Methods, Treatise on Geophysics: Second Edition. Elsevier B.V. <https://doi.org/10.1016/B978-0-444-53802-4.00192-5>
- Binley, A., Kemna, A., 2005. DC Resistivity and Induced Polarization Methods, in: Hydrogeophysics. Springer Netherlands, pp. 129–156. https://doi.org/10.1007/1-4020-3102-5_5
- Blanchy, G., Saneiyani, S., Boyd, J., McLachlan, P., Binley, A., 2020. ResIPy, an intuitive open source software for complex geoelectrical inversion/modeling. *Comput. Geosci.* 137, 104423. <https://doi.org/10.1016/j.cageo.2020.104423>
- Cadelano, G.; Bortolin, A.; Ferrarini, G.; Molinas, B.; Giantin, D.; Zonta, P.; Bison, P. Corrosion Detection in Pipelines Using Infrared Thermography: Experiments and Data Processing Methods. *J. Nondestruct. Eval.* 2016. <https://doi.org/10.1007/s10921-016-0365-5>.
- Cassiani, G., Bruno, V., Villa, A., Fusi, N., Binley, A.M., 2006. A saline trace test monitored via time-lapse surface electrical resistivity tomography. *J. Appl. Geophys.* 59, 244–259. <https://doi.org/10.1016/j.jappgeo.2005.10.007>
- Day-Lewis, F.D., Johnson, C.D., Singha, K., Lane, J.W.J., 2008. Best practices in electrical resistivity imaging: Data collection and processing, and application to data from Corinna, Maine.
- Ferrarini, G.; Bison, P.; Bortolin, A.; Cadelano, G.; Finesso, L. Performance Assessment of Clustering Algorithms for the Thermal Testing of Industrial Components.; 2020. <https://doi.org/10.21611/qirt.2020.124>.
- G162-99(2010). Standard Practice for Conducting and Evaluating Laboratory Corrosions Tests in Soils. In ASTM Book of Standards; 2004.
- Gehlin S. 2002. Thermal Response Test, Method Development and Evaluation. Doctoral Thesis 2002:39. Luleå University of Technology. Sweden.

- Gehlin, S. E. A.; Nordell, B. Determining Undisturbed Ground Temperature for Thermal Response Test. In ASHRAE Winter Meetings CD, Technical and Symposium Papers; 2003.
- Geotechnical test method gtm-24. 2015. Test method for the determination of ph value of water or soil by pH meter.
- Ibarra-Castanedo, C. Quantitative Subsurface Defect Evaluation By Pulsed Phase Thermography : Résumé. Time 2005.
- ISO 11357-4:2021(en) Plastics — Differential scanning calorimetry (DSC) — Part 4: Determination of specific heat capacity.
- Klein, M., Ibarra-Castanedo C., Maldague X., Bendada A. A straightforward graphical user interface for basic and advanced signal processing of thermographic infrared sequences.” SPIE Defense + Commercial Sensing, 2008.
- Laaidi, N.; Belattar, S.; Elbaloutti, A.; Jadida, E. Thermal And Thermographical Modeling Of The Rust Effect In Oil Conduits. In 10th European Conference on Non-Destructive Testing; 2010.
- Maldague X. P. 2001, Theory and Practice of Infrared Technology for Nondestructive Testing, John Wiley & Sons, N. Y.
- Maldague X., Jones T.S., Kaplan H., Marinetti S., Prystay M. (2001). Fundamentals of infrared and thermal testing. In Maldague K, Moore PO (eds.). Nondestructive Handbook, Infrared and Thermal Testing. Vol. 3 (3rd ed.). Columbus, Ohio: ASNT Press.
- Parker, W. J.; Jenkins, R. J.; Butler, C. P.; Abbott, G. L. (1 September 1961). Flash Method of Determining Thermal Diffusivity, Heat Capacity, and Thermal Conductivity. *Journal of Applied Physics*. 32 (9): 1679–1684. doi:10.1063/1.1728417. ISSN 0021-8979.
- Sanner, Burkhard; Hellström, Göran; Spitler, Jeff; Gehlin, Signhild (April 2005). Thermal Response Test – Current Status and World-Wide Application (PDF). *Proceedings World Geothermal Congress 2005*. CiteSeerX 10.1.1.702.2864.
- Tao, N.; Wang, C.; Zhang, C.; Sun, J. Quantitative Measurement of Cast Metal Relics by Pulsed Thermal Imaging. *Quant. Infrared Thermogr. J.* 2022. <https://doi.org/10.1080/17686733.2020.1799304>.
-

8 Themed topic chapter: Design of innovative coaxial heat exchangers for shallow geothermal

This chapter is dedicated to the development phases of new types of vertical coaxial heat exchangers that have the outer tube in metal. Moreover, such GHEs are compatible with the innovative drilling methodology developed within the EU Cheap-GSHPs and GEO4CIVHIC projects, that allows the metal pipes to be in direct contact with the ground. A variant of the same design, called the “well-point” type, has been extensively tested on site, together with the experimentation of different passive anti-corrosion measures.

Based on two manuscripts:

- L. Pockelé, G. Mezzasalma, D. Righini, F. Cicolin, G. Cadelano, A. Galgaro, G. Della Santa, M. De Carli, G. Emmi, A. Bernardi, 2020: H2020 Cheap-GSHPs Project: **Innovative Coaxial Heat Exchangers for shallow geothermal**, in: Proceedings World Geothermal Congress 2020, Reykjavik, Iceland, 24–27 October 2021, Contribution no. 29052, 2020.

The manuscript has been in published proceedings of World Geothermal Congress 2022. LP, DR, GC, AG designed the study; LP and DR developed the methods; GC, DS and GE collected the data. All the authors discussed the data and agree on their interpretation and wrote the manuscript. All the co-authors contributed to the final polishing of the manuscript.

- G. Dalla Santa, A. Galgaro, E. Di Sipio, G. Cadelano. Deliverable D2.6: **Adapted well point technique and subsequent field evaluation for the installation**. GEO4CIVHIC project, 06/04/2020.

The manuscript has been in submitted and approved by European Commission in the frame of GEO4CIVHIC project. AG designed the study; GC, G.DS and E. DS developed the methods; GC, G.DS and E. DS collected the data. All the authors discussed the data and agree on their interpretation and wrote the manuscript. All the co-authors contributed to the final polishing of the manuscript.

8.1 Innovative Coaxial Heat Exchangers for shallow geothermal

8.1.1 Abstract

One of the main innovations of the H2020 “Cheap and efficient application of reliable Ground Source Heat exchangers and Pumps” (acronym Cheap-GSHPs) research project, was the development of a coaxial ground source heat exchanger and drilling machine components to reduce the total installation cost using the piling method. These developments include the geometry of the heat exchanger, primarily a larger diameter and a co-extruded internal plastic pipe, to improve thermal extraction as well as the development of a drilling head combined with high pressure water injection to reduce the installation time. All these innovations, reduce significantly the installation costs in unconsolidated ground, especially when borehole stabilization measures are needed. The drilling machine remains small and compact since the installation method used requires much less power. A patent request has been filed in Italy (patent request n.102018000011157 of 17/12/2018).

The enlarged coaxial heat exchanger was installed at five demonstration sites using the new drilling machine components and installation methodology. Historical buildings are part of these demonstration cases supporting the applicability of this technology in this type of buildings. All sites are monitored and demonstrated important gains of thermal energy extraction rate under transitory operating conditions when compared to the state of art. The developments are being improved further as part of the on-going “Most Easy, Efficient and Low Cost Geothermal Systems for Retrofitting Civil and Historical Buildings” (acronym GEO4CIVHIC) H2020 research project. One of the objectives of this latter project is to improve the power of the drilling head and making the machine more compact to enable the cost-effective application of this installation method and the coaxial heat exchanger in retrofitted buildings in built environments and historical districts. This paper evaluates the yield obtained and the potential cost reduction of this novel heat exchanger combined with this innovative drilling technique. Cheap-GSHPs project has received funding from the European Union’s Horizon 2020 research and innovation program under grant agreement No. 657982. GEO4CIVHIC project has received funding from the European Union’s Horizon 2020 research and innovation program under grant agreement No. 792355.

8.1.2 Introduction

In closed loop shallow geothermal systems, the heat is exchanged between the building and the ground by means of Ground Source Heat Exchangers (GSHEs). These can be of different shape and length. Usually, a borehole with a diameter of about 15cm is drilled and one single-U or double-U probe is inserted. Then, the borehole is sealed with grout. The heat exchangers can be U-shaped, or in the coaxial configuration. In the latter case the tubes have different diameters and are inserted one into the other. The heat transfer fluid flows downwards in the annular space and upwards in the internal tube or vice versa. Coaxial GSHEs can be installed in two ways: drilling of a borehole and subsequently inserting the external and internal tubes followed by grouting or by piling the external tube into the ground and inserting the internal tube afterwards. One of the innovations in the Cheap-GSHPs project, is the development of a coaxial GSHE and related drilling machine using the piling technique. The AISI 304 steel pipes are piled into the ground by using a pile-driving machine with a roto-vibrating head. The aim is the reduction of the installation cost, thanks to the direct piling of the external tube without the use of a support casing in combination with a higher heat exchange rate thanks to the larger diameter and the direct contact between the coaxial external tube and the ground.

The history of developments of this methodology describes the state of art at the start of the project. The piling technique was developed to cut down the installation time and, therefore, the cost of drilling in unconsolidated ground. Usually in such undergrounds the traditional drilling technology requires the use of casings to avoid the collapse of the borehole and large amounts of water as drilling fluids to remove the drilling residues. These aspects lead to significant drilling costs. The starting point of the piling technique consists in the installation of stainless-steel tubes with a diameter of 50 mm as a new type of GSHE. These tubes fulfil a dual function as drilling rods and as geothermal pipes. The idea behind the installation technology is to drill directly with a stainless steel pipe that will become a part of the BHE using the piling technique. Hence, the new coaxial borehole heat exchanger is built with an external stainless-steel pipe to avoid corrosion problems and an internal plastic HDPE or PEXa pipe. The installation of coaxial steel GSHE's with the piling methodology was patented in Italy by TecnoPenta Sas in 2006. Following the original patent, Hydra Srl (a Cheap-GSHPs project partner) and TecnoPenta Sas obtained another Italian patent (patent number 0001398341), that covers the installation of this GSHE using the piling methodology with a vibrating head. The drilling machines were marketed under the name "Vibrasond" (figure 1). One of the objectives of this project is to achieve the installation of coaxial probes with an external diameter larger than 50 mm, in more difficult unconsolidated grounds to depths up to 100 m and with shorter installation

times. The development in the Cheap-GSHPs project consisted in designing and manufacturing a drilling head with rotation and vibrating functionalities as well as the use of small quantities of water injection through the drill bit during the piling operation. Both developments were tested in the field in Molinella (in the Po Plain, Italy), providing experience and learning for the installations in the demonstration cases. This technique has been applied in 2 demonstration cases (Pikermi Attiki in Greece and Mechelen in Belgium) to evaluate the installation time and the heat exchange rate in different geological settings and building energy loads.



Figure 1: The newly developed drilling machine JOY 4 (left) and the “Vibrasond” machine (right)

It is generally known that using a fluid, such as water, facilitates drilling operations and is necessary in conventional drilling. Conventional drilling methods often use large quantities of water. The use of water in the installation of the coaxial GSHPs into the ground using the piling methodology is less common. However, the roto-vibro technique brings improvements either in a reduction of installation time and hence cost or by widening the application of the piling methodology in different ground types. The original Vibrasond technique did not use water due to the fact that the stainless-steel tube had to be closed for water recirculation during the heat extraction operation. The design of water nozzles as part of the project has allowed water to be used during the drilling operation and then to seal the nozzle assembly for the geothermal operation.

8.1.3 Rotating and vibrating machine head for penetrometers

Drilling head improvements

The first improvement is the development of a rotating and vibrating machine head. The combination of vibration, rotation and downward push, allows the installation of probes of larger diameters (60-80 mm) to be installed in more types of grounds than with the Vibrasond technique that used only vibration. The drilling unit manufactured by HYDRA, is a stand-alone machine with four main elements: a frame, a power pack, a crawler and a mast (see figure 1). The newly developed drilling head, called Roto-Vibro head (RV1), combines the effect of rotation with the effect of vibration. This unique head differs from the others since it is characterized by higher torque and low frequency in comparison to the previously used sonic heads. Such a solution was adopted as it is able to provide high torque to drill through harder material. The lower vibration frequencies produce less stress to the mechanical components but are still able to reduce the wall frictional forces especially in combination with a small flow of water. In addition, a low-cost drilling bit that remains in the borehole was manufactured on purpose; the design of the tip of the GSHE was completed in order to loosen the underground when the machine head is rotating. In more difficult grounds, a tri-lame or a tri-cone can also be deployed. A first series of tests was performed at the test site of Molinella (Italy) in order to compare the RV1 head performance using one or more of its functionalities. The lithological sequence is typical of a quaternary floodplain deposition environment, dominated by silt and silty clay deposits, alternated with sandy layers, as described in [1,2]. All the tests were carried out without water injection in order to stretch all the tests to their limit. The rods used had a length of 2m. Only one operator was used for all the operations. Each trial consisted of drilling 12 m and measuring the time required to achieve this depth. The average time reported below consists of the total drilling time, which means that the time includes the effective drilling time plus the rod handling and assembly time. Overall, about 40 % of the measured time comprises the drilling time and the remaining 60% of the time for the handling and assembly of the rods. The tests show significant improvement with the employment of vibration in the drilling operation. Moreover, the best results were obtained when the rotation was coupled with vibration. Figure 2 illustrates the percentage time drilling reduction for the different drilling head tested. In addition, the penetration capability test was carried out to understand the time needed to reach a depth of 48 m with the full capacity of the RV1 in real drilling conditions with 76mm rods. The drilling was carried out with the simultaneous effects of rotation, vibration and thrust. Water was injected during the test, with the following operating conditions:

20 lt/min and 90 bar of maximum pressure. During the test, a depth of 48m was reached in 53 minutes, including rod handling and assembly time. During the test a pushing speed of approximately 15 s/m was achieved whilst the time for rods handling was measured at approximately 45 s/rod. Only one operator was involved in the test (see Bernardi et al., 2019, Chapter 3).

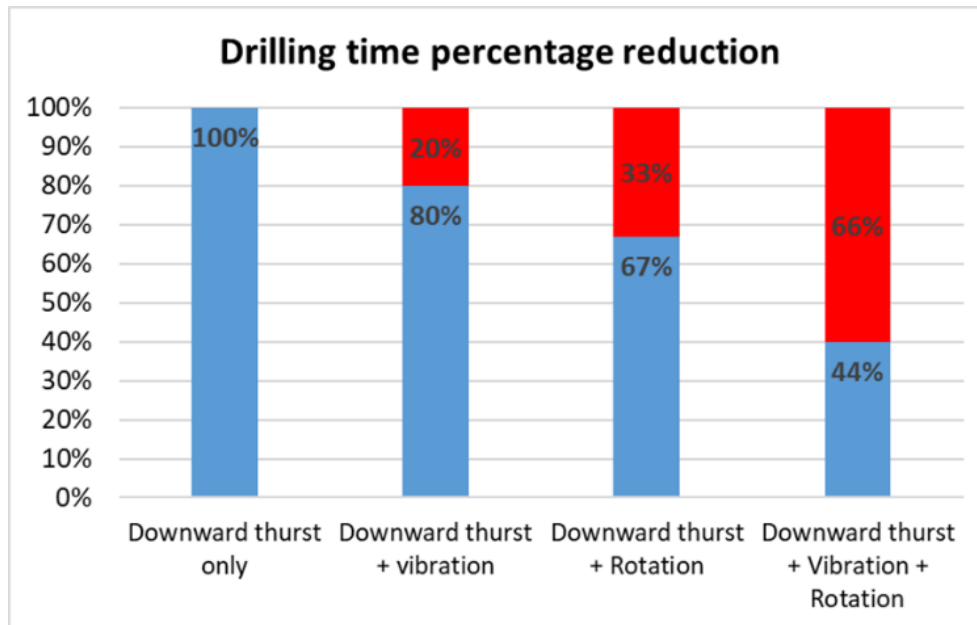


Figure 2: Drilling head performance comparison: time percentage reduction (from Bernardi et al., 2019).

The range of operation for this technique is unconsolidated ground such as sand, silt and clay. Usually, in such undergrounds the traditional drilling technology requires the use of casings to avoid the collapse of the borehole, large amounts of water as drilling fluids and disposal of the drilling residues. These lead to significant costs. The piling method is, therefore, cheaper and also less invasive than traditional methods.

Injection nozzle assembly at the tip of the coaxial GSHE

The second development concerns the design of a water injection nozzle integrated in the drill bit injecting water during the piling operation using a high-pressure pump. After drilling, the nozzle assembly needs to be sealed. Only small quantities of water are injected to loosen the ground and to decrease the friction on the walls of the stainless-steel pipe being piled into the ground. Finally, to increase the mechanical couple at the rotating drill bit an internal shaft has been connected to this drill bit. To

further improve the piling methodology performance, a high-pressure water injection system was designed. The water pump selected for the water injection is a Triplex pump. Conversely to the conventional drilling where the recirculation of water is characterized by high flow rates and low pressures to remove the cuttings, here the working conditions requires the flow to be set to c. 20 l/min and the pressure to be defined by the resistance of the injection system and the ground resistance that the water has to overcome. In fact, the objective is only to create a thin water layer on the tube outer surface that lubricates, as well as softening, weakening and displacing the unconsolidated ground at the tip of the probe. The water is injected within the internal rods through the drilling tip, where proper nozzles are installed. The design of the nozzle system needs to be able to allow water flow during the drilling activities and, once the desired depth is achieved, to close the tube in order to be used as heat exchanger. Three different nozzle designs were performed and, finally, the best design was chosen and optimized based on the results obtained in field tests (see Figure 3) [3].

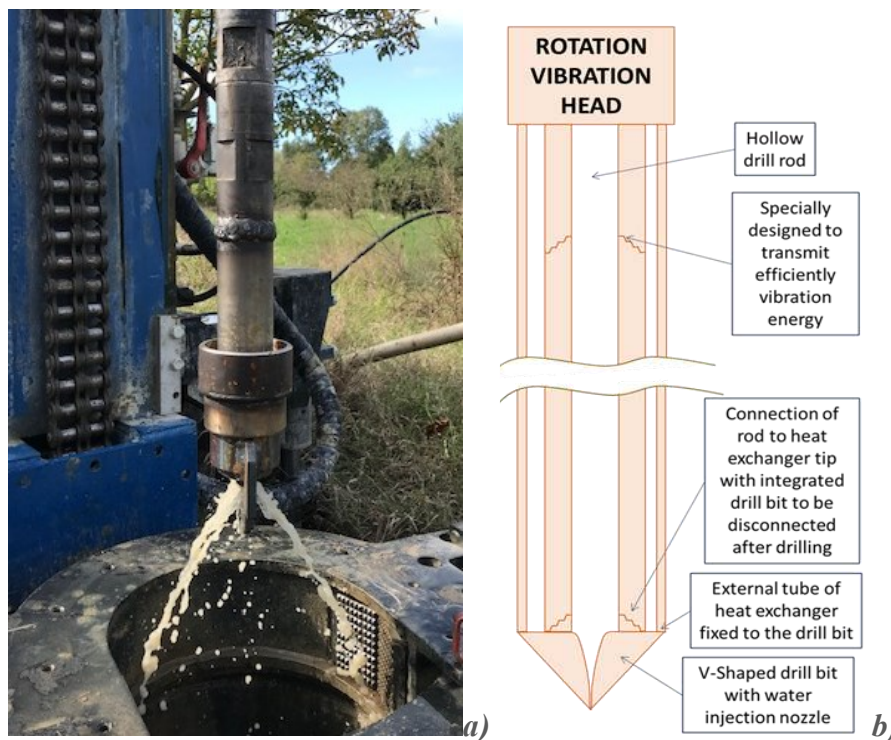


Figure 3: The drill bit (a), (b) one of the nozzles designed.

8.1.4 New inner and outer coaxial GSHE tube material

Different material options for the inner and outer tube of the coaxial GSHE have been studied based on their installation methodologies (traditional drilling of the well completed with sealing grout or piling technique). Several thermoplastic and metal

based materials have been investigated for their use as borehole heat exchanger (BHE) piping material. These include mild steel, galvanized steel, various coating options, stainless steel, copper and its alloys, aluminium, titanium, as well as reinforced polymers and other plastic materials including thermally enhanced polyethylene. The general assumption is that the BHE is installed into the ground by standard drilling which will disturb the natural underground conditions. The GSHE service life was estimated in function of their material characteristics, the installation methodology, the operating parameters and underground conditions. In addition, the length of a reference BHE for a 5 kW (thermal) heat pump used in a central European climate was estimated using the Earth Energy Designer (EED) software. The cost per geothermal kW of the coaxial BHE was evaluated using the sale price of pipes for the different materials examined. An internal pipe of HDPE of 32 mm in diameter with a cost of 1,38 €/m was used. As this exercise addresses the materials a typical drilling and grouting costs of 36 €/m was assumed to avoid the introduction of another variable. The results are reported in Figure 4.

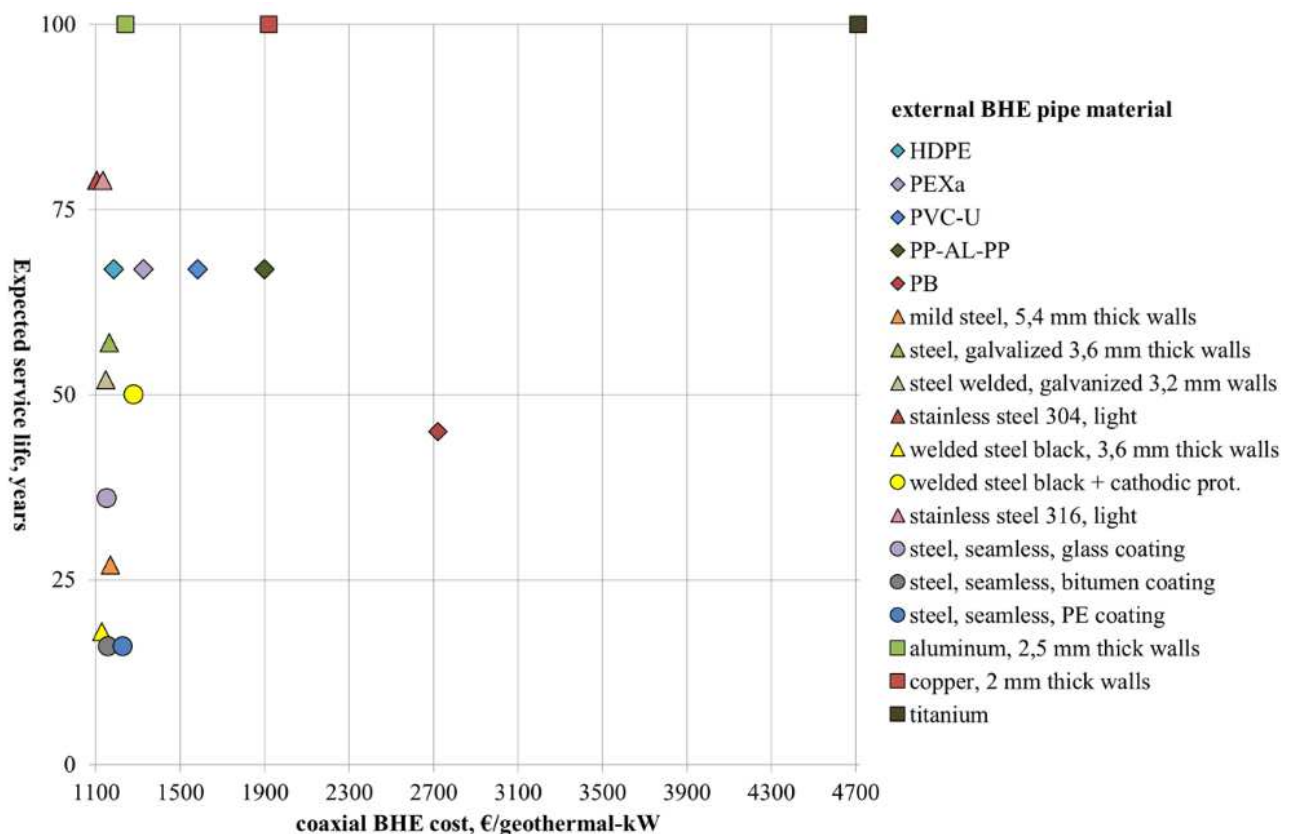


Figure 4: Expected service life versus coaxial BHE cost/geothermal kW extracted for moderate corrosive geologic formations and groundwater (pH 6,5 and resistivity 25 Ohm·m).

The effective borehole thermal resistances for each one of the cases presented in Figure 4 are presented in Table 1.

Table 25: Effective borehole thermal resistances of the BHE types considered in Figure 1.

BHE external pipe material	Outer diameter [mm]	Wall thickness [mm]	BHE length [m]	Effective Borehole Thermal Resistance, [(m·K)/W]
HDPE	63	3.8	118.5	0.1862
PEXa	63	3.8	121.3	0.1959
U-PVC	63	3.0	135.8	0.2452
PP-Al-PP	63	5.8	169.0	0.3586
PB	63	10.5	188.8	0.4266
Mild steel	60.3	5.54	103.6	0.1359
Steel, galvanized, seamless	60.3	3.6	105.5	0.1420
Steel, galvanized, welded	60.3	2.5	106.4	0.1453
SS 304L	60.3	2.0	107.0	0.1474
Steel, black	60.3	3.6	105.5	0.1422
Steel, black, cathodic prot.	60.3	3.6	105.5	0.1422
SS 316	60.3	1.5	107.4	0.1485
Steel, glass coating	60.3	2.9	106.1	0.1443
Steel, bitumen coating	60.3	2.9	106.6	0.1460
Steel, PE coating	60.3	2.9	112.7	0.1666
Aluminium	63	2.5	106.1	0.1443
Copper	64	2.0	106.4	0.1451
Titanium	73.02	3.05	104.7	0.1393

Thermoplastics and coated metals cannot be used with the piling methodology. Thermoplastic materials cannot withstand the compression load during the piling operation. Galvanized metallic materials cannot be considered due to the risk of damaging the coating or the galvanized layer during the piling process [3]. In addition, due to the absence of grouting, the borehole resistance between the external metallic tube and the ground is significantly lower than that of convention grouted heat exchangers, thereby increasing the yield of the coaxial GSHE. From this analysis, stainless steel 304L has been found to be the materials of choice, having the lowest cost per extracted kW and service lives of at least 50 years. The ground conditions when using stainless steel as outer tube material need to be checked on a case by case basis. Many factors can influence metal corrosion in the underground, almost all related to the chemical and physical characteristics of the underground. These are the conductivity, the permeability, the pH or acidity and the water content. These factors are also correlated amongst them. In addition, the presence of sulphates and chlorides, biological agents and eddy-currents can have an important influence and may require protective measures. Where cathodic protection is required, a BHE cathodic protection layout using a Magnesium sacrificial anode or a BHE cathodic protection layout by imposed current anode can be considered. Commercially available special alloys or cathodic protection equipment needs to be considered to prevent corrosion if this is deemed necessary. Experience of these installations in Belgium and Italy have shown that when underground conditions are not particularly aggressive, stainless steel tubes have an acceptable service life. An insulated inner tube has been developed; the insulation of the inner tube should prevent the heat transfer fluid going up being cooled down by the colder fluid coming down through the external tube. Numerical simulations performed during the design phase showed that efficiency improvements are limited. In addition, the beneficial effect of using the insulated pipe is the velocity increase of the fluid at moderate flow quantities, which improves the convective exchange coefficient through the pipe wall. Because the insulated pipe has a greater thickness, it reduces the annular flow section and, at the same flow rate, the fluid velocity increases leading to an increase of the convective exchange. In conclusion, stainless steel is used to avoid corrosion problems whilst the internal pipe is a co-extruded internal plastic pipe (figure 5).



Figure 5: The external coaxial tubes and the internal pipe at the Molinella test site.

8.1.5 Demonstration sites and costs and heat extraction rates comparison

These Ground Source Heat Exchanger (GSHE), with a larger diameter and a co-extruded internal plastic pipe, have been installed in demonstration sites using the new drilling machine and the new installation methodology. All sites are monitored and demonstrated important gains of thermal energy extraction under transitory operating conditions when compared to the state of art. The results of this monitoring are discussed in more detail in next sections.

The efficiency increases from the larger diameters, from the inner tube developments and the shorter installation times with smaller machines favour this methodology in unconsolidated ground where casings are needed to stabilize the borehole. The enlarged coaxial stainless-steel heat exchanger was tested on site in Pikermi Attiki (Greece) and in Mechelen (Belgium) in order to consider different geological settings, climates and building thermal requests. The installation times were measured as well as the energetic performances. The heat exchange capacity was measured by Thermal Response Tests performed both on the coaxial probes as on the traditional ones. Thermal energy meters were installed on each coaxial heat exchanger and on the double-U's [4] to measure the extracted energy during the different cycles of the heat pump.

Demonstration site: residential eco-house in Belgium

In Mechelen (Belgium) the demonstration building was a two story single-family house, with a total surface area of 170 m² and a 12 kW geothermal heat pump. It is a NZEB building with a wooden structural frame and 35 cm thick pressed straw bale walls. A chalk render protects the straw bales from the rain and a clay internal render provides breathing functionalities. The windows are triple glazed filled with Argon. The building is equipped with radiant floor and ceiling panels. 6 BHE's are installed down to 78 m depth: 2 double U's, 2 coaxial with diameter of 50 mm and, finally 2 coaxial of 76 mm (one with an insulated internal tube). The geological context is characterized by the presence of the over-consolidated Boom clay. In this demonstration case the feasibility of the piling method in hard clay layers was proven at rates of 1-2 meters/min. The thermal response tests confirm (figure 6) the lower borehole resistance of the steel coaxial BHE's compared to double U's. The borehole resistance of 0,076 for double U's fits very well with the average values found in that region with GRT tests. By integrating the surface area under the energy extraction curves, the thermal energy meters demonstrate up to 20% higher energy extraction rates during heat pump operation cycle when compared to the double- U's.

Table 2: Specification of GHE installed at the demonstration site in Belgium.

BHE	Borehole resistance (K/Wm)	Thermal Conductivity (W/mK)
Coaxial 76 mm w/insulated	0.036	2.06
Coaxial 76 mm w/o insulated	0.061	2.27
Double U	0.076	2.16
Coaxial 50 mm	0.048	2.31

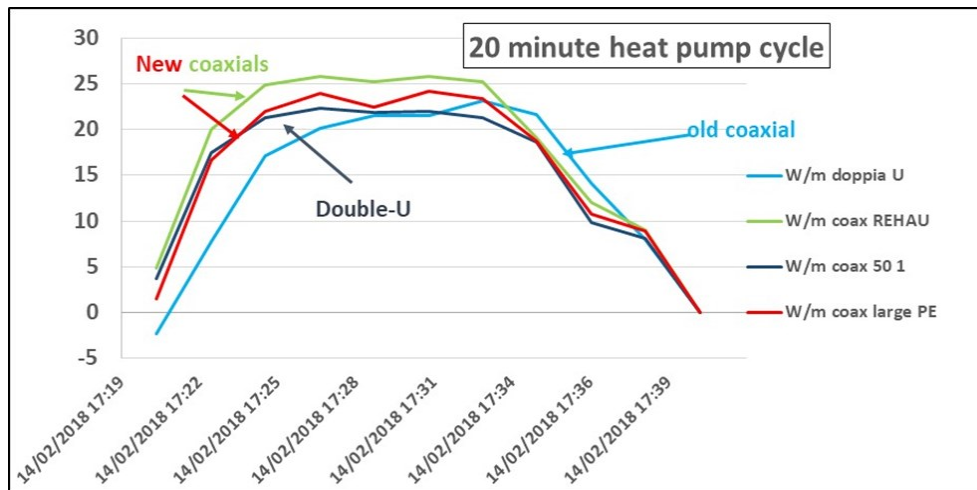


Figure 6: The performances measured at the demonstration site in Belgium. (image from Cheap-GSHPs Training manual)

Demonstration site: Bioclimatic office building in Pikermi Attiki in Greece

This is a NZEB building constructed in 2001, that integrates several renewable energy technologies. The ground source heat pump produces 21 kWth of heating at 45°C and 16 kWth of cooling at 10°C. The tested bore field is composed by 4 BHEs (single-U, double-U, coaxial, spiral) & open loop doublet. The site has a real time monitoring system that displays online all the thermal and energetic parameters, graphs and calculations allowing user friendly assessment of the demonstrated systems (see the project homepage of Cheap-GSHPs [5]). Also in this case the stainless steel coaxial BHE shows to be very high energy output (equal to 2.643 W/mK), low borehole thermal resistance (equal to 0.050mK/W) and low cost per kWth of geothermal yield [6]. Compared to the double U probe, coaxial probes reached a 30 % higher yield (80-100W / m compared to 50 W / m) during the operational phase of the heat pump in heating mode.

8.1.6 Conclusions and further developments

The developments in the geometry and composition of the coaxial heat exchanger improve the thermal exchange yields. The monitoring data of the instantaneous energy exchange with the ground support this fact as explained in paragraphs 3.1 and 3.2. The drilling head developments and the use of high-pressure water injection reduce the installation time as shown in figure 2. In the demonstration cases this increased rate of

penetration and avoiding the need to consolidate the borehole with a casing results in a reduction of installation times in the order of 30 – 50 %. A patent request has been filed in Italy covering the above described improvements of the drilling method (patent request n.102018000011157 of 17/12/2018). Despite the limitation of this technique that can be applied primarily in unconsolidated ground such as sand and clay the following advantages have been confirmed within the Cheap-GSHPs project and further developments within the GEO4CIVHIC project will further enlarge its field of application: (I) The external tube is in tight or direct contact with the ground and this leads to the reduction of the borehole resistance (R_b). In addition, the use of stainless steel with its high thermal conductivity ($\approx 16 \text{ W/(m K)}$) enhances the heat exchange between the underground and the probes. The heat exchange rate has been shown to be up to 30% higher with respect to a traditional Double-U in transient operating mode (figure 6). (II) The use of the piling methodology removes the need for grouting the borehole, resulting in substantial savings in terms of time, complexity and cost of the heat exchanger installation. This technique also avoids all the common operations of drilling with rods and casing, saving in rod handling time due to the fact that the stainless steel rods remain in the borehole and are then used as heat exchanger. Thus, we get a faster installation in grounds that usually require the use of casings. (III) The higher installation speed and the better thermal exchange with the ground lowers the total installed cost with 20-30 % compared to state of art in unstable ground conditions where the use of a stabilizing casing is necessary. Therefore, shallow geothermal technology could gain market share in several markets where prices today are in the order of 40 – 50 €/m and become more competitive against other renewable energy based heating and cooling systems like air to water heat pumps. (IV) The installation method requires a lot less power to displace the ground than required by removing the grounds. Smaller, less capital intensive drilling machines and ancillaries can be used whilst the method is also much less invasive. In conclusion, the potential cost reduction of 20 -30 % has been confirmed, in several demonstration cases for situations where the borehole needs to be supported by casings and/or where the market competition is not well developed. In situations where the ground is sufficiently stable to avoid casings and where the market is very competitive and mature, this methodology is able to match the state of art costs but with a less invasive and more compact drilling rig. The velocity of installation, compactness of the drilling machine and high energetic performance make this technology particularly interesting for the application to historical buildings. For this reason, this technology conceived within the Cheap-GSHPs project is the starting point for the further developments and optimizations foreseen within the EU funded project GEO4CIVHIC that aims at applying the shallow geothermal technology in retrofitted buildings and historical buildings in built environment.

Aknowledgments

Cheap-GSHPs project has received funding from the European Union’s Horizon 2020 research and innovation program under grant agreement No. 657982. GEO4CIVHIC project has received funding from the European Union’s Horizon 2020 research and innovation program under grant agreement No. 792355.

8.1.7 References

1. Galgaro, A., Dalla Santa, G., Cultrera, M., Bertermann, D., Mueller, J., De Carli, M., Emmi, G, Zarrella, A., Di Tuccio, M., Pockelé, L., Mezzasalma, G., Psyk, M., Righini, D., Bernini, M., Bernardi, A: EU project “Cheap-GSHPs”: The geoexchange field laboratory. *Energy Procedia*, 2017, 125, 511–519. <https://doi.org/10.1016/j.egypro.2017.08.175>
2. Zarrella, A.; Emmi, G.; Graci, S.; De Carli, M.; Cultrera, M.; Dalla Santa, G.; Galgaro, A.; Bertermann, D.; Muller, J.; Pockelé, L.; Mezzasalma, G.; Righini, D.; Psyk, M.; Bernardi, A. Thermal response testing results of different types of borehole heat exchangers: an analysis and comparison of interpretation methods. *Energies* 2017, 10, 801, <https://doi.org/10.3390/en10060801>
3. Mendrinos, D., Katsantonis S., and Karytsas C. Review of Alternative Pipe Materials for Exploiting Shallow Geothermal Energy. *Innovations in Corrosion and Materials Science*, 2017, 7, 13-29
4. Bernardi, A. and all the partners of Cheap-GSHPs EU Project: Cheap and Efficient Application of Reliable Ground Source Heat Exchangers and Pumps – Technical Manual of Cheap-GSHPs EU project (English version). 2019
5. Horizon 2020 project Cheap and efficient application of reliable ground source heat exchangers and pumps. <http://cheap-gshp.eu/>
6. Capozza, A.; De Carli, M.; Zarrella, A. Design of Borehole Heat Exchangers for Ground-Source Heat Pumps: A Literature Review, Methodology Comparison and Analysis on the Penalty Temperature. *Energy Build.* 2012. <https://doi.org/10.1016/j.enbuild.2012.08.041>.

8.2 Adapted well point technique and subsequent field evaluation for the installation

8.2.1 Abstract

For construction sites where deep well dewatering is not suitable, the well point dewatering system is an effective and economical way to reduce the level of the water table to below the required excavation level. The well point system is constituted by a series of tubes inserted into the ground at a distance of about 6-8m, all around the excavation area. Usually, after their utilisation, the well point systems are removed from the ground and the equipment can be exploited for new installations. The basic idea developed in the Task 2.6 is to exploit the well point systems by maintaining and adapting the equipment in order to develop shallow coaxial heat exchangers linked to a ground source heat pump as a closed loop system.

In addition, given that the basic idea is to re-use an installation already used in the building site, the adaptation of the well point system was supposed to be very cheap and suitable to be applied in the urban areas, also thanks to the limited dimensions of the excavation machines used. Nevertheless, the length of these probes is very limited (down to about 10 m), therefore it is necessary to check the real energetic performances and benefits of this kind of installation by testing it. For this reason, a pilot site was foreseen at the CNR – ISAC premises in Padova (Italy) where the well point installation provide heating and cooling to a testing building by means of two Heat pumps. The system is completed with a dedicated monitoring system, in order to evaluate the energetic performances of the tested ground heat exchangers.

During the development of the Task, first of all we performed a general survey about the diffusion of the well point systems in all the countries around Europe (each partner in its Country), and about the most used materials, geometries (diameters, depth of installation) and installation techniques (type of ground, size of the machines, costs). This survey was performed in order to check the parameters affecting the installation of these kinds of GSHEs.

Based on the local stratigraphy, the simulations run by UNIPD-DII provided the sizing of the well point system by indicating the number, the length and the geometry (external and internal diameters) of the co-axial probes, in order to provide the requested heat transfer between the ground and the building.

Currently, the pilot facility installation has not been completed due to several difficulties caused by the authorization processes provided by the local administration and to the coronavirus prohibitions to perform activities in building sites.

The heat exchangers are made of different materials (carbon steel and stainless steel) and treated with different methods, in order to test their thermal exchange performance and durability in terms of corrosion. The installation procedure applied will indicate the potentials and risks of this kind of installations in the urban context (to be used in Task 6.3 and in the market analysis Task 7.3).

The installation of this system at the pilot facility n.1 in CNR will provide data about its efficiency by means of a dedicated advanced monitoring system. In addition, while installing the heat exchangers in the pilot facility, the resolutions of the possible issues encountered during the installation help to achieve TRL 7.

8.2.2 Introduction

Description of the well point technique

For construction sites where deep well dewatering is not suitable, well point dewatering system is an effective and economical way to reduce the level of the water table to below the required excavation level.

In addition to lowering the groundwater table to facilitate a dry working platform, well points can also prevent groundwater build-up behind the shoring wall. Where applicable, this allows ground anchors to be installed in dry conditions. Well point dewatering can effectively draw the water table down to between 5 and 7 metres depending on pump selection and the ground permeability.

The well-point plant was born in 1901 in the United States and is now the temporary drainage system of the excavations in civil engineering most used, known and tested. This dewatering system is exploited more and more on urban areas, where there issues due to the limited space availability and the need to build underground civil structures, such as garages or other indoor spaces.

Drainage is produced by a battery of microwells (hence the name well-point, point well) put in lowered pressure by self-priming centrifugal pumps. These pumps have the ability to generate a pressure decrease in the pipelines to which they are connected. Schematically the well-point system consists of a series of microwells of 1", ¼", 1½" of diameter, to whose end a filter is screwed through which offtakes occur.

The microwells are connected through a flexible sleeve to an intake manifold and therefore to the pump that has the task of generating the pressure decrease inside the

suction pipes, which generates the acceleration and deviation of the groundwater flow towards the points of pumping, bringing the surface of the water to take the form of an inverted fan (influence cone) with the axis at each single well-point. The shape and geometry of the depression cone depend on the flow rate emitted, the duration of the pumping, the hydraulic conductivity of grounds.

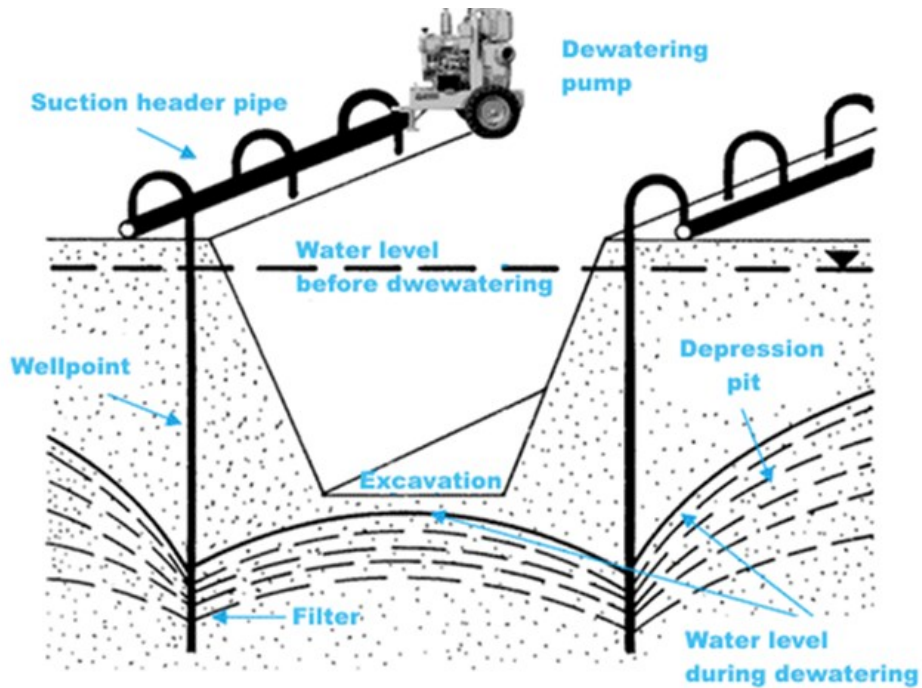


Figure 1: Schematic representation of the well-point system for dewatering.



Figure 2: On field well-point system for dewatering applied to a wide excavation

There are different kind of well point systems, with different diameters, length, filters and openings for the water. The choice depends on the geological setting of the area affected by the excavations. It is necessary to define the stratigraphic sequence, the physical characteristics of the grounds, the particle size analysis, the hydraulic conductivity of the coarse sediments (sands and gravel) and the groundwater flow. In addition, these characteristics also affect the operational choices to be used on site as the installation methodology. First of all, at the design stage, the discharge of dewatering has to be evaluated in order to correctly size the drainage system. In the case of well-point systems this means to establish the number of pumps to be served by the respective pumping system and the number and type of well-points to be installed around the excavation. The pump must have sufficient hydraulic performance to guarantee both the scope that was foreseen by the project and the adequate head to be able to extract the water from the ground and transfer it to the established delivery points. As regards instead the choice of the number of well-points to be used, it is possible to use a nomogram that allows, on the basis of the lowering of the pitch required by the project and on the basis of the types of existing land, to estimate the distance between the well-points.

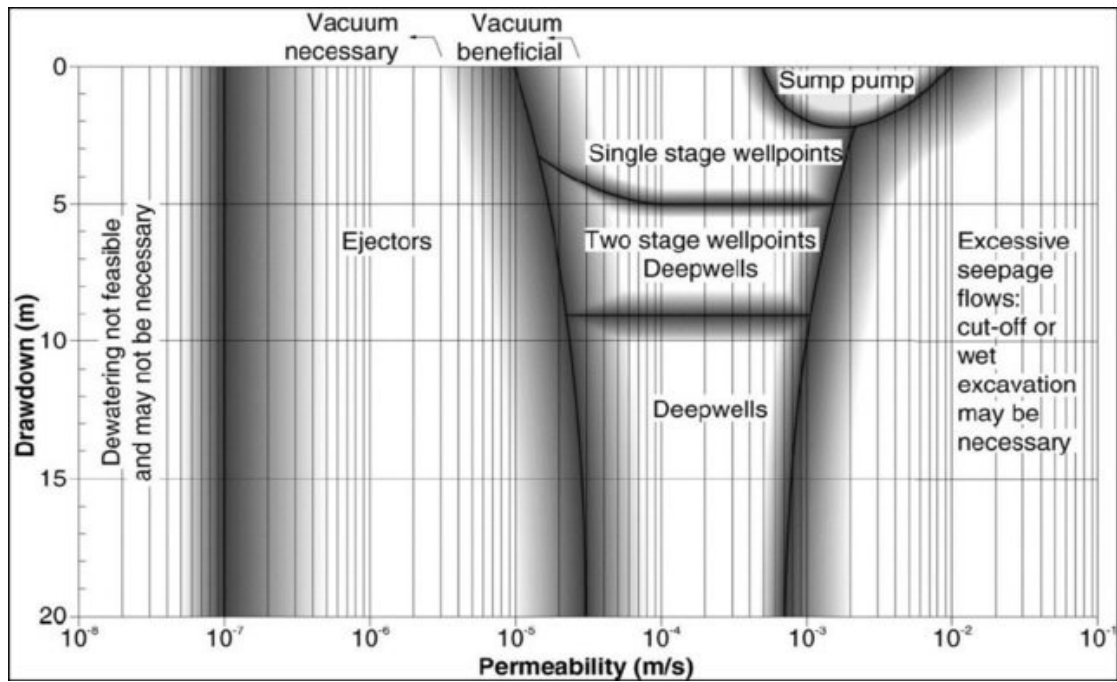


Figure 3: Schematic range of applicability of different kinds of well points systems (CIRIA C750, London 2016).

As stated, well point systems are most suitable in shallow aquifers where the water level needs to be lowered no more than 6-8 meters. Due to the vacuum limitation of the pump, excavations that are deeper will require multiple stages of well point systems or different technologies. Filters that are generally used with well-point systems are of two types: for sand and for gravel. Sand filters have a passage of 0.2 mm and are generally used in sandy or silty-clayey grounds. The gravel filters are from shorter length and are characterized by 36 holes with a diameter of 8 mm. With these types of filters the water pressure drops are extremely reduced and this entails a capacity of approx. 50% higher suction than a classic sand filter.



Figure 4: The filter usually used for gravel grounds.

As for the arrangement of the well-point systems on site, this depends on the type of excavation that must be done. For example, in the context of a foundation excavation, the plant is arranged along the perimeter of the work area, constituting a hydraulic barrier that intercepts the flow of the groundwater, depressing its level. The alignment of the microwells is generally arranged at about 1.0 m of distance from the upper edge of the excavation. As far as the depth of the filter is concerned, in order to create the depression cone which allows the execution of the works in drained conditions, this is generally positioned to at least 1.5 m below the bottom of the excavation.



Figure 5: Example of well point dewatering system around an excavation for building foundation.

The installation of well-point systems is often executed manually, but can be performed even with a drilling machine. The well-point installation process involves the injection of pressurized water (4-5 bar) into the lifting and then to the filter. The sphere located on the tip of the filter moves due to the jet effect, allowing water to flow out of both the tip and the filter. The jet of water removes the ground in a sort of core destruction drilling, partially bringing it back to the surface. The removal of the material favours the self-sinking of the well-points up to the depth at which it was decided to place the filter. Once the pressure in the microwell is decreased, the sphere placed on the tip of the well-point blocks the access of the water from the terminal part of the filter allowing it the entrance from the filter walls only. In case of fine-grained grounds, the installation of well-points is preceded by the construction of a cylindrical, vertical, sand drain. After drilling the grounds, the microwell is placed inside the hole, making at the same time a very light wash to remove the fine material, if necessary, deposited on the walls. At the same time, coarse sands rise to constitute a vertical drain immediately

behind the filters while the finer fraction is at a greater distance from the pumping point.

8.2.3 Investigation survey about the use of the well point across Europe

In order to understand how much the well point technique is actually applied in Europe, all the partners that are expert in drilling operations have been involved in an investigation survey about their country. The following Table 1 shows the obtained outputs.

Table 1: The outputs obtained by the survey among the partners.

	GERMANY	SPAIN	BELGIUM	GREECE	SWITZERLAND	IRELAND	ITALY	ROMANIA
material	PVC-U steel (possible longer with submerged pumps BUT expensive)	Concrete Metallic PVC PE	PVC or only a hole	Steel Stainless steel PVC-U	-	uPVC	Steel PVC	1. Ground is very hard → difficult to penetrate 2. underground water table usually lower than 6m
Length [m] (usual)	2.5m or 15.0m	5-10 (5)	5-40 (10)	3-6 (4)	4-10 (7)	3-20 (3-10)	2-6 (5+0,6)	
Diameter [mm]	150-300	125-200 (150)	100-250 (150)	70-89 (75)		30-75 (54)	25-76 (25)	
Length of the slotted part [m]	1-2			1-6	1-1.5	1.5-3	2-6	
Distance between tubes [m]		3-5	5	5	1,2	6-10	1.5	
Diffusion	NOT USED AS STANDARD METHOD	USED WHEN HIGH WATER LEVEL	USED VERY OFTEN IN FIANDERS	NOT VERY COMMON	RARELY USED	NOT SO COMMON	HIGHLY DIFFUSED IN THE WHOLE NATION	NOT USED AT ALL

The obtained outputs point out that only in Spain, in the Flanders (Belgium) and Italy (in particular in the Po Plain) the well point technique is widely diffused, while in the

other countries is not so common. Obviously, it depends on the geological setting: given that the prior application is the lowering of the water table, this technique is applied in the low-plain geological context, where the water table is very close to the surface (1- 2 m) and shallower layers mainly consist of deposits of sands and silts and, more rarely, of gravel. In addition, the sediments have to be loose and not too hard to insert the well points with the techniques usually used.

8.2.4 The pilot site

In order to test the practical feasibility of the reuse of the well point system and test its energetic performance, a pilot site has been engineered. The pilot site is located in Padova (Italy) at the National Research Council premises, in Corso Stati Uniti. Figures 6-7 depict the location of the pilot site (source: Google Maps).

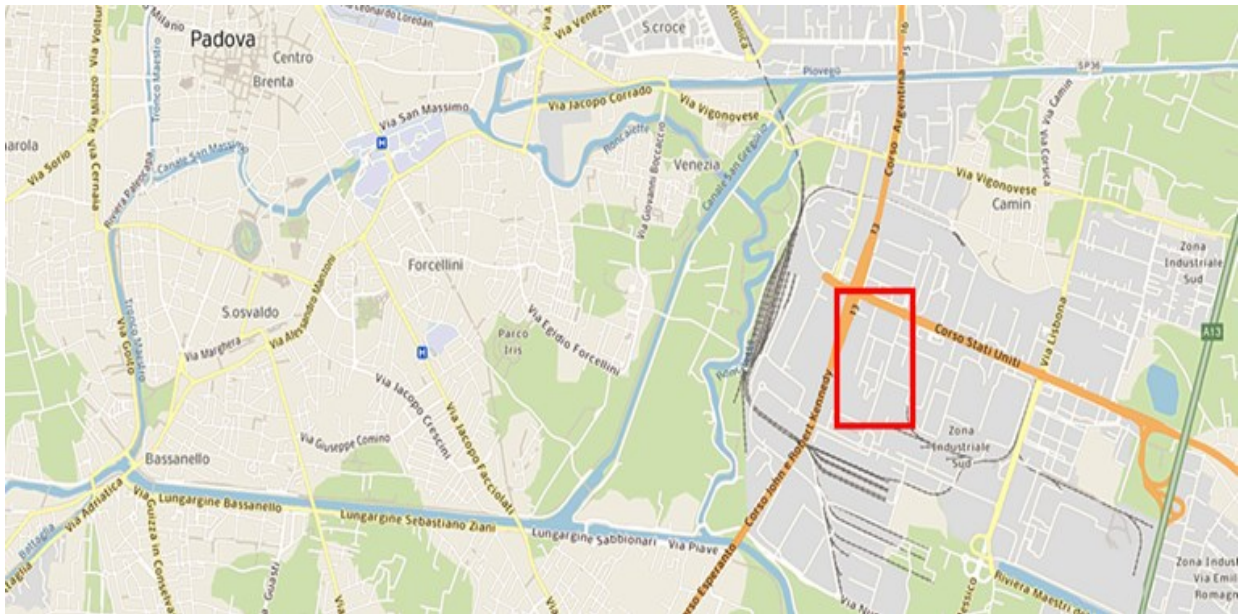


Figure 6: Overview of the location of the pilot site at CNR, Padova (Italy), Corso Stati Uniti.



Figure 7: Overview of the building of the pilot site at CNR, Padova (Italy), Corso Stati Uniti.

The local geological setting

Given that the city of Padova is located in the North East of Italy, in the lower part of the Po Plain, next to the Adriatic see (see Figure 8a), the local geological setting is the typical one of the low-plain areas. The local stratigraphic sequence is characterized in the shallower layers by silts and sands, as represented in Figure 8b. These data have been derived from previously available corings, represented in Figure 9.

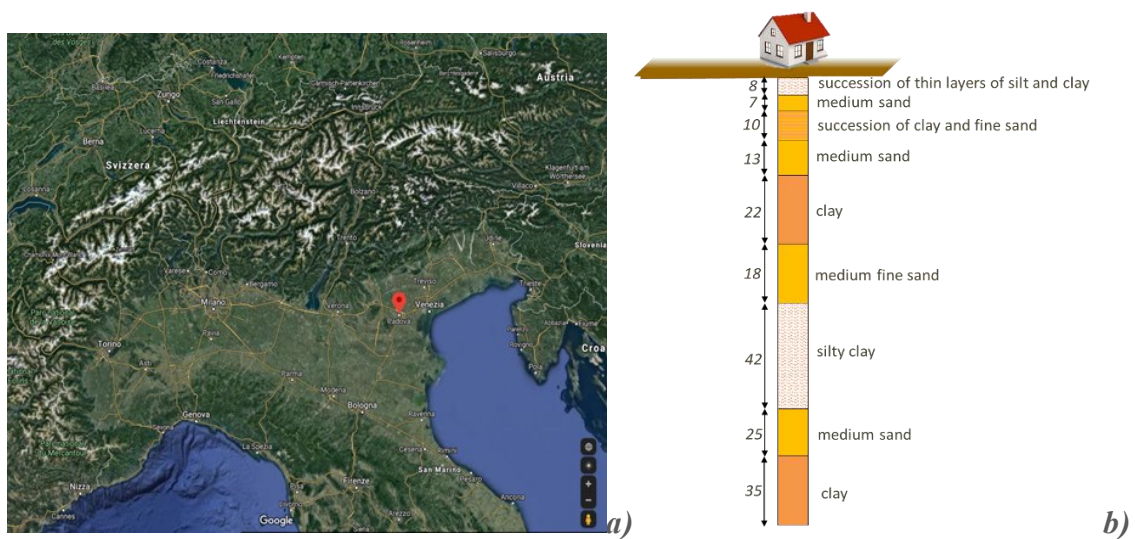


Figure 8: a) Overview of the location of the city of Padova in the Po plain and b) the schematic representation of the local stratigraphic sequence.

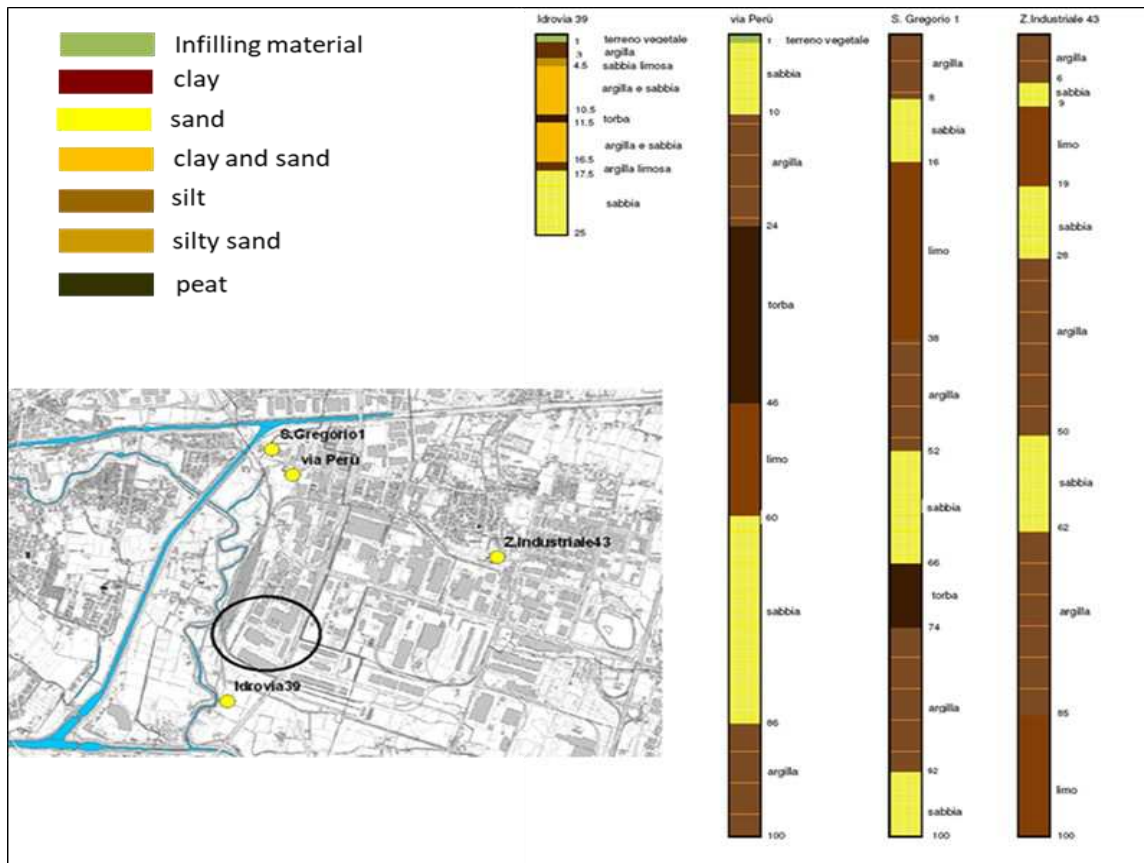


Figure 9: Available corings in the area.

With regard to the hydrogeological conditions (Figure 10), the local underground is inserted in the multi-pitch system of the low Venetian plain characterized by an alternation of permeable and impermeable levels. Therefore, there are free and pressurized aquifers. Generally, the groundwater flow could be considered from very shallow to modest groundwater flow. This aquifers system is recharged mainly from rainwater and indirectly from the contributions of the waterways present in the area.

The most shallow aquifer assumes a prevalent direction towards south-west. The underlying aquifers are mostly under pressure in mainly sandy aquifers, separated by impermeable clayey layers. In the area of Padova, the superficial aquifer has a depth of between 1.0-1.5 m from the ground, with a water table increase from the North-West to the South-East. The average oscillations of the aquifer are estimated as ± 1 m during the annual variations.

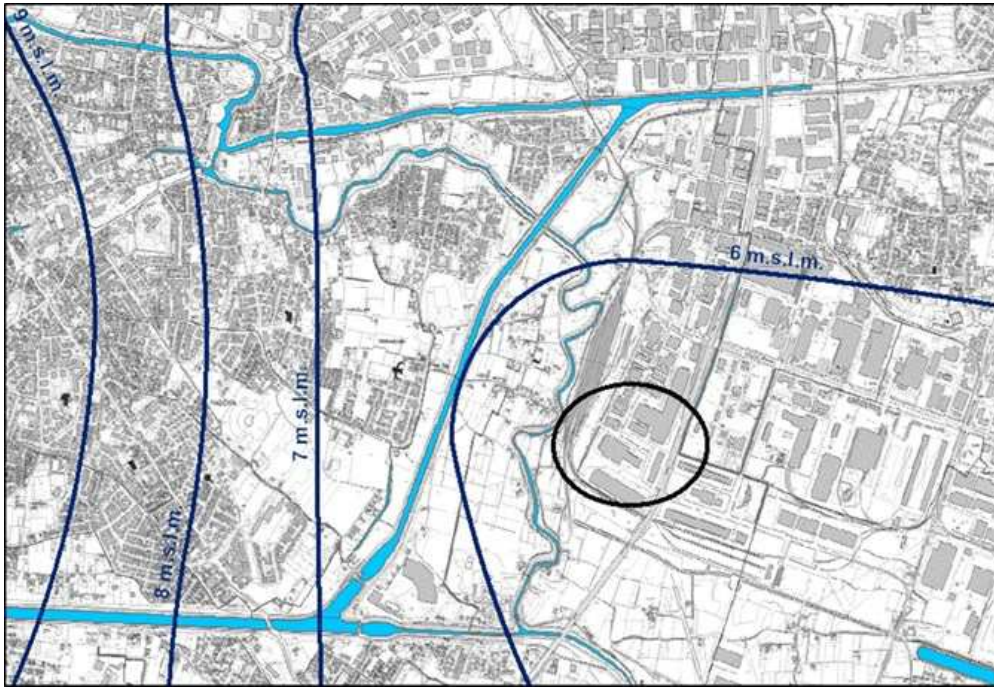


Figure 10: Local isophreatic map. The blue lines represent the medium isophreatic lines.

8.2.5 The modelling analysis

The modelling analysis of the system has been conducted by considering the use of a couple of heat pumps, one with the ‘inverter’ technology and the other ‘ON/OFF’.

The system is combined also with other 2 heat exchangers to be tested during the GEO4CIVHIC project, as it will be described in the Deliverables 3.5 ‘*First report on the results of pilot Facilities demonstration n.1 in Padua: performance of the plug & play solutions and of the adaptation of well point technique*’ and D 3.7 ‘*Second report on the results of pilot Facilities demonstration n.1 in Padua: performance of the novel co-axial heat exchangers*’. The parameters used for the underground are listed in Table 2.

Table 2: Thermal parameters for the sediment in the stratigraphic succession.

top	bottom	thickness	geological description	thermal conductivity W/(m*K)	specific heat MJ/(m³*K)	density (in 10³ kg/m³)
0	8	8	continuous succession of silts and clayey silt	2.50	2.8	2.2
8	15	7	medium sand	2.20	2.6	2.1
15	25	10	continuous succession of clay and fine sands	2.50	2.8	2.2
25	38	13	medium sand	2.20	2.6	2.1
38	60	22	clay	1.80	2.50	2.10
60	78	18	medium fine sand	2.20	2.6	2.1
78	120	42	silty clay	2.50	2.8	2.2
120	135	15	medium sand	2.20	2.6	2.1
135	160	25	clay	1.80	2.50	2.10
160	195	35	medium sand hosting aquifer	2.20	2.4	2

The modelling outputs provide the sizing of the well point system.

The actual tubes constituting the heat exchanger have the following size:

- Heat exchanger total length: 8 m
- External tube: steel alloy (refer to Table 5)
- Length: 8 m as result of the assembly (butt join welding) of 2 m and 6 m tubes.
- External diameter: 76.2 mm (3")
- Wall thickness: 3 mm
- Internal diameter: 70.2 mm
- Internal tube: PE SDR17
- external diameter: 40 mm
- Average well thickness: 2.5 mm
- Average Internal diameter: 35 mm

The dimensions of the well-point tube, that is the external tube of the coaxial heat exchanger, is larger than the normally used; otherwise, the pressure drops evaluated for the circulation of the fluid inside the inner pipe and within the annulus of the coaxial heat exchanger were too high.

8.2.6 Heat exchanger materials

Tubes

Many factors influencing the corrosion mechanism of metallic GHEs are related to physical-chemical characteristics of the ground, including mineralogical composition of rocks/sediments, ground pH and water content. Also the chemistry interaction between underground and GHE materials, as well as the underground electrical conditions have an important effect. GHEs installation implies altering the undisturbed underground conditions, which could lead to significant development of corrosion, mainly due to the penetrating atmospheric oxygen into the underground and the presence of ground water in contact with the GHE. According to best practices, using metallic GHEs is an unfavourable choice if the tubes are not made of corrosion resistant alloys and it is discouraged by actual regulations, despite the good heat exchange performance and the relatively low cost of carbon steel. Following tables 3 and 4 show that stainless steel is more resistant to corrosion but it costs over three times more than carbon steel, with worse thermal properties.

Table 3: Thermal conductivity of reference materials (Source: US NIST, matweb.com, engineeringtoolbox.com)

Material	W/ (m K)
HDPE	0.5
Mild/low-carbon steel AISI 1018	51.9
Stainless steel AISI 304	14.4
Stainless steel AISI 316	16.2

Table 4: Market price of reference materials (Source: Milano Finanza/Camera di Commercio di Milano. Average market price from the producer/importer to the industry, VAT excluded)

Material	€/ton
HDPE	1080
Mild/low-carbon steel	900
Stainless steel AISI 304	2900
Stainless steel AISI 316	3480

After a screening of the materials and methods commonly used to prevent or limit corrosion in metal underground applications, a selection of best practice measures were selected and applied to the well point heat exchangers at the CNR pilot site. The purpose of this operation is identifying the most suitable materials for GHEs and the best protection systems to improve durability, thermal performance and safety of metallic tubes, that can be feasible, and also really admissible by the regulations. Concerning durability and performance, if metal GHEs are used, it is preferable to implement anti-corrosive measures such as cathodic protections, thus a sacrificial anode has been applied too.

Table 5: Overview of the well point tubes materials and related protection systems

No. of tubes	Tube material	Protection system
2	Carbon steel	Zinc based coating
2	Carbon steel	Tar coating
1	Carbon steel	Zinc alloy sacrificial anode
2	Carbon steel	Galvanic Zinc plating, Zinc based coating applied on the welding joint between the 2 and 6 metres sections.
1	Carbon steel	Nothing
7	Stainless steel AISI 304	Nothing
1	Stainless steel AISI 316	Nothing

Heat exchanger heads

At first, stainless steel heads were foreseen, i.e. the very same item used for the coaxial heat exchangers developed in GEO4CIVHIC. Such heads required a joint piece to fit the 3” steel pipe constituting the outer tube of the well-point heat exchangers. Such piece was designed but discarded as soon as the stainless steel head option was dropped. In fact, due to economic evaluation, it became obvious that using such head would be unfeasible, as the cost was equal to that of the whole heat exchanger itself. While the stainless steel head is a good option indeed for the standard length coaxial heat exchangers, that is not true considering the relatively short length of the well points tubes, resulting in a high cost per meter of heat exchanger. The design is represented in Figure 11.

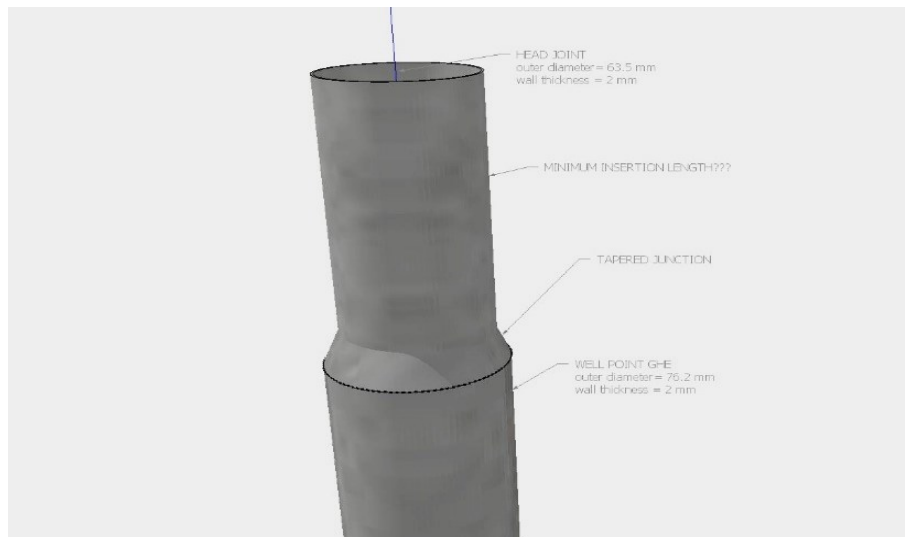
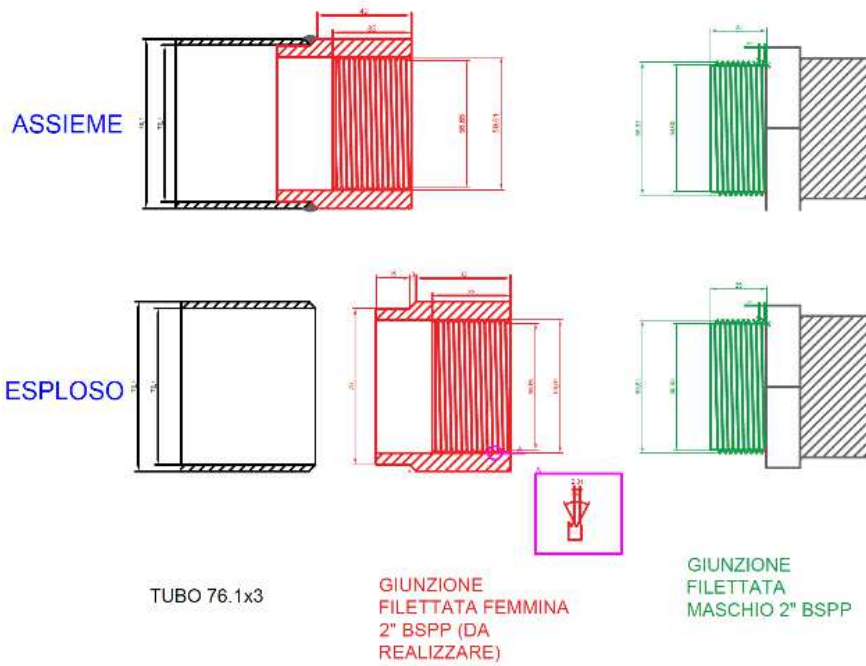


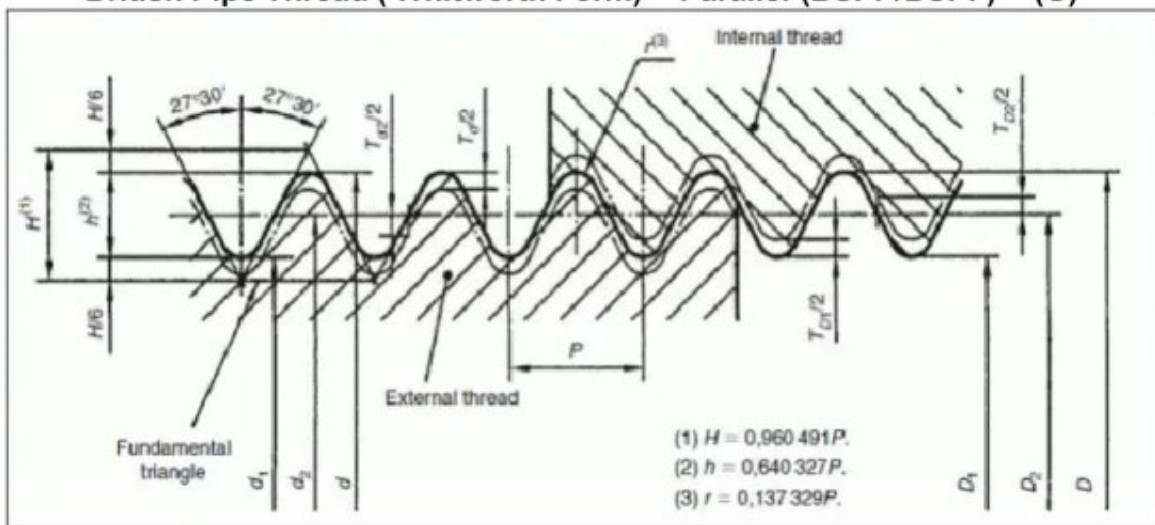
Figure 11: Drawing of the fitting piece allowing junction between well point heat exchanger external tube to the stainless steel head

A cheaper plastic heat exchanger head in PE was thus preferred. Nonetheless, a joint piece to fit the plastic head to the 3” steel pipe was compulsory as well (see Figure 14). Specifically, such piece was made to fit a brass spigot 2” BSPP male thread already jointed to the external pipe junction of the head.



(a)

**BS EN ISO 228-1: 2003 Table 1 Thread dimensions
British Pipe Thread (Whitworth Form) -- Parallel (BSPP/BSPF) -- (G)**



				Tolerances on pitch diameters						Tolerance on minor diameter		Tolerance on major diameter			
				Internal thread TD2			External thread Td2			Internal thread TD1		External thread Td			
Designation of thread	Number of threads in 25.4 mm	Pitch P	Height of thread h	Diameters			Lower deviation	Upper deviation	Lower deviation Class A	Lower deviation Class B	Upper deviation	Lower deviation	Upper deviation	Lower deviation	Upper deviation
				major d = D	pitch d2 = D2	minor d1 = D1									
2	11	2.309	1.479	59.614	58.135	56.656	0	0.18	-0.18	-0.36	0	0	0.64	-0.36	0

(b)

Figure 12: Drawing of the fitting piece allowing the connection of the plastic head to the externa steel pipe (a); Detail of the joint thread taken from BSPP standard.

This metal part has been produced in two different metal alloys (8 pieces in carbon steel and 8 in stainless steel) for optimal welding to the matching steel pipes, as represented in Figure 13.



Figure 13: Example of a fitting piece machined in carbon steel alloy. The tapered/recessed section is meant to be inserted into the 3" steel pipe for optimal joint.

The selected design of the plastic head is shown in the following Figure 14.



Figure 14: Picture of the prototype of the plastic head assembly (a). Note that the elbow joint was missing in this early design. Detail of the brass 2" male threaded BPS spigot (b). Section of the inner and outer PE tubes constituting the core of head (c).

Each plastic head is an assembly of the following PE hydraulic items, as depicted in Figure 15:

- 1 No. EF 63mm T piece kit
- 2 No. EF 63mm to 40mm reducers
- 1 No. Transition fitting 63mm to 2" Male BSP
- 1 No. EF 40mm 90° Elbows
- 0.75 metres of 63mm SDR 11

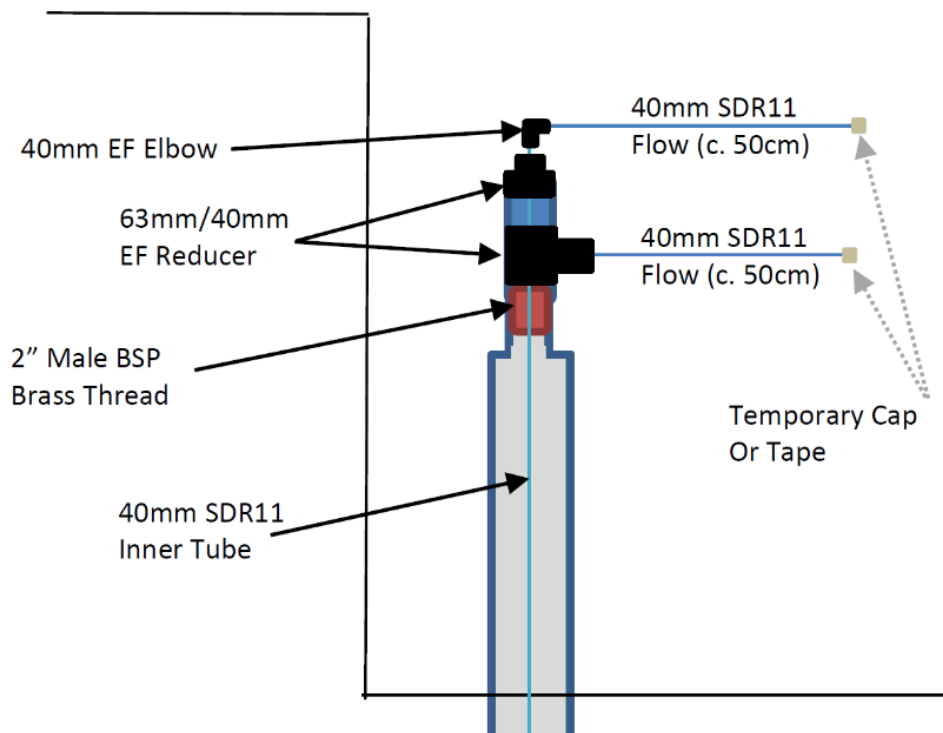


Figure 15: Scheme of the assembled and installed plastic head. Caps at the end of the inlet and outlet pipes are meant to avoid dirt or debris inside the hydraulic circuit during the installation.

Such PE components are partially pre-assembled, nonetheless some electro-fusion welding is needed on site to attach the inner heat exchanger pipe to the head, and for the inlet and outlet connections. The basic head installation methodology is the following:

(Note: Well point steel outer tube already installed)

- Push 40mm inner pipe into steel well point and cut above final head height;
- Place sealant or PTFE tape on the 2" brass male thread ;
- Slide head through the inner tube top section and screw to well point;

- Weld 63mm to 40mm reducer at top of head;
- Weld 40mm elbow at the top;
- Weld 63mm to 40mm reducer.

8.2.7 Well point heat exchangers installation method at Padova Pilot site

The following Figures 16-17 report the installation layout. In the upper part the building is represented: the yellow part represents the location of the heat pump; whilst the orange squares in the lower part represent the excavation foreseen for the heat exchangers installation.

Given the local stratigraphic setting, the laying of well-points/heat exchanger is performed by using the same technique used in case of presence of fine-grained grounds, hence it is preceded by the construction of a cylindrical, vertical, sand drain. Firstly, a squared excavation is made, in order to lower the surface. After this operation, the vertical hole is drilled; the well-point (heat exchanger) is placed inside the hole and, at the same time, it is washed with water in order to remove any fine material that may have settled on the walls. Coarse sand is introduced into the hole until it forms a vertical drain. For the well-points, the drain has the double function of protecting the filter from any blockages due to the fine fraction present in the ground, and it puts in communication different sandy layers, increasing the drainage capacity of the system. In this case, the vertical drain also enhances the thermal exchange thanks to the high thermal conductivity of the sandy material used.

The procedure is summed up in Figure 18.

Figure 18: Overview of the procedure for the well-points/ heat exchanger installation.



(a) Drilling and casing from -1.50 (pit depth) to -8.50 m below g.l..



(b) Positioning of the GHE and connection between GHE and hydraulic pump.



(c) GHE insertion using the excavator and pressurized water.



(d) Extraction of the case.



(e) Filling the borehole.



(f) Closing the open end with cement.

In order to allow optimal handling of the steel pipe during the installation, a custom metal hub was made, represented in Figure 19. The hub is male threaded 2" BSP to be screwed to the welded 2" BSP female thread of the steel pipes. A pass-trough hole is for easy attach of ropes, chains or other mediums during the lifting of the steel tubes on site.



Figure 19: Custom made 2" BSP threaded steel hub.

Sealing of the well point

After inserting the steel pipe into the ground, the open edge at the bottom end of the heat exchanger is sealed in order to obtain the water-tightness of the outer pipe of the coaxial configuration. A specific material has been selected to be injected by means of a pipe passing through the upper opening of the heat exchanger (2" BSP female threaded opening) before the installation of the head and the inner tube.

The ideal grout mixture able to seal the wide opening of the well points must be characterized by:

- low fluidity;
- best chance of clogging / sealing the wide opening, avoiding the water inflow from the surrounding environment within the heat exchanger;
- the ability to be made less fluid, if required by the surrounding environmental conditions, by slightly reducing the water / powder mixture ratio during the preparation phase, without suffering a variation in the thermo-mechanical properties.

According to the results obtained by the laboratory measurements already described in the deliverable 2.5 (see D2.5 “*Definition of best grouting mix and process for developed geothermal heat exchangers*”), the preferred mixtures are:

- Masterflow 928 by Basf (MF928)
- MapegroutSV + IdrocreteS by Mapei (SV)

Therefore, these 2 different grouts (MF228 and SV) have been used to seal 4 well points (2 made of stainless steel AISI 304 and 2 of carbon steel) with external diameter (Dex) of 3”. The material of the well point casing does not affect their hydraulic characteristic, therefore for the purposes of the sealing test the behaviour of both stainless steel and carbon steel well point is considered the same.

Two different material, a gravel and a fine fluvial gravel (named “Ghiaiotta del Brenta”) have been considered as reference material to verify the sealing ability of the selected grouts. In fact, if the grouts work well with gravel, a sediment characterized by high hydraulic permeability, it is expected that their behaviour remains promising also in case of finer material as sand, silt and clay.

The sealing performance has been tested in laboratory between 11 and 14 November 2019. At first 4 boxes (38x26.5x28 cm) have been filled with fine gravel (Figure 20 a-c) and gravel (Figure 20 b-d). The main idea is to seal the first 25 cm from the well point bottom, so 2.3 kg of dry material were prepared for each grout (MF928 and SV) following the corresponding technical data sheet (see Appendix A, D2.5).

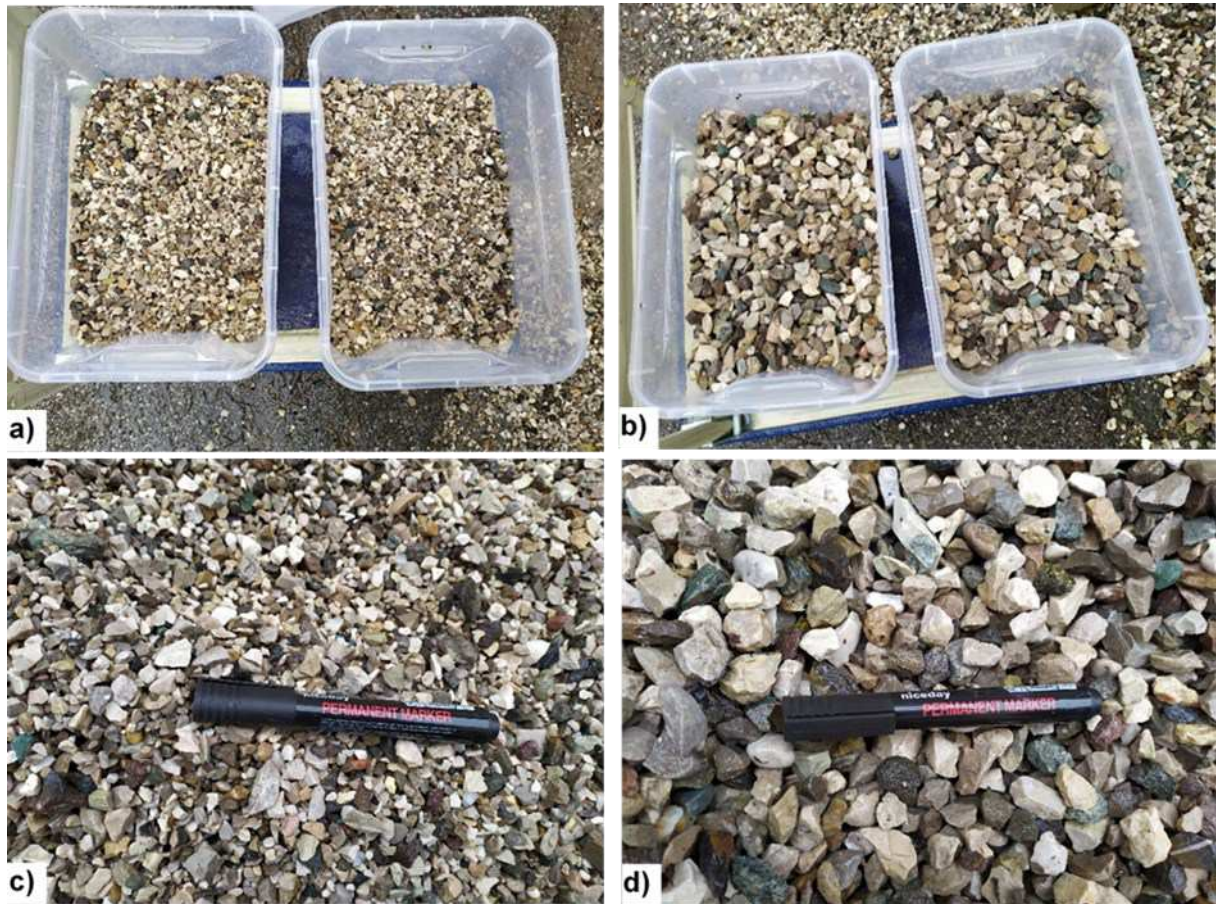


Figure 20: Boxes filled with fine gravel (a) and gravel (b) for the well points sealing tests; detail of fine gravel (c) and gravel (d).

At first **SV mixture** was prepared (Figure 21).

Meanwhile 2 well points have been driven into the two selected grounds (fine gravel and gravel) by hand and secured to a stone support to maintain their vertical stability (Figure 21).

Finally, the grout was inserted in the "well point" with the aid of a funnel and its descend was enhanced by beating a hammer on the pipe walls (Figure 23).



Figure 21: MapegroutSV + IdrocreteS by Mapei (SV) preparation: from left to right the raw material, the additive and the powder mixed to the additive as required by the technical sheet.



Figure 22: From left to right, preparation to driving the well point into the gravel, securing of the well points and note about the dry material to be used.



Figure 23: From left to right, SV inserted into the well point, a detail of the low viscosity of the material, use of the hammer to enhance the grout descend.

Then, the **MF928** was prepared (Figure 24).

During MF928 preparation, the remaining 2 well points have been driven into the two selected grounds (fine gravel and gravel) by hand and secured to a stone support to maintain their vertical stability (Figure 25).

Finally, the grout was inserted in the "well point" with the aid of a funnel and its descend was enhanced by beating a hammer on the pipe walls (Figure 26).



Figure 24: From left to right MF928 raw material, dry powder weighing, mixing with water according to the technical sheet.



Figure 25: From left to right securing of the well points in gravel and fine gravel, top view of the well point with the space for inserting the grout, preparation for the grout filling.



Figure 26: From left to right, MF928 inserted into the well point, a detail of the higher viscosity of the material, detail of the filling operation.

Once the grout filling was completed, the 4 well points have been left on site for a couple of days in order to let the grout mature (Figure 27).



Figure 27: The 4 well points with the sealed heads.

After a couple of days, on 14.11.2019, the 4 well points were removed from the ground and the grout performance has been visually analysed.

The grout-sediment-well point combinations are summarized in Table 6.

Table 6: Summary of the grout-sediment-well point combinations

GROUT	SEDIMENT	WELL POINT
MapegroutSV (Mapei) - SV	<ul style="list-style-type: none"> • fine gravel (Ghiaietta del Brenta) • gravel 	<ul style="list-style-type: none"> • stainless steel AISI 304 • carbon steel
MasterFlow 928 (BASF) - MF928	<ul style="list-style-type: none"> • fine gravel (Ghiaietta del Brenta) • gravel 	<ul style="list-style-type: none"> • stainless steel AISI 304 • carbon steel

The visual inspection of the well points' heads does not show any loss of material in the surrounding ground.

SV and MF928 show a similar behaviour: they are able to completely seal the well points' head as shown by the fine gravel and gravel material cemented by the grout where the pipe opening is located as shown in Figures 28-31.



Figure 28: SV after removal: both fine gravel (left) and gravel (right) are completely cemented by the grout where the pipe opening is located. No loss of grout has been detected in the ground.



Figure 29: MF928 after removal: both fine gravel (left) and gravel (right) are completely cemented by the grout where the pipe opening is located. No loss of grout has been detected in the ground.

The SV grouting is really effective both for fine gravel and gravel (Figure 29 left). The same is observed for ME928 (Figure 29 right). Moreover, no differences are observed in the grouting when comparing the heat exchangers inserted in the fine gravel (Figure 30 left) to those in the gravel (Figure 30 right).



Figure 30: SV (left) and MF928 (right) grouting with different materials (fine gravel and gravel).



Figure 31: The well points inserted in fine gravel (left) and gravel (right) do not show loss of grouting material, neither SV nor MF928.

Therefore, both products are expected to work well also when sediments with finer grain size are present.

In detail, both SV and MF928 can be considered as a valuable solution to seal the well points. However, MF928 is the preferred grout as it is a less fluid mixture and has a better chance of clogging / sealing the wide opening of the well-points in the presence of any kind of grain-size. In addition, if needed, the water / powder mixture ratio can be lowered to 0.145 to reduce its fluidity.

To seal the first 25 cm from the well point bottom, 2.3 kg of dry material are prepared for each well point.

In the CNR demo site in Italy, to seal 16 well points, in total 36.8 Kg of dry material are required. With regards to the possibility of losses during grouting mixing, it seems that 50 kg could be sufficient to prepare the grout on site and 75 kg allows to be on the safe side. If the well point is sealed the day after the completion of the installation on site, the setting time required by the grout can be estimated finalized at three hours.

The monitoring system

In the same pilot site, other 3 coaxial heat exchangers will be tested. The installation is served by 2 heat pumps, one is managed with an ‘inverter’ whilst the other is ON/OFF. The two pumps and the heat exchanger will be managed by a software tool developed on purpose. The whole installation is described in Figure 32, where the ground heat exchangers as well as the horizontal connections and the heat pumps systems are reported.

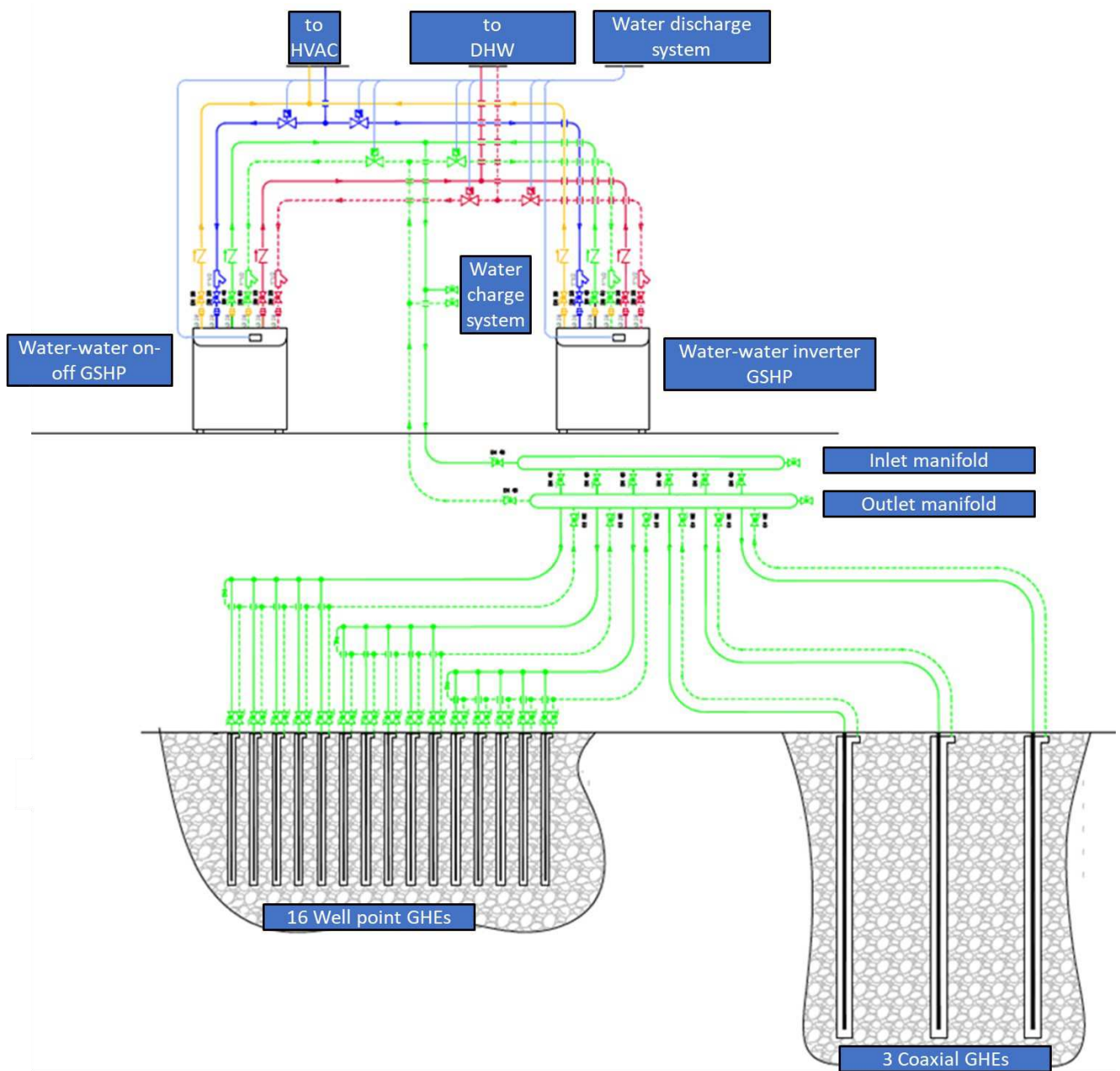


Figure 32: Ground heat exchangers (well point and coaxial heat exchangers), horizontal connections and heat pumps systems foreseen in the CNR pilot site.

The installation is completed with a dedicated an advanced monitoring system, depicted in Figure 32. The Temperature and the Pressure of the fluid are registered continuously in several points, both at the user and the source (i.e. the ground) sides of the heat pumps. In addition, also the energetic consumption will be registered, as well as the Coriolis velocity within the heat pump, in order to test the innovative refrigerant fluid used. These aspects will be better described and reported in the *Deliverables 3.5 'First report on the results of pilot Facilities demonstration n.1 in Padua: performance of the plug & play solutions and of the adaptation of well point technique'* and *D 3.7*

‘Second report on the results of pilot Facilities demonstration n.1 in Padua: performance of the novel co-axial heat exchangers’

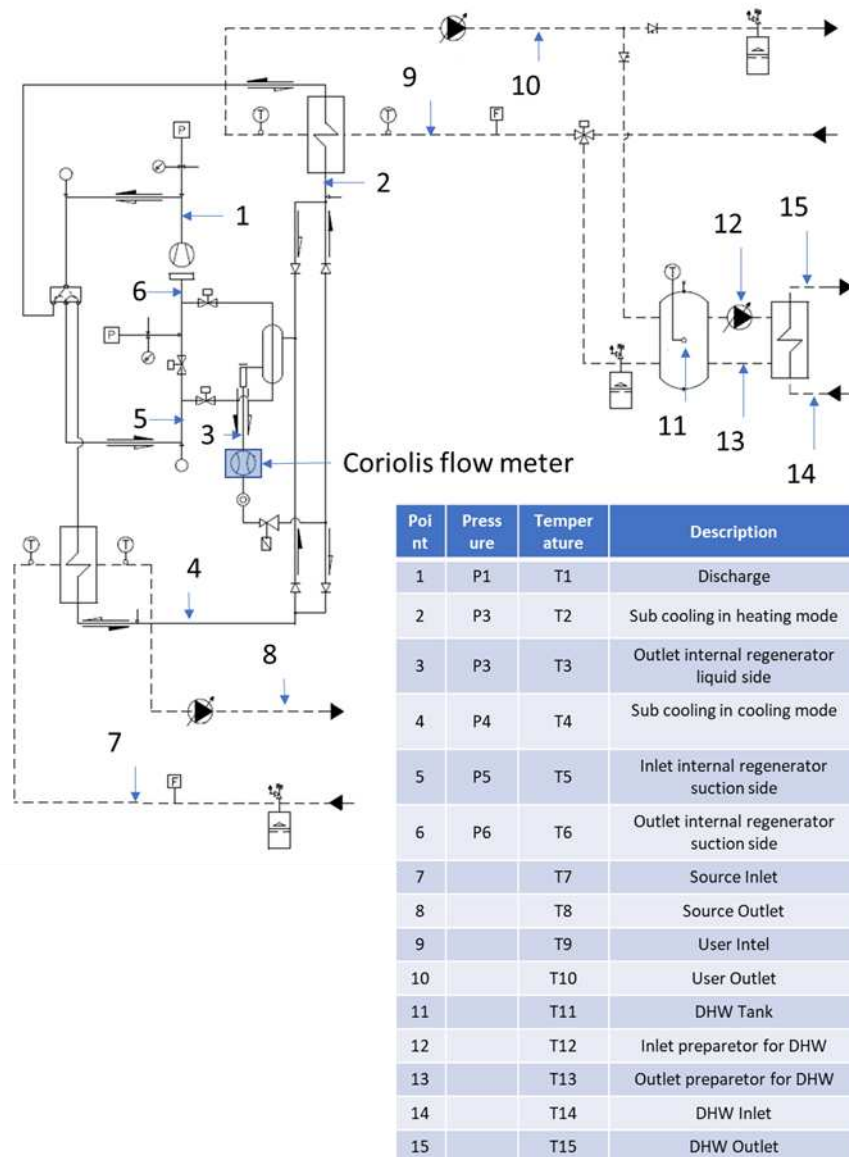


Figure 32: Monitoring system of the pilot site at the CNR in Padua.

8.2.8 Conclusions

All the components for the installation of the test site are designed and sized and ready to be installed, but the particular conditions determined by the coronavirus pandemic interrupted the works. The installation will be completed when it will be possible, and the foreseen monitoring of the energetic performances of the system then will be finalized.

9 Themed topic chapter: Evaluation of the thermal performance of metal GHEs

This chapter is dedicated to the thermophysical characterization of the new vertical coaxial metal heat exchangers. The thermophysical properties of the materials of the outer pipes were assessed in the laboratory. Several techniques were employed, most notably the laser flash method. Finally, the measured thermophysical properties allowed to perform the modelling of the thermal performances of the metallic solutions both in steady state and transient conditions.

Based on two manuscripts:

- G. Cadelano, A. Bortolin, G. Ferrarini, P. Bison, G. Dalla Santa, E. Di Sipio, A. Bernardi, A. Galgaro. **Evaluation of the Effect of Anti-Corrosion Coatings on the Thermal Resistance of Ground Heat Exchangers for Shallow Geothermal Applications.** *Energies* **2021**, *14*, 2586. <https://doi.org/10.3390/en14092586>

The manuscript has been published and indexed in bibliometric area. GC designed the study; GC and AG developed the methods; GC, AB and AG collected the data. All the authors discussed the data and agree on their interpretation; GC, AB, E.DS, G.DS and AG wrote the manuscript. All the co-authors contributed to the final polishing of the manuscript.

- G. Cadelano, G. Ferrarini, A. Bortolin, G. Dalla Santa, E. Di Sipio, A. Galgaro. **FEM evaluation of heat exchange efficiency variability under transient conditions for different coaxial ground heat exchangers materials and subsoil contexts.** Draft to be submitted to MDPI Energies.

The manuscript has not been peer-reviewed for publication yet. GC and AG designed the study; GC, GF and AG developed the methods; GC and GF a collected the data. All the authors discussed the data and agree on their interpretation; GC, GF, AB, E.DS, G.DS and AG wrote the manuscript. All the co-authors contributed to the final polishing of the manuscript.

9.1 Evaluation of the Effect of Anti-Corrosion Coatings on the Thermal Resistance of Ground Heat Exchangers for Shallow Geothermal Applications

9.1.1 Abstract

The materials and the technology used to build the ground heat exchangers significantly affect the heat transfer performance of a geothermal system, in addition to the local geological and hydrogeological context. Among expense items such as the coupled heat pumps and the applied drilling technology, the heat exchangers play a key role in the shallow geothermal market. For this reason, they are usually made with plastic. Metal tubes are not widely used because of corrosion issues, which can compromise the reliability of the system over time. According to best practices, metal is an unfavorable choice if the pipes are not made of corrosion resistant alloys, such as stainless steel, but the overall performance is strongly related to the heat transfer efficiency. In this study, laser-flash technique is applied on carbon steel samples with anti-corrosion coatings and on corrosion resistant materials (stainless steel grades used for pipes), thus, allowing the comparison of their thermophysical properties. These properties are used to evaluate each solution in terms of thermal resistance. This study demonstrates that there are no particular corrosion resistant steel pipe configurations that are thermally favorable over others in a critical way.

9.1.2 Introduction

Shallow geothermal systems have proved reliability in efficiently supplying heating and cooling to buildings. Ground heat exchangers (GHEs) are tubes inserted into the ground, where a fluid flows inside, allowing the heat exchange between the ground and the building. The heat transfer fluid can be only water, or water with anti-freezing and anti-algal additives. In winter, the heat is extracted from the underground and supplied to the building, which is vice-versa in the summer. The whole system is managed by a heat pump, granting the heat transfer between the GHE and the building. The heat exchange capacity of the system mainly depends on the local geological setting such as stratigraphy, hydrological conditions, and undisturbed ground temperature, and on the materials and technology used to build the GHEs [1,2].

Recently, an improved GHE installation method was proposed [3–6], which is an enhancement of the well-known piling technique. Such a method is specific for coaxial

GHE and it implies the absence of grouting, so the outer pipe is in direct contact with the surrounding underground. In this way, the borehole resistance between the external metallic tube and the ground is significantly lower than that of standard, grouted, heat exchangers, thereby increasing the thermal performance of the coaxial GHE.

In addition, the characteristics of the properly designed drilling head and its operation significantly limit the abrasion with the underground. In fact, using this drilling technique, the external tube does not rotate during installation because the torque is transferred to the drill, but from an internal shaft, while the tube is mechanically decoupled by means of ball bearing elements while it is dragged into the ground. This is crucial because it opens the possibility to use thermoplastics and coated metals for the outer pipe, which cannot be easily used with other methodologies. In fact, thermoplastic materials, such as HDPE, cannot easily withstand the compression load during the piling operation. Moreover, galvanized metallic materials can suffer the risk of damaging the coating or the galvanized layer during the piling process [7,8]. With this newly developed drilling methodology, three kinds of materials can be more safely selected as the outer pipe in order to optimize cost, corrosion-safety, and thermal performance, which include HDPE, stainless steels, and coated carbon steel. The thermal performance of pipe or pipe-coating systems, represented here by thermal resistance values (as defined in Section 3.3), is a combination of the thermal properties of pipes and coatings, and their geometries (i.e., the thickness of each layer and the ratio of radii). It is well known that there are other factors that could affect the heat transfer between the fluid and the ground (e.g., the viscosity of the fluid, its laminar or turbulent flow, and the presence of fins or other elements [9,10], such as changes in the diameter or the presence of incrustations on the inside wall of the pipe). However, they have not been considered because they do not influence the goal of this study focused on assessing and comparing the effects of anti-corrosion measures applied on the outer wall only. In particular, a laboratory measurement of anti-corrosion coatings represented a core part of the work. The application of the experimental techniques used to obtain thermal conductivity, i.e., by measuring the thermal diffusivity in single-side configuration, has been proposed as a method, which could be worth considering for future research in the field of thin coatings for ground, geothermal, heat exchangers. While the general issues of characterizing the thermal properties of materials and modeling the thermal behavior of pipes have been discussed in the literature [11], this work proposes an alternative, clear, and reliable path to measure the properties of coated pipes, leading to an optimal choice and design of heat exchangers. The ultimate goal is to evaluate and compare the thermal performance of different solutions that are very specific for the new installation method. This is meant to provide indications that can allow for more precise design choices, which can, therefore, be based on other parameters, such as costs or geological/hydrogeological compatibility.

Table 1 shows that stainless steel costs over three times more than carbon steel. The latter costs about as much of HDPE plastic, but presents significantly better thermal properties.

Table 1: Market price of reference materials (Source: Milano Finanza/Camera di Commercio di Milano. Average market price from the producer/importer to the industry, VAT excluded).

Material	€/ton
HDPE	1080
Mild/low-carbon steel	900
Stainless steel AISI 304	2900
Stainless steel AISI 316	3480

Concerning durability and performance, if carbon steel GHEs are used, it is mandatory to implement anti-corrosive measures, such as coatings or a sacrificial anode. The environmental aspect is paramount. It is fundamental to avoid issues concerning leaks of the heat-transfer fluids flowing inside the pipes (e.g., glycol mixtures often with anticorrosive/antialgal additives). For coaxial GHEs in direct contact with the underground, the addition of a coating layer around the pipe might be a factor impacting on the thermal performance of the system. In order to evaluate different GHE solutions, a comparison in terms of thermophysical properties has been held. Six different solutions have been considered: (I) HDPE, (II) Stainless steel AISI 304, (III) Stainless steel AISI 316 (Marine grade stainless steel), (IV) Carbon steel S235JRH, (V) Carbon steel S235JRH with bitumen coating, and (VI) Carbon steel S235JRH with alkyd-based primer coating. For each of them, we obtain the thermal properties of the material used for the pipe, the coatings, and, then, evaluate the total thermal resistance as the sum of the thermal resistance of both the pipe and the coating, if any. Finally, the different solutions have been compared.

9.1.3 Materials and Methods

Passive and Active Anti-Corrosion Measures for Buried Carbon Steel Pipes

Passive protection is used to mechanically insulate the metal surface from the external environment by means of a coating. The most common are:

1. protective films of proper paint applied over the entire length of the pipe or only in points subject to corrosion, such as polyethylene-based protective coatings as prescribed by UNI 9099 [12] (other coatings are applicable as a paint, i.e., primer), or bitumen according to UNI 5256 [13];
2. oxidation products obtained, e.g., by anodic oxidation of metals such as Al, Ni, or Co. The oxides of these materials are very tough and adherent to the surface layer, insulating them from the environment. Metals, such as Zn, could be applied by immersing the Fe-alloy in a galvanic bath of molten Zinc or attaching a bulk sacrificial anode made of Zinc alloy to the pipe in case of stray currents. With Zn being more reducing than Fe, oxidation proceeds on the Zn and the pipe remains protected until all the Zn has been consumed. Moreover, other metals such as Cr, could be applied by plating/cladding the pipes.

Other coverings with an insulating effect due to their materials and thickness, widely used in aerial pipelines [14], cannot be used for GHEs because they would critically limit the overall efficiency.

Conversely, active methods consisting of applying a reverse electromotive force, where the pipe is connected to the negative pole of a direct current generator whose positive pole is, in turn, connected to an inert electrode, would not add any additional thermal resistance to the GHE. This system is called Impressed Current Cathodic Protection (ICCP) and has a higher installation and maintenance cost than the previously mentioned methods. Therefore, it is quite inconvenient for cost-effective/long-term applications, such as GHEs. Another method is the use of a sacrificial anode, but it is not suitable in the case of piled GHEs because it protrudes with respect to the tube profile and this is not acceptable during drilling/installation procedures.

For the sake of this study, only bitumen and primer were considered. They were also found to be very relevant because such coatings are still used to protect the weld joints when the carbon steel pipe is galvanized or even plated.

Stainless-Steel Grades with Anti-Corrosive Action Used for Piping

Stainless steel is an alloy of Fe, Cr, and C. Occasionally, it has other complementary elements, such as Ni (the most common) and Mo. Cr is the element that provides the stainless characteristic of the material. In an oxidizing environment, Cr produces a very dense and thin oxide layer that allows us to isolate the material from any corrosive action as long as it is kept intact. Stainless steels are subdivided in martensitic, ferritic, and austenitic, according to the amount of the elements in their composition. Austenitic is the group with the greatest advantages in manufacturing, as well as in service performance, such as easy welding and great corrosion resistance. AISI 304 contains 18% Cr and 8% Ni, whereas AISI 316 contains 16% Cr, 10% Ni, and 2% Mo. The

latter is added to enhance resistance to corrosion from chlorides (common in seawater and marine environments).

Being among the most common materials for structural pipes and underground structures, such stainless steel grades were selected in their category as representatives for the purpose of this study.

The Laser Flash Method Procedure to Measure Thermal Properties

Several methods are available to measure the thermal properties of materials. The laser flash method (LFM), which is one of the most widespread and reliable methods [15–17], has been chosen for this work.

In the typical LFM setup, the specimen under the test is stimulated by a heat flux on his front face and a temperature sensor records the temperature increase on the back face of the specimen. The samples are usually disc-shaped ones, sizing in the order of magnitude of 1 cm², but it could be modified to measure the thermal diffusivity value (α) of other kinds of specimens [18]. This method is popular for different reasons. It is very straightforward, the measurement is not time-consuming, it allows us to test the thermal diffusivities of a wide range of materials, and it can be performed at room temperature but also at very high temperatures. Another advantage is that LFM could provide an indirect evaluation of the thermal conductivity. In fact, after measuring the density (ρ) [19] (e.g., using the Archimedes principle), and the specific heat (c_p) (e.g., using the Differential Scanning Calorimetry—DSC) [20], the thermal conductivity (λ) could be obtained as the product of thermal diffusivity, specific heat, and density.

Several manufacturers provide turnkey solutions, while the instrument used in this experiment is based on a commercial solution but has been modified, guaranteeing the same performance level. The instrumentation includes seven elements. The first one is an Nd-doped YAG solid state laser (wavelength of 1064 nm) pumped by two xenon-filled flash lamps. The second one is a sample holder ring made with graphite and molybdenum. It is placed inside the third element, which is a furnace, made of a tantalum foil, allowing for high-temperature measurements. The latter is, in turn, inserted into the fourth element, which is a bell jar with two infrared transparent windows. The fifth element is a dual stage vacuum system, which allows the sample to be placed in vacuum or in gas atmosphere. The sixth element is a Teledyne J10D (InSb, range 2–5.5 μm) detector. It operates in a photovoltaic mode and it is connected to a Teledyne P9 transimpedance amplifier. The final element is a control and data acquisition system, which has been designed to measure the thermal diffusivity of different materials. It adopts a multiple averaging technique [21] that makes it possible to automatically repeat the measurements for a preselected number of times, thus, significantly improving the measured signal-to-noise ratio. Such a technique has been

applied to measure the thermal diffusivity of the pipe materials. A typical example of the output is given in Figure 1.

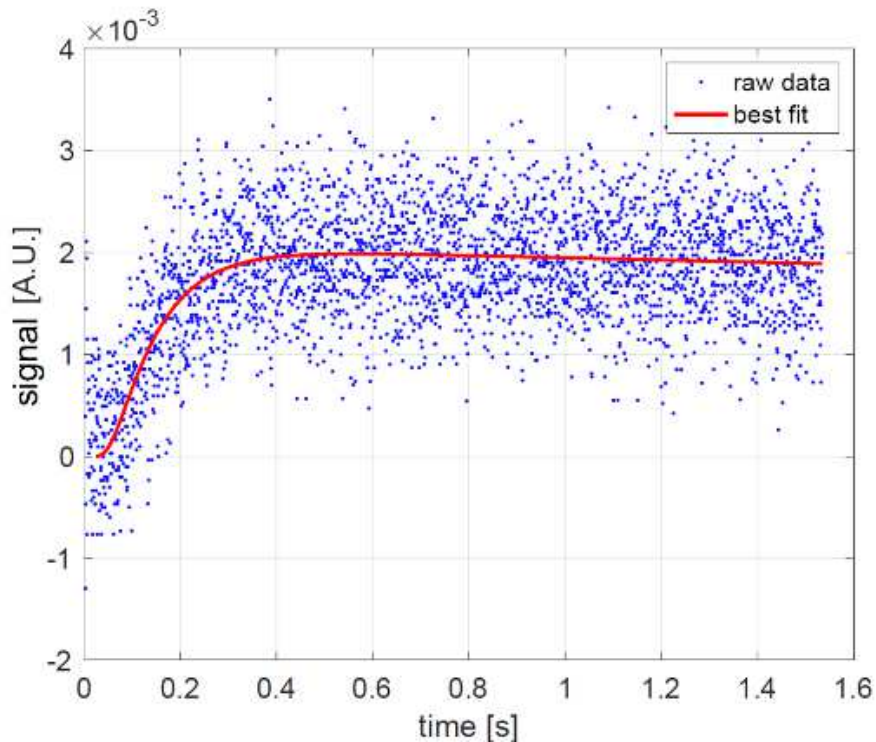


Figure 1: . Results of the AISI 304 specimen measurements given as an example of the raw output. Experimental data and fitting curve for the average of 100 shots [21].

Moreover, the LFM technique allows a single-side configuration, which is very convenient when the material to be tested is a layer of a multi-layer system. This configuration has been applied to study the characteristics of the two protective layers applied as anti-corrosion coating on the steel substrate (bitumen and primer). Figure 2 shows the experimental procedure of the technique used to measure the thermal diffusivity of the coatings. A pulsed laser heats the anti-corrosion coating of the specimen. On the same side, an infrared camera acquires a set of thermal images measuring the temperature evolution on the surface of the sample. The thermal exchange toward the room is neglected [22]. The thermal model of the sample is represented in Figure 3. The model considers a plane layer (coating) with thickness l_c . The other parameters of the models are: the thermal conductivity, the density (ρ_c), and the specific heat (c_c) of the coating. With regard to the substrate, it is considered isotropic and semi-infinite. Its parameters are the thermal conductivity λ_s , the density ρ_s , and the specific heat c_s . The laser heat pulse is submitted to the observed surface with a Gaussian spatial distribution. It has been demonstrated [23] that, when the temperature integration area includes the entire heated area, the thermal problem is one-dimensional, regardless of the energy distribution of the heating source. Knowing

the characteristics of the semi-infinite substrate, the thermal characteristics of the coating are derived.

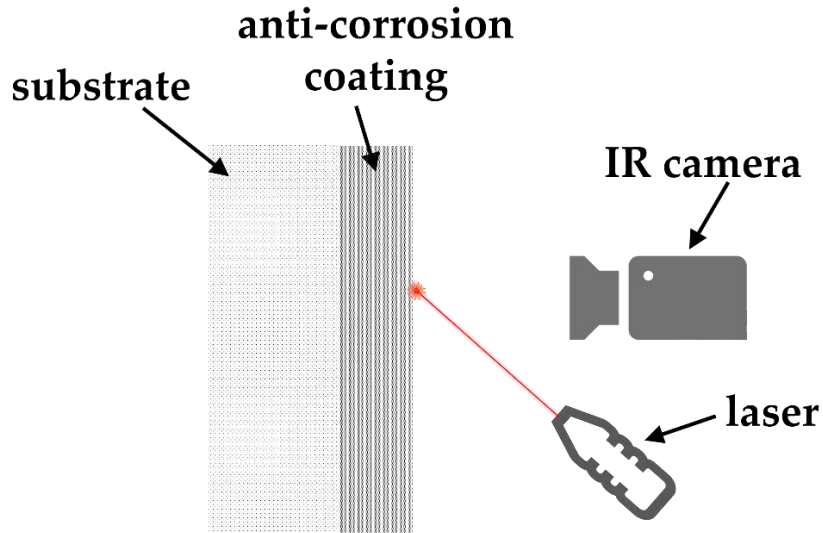


Figure 2: Experimental setup of in-plane and in-depth thermal diffusivity measurement.

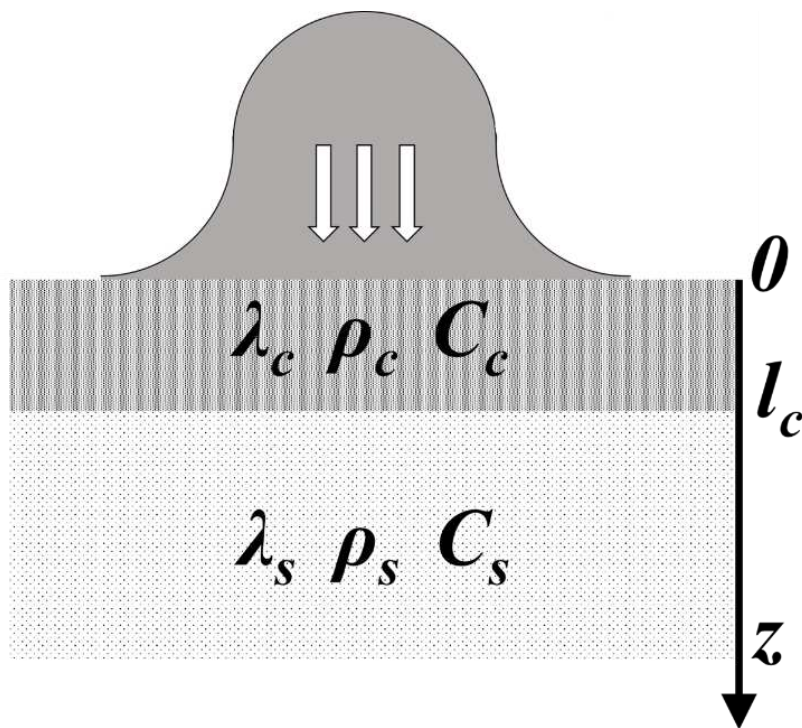


Figure 3: Schematic diagram of the experiment. Substrate is much thicker than the coating and is considered endlessly extended along the z -axis. On the observed surface, a laser heat pulse is released with a Gaussian spatial distribution [24].

The data acquisition includes images of the temperature evolution in three different stages: before the laser shot (this acts as the reference), during the laser pulse, and after the laser shot, during the cooling stage. In this way, it is possible to analyze the cooling curve after subtracting the baseline reference temperature that is acquired at the beginning of the test. As already depicted in Figure 3, the model consists of a thin layer coating on a semi-infinite substrate (steel sample) [25,26]. A heat pulse (Dirac delta $\delta(t)$) is imposed to the front face of the sample. The temperature T has to satisfy the following equations:

$$\frac{\partial T}{\partial t} = \alpha_c \frac{\partial}{\partial z} \left(\frac{\partial T}{\partial z} \right); 0 \leq z \leq l_c; t \geq 0 \quad (1)$$

$$\frac{\partial T}{\partial t} = \alpha_s \frac{\partial}{\partial z} \left(\frac{\partial T}{\partial z} \right); z > l_c; t \geq 0 \quad (2)$$

$$T(t=0)=0 \quad (3)$$

$$-\lambda_c \frac{\partial T}{\partial z} = Q\delta(t); z = 0 \quad (4)$$

The exact solution on the front face ($z = 0$) of the specimen is:

$$T(t) = \frac{Q}{e_c \sqrt{\pi t}} \left(1 + 2 \sum_{n=1}^{\infty} \Gamma^n e^{-\frac{n^2 l_c^2}{\alpha_c t}} \right) \quad (5)$$

e_c is the effusivity of the coating [$\text{J m}^{-2} \text{K}^{-1} \text{s}^{-1/2}$] $e_c = \sqrt{\rho_c \lambda_c c_c}$;

e_s is the effusivity of the substrate [$\text{J m}^{-2} \text{K}^{-1} \text{s}^{-1/2}$] $e_s = \sqrt{\rho_s \lambda_s c_s}$;

ρ is the density [kg m^{-3}];

λ is the thermal conductivity [$\text{W m}^{-1} \text{K}^{-1}$];

c is the specific heat capacity [$\text{J kg}^{-1} \text{K}^{-1}$];

Γ is the function of the effusivity of both coating and substrate $\Gamma = \frac{e_c - e_s}{e_c + e_s}$;

l_c is the thickness of the coating [m];

α_c is the thermal diffusivity of the coating [$\text{m}^2 \text{s}^{-1}$] $\alpha_c = \frac{\lambda_c}{\rho_c c_c}$;

The measured temperature evolution over time can be approximated by Equation (5). The parameters of the analytical solution are optimised in such a way that the analytical solution best fits the experimental data. An example of the data and of the analytical best fit is reported in Figure 4, where they are represented on a log-log scale. In Equation (5), a few unknown parameters are present.

$$P = \{p_1, p_2, p_3\} = \left\{ \frac{Q}{e_c \sqrt{\pi}}, \frac{\alpha}{l^2}, \Gamma \right\} \quad (6)$$

An iterative procedure changes the previously mentioned parameters in such a way to minimize the error between the experimental data and the mathematical model. Once the condition is achieved, the parameter $p_2 = \alpha/l^2$ is known and, therefore, the thermal diffusivity α is also known.

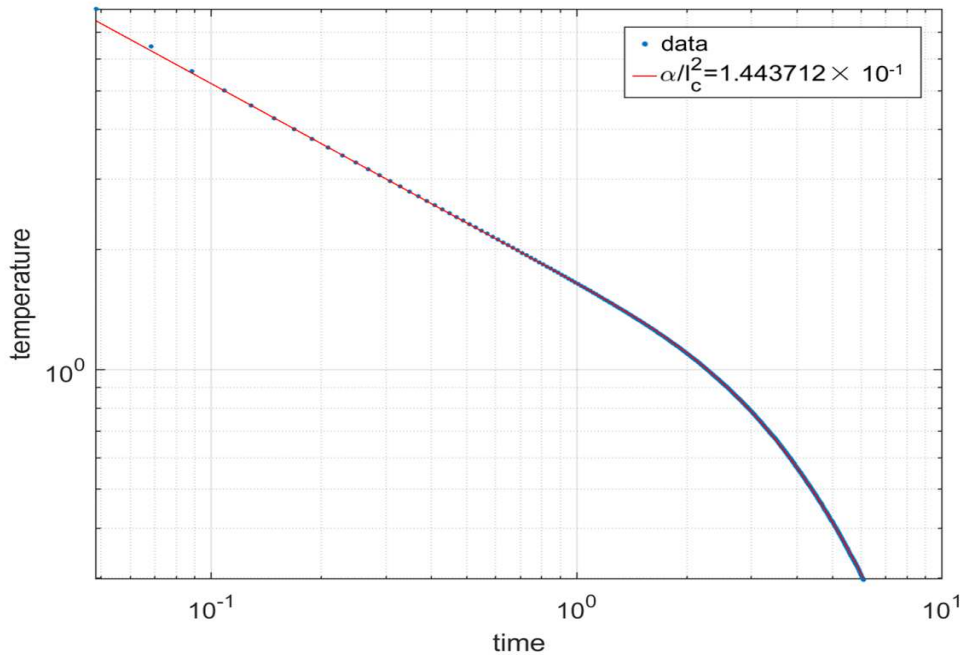


Figure 4: Log-log representation of the spatial average of the surface temperature in time given as an example of the processed output. The red line is the fit curve calculated on the experimental data (blue points).

Six different specimens have been measured in order to obtain the thermal diffusivity of HDPE, stainless steels (AISI 304 and AISI 316), carbon steel (S235JRH), and anti-corrosion coatings (bitumen and primer). In Table 2, the thickness values of each specimen are listed. Such values have been measured directly on the samples with a micrometer screw gauge. Bitumen and primer were applied on a carbon steel sample. Their thickness values have been obtained by subtracting the carbon steel thickness from the total thickness of the samples. As a result, their experimental uncertainties are significantly higher than the others.

Table 2: Thickness of the specimens: pipe materials and coatings.

Specimen	Thickness [mm]
HDPE	$0.570 \pm 1\%$
Stainless steel AISI 304	$1.024 \pm 0.5\%$
Stainless steel AISI 316	$1.100 \pm 0.5\%$
Carbon steel S235JRH	$5.486 \pm 0.5\%$
Bitumen	$0.657 \pm 4\%$
Primer	$0.150 \pm 12\%$

Modelling the Thermal Resistance of Each Material and of Different GHE Configurations

Several methods are available to model the heat transfer through the pipe, depending on the type and configuration of the heat exchanger [27–29]. In this section, a simple pipe model is proposed, with the purpose of comparing different materials. The heat flux Q^* exchanged by conduction through the pipe, where the inner temperature T_1 is higher than the outer temperature T_2 , is represented in Figure 5 by a red arrow.

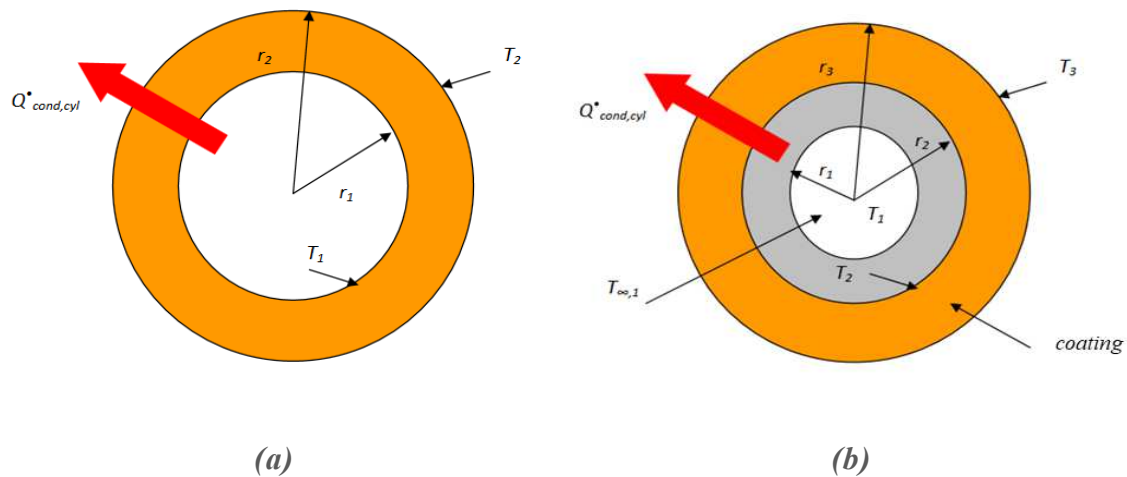


Figure 5: Heat flux exchanged by conduction in a pipe where the inner temperature is higher than the outer one. Left side (a) is a single layer pipe and the right side (b) is a pipe with a coating layer (not in scale).

The thermal resistance of a pipe wall is calculated using the following formula:

$$R_{pipe} = \frac{\ln\left(\frac{r_2}{r_1}\right)}{2\pi\lambda L} \quad (7)$$

where with reference to Figure 5a:

R = the thermal resistance per unit area of the piece of material ($\text{m}^2 \cdot \text{K} \cdot \text{W}^{-1}$),

r_1 = represents the inner radius of the pipe (m),

r_2 = represents the outer radius of the pipe (m),

λ = represents the conductivity of the material ($\text{W} \cdot \text{m}^{-1} \cdot \text{K}^{-1}$),

L = represents the length of the pipe, that is assumed to be unitary (m).

A pipe protected with a coating can be considered to act as two layers of different materials.

When materials are positioned in this way, their thermal resistances are added so that the same area conducts less energy for a given temperature difference. Hence, the actual resistance is given by adding the thermal resistance of each layer as an additional piping layer. Equation (7) is modified as follows:

$$\begin{aligned}
 R_{pipe+coating} &= R_{pipe} + R_{coating} \\
 &= \frac{\ln\left(\frac{r_2}{r_1}\right)}{2\pi\lambda_{pipe}L} + \frac{\ln\left(\frac{r_3}{r_2}\right)}{2\pi\lambda_{coating}L}
 \end{aligned} \tag{8}$$

where with a reference to Figure 5b:

R = the thermal resistance per unit area of the piece of material ($\text{m}^2 \cdot \text{K} \cdot \text{W}^{-1}$),

r_1 = represents the inner radius of the pipe (m),

r_2 = represents the outer radius of the inner pipe (m),

r_3 = represents the outer radius of the outer pipe (coating layer) (m),

λ_{pipe} = represents the conductivity of the carbon steel pipe ($\text{W} \cdot \text{m}^{-1} \cdot \text{K}^{-1}$),

$\lambda_{coating}$ = represents the conductivity of the coating material ($\text{W} \cdot \text{m}^{-1} \cdot \text{K}^{-1}$).

9.1.4 Results

Outcomes of LFM and Thermal Diffusivity Values

In Table 3, the outcomes of the LFM measurements are listed on the previously mentioned specimens of the materials constituting the pipes and the coatings.

The values are presented before and after taking into account the thickness of each specimen (l).

Table 3: Outputs of the LFM measurement of the specimens.

Specimen	Estimated Parameter α/l^2 [s ⁻¹]	Thermal Diffusivity [m ² s ⁻¹]
HDPE	0.708 ± 0.4%	0.23 × 10 ⁻⁶ ± 5%
Stainless steel AISI 304	3.96 ± 0.5%	4.1 × 10 ⁻⁶ ± 5%
Stainless steel AISI 316	2.98 ± 0.5%	3.6 × 10 ⁻⁶ ± 5%
Carbon steel S235JRH	0.422 ± 0.5%	12.7 × 10 ⁻⁶ ± 5%
Bitumen	0.176 ± 0.4%	0.08 × 10 ⁻⁶ ± 9%
Primer	11.21 ± 0.5%	0.25 × 10 ⁻⁶ ± 25%

Thermophysical Properties of the Specimens

For each material, the density and the specific heat have been measured in order to calculate the thermal conductivity values (Table 4).

Table 4: Thermophysical properties of the specimens.

Material	Specific Heat [J·kg ⁻¹ ·K ⁻¹]	Density [kg·m ⁻³]	Thermal Conductivity [W·m ⁻¹ ·K ⁻¹]
HDPE	1930 ± 2%	940 ± 2.5%	0.41 ± 5%
Stainless steel AISI 304	500 ± 5%	7850 ± 2.5%	16.2 ± 7.5%
Stainless steel AISI 316	500 ± 5%	8000 ± 2.5%	14.4 ± 7.5%
Carbon steel S235JRH	460 ± 5%	7700 ± 2.5%	45 ± 7.5%
Bitumen	1720 ± 5%	1500 ± 2.5%	0.20 ± 10%
Primer	1100 ± 5%	2200 ± 2.5%	0.62 ± 27%

Calculation of the Thermal Resistance of Each Material and of Different GHE Configurations

Given the obtained experimental results, the thermal resistance of each material has been calculated by applying the method reported in Section 2.4. Considering the wall pipe thickness equal to 2 mm, and assuming the outer and the inner radius equal to 82 and 80 mm, respectively, the thermal resistance for each of the considered materials is given as follows:

$$R_{\text{HDPE}} = 9585 \times 10^{-6} [\text{m}^2 \cdot \text{K} \cdot \text{W}^{-1}],$$

$$R_{\text{S235JRH}} = 87 \times 10^{-6} [\text{m}^2 \cdot \text{K} \cdot \text{W}^{-1}],$$

$$R_{\text{AISI316}} = 273 \times 10^{-6} [\text{m}^2 \cdot \text{K} \cdot \text{W}^{-1}],$$

$$R_{\text{AISI304}} = 243 \times 10^{-6} [\text{m}^2 \cdot \text{K} \cdot \text{W}^{-1}].$$

Considering 2 mm of thick carbon steel pipe coated with 0.1 mm of bitumen, the total thermal resistance is:

$$R_{\text{bitumen}} = 97 \times 10^{-6} [\text{m}^2 \cdot \text{K} \cdot \text{W}^{-1}],$$

$$R_{\text{total}} = R_{\text{S235JRH}} + R_{\text{bitumen}} = 184 \times 10^{-6} [\text{m}^2 \cdot \text{K} \cdot \text{W}^{-1}].$$

Considering the previously described 2 mm of thick carbon steel pipe coated with 0.1 mm of polymeric paint, the total thermal resistance is:

$$R_{\text{Primer}} = 32 \times 10^{-6} [\text{m}^2 \cdot \text{K} \cdot \text{W}^{-1}],$$

$$R_{\text{total}} = R_{\text{S235JRH}} + R_{\text{Primer}} = 120 \times 10^{-6} [\text{m}^2 \cdot \text{K} \cdot \text{W}^{-1}].$$

The total thermal resistance of the considered solutions for corrosion-resistant GHEs are listed in Table 5. A wall thickness equal to 2 mm is considered, as it represents a reasonable situation. Among the analyzed configurations are pipe-only solutions (i.e., HDPE, stainless steels) or combination of carbon steel and coatings (i.e., carbon steel with bitumen, carbon steel with primer). The thickness of the coatings is equal to 0.1 mm, which represents a realistic value.

Table 5: Thermal resistance of different corrosion-resistant, pipe-coating systems, and how they compare to an unprotected carbon steel pipe 2 mm thick.

Corrosion-Resistant Pipe Configuration	Total Thermal Resistance [m²·K·W⁻¹]	Increased Resistance Compared to Unprotected Carbon Steel
2 mm thickness HDPE	9585×10^{-6}	×110
2 mm thickness stainless steel AISI 304	243×10^{-6}	×2.8
2 mm thickness stainless steel AISI 316	273×10^{-6}	×3.1
2 mm thickness Carbon steel S235JRH coated with 0.1 mm of bitumen	184×10^{-6}	×2.1
2 mm thickness carbon steel S235JRH coated with 0.1 mm of primer	120×10^{-6}	×1.4

9.1.5 Discussion

The results obtained from the experimental tests conducted show that, while the thermal diffusivity of each material varies, and, thus, possibly impacts the dynamic behaviour of a shallow geothermal system, the thermal resistance values of the pipes are not so different among the considered configurations. Therefore, they appear not to potentially affect the steady state performance of the GHEs significantly. Exceptions are pipe made of HDPE and unprotected carbon steel.

Notwithstanding the price point, HDPE has, by far, the worst thermal resistance (meaning the highest), making an unfavourable choice for coaxial GHEs in contact with the ground. Therefore, the use of this material could likely find better application with configuration where the grouting is present. As for the carbon steel, which is in the same price range of HDPE, it has the highest thermal conductivity among the measured materials, which is even higher than AISI 304 and AISI 316 stainless steel.

Nevertheless, carbon steel is necessary to use, and, thus, here evaluated, in combination with a coating for corrosion safety reasons. When the bitumen or primer are applied on carbon steel, the resulting thermal resistance is in the same order of magnitude of the stainless steel ones.

Therefore, the choice among stainless steels or carbon steel with coating should be suggested by other aspects, such as the material cost or the compatibility with the characteristics of the underground where the GHE has to be installed. For example, in case of gravels or presence of hard rock fragments, it is preferable to not use GHE made of carbon steel with coating because they could damage the coating during the installation phase, even if the new drilling methodology is used. Therefore, these kinds of GHE are preferably installed in finer sediments. In this respect, other anti-corrosion measures should be evaluated. For instance, the galvanic plating with zinc could be possibly favoured if the previously mentioned coatings could not withstand the abrasion during the installation. Nonetheless, the weld joints still require bitumen or primer, with possible damages on such spots. This possibility is not considered in the frame of this study, as the small ratio between joints and the entire length of the GHE (up to 120 m or even more) is negligible because it will not affect the thermal performance of the system, even if a low thermal conductivity paint is used. This study demonstrated that there are no particular corrosion-resistant steel pipe configurations that are thermally favourable over others in a critical way. This is valid for the size and geometry of the pipe considered, which are typically used in shallow geothermal installations. However, it can be assumed that, in applications where high external pressure could cause the tube to collapse, and, therefore, the tube must be thick enough to withstand this force, higher conductivity materials may be preferred.

Funding

This research was funded by H2020 GEO4CIVHIC project, grant number 792355. GEO4CIVHIC project has received funding from the European Union's Horizon 2020 research and innovation program under grant agreement No. 792355.

9.1.6 References

1. Boban, L.; Miše, D.; Herceg, S.; Soldo, V. Application and Design Aspects of Ground Heat Exchangers. *Energies* **2021**, *14*, 2134, doi:10.3390/en14082134.
2. Badenes, B.; Sanner, B.; Mateo Pla, M.Á.; Cuevas, J.M.; Bartoli, F.; Ciardelli, F.; González, R.M.; Ghafar, A.N.; Fontana, P.; Lemus Zuñiga, L.; et al. Development of Advanced Materials Guided by Numerical Simulations to Improve Performance and Cost-Efficiency of Borehole Heat Exchangers (BHEs). *Energy* **2020**, *201*, 117628, doi:10.1016/j.energy.2020.117628.
3. Pockelé, L.; Mezzasalma, G.; Righini, D.; Vercruyse, J.; Cicolini, F.; Cadelano, G.; Galgaro, A.; Dalla Santa, G.; De Carli, M.; Emmi, G.; et al. Innovative

- Coaxial Heat Exchangers for Shallow Geothermal. In *World Geothermal Congress*; Elsevier: Reykjavik, Iceland, 2021.
4. Galgaro, A.; Dalla Santa, G.; Cultrera, M.; Bertermann, D.; Mueller, J.; De Carli, M.; Emmi, G.; Zarrella, A.; Di Tuccio, M.; Pockelé, L.; et al. EU Project “Cheap-GSHPs”: The Geoexchange Field Laboratory. In *Energy Procedia*; Elsevier: Vienna, Austria 2017, doi:10.1016/j.egypro.2017.08.175.
 5. Zarrella, A.; Emmi, G.; Graci, S.; De Carli, M.; Cultrera, M.; Dalla Santa, G.; Galgaro, A.; Bertermann, D.; Müller, J.; Pockelé, L.; et al. Thermal Response Testing Results of Different Types of Borehole Heat Exchangers: An Analysis and Comparison of Interpretation Methods. *Energies* **2017**, *10*, 801, doi:10.3390/en10060801.
 6. Quaggiotto, D.; Zarrella, A.; Emmi, G.; De Carli, M.; Pockelé, L.; Vercruysse, J.; Psyk, M.; Righini, D.; Galgaro, A.; Mendrinós, D.; et al. Simulation-Based Comparison between the Thermal Behavior of Coaxial and Double u-Tube Borehole Heat Exchangers. *Energies* **2019**, *12*, 2321, doi:10.3390/en12122321.
 7. Mendrinós, D.; Katsantonis, S.; Karytsas, C. Pipe Materials for Borehole Heat Exchangers. *Eur. Geotherm. Congr.* **2016**, 2016.
 8. Mendrinós, D.; Katsantonis, S.; Karytsas, C. Review of Alternative Pipe Materials for Exploiting Shallow Geothermal Energy. *Innov. Corros. Mater. Sci. Former. Recent Pat. Corros. Sci.* **2017**, *7*, 13–29, doi:10.2174/2352094907666170327163227.
 9. Tang, F.; Nowamooz, H. Factors Influencing the Performance of Shallow Borehole Heat Exchanger. *Energy Convers. Manag.* **2019**, *181*, 571–583, doi:10.1016/j.enconman.2018.12.044.
 10. Zanjani, A.M.; Gharali, K.; Al-Haq, A.; Nathwani, J. Dynamic and Static Investigation of Ground Heat Exchangers Equipped with Internal and External Fins. *Appl. Sci.* **2020**, *10*, 8689, doi:10.3390/app10238689.
 11. Paul, K.C.; Pal, A.K.; Ghosh, A.K.; Chakraborty, N.R. Thermal Measurements of Coating Films Used for Surface Insulation and Protection. *Surf. Coatings Int. Part B Coatings Trans.* **2004**, *87*, 137–141, doi:10.1007/BF02699608.
 12. UNI 9099:1989, Tubi Di Acciaio Impiegati per Tubazioni Interrate o Sommerse. Rivestimento Esterno Di Polietilene Applicato per Estrusione.
 13. UNI ISO 5256:1987, Tubi Ed Accessori Di Acciaio Impiegati per Tubazioni Interrate o Immerse. Rivestimento Esterno e Interno a Base Di Bitume o Di Catrame.

14. Cadelano, G.; Bortolin, A.; Ferrarini, G.; Molinas, B.; Giantin, D.; Zonta, P.; Bison, P. Corrosion Detection in Pipelines Using Infrared Thermography: Experiments and Data Processing Methods. *J. Nondestruct. Eval.* **2016**, doi:10.1007/s10921-016-0365-5.
15. Parker, W.J.; Jenkins, R.J.; Butler, C.P.; Abbott, G.L. Flash Method of Determining Thermal Diffusivity, Heat Capacity, and Thermal Conductivity. *J. Appl. Phys.* **1961**, *32*, 1679–1684, doi:10.1063/1.1728417.
16. Akoshima, M.; Baba, T. Thermal Diffusivity Measurements of Candidate Reference Materials by the Laser Flash Method. *Int. J. Thermophys.* **2005**, *26*, 151–163, doi:10.1007/s10765-005-2361-3.
17. Jannot, Y.; Degiovanni, A. *Thermal Properties Measurement of Materials*; ISTE: London, UK 2018, doi:10.1002/9781119475057.
18. Ferrarini, G.; Bison, P.; Bortolin, A.; Cadelano, G.; Rossi, S. Thermal Diffusivity Measurement of Ring Specimens by Infrared Thermography. In *Thermosense: Thermal Infrared Applications XXXIX*; SPIE: Anaheim CA, USA 2017, doi:10.1117/12.2262512.
19. Spierings, A.B.; Schneider, M.; Eggenberger, R. Comparison of Density Measurement Techniques for Additive Manufactured Metallic Parts. *Rapid Prototyp. J.* **2011**, *17*, 380–386, doi:10.1108/13552541111156504.
20. O'Neill, M.J. Measurement of Specific Heat Functions by Differential Scanning Calorimetry. *Anal. Chem.* **1966**, *38*, 1331–1336, doi:10.1021/ac60242a011.
21. Ferrarini, G.; Bortolin, A.; Cadelano, G.; Finesso, L.; Bison, P. Multiple Shots Averaging in Laser Flash Measurement. *Appl. Opt.* **2020**, *59*, E72–E79, doi:10.1364/ao.389564.
22. Bison, P.; Clarelli, F.; Vannozzi, A. Pulsed Thermography for Depth Profiling in Marble Sulfation. *Int. J. Thermophys.* **2014**, *36*, 1123–1130, doi:10.1007/s10765-014-1734-x.
23. Bison, P.G.; Cernuschi, F.; Grinzato, E.; Marinetti, S.; Robba, D. Ageing Evaluation of Thermal Barrier Coatings by Thermal Diffusivity. *Infrared Phys. Technol.* **2007**, *49*, 286–291, doi:10.1016/j.infrared.2006.06.019.
24. Bison, P.; Cernuschi, F.; Grinzato, E. In-Depth and in-Plane Thermal Diffusivity Measurements of Thermal Barrier Coatings by IR Camera: Evaluation of Ageing. *Int. J. Thermophys.* **2008**, *29*, 2149–2161, doi:10.1007/s10765-008-0421-1.
25. Balageas, D.L.; Krapez, J.C.; Cielo, P. Pulsed Photothermal Modeling of Layered Materials. *J. Appl. Phys.* **1986**, *59*, 348–357, doi:10.1063/1.336690.

26. Luo, Y.; Xu, G.; Yan, T. Performance Evaluation and Optimization Design of Deep Ground Source Heat Pump with Non-Uniform Internal Insulation Based on Analytical Solutions. *Energy Build.* **2020**, *229*, 110495, doi:10.1016/j.enbuild.2020.110495.
27. Lamarche, L.; Kajt, S.; Beauchamp, B. A Review of Methods to Evaluate Borehole Thermal Resistances in Geothermal Heat-Pump Systems. *Geothermics* **2010**, *39*, 187–200, doi:10.1016/j.geothermics.2010.03.003.
28. De Carli, M.; Tonon, M.; Zarrella, A.; Zecchin, R. A Computational Capacity Resistance Model (CaRM) for Vertical Ground-Coupled Heat Exchangers. *Renew. Energy* **2010**, *35*, 1537–1550, doi:10.1016/j.renene.2009.11.034.
29. Carslaw, H.S.; Jaeger, J.C. *Conduction of Heat in Solids*; Oxford University Press: Oxford, UK, 1980

9.2 FEM evaluation of heat exchange efficiency variability under transient conditions for different coaxial ground heat exchangers materials and subsoil contexts

9.2.1 Abstract

In the framework of the EU Horizon 2020 Cheap-GSHPs and GEO4VICHIC projects an innovative vertical Ground Heat Exchanger (GHE) has been developed combined with a specific drilling methodology, with the aim of maximizing the heat exchange efficiency. It is coaxial, formed by an external metal pipe in direct contact with the ground. A simplified finite element method (FEM) has been developed to compare the heat exchange efficiency of this new vertical coaxial GHE with the traditional, plastic one, in transient working conditions. The paper presents the results obtained considering different conditions on terms of materials (metallic or plastic tubes), annular space filling grout, presence or absence of tube coating and different surrounding ground environments. Comparison of different pipe configurations and ground conditions indicates that thermal performance under transient conditions is mostly affected by the moisture content of the ground. In this regard, the presence of underground saturated materials and grouting is more relevant in specific lithologies such as clays.

9.2.2 Introduction

Recently, research in the field of surface geothermal energy has embraced the attempt to broaden the base of exploitable sites, seeking new solutions that overcome installation barriers such as constraints of available area for the installation of ground heat exchangers or drilling depth. Increasing the thermal efficiency of the ground heat exchangers was chosen as one of the possible solutions. In fact, more efficient ground heat exchangers would require a shorter total length of pipes inserted into the ground to cover the building energy needs, compared to less performing solutions. As a result, fewer ground heat exchangers would be used in case of constrained available area, or shorter in case of depth limitations due to regulatory bans or geological constraints. As part of the EU Horizon 2020 Cheap-GSHPs and GEO4VICHIC projects [1,2,3], a new drilling methodology was developed that would allow the installation of vertical ground heat exchangers with external metal pipes in direct contact with the ground.

This solution would benefit both from the high thermal conductivity of the metal (e.g., thermal conductivity of carbon steel and HDPE is 45 and $0.41 \text{ W}\cdot\text{m}^{-1}\cdot\text{K}^{-1}$, respectively) and from the absence of the grouting layer which is generally present to fill the annular space around the ground heat exchanger where traditional installation methods are applied, thus acting as additional thermal resistance between the pipe and the ground. The innovative proposed materials for the GHE pipe were stainless steel (i.e. AISI 304 and 316) and carbon steel, the latter requiring coating to prevent corrosion (e.g. primer paint or bitumen). As part of the GEO4VICHIC project, these metallic GHEs were developed and installed on site to assess the practical feasibility and to allow experimental measures (Figure 1).

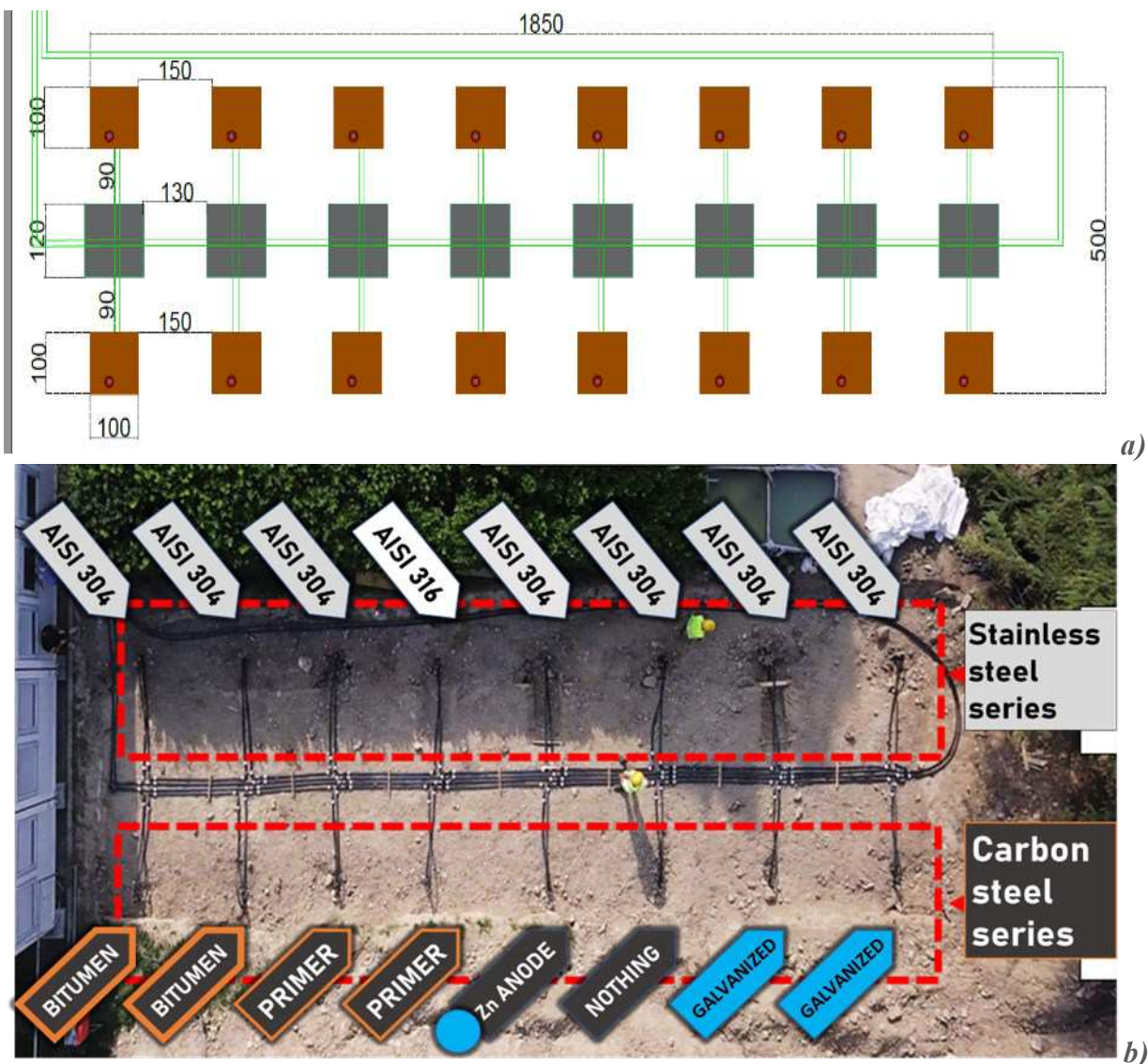


Figure 1: (a) Layout of the geothermal field, showing the pits for housing the metallic GHE (brown areas) and the horizontal hydraulic connection switch systems (gray areas). (b) Aerial view of the site. The labels indicate the material and the anti-corrosion measures applied.

The development also included laboratory measurement of the thermophysical properties of GHE materials, coatings, grouting and a range of ground lithologies. While a comparison of the metal choices and their behaviour against the grouted or plastic (HDPE) heat exchanger can be made based on the equivalent thermal resistance provided by each configuration, this does not reflect actual Ground Source Heat Pump (GSHP) system operation. In fact, during operation, a geothermal heat pumps continuously switches on and off according to the variable energy demand of the served building. Therefore, a more complete evaluation of the efficiency of the newly developed metallic coaxial GHE inserted in the whole GSHP system should analyse the thermal behaviour in transient conditions. Additionally, the thermal behaviour of the GHE coupled with different stratigraphic and hydrogeological conditions is expected to lead to different results. The ultimate goal is to determine the best performing configuration of the GHE pipes for each of the considered underground contexts.

9.2.3 Materials and methods

Several methods are available to simulate the thermal behaviour of shallow geothermal systems, ranging from analytical to numerical models [4]. In this work, the comparison of different pipe solutions has been done using finite elements method software COMSOL Multiphysics® [5]. The coaxial system has been simplified by taking into account a cross section consisting of three concentric annular layers. The layers, as shown in Figure 1, from internal to external, represent the external pipe of the ground heat exchanger, the anti-corrosion coating (in case of carbon steel pipe) or grouting (in case of plastic pipe) and the homogeneous surrounding ground, respectively. The simulation was performed solving the heat equation in transient conditions. The initial temperature of the undisturbed ground was set to 14 ° C. A constant heat flow was applied on the internal surface of the pipe, resulting in a fluid temperature higher than the ground temperature, similarly to what would happen during real operation in the summer season for cooling. Thereafter, heat propagation and ground temperature rise were simulated for 24 hours at a rate of 10 seconds.

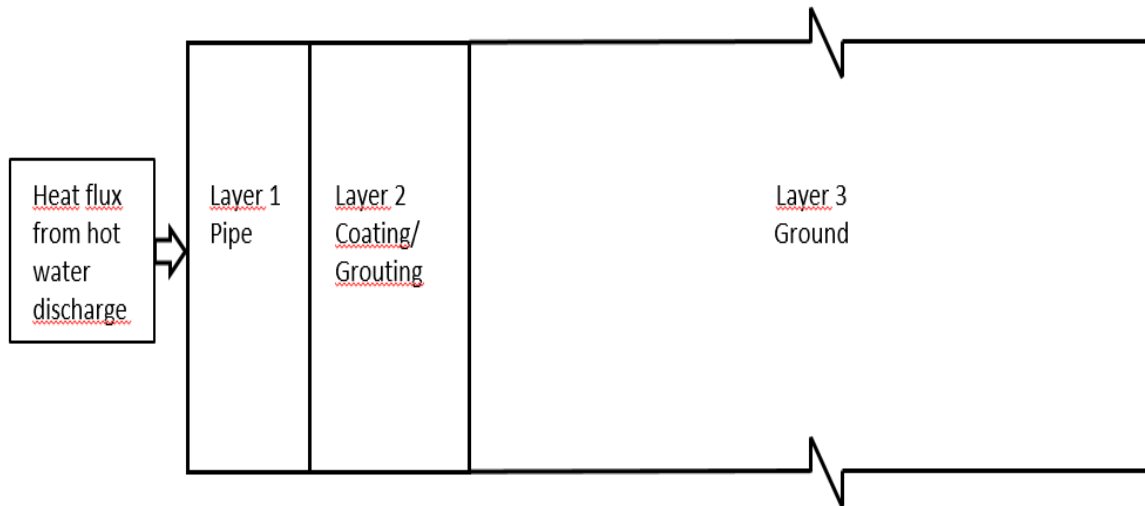


Figure 1: Scheme of the thermal model. The thickness of each layer varied according to Table 1.

As shown in table 1, there are several possible options for each layer, covering possible materials and geometries, as well as dry or wet conditions in the surrounding ground. By combining the different options available for each layer, a total of 90 distinct scenarios have been simulated. The possible materials variability for each layer was made on the basis of those compatible with the new groutless GHE installation method developed during EU Horizon 2020 Cheap-GSHPs and GEO4VICHIC projects.

Table 1: Diagram of the possible options for each layer which constitutes the simplified model of a ground coaxial heat exchanger.

Layer	Material	Thickness [mm]	Moisture condition
Pipe	Carbon steel, stainless steel, plastic (HDPE)	2	Not applicable
Coating/Grouting	bitumen, primer, grouting	1 (bitumen), 0.5 (primer), 50-100-150 (grouting)	(not applicable to coatings) Dry/Saturated
Ground	Gravel, medium sand, clayey-silt	Semi-infinite	Dry/Saturated

Each layer is characterized by its geometry, variable depending on the material itself, and its thermophysical properties that regulate the heat diffusion : thermal conductivity, density and specific heat capacity. These values have been taken from recent literature in which materials have been measured in laboratory, even at different water content [6,7,8,9]. Where the measured values of wet materials were not available in the literature, they were approximated [10,11] by taking into account the effect of water as a function of the saturation (ratio between the volume filled by water and the volume of the pores, otherwise filled by air) and the total volume of the layer. Table 2 shows the thermophysical properties adopted for pipe and coating materials; those adopted for grouting and ground materials are shown in table 3.

Table 2: Thermophysical properties of non-porous materials (pipe and coating) taken from literature [6].

	Thermal conductivity [W·m ⁻¹ ·K ⁻¹]	Density [kg·m ⁻³]	Specific Heat [J·kg ⁻¹ ·K ⁻¹]
Carbon steel – pipe	45	7700	460
Stainless steel AISI 304 – pipe	16.2	8000	500
Plastic (HDPE) – pipe	0.41	940	1930
Bitumen – coating	0.2	1500	1720
Primer – coating	0.62	2200	1100

9.2.4 Results

The simulation results provide the temperature distribution through the different layers. To compare the results of the 90 modelled scenarios, the increase in ground temperature over time was registered at a control point located at 25 cm from the ground heat exchanger from the external surface of the pipe,. Figure 2 directly compares the trend of the temperature increase over time considering different ground lithologies (clayey silt, medium sand and gravel) both in water saturated (Figure 2a) and in dry conditions (Figure 2b), respectively. The comparison clearly highlights the

different thermal behaviour of the lithologies on the thermal response of the modelled system.

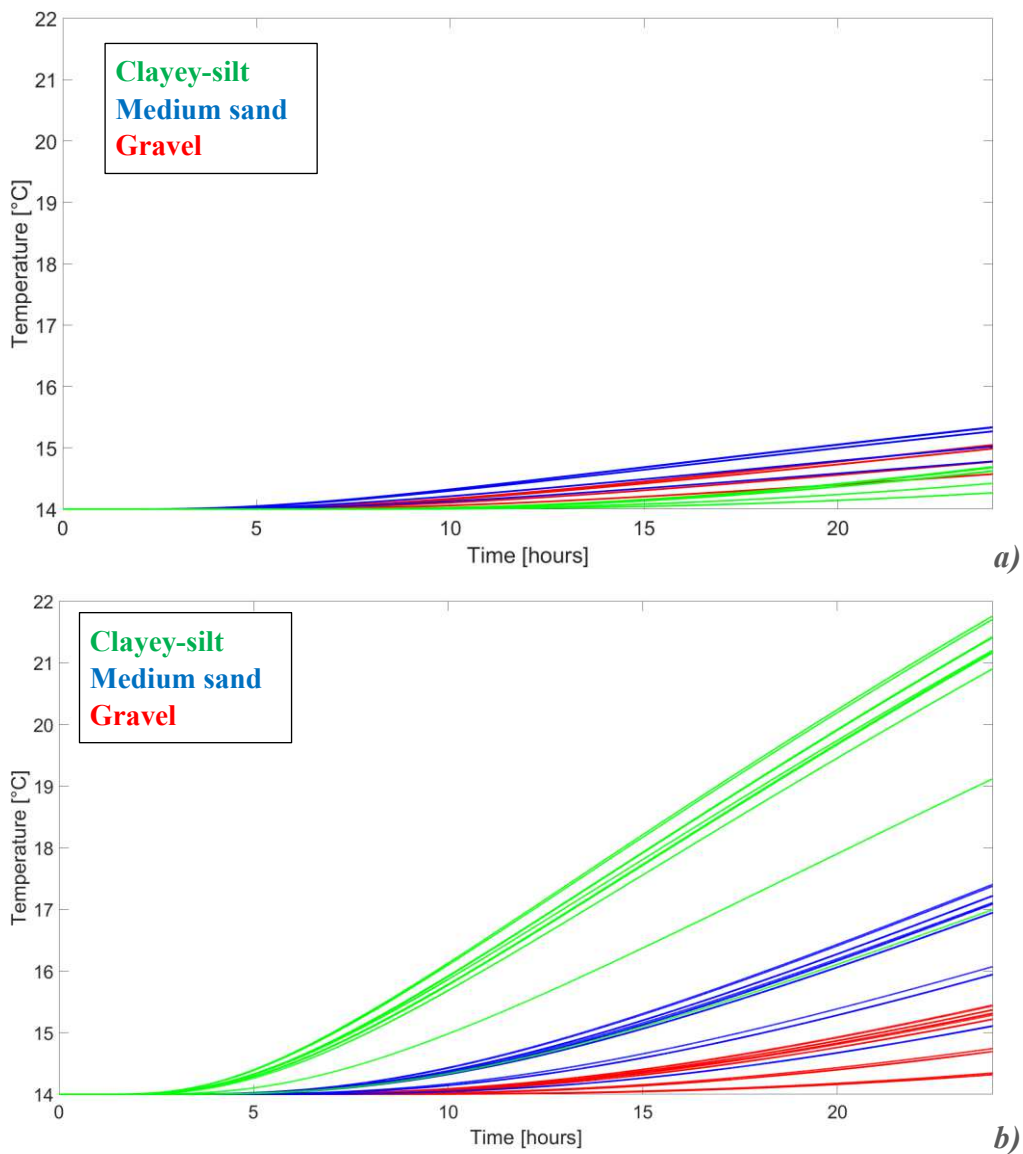


Figure 2: The increase in the temperature of the soil at 25 cm from the pipe shows a differentiated thermal behaviour between the types of ground in (a) saturated, and (b) dry conditions.

Comparing the results presented in the figure above, it is evident that, despite the variations in thermal conductivity and mass density between saturated and dry materials, the material's specific heat plays a key role in the heat propagation mechanism governed by thermal diffusivity (α). Since the heat capacity (ρc) of water is significantly greater than the heat capacity of the selected lithologies (as shown in table 3), thus the inertia of the system in water saturation condition is higher than dry conditions. The hypothesis that derives from this is that a heat waves that cross the wet

material would be attenuated (have a lower amplitude) and out of phase with respect to the heat wave that passes through the dry material, resulting in a lower temperature increase over time. The presence of water is critical with respect to the maximum values of overall temperature reached after 24 hours: much higher in dry conditions than in saturated ones. The presence of water has also determined that in saturation conditions the medium sand values are higher, while in dry conditions the clayey silt values are higher. The mineralogical composition of the sediments themselves plays a role (for example, sand is usually composed of minerals such as quartz and/or limestone which have a relatively high thermal conductivity, while fine materials are composed of minerals with lower thermal conductivity). Furthermore, one would expect the explanation to concern the coarser grain of the gravel, whereby in dry conditions the heat transfer passes through the contact points between the clasts, which are few. Despite this, at this modelling scale the driving parameters of heat diffusion are specific heat and density, and the result reflects the thermal diffusivity values (i.e., in dry conditions, the α value of clayey silt is more than double that of gravel and sand).

Table 3: Thermophysical properties of porous dry materials) taken from literature [7,8,9]. and water.

	Thermal conductivity [W·m⁻¹·K⁻¹]	Density [kg·m⁻³]	Specific Heat [J·kg⁻¹·K⁻¹]
Grout “fassageo100” (dry)	0.36	1292	1000*
Gravel (dry)	0.4	2000	1450
Medium sand (dry)	0.4	2000	945
Clayey silt (dry)	0.5	1200	935
Water	0.6	1000	4182

*estimated value

The following figure 3 shows the same temperature trends over time, this time focusing on the comparison between the new metal coaxial HE in direct contact with the ground, and the more traditional HDPE ones than filled with grout, as usual. Each trend plotted in figure 3 represents each of the 90 modelled scenarios. Most of them overlap, which

means there are no significant differences in terms of thermal response. In particular, metal solutions behave the same, regardless of the type of metal and the presence of coatings, and the only difference is due to the surrounding context. The comparison takes into account the saturated (Figure 3a) and dry condition (Figure 3b) separately.

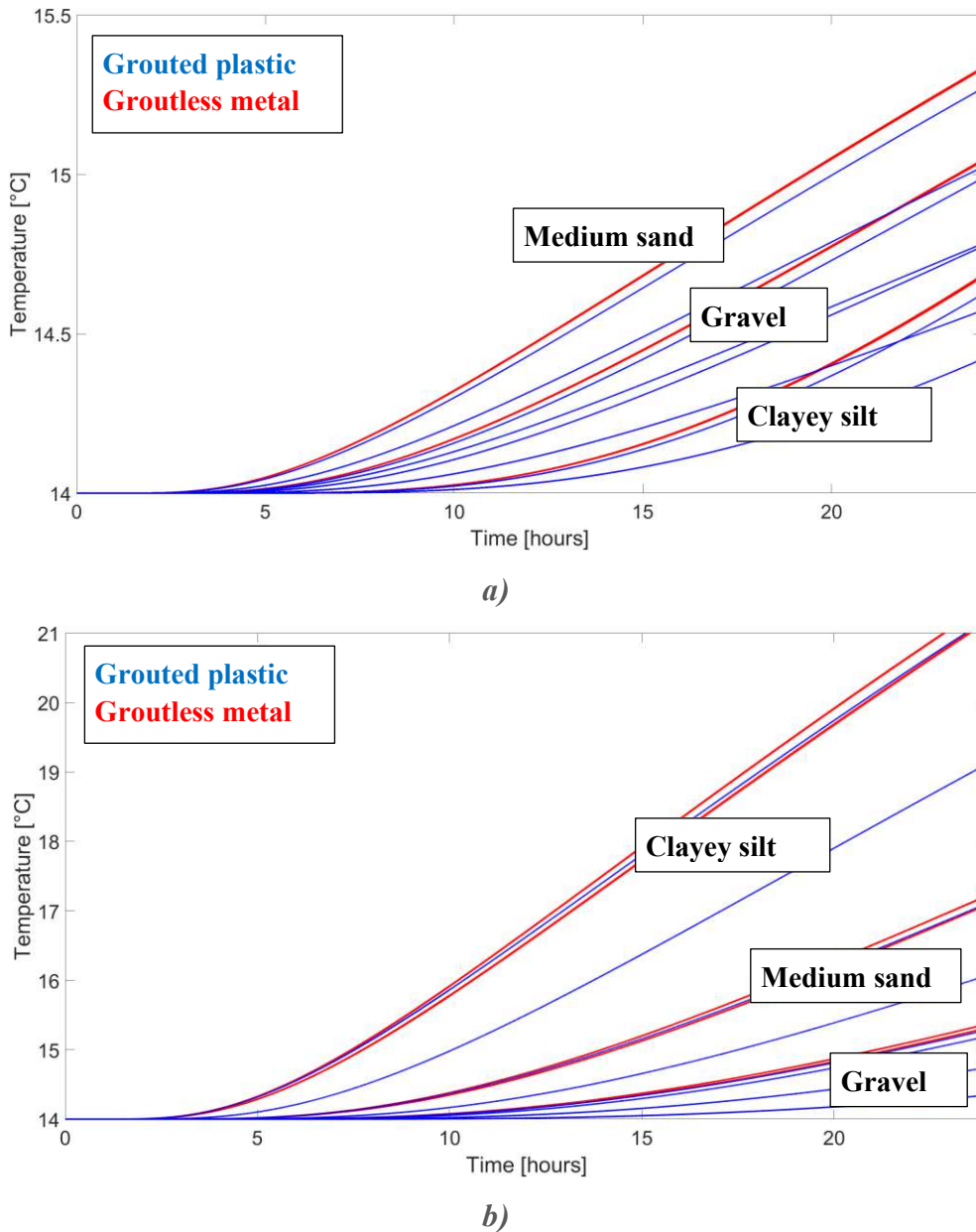


Figure 3: Metallic solutions (red) have superior thermal performance compared to grouted plastic (blue) for all types of ground in (a) saturated, and (b) dry conditions. (a is saturated, b is dry).

The results show no evidence of significant differences between stainless steel and coated carbon steel (in red). The advantage of the metal is less relevant in conditions of water saturation. As expected [6], the higher conductivity of carbon steel is partially

offset by the thermal resistance given by the necessary coating. Thus, protected carbon steel tubes have the same overall thermal resistance of the stainless steel ones. Furthermore, as observed, the lower thermal performance of plastic solutions (in blue) compared to metal ones is not linked to the pipe itself, but is almost entirely ascribable to the grouting and its thickness. The material of which the tube is made does not play a determining role. In fact, the wall thickness of the pipe is far less than that of the grouting, which is the main thermal resistance in the system. Consequently, the modelling results highlight that with respect to the heat exchange capacity, the grouted plastic solutions are comparable to the metal GHE, as long as the thickness of the grout is very small (less than 1 cm). In dry conditions, there are significant advantages in using groutless metal solutions over grouted plastic ones, particularly in clayey silty grounds, and to a lesser extent, also in sand or gravel. Under water saturation conditions, due to the predominant effect of water on the thermal inertia, there are no significant differences between the modelled scenarios.

9.2.5 Conclusions

The need for high efficiency ground heat exchangers for shallow geothermal applications has led to the experimentation of groutless metal solutions. However, underground metal pipes suffer corrosion (e.g. carbon steel) or are expensive (e.g. stainless steel). Therefore, this study was necessary to evaluate the compensation of these drawbacks in terms of thermal performance improvement compared to traditional solutions such as grouted plastic pipes.

A computational modelling in transient conditions took into account the different possible configurations of the pipes given by the combination of pipe materials, pipe coatings, grouting, together with the coupling with different underground lithologies, also with regard to the presence of groundwater. During operation, the Ground Source Heat Pump system switches on and off continuously according to the varying energy needs of the building being served. For this reason, the reactivity of the GHE to variations in thermal regimes was evaluated by running the simulation in transient mode. Therefore, the thermal conductivity of the materials was taken into account, along with other properties as the thermal diffusivity that governs heat propagation. In particular, the switching-on of the GSHP in summer mode was modelled. In this circumstance the water was critical with respect to the maximum values of the soil temperature, reached at 25 cm from the pipeline after 24 hours. Temperature value was much higher in dry conditions than in saturated conditions. The phenomenon is attributable to the increase in thermal inertia due to water. In this regard, the ground

materials responded differently, as the overall thermal diffusivity of the ground layer was based on the combination of the specific properties of the mineral composition and the amount of water in saturation conditions. In dry conditions, the models in clayey silt environment reached higher temperature than other materials, due to its higher thermal diffusivity. By way of reference, all the considered lithologies are an order of magnitude lower in terms of thermal diffusivity than a rock material, which would have performed better and which would probably have been less affected by the presence of water. Rock lithology, however, cannot be addressed with the deemed drilling method, and therefore it has not been presented in detail.

The results showed that groutless metal solutions performed better than grouted plastic ones in dry underground conditions, especially in clayey underground. The thickness of the grouting is the most relevant parameter in this regard. In underground conditions saturated with water, metallic solutions are still superior to plastic ones, but to a much lesser extent, due to the high thermal inertia of the system which makes the contribution of the pipe itself less relevant.

Acknowledgements



GEO4CIVHIC project has received funding from the European Union's Horizon 2020 research and innovation program under grant agreement No. 792355

9.2.6 References

1. Horizon 2020 Cheap GSHPs project, grant no. 657982. <https://cordis.europa.eu/project/id/657982/>. Last access: 20 July 2022.
2. Horizon 2020 GEO4CIVHIC project, grant no. 792355 <https://cordis.europa.eu/project/id/792355/>. Last access: 20 July 2022.
3. Pockelé, L.; Mezzasalma, G.; Righini, D.; Verduyck, J.; Cicolini, F.; Cadelano, G.; Galgaro, A.; Dalla Santa, G.; De Carli, M.; Emmi, G.; et al. Innovative Coaxial Heat Exchangers for Shallow Geothermal. In World Geothermal Congress; Elsevier: Reykjavik, Iceland, 2021.
4. Christodoulides, P.; Vieira, A.; Lenart, S.; Maranhã, J.; Vidmar, G.; Popov, R.; Georgiev, A.; Aresti, L.; Florides, G. Reviewing the Modeling Aspects and

- Practices of Shallow Geothermal Energy Systems. *Energies* **2020**, *13*, 4273. <https://doi.org/10.3390/en13164273>
5. COMSOL Multiphysics® v. 5.4. www.comsol.com. COMSOL AB, Stockholm, Sweden.
 6. Cadelano, G.; Bortolin, A.; Ferrarini, G.; Bison, P.; Santa, G. D.; Di Sipio, E.; Bernardi, A.; Galgaro, A. Evaluation of the Effect of Anti-Corrosion Coatings on the Thermal Resistance of Ground Heat Exchangers for Shallow Geothermal Applications. *Energies* 2021. <https://doi.org/10.3390/en14092586>.
 7. Mascarin, L.; Garbin, E.; Di Sipio, E.; Dalla Santa, G.; Bertermann, D.; Artioli, G.; Bernardi, A.; Galgaro, A. Selection of Backfill Grout for Shallow Geothermal Systems: Materials Investigation and Thermo-Physical Analysis. *Constr. Build. Mater.* 2022. <https://doi.org/10.1016/j.conbuildmat.2021.125832>.
 8. Dalla Santa, G.; Peron, F.; Galgaro, A.; Cultrera, M.; Bertermann, D.; Mueller, J.; Bernardi, A. Laboratory Measurements of Gravel Thermal Conductivity: An Update Methodological Approach. In *Energy Procedia*; 2017. <https://doi.org/10.1016/j.egypro.2017.08.287>.
 9. Dalla Santa, G.; Galgaro, A.; Sassi, R.; Cultrera, M.; Scotton, P.; Mueller, J.; Bertermann, D.; Mendrinós, D.; Pasquali, R.; Perego, R.; Pera, S.; Di Sipio, E.; Cassiani, G.; De Carli, M.; Bernardi, A. An Updated Ground Thermal Properties Database for GSHP Applications. *Geothermics* 2020. <https://doi.org/10.1016/j.geothermics.2019.101758>.
 10. S. Torquato. *Random Heterogeneous Materials – Microstructure and Macroscopic Properties*, Springer, 2002
 11. F. Ochs, W. Heidemann, H. Müller-Steinhagen, Effective thermal conductivity of moistened insulation materials as a function of temperature, *International Journal of Heat and Mass Transfer*, 51(3-4), 539-552, (2008).

10 Themed topic chapter: Evaluation of the durability of metallic GHEs and the effectiveness of passive anti-corrosion measures

This chapter is dedicated to evaluating the durability of the new vertical coaxial metal heat exchangers. The measurements of the corrosion rate in the laboratory allowed to evaluate the coupling between a metal alloy exposed to specific conditions of the underground. Applicable measures to limit corrosion of carbon steel pipes were tested on site on the “well point” ground heat exchangers. This allowed to evaluate the anti-corrosion measures in terms of their impact on the heat transfer performance.

Based on two manuscripts:

- G. Cadelano, A. Bortolin, E. Di Sipio, G. Ferrarini, P. Bison, A. Bernardi, G. Dalla Santa, A. Galgaro. **Laboratory assessment of corrosion rate of carbon steel ground heat exchangers**, *Adv. Geosci.*, 58, 41–46, 2022; <https://doi.org/10.5194/adgeo-58-41-2022>

The manuscript has been published by European Geosciences Union Division Energy, Resources & Environment (ERE) special issue 2022 in *Advances in Geosciences (ADGEO)*. GC designed the study; GC, PB and GF developed the methods; GC, AB and GF collected the data; GC, GF and PB developed the numerical model. All the authors discussed the data and agree on their interpretation; GC, AB, PB and GF wrote the manuscript. All the co-authors contributed to the final polishing of the manuscript.

- G. Cadelano, A. Galgaro, G. Dalla Santa, E. Di Sipio, A. Bortolin, A. Bernardi. **Evaluation of different metal anti-corrosion countermeasures on coaxial ground loop heat exchangers for shallow geothermal applications.**

The manuscript has been presented to European Geothermal Congress 2022 (EGC 2022). GC designed the study; GC and AG developed the methods; GC, AB and AG collected the data. All the authors discussed the data and agree on their interpretation; GC, AB, E.DS, G.DS and AG wrote the manuscript. All the co-authors contributed to the final polishing of the manuscript.

10.1 Laboratory assessment of carbon steel corrosion rate of grout-less ground heat exchangers

10.1.1 Abstract

The materials used in the manufacture of geothermal heat exchangers for shallow geothermal applications play an important role in the overall system performance, especially if grout is not being used to seal the boreholes in which the heat exchanger is installed. The subject of this study is the durability evaluation of a vertical coaxial ground heat exchangers made of steel that is coupled directly to the ground. This solution minimizes the thermal resistance between the heat exchanger and the ground, but presents the important drawback of removing any protection toward the surrounding environment. This type of metal heat exchanger is promising because it offers higher heat exchange efficiency. Moreover, thanks to an innovative drilling technology that combines vibrating pile driving and high pressure water jetting, the installation time in certain type of undergrounds are reduced in comparison with other more established installation methodologies. Among the materials proposed for manufacturing such vertical geothermal heat exchanger, carbon steel is suitable and have potential, due to its low cost and high thermal conductivity. The main disadvantage of this material is that it is strongly subject to corrosive attack, according to the chemo-physical properties of the underground. This study investigated the corrosion behaviour of carbon steel used in an experimental underground heat exchanger and assessed its durability over time. Corrosion rate of steel samples were measured in the laboratory by weight loss method after exposure over a specified period in a selected ground medium. Different ground conditions were tested, resulting in different densities and moisture contents of ground samples collected on the field. Based on the results, the corrosion rate of carbon steel is evaluated as a function of water content and rate of ground compaction. This information has allowed to advance more accurate quantitative forecast of the expected operational life of installed geothermal exchangers and their safety over time.

10.1.2 Introduction

As practice of the European research projects Cheap GSHPs [1], and GEO4CIVHIC [2], a holistic approach has been taken to make shallow closed-loop geothermal energy

more convenient, safe and efficient. During projects implementation, various aspects were addressed, such as pumps, secondary fluids, as well as drilling methods and the design of ground heat exchangers. Focusing on vertical ground heat exchangers (GHEs), the coaxial types have been researched and improved by optimizing the general design [3]. One of the new technologies being developed during GEO4CIVHIC is a methodology that allows both borehole drilling and pipe installation at the same time. This greatly reduces costs and opens up the possibility to have the pipe in direct contact with the ground. In this way, there is no extra thermal resistance between the heat transfer fluid and the ground because there is no injection of grout into the borehole. In fact, there is no annular gap at all, as result of the installation procedure. The only remaining thermal resistance due to a physical item is the pipe itself. Based on these advances, the research focused at further improving the system by exploring alternative GHE materials [4,5] such as metals, that have very good thermal properties [6,7]. Plastic represents the most common pipe material in shallow geothermal systems, despite its poor thermal properties, as it is affordable and does not degrade by corrosive attack. Corrosion of pipe used for GHEs is crucial because it leads to system failure and is thought to be an environmental hazard in the event of a liquid leak (in particular if antifreeze liquids are used). Stainless steel is almost not subject to corrosion but it is very expensive and thus not economically sustainable. Therefore, research moved to study the advantages and drawbacks of carbon steel, a quite affordable material that is characterized by an excellent thermal conductivity [8]. Corrosion is renowned as a major problem for the long-term function and integrity of all kind of pipelines [9] including buried carbon steel components such as electric poles or pipes. In the case of geothermal heat exchangers, this aspect is especially important as it causes damage beyond system failure. Indeed, the leakage of heat transfer fluid through corroded piping causes serious environmental problems. The mechanism of corrosion is variable and depends on the specific composition of the metal alloy and the local underground conditions. The dissolution of carbon steel is caused by electrochemical processes due to the presence of both oxygen and water. Additionally, other parameters, related to ground properties, can potentially enhance corrosion issues [10]. Such parameters are pH, resistivity, humidity and oxygen. However, the operational criteria for assessing ground corrosion only take into account ground properties from a qualitative point of view. The corrosion rate, defined as the mass of metal per unit time destroyed, can be assessed using standard laboratory procedures based on measuring weight loss over time. These methods are used in many fields of engineering but not yet exploited in shallow geothermal systems. By applying these methods to metal samples such as GHE piping material buried under known conditions, it is possible to quantitatively assess the site-specific corrosion rate.

10.1.3 *Materials and methods*

The severity of corrosion can be expressed by the corrosion rate (CR) that consists in the material loss over time of metals exposed to corrosive environments. Concerning geothermal components, it depends on the coupling of the metal constituting the outer pipe of the exchanger with a specific ground that can be found in the strata where the pipe is buried. Usually, CR is expressed in terms of depth of penetration, so in metric units it is millimeters per year. Corrosion rates can be measured in the laboratory according to standard test methods. They generally consist of exposing metal samples of known density and shape in a corrosive environment for a period of time. The material loss is then measured by gravimetric analyses. In this study, the ASTM G162-18 method [11] was applied to calculate the corrosion rate of structural carbon steel specimens. It is based on weight loss, which is expressed by the following equation (1):

$$CR = 87.6 \cdot \frac{W}{\rho \cdot A \cdot t} \quad (1)$$

Where:

W: weight loss in milligrams;

A: area of the sample (cm²)

ρ : metal density (g/cm³)

t: time of exposure in corrosive environment (hours).

C: Corrosion Rate: the weight loss of a pipe system or other metallic surfaces after exposure to a corrosive environment (mm/y)

This practice does not replicate all field conditions and variables existing underground, such as stray currents, microbiologically influenced corrosion, non-homogeneous electrochemical conditions, but it allows to simulate the most common and relevant conditions that determine the corrosiveness of a soil.

Corrosion rate is a useful parameter to assess the lifespan of metal-based buried structures, and therefore it also determines the maintenance requirements for components. Assuming, according to NACE Corrosion Engineer's Reference Book [12], a uniform corrosion over the entire component surface, and CR as constant, obtaining the maximum theoretical lifetime of a buried pipe as (2):

$$\textit{Estimated lifetime} = \frac{\textit{pipewallthickness}}{CR} \quad (2)$$

It is worth remarking that the estimated lifetime refers to the complete destruction of the pipe. Actual service life should presumably be much shorter, especially if mechanical integrity is compromised due to external stresses or forces, e.g. water pressure, vibrations, etc. Moreover, the possible simultaneous corrosion attack on the internal side of the pipe is neglected in this study. The expected lifetime of any geothermal system is always limited. For the sake of having a reference value, in most cases the lifetime can be considered economically sustainable when it is over 30 years [13] of actual service life.

Experimental process and samples preparation

The experiment was conducted by collecting the ground samples from a shallow geothermal site in the frame of GEO4CIVHIC project located in Padua, Italy. In such site, carbon steel groutless vertical experimental ground heat exchangers were installed. The samples were collected 1.5-1.8 meters below ground level which is very shallow but consistent with the specific type of GHEs which are very short (average thermal exchange length is less than 7 meters). In addition, it represents a worst-case scenario, as it was assumed that corrosion would be more critical near ground level due to the abundance of oxygen and water from precipitation. The ground samples typology is clayey silt and the average measured pH is 8.16 at the sampling depth [14]. A total of 30 specimens (i.e. 30 collected ground samples from the same location) were inserted in a container. Then, the parameters known to critically impact on the corrosion rate, as oxygenation (in relation to the compactness of the soil) and water content, were gradually changed. The samples were prepared according to the ASTM G162-18 (Standard Practice for Conducting and Evaluating Laboratory Corrosion Tests in Soils), also paying attention to the ground quantities and the specifications of the containers.

Firstly, the ground samples were dried in a ventilated oven at 105 ° C constant temperature for several days, regularly monitoring their drop in mass to equilibrium. In order to evaluate the corrosion behaviour of the soil with varying moisture content (MC), samples were prepared by artificially setting different quantities of water, as a fraction percentage of the saturation moisture content (SMC) of the soil materials. SMC is defined as the maximum amount of water that can be contained in a ground type when all pore spaces are filled with water. The reference moisture contents of the

analysed ground samples were: 0%, 20%, 40%, 70% and 85% obtained by gravimetric method. By pressing the samples, two levels of compactness were arbitrarily obtained: 7 g/cm³ and 13 g/cm³ to simulate loose and compacted ground respectively. For each combination of MC level and compactness, three different ground samples were prepared for redundancy, as reported in Table 1.

Table 1: Experiments organization scheme. The numbers of experiment for each MC and ground compactness level are reported.

		Moisture content levels				
		0%	20%	40%	70%	85%
Ground Compactness levels	Loose	3	3	3	3	3
	Compact	3	3	3	3	3

Subsequently, for each of the 30 polyethylene containers filled with ground with varying compactness and MC, a metal coupon of known size and mass was inserted inside, as schematized in Figure 1.

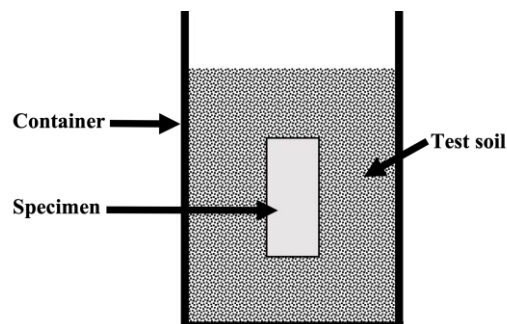


Figure 1: Experimental setup scheme during the exposure of metal coupons, according to ASTM standard.

The coupons were made of S235JRH carbon steel plates having surface area equal to 1.8 cm². Oily greases or other corrosion inhibiting substances can be often found on metal components, as results of metal manufacturers practices to protect the metal from corrosion where no enamel or other proper passive anti-corrosion measures are present. Therefore, the coupons were cleaned by rinsing them in ethylic alcohol solution. The

coupons were intended to simulate the outer pipe of the ground heat exchangers that were installed in the field, which are in fact made of carbon steel in direct contact with the ground, without grouting or filling in the borehole. The prepared containers, thus including the ground and the metal coupons, were sealed with plastic film, then kept undisturbed for an exposure time of 2304 hours at constant room temperature. During that period, the moisture content was also kept constant by refilling the water if necessary. In fact, a periodic monitoring by gravimetric method were implemented to check the containers for possible weight loss due to water evaporation. Finally, the metal specimens were extracted, cleaned, rinsed with alcohol solution and then weighed to evaluate the mass drop. Finally, the corrosion rate for each of them was calculated according to (1).

10.1.4 Results

The visual appearance of the carbon steel coupons surface after exposure to the corrosive ground environment is shown in Figure 2 that depicts unaltered photographic images of some coupons at the end of the test. It is evident that the corrosive attack progressed the most in soil environments where the moisture content was higher.

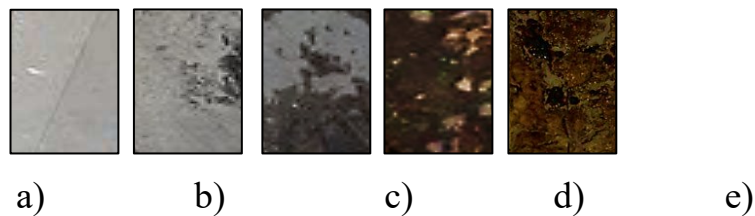


Figure 2: Visual images of specimens after 2304 hours exposition at different moisture contents; from left to right: 0% (a), 20% (b), 40% (c), 70% (d) and 85% (e). Ground density has not significant evidence on visual inspection.

The result of the gravimetric test shows that the corrosion rate increases non-linearly with the moisture content, as shown in Figure 3.

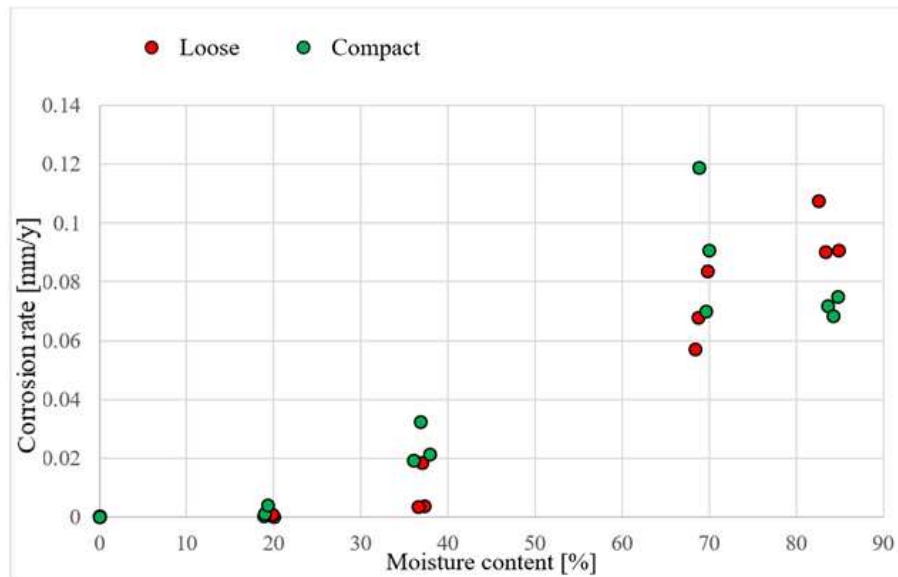


Figure 3: Corrosion rate of metal coupons as function of water content. Loose and compacted ground samples are represented in red and green, respectively.

Based on the results, the corrosion rate of the carbon steel coupons is highest (values of around 0.1 mmy) at >70% moisture content. At even higher moisture content, CR is greater for loose soil conditions. Corrosion rate is almost zero at 20% water content. Nonetheless, CR it is not negligible for coupons exposed at 40% of moisture content, especially in compact ground environment. At moisture content equal to 0%, the corrosion attack is negligible. As expected, results indicate that the corrosion rate of carbon steel under constant boundary conditions is higher when the soil has a higher moisture content, so the water content percentage seems to affect more the metal corrosion compared to the rate of ground compactness. It can be hypothesized that at low moisture content, the lower rate of ground compaction limits the corrosion due to a drainage effect. At higher moisture content, higher rate of ground compaction enhances corrosion because it would favor a differential oxygenation. The evaluation of the corrosion rate allows to advance the forecast of the maximum expected life of the ground heat exchangers. The number of years necessary to corrode completely the carbon steel pipe was calculated according to (2), and taking into account a pipe wall thickness equal to 2 mm. Results are shown in Table 2. The measurement uncertainty has been expressed as the standard deviation σ over the three values obtained from the redundant specimens.

Table 2: Maximum estimated life time in years, assuming a wall thickness of the pipe equal to 2 mm.

Water content [%]	Compact ground [years±σ]	Loose ground [years± σ]
0	-	-
20	>2500	>2500
40	87±22	550±30
70	25±3	30±5
85	28±1	21±2

The corrosion rate values obtained as a function of the moisture content can also be used to define more refined durability models that take into account the effect of precipitations, which can be relevant for very shallow installations. The annual variation in soil moisture directly affects the CR, which would therefore not be constant. In order to evaluate the effect of considering CR not constant, the rainfall data of the studied site were recovered from the meteorological data collected by the ARPAV (Regional Agency for the Protection of the Environment of Veneto) [15]. Data record of Padua weather station was processed to obtain a simplified model of variable moisture content. Assuming the average number of rainy days and individual rain events over the last 10 years, the adjusted annual CR would be ca. 0.04 mmy, which allows us to predict complete perforation of the pipe after about 50 years. However, the alternating cycles of wet-dry conditions as further aggravating parameters affecting the corrosion has not been considered, and it should be examined by future investigations.

10.1.5 Conclusions

In order to evaluate the durability of a new type of metal ground heat exchanger for shallow geothermal applications, a dedicated laboratory testing methodology was applied to assess the corrosiveness of the ground at the site where such GHEs were installed. Specifically, the test were mean to evaluate corrosion at very shallow depths, where corrosive attack is considered to be more critical due to the presence of moisture due to precipitations. Carbon steel metal samples were exposed in ground environment

collected on site. The corrosion rate was evaluated, also as a function of the main parameters that are known to affect corrosion, i.e. water content and rate of ground compaction, the latter related to ground oxygenation. This way of evaluating the expected life is partial and takes into account only the main corrosion mechanisms in the underground environment, and does not consider other corrosion phenomena induced e.g., by bacteria, stray currents or presence of organic matter. However, the applied methodology represents a promising introduction in the field, because it provides an indication that would help assess sites when designing a geothermal system. Under constant conditions, the worst-case corrosion rate is within 0.1 mmy at the site under consideration, assuming a constant moisture content $> 70\%$. In this context, the durability of a metal pipe with a wall thickness of 2 mm is approximately 20 years.

The results of this study allow for the introduction of ground corrosiveness assessment as a suggested methodology for evaluating a site. In fact, it would provide site-specific and quantitative forecast of the expected life of the GHEs. Furthermore, this methodology can be easily adapted to replicate site specificities that can impact soil corrosivity, such as precipitations, temperature variations, etc..

If the ground samples are collected at different depths, it would also be possible to test different tube materials against the different lithologies present in the different layers. This would imply the interesting possibility of designing a new type of vertical ground heat exchanger built not in a single tube material, but in sections of different materials, that are selected to ensure optimal coupling with the corresponding ground layer. For example, plastic should be used in the most superficial layers, where corrosion is more significant due to a greater presence of water and oxygen, and metal in the deeper layers.

Acknowledgements



GEO4CIVHIC project has received funding from the European Union's Horizon 2020 research and innovation program under grant agreement No. 792355

10.1.6 References

1. Horizon 2020 Cheap GSHPs project, grant no. 657982. <https://cordis.europa.eu/project/id/657982/it>. Last access: 20 June 2022.
2. Horizon 2020 GEO4CIVHIC project, grant no. 792355 <https://cordis.europa.eu/project/id/792355/>. Last access: 20 June 2022.
3. Pockele', L., Mezzasalma, G., Righini, D., Vercruyssen, J., Cicolin, F., Cadelano, G., Galgaro, A., Dalla Santa, G., De Carli, M., Emmi, G., Mendrinis, D., Pasquali, R., Bernardi, A.: Innovative Coaxial Heat Exchangers for Shallow Geothermal, Proceedings World Geothermal Congress 2020. Reykjavik, Iceland, 2020.
4. Mendrinis, D., Katsantonis, S.; Karytsas, C. Pipe Materials for Borehole Heat Exchangers. In Proceedings of the European Geothermal Congress 2016, Strasbourg, France, 19–23 September 2016; 2016.
5. Boban, L., Miše, D., Herceg, S., Soldo, V.: Application and Design Aspects of Ground Heat Exchangers. *Energies*, 14, 2134, 2021.
6. Ashby, M. Materials selection in mechanical design: Fourth edition, pp. 1-646. Doi:10.1016/C2009-0-25539-5, 2010.
7. Ferrarini, G., Bortolin, A., Cadelano, G., Finesso, L., Bison, P.: Multiple shots averaging in laser flash measurement, *Applied Optics*, 59 (17), pp. E72-E79. Doi: 10.1364/AO.389564, 2020
8. Cadelano, G., Bortolin A., Ferrarini, G., Bison, P., Dalla Santa, G., Di Sipio, E., Bernardi, A., Galgaro, A.: Evaluation of the effect of anti-corrosion coatings on the thermal resistance of ground heat exchangers for shallow geothermal applications, *Energies* 14, 2586. Doi: 10.3390/en14092586, 2021.
9. Cadelano, G., Bortolin, A., Ferrarini, G., Molinas, B., Giantin, D., Zonta, P., Bison, P.: Corrosion Detection in Pipelines Using Infrared Thermography: Experiments and Data Processing Methods, *Journal of Nondestructive Evaluation*, 35 (3). Doi: 10.1007/s10921-016-0365-5, 2016.
10. Arriba-Rodriguez L.; Villanueva-Balsera, J., Ortega-Fernandez F., Rodriguez-Perez F.: Methods to Evaluate Corrosion in Buried Steel Structures: A Review. *Metals* 8, 334, doi: <https://doi.org/10.3390/met8050334>, 2018.
11. ASTM Committee G162-18 Standard Practice for Conducting and Evaluating Laboratory Corrosion Tests in Soils.
12. Baboian R., Munger C. G., Treseder R.S. Nace Corrosion Engineer's Reference Book, Houston, TX: NACE, 1991.

13. Hähnlein S., Bayer P., Ferguson G., Blum P.: Sustainability and policy for the thermal use of shallow geothermal energy, Energy Policy, Volume 59, doi: <http://dx.doi.org/10.1016/j.enpol.2013.04.040>, 2013.
14. Geotechnical test method gtm-24: test method for determination of ph value of water or soil by ph meter. Department of transportation - Geotechnical engineering bureau, 2015.
15. ARPAV website.
https://www.arpa.veneto.it/bollettini/storico/2022/0234_2022_TEMP.htm. Last access: 20 June 2022.

10.2 Evaluation of different metal anti-corrosion countermeasures on coaxial ground loop heat exchangers for shallow geothermal applications

10.2.1 Abstract

The materials and technology used to build ground heat exchangers (GHE), as well as the local geological and hydrogeological context, significantly affect the thermal performance of a geothermal system [1]. The use of metallic pipes was explored, evaluating corrosion problems and proposing measures to improve the reliability of the systems over time. The well point technique is used in the construction field to reduce groundwater level before excavation works. It consists of a series of metal tubes (length 7-10 m) inserted into the ground to draw water. These tubes are normally removed after use, but on the frame of Horizon 2020 GEO4CIVHIC project their exploitation as low-cost GHEs was investigated. These tubes have become coaxial GHE, with the outer metallic tube in direct contact with the ground. A hypothetical benefit of such solution is that the use of pipes made in carbon steel (CS) or stainless steel (SST) should lead to increased heat transfer against a traditional plastic single or double U layout, according to previous literature [2]. However, the implementation of anticorrosive measures is mandatory, and the possible negative effect of such measures on the thermal performance and leakage hazard should be evaluated. Two different grades of SST (AISI 316 and AISI 304) and four passive anti-corrosion measures for CS (sacrificial anode, bitumen, paint, galvanized zinc) have been arranged and installed into the ground, in a pilot case in Padua (Italy). Their thermal performance have been evaluated by Ground Response Test. The results are consistent with the pipe wall resistivity model, based on the measured thermal conductivity of the individual materials constituting each installed GHE solution.

10.2.2 Introduction

The chemical interaction between the underground and GHE materials, as well as the underground electrical conditions, have an important effect on the durability of GHEs. The installation of the GHE implies the undisturbed underground conditions alteration, which could lead to a significant development of corrosion, mainly due to the

penetration of atmospheric oxygen into the underground and the presence of groundwater in contact with the GHE. According to best practices, the use of metal GHE is an unfavourable choice if the pipes are not made of corrosion resistant alloys and is discouraged by regulations, despite the good thermal performance and the relatively low cost of carbon steel. A suitable material that might be considered is stainless steel, which have worse thermal properties and is much more expensive. Depending on the SST grading, its thermal conductivity is around $14\text{-}16 \text{ W}\cdot\text{m}^{-1}\cdot\text{K}^{-1}$, while CS is $45 \text{ W}\cdot\text{m}^{-1}\cdot\text{K}^{-1}$. 1.1 Passive anti-corrosion measures for buried steel artefacts. In many fields, such as plumbing or the installation of electricity poles, there are methods and standards to limit the occurrence of corrosion in underground pipes or similar metal artifacts. These anti-corrosion measures include both active and passive solutions. Since reducing the overall costs of installing shallow geothermal systems is a major concern, we have discarded the active ones from this study, because they involve additional costs to keep the protection on. Passive protection is used to mechanically insulate the metal surface from the external environment by means of a coating. The most common coatings are:

- i) protective films of paint applied over the entire length of the pipe or only in points subject to corrosion, such as polyethylene-based protective coatings as prescribed by UNI 9099, or bitumen according to UNI 5256;
- ii) oxidation products obtained e.g. by anodic oxidation of metals such as Al, Ni or Co. The oxides of these materials are very tough and adherent to the surface layer, insulating them from the environment; metals, such as Zn, could be applied by immersing the Fe-alloy in a galvanic bath of molten Zinc.
- iii) Attaching a sacrificial anode made of bulk Zinc or Magnesium to the pipe. Being Zn more reducing than Fe, oxidation proceeds on the Zn (with the formation of white rust by zinc hydroxide and minimally by oxide and carbonate) and the pipe remains protected until all the Zn has been consumed. Moreover, other metals such as Cr could be applied by plating/cladding the pipes.

Stainless-steel grades with anti-corrosive action used for piping

SST is an alloy of Fe, Cr and C. Occasionally it might contain other complementary elements, such as Ni. Cr is the element that gives a protection from corrosion. In oxidizing environment, Cr produces a very dense and thin oxide layer (also referred as passivating layer) insulating the material from any corrosive action as long as it is kept intact. SSTs are classified according to the amount of the elements in their

composition: martensitic, ferritic, and austenitic. Austenitic is the group with the greatest advantages in manufacturing, as well as in service performance such as easy welding and great corrosion resistance. AISI 304 contains 18% Cr and 8% Ni while AISI 316 contains 16% Cr, 10% Ni and 2% Mo; the latter is added to help resist corrosion from chlorides (common in seawater and marine environments). In summary, the use of metal as a material for the external tubes in the ground heat exchanger [3] involves trade-offs: while the bare SST can be considered safer, its thermal performance is theoretically worse than the CS. However, also the additional thermal resistance of the passive protection layer (e.g. bitumen or paint) must be taken into account too. A laboratory study has shown [4] that bare SST pipes have greater thermal resistance than coated CS ones. However, both materials have lower thermal resistance than plastic, which is commonly used in shallow geothermal installations. The present study aims to test the metal pipes in a real operating environment.

10.2.3 Materials and methods

Case study: CNR area site (Padua, Italy)

This investigation took place in a site in the premises of CNR area in Padua-Italy, starting from June 2020. Such case study act as testbench for different anti-corrosion materials and methods in real operative conditions. A great effort was made to develop the GHEs, in such a way to adapt the well point pipes and installation methodology, while assuring thermal performances, practical feasibility and sustainability during the production and the installation phases. Such work included tailored solutions for outer pipes, heads (connecting the GHE to the hydraulic circuit to the heat pump) and ancillary hydraulic pieces. The GHEs specifications are as follows:

- Heat exchanger total length: 8 m
- External tube: steel alloy (refer to Table 2)
- Length: 8 m as result of the assembly (butt join welding) of 2 m and 6 m tubes.

Table 1: Geometrical properties of the well point GHEs.

	External tube	Internal tube
Material	See Table 2	PE100
External diameter (mm)	76.2	40
Internal diameter (mm)	70.2	35.2
Thickness (mm)	3	2.4

The tubes constituting the GHEs were not the actual well point pipes, instead they have been built on purposes and engineered in order to use the well point installation procedure. The local geological setting of the site is the typical one of the low-plain areas. The local stratigraphic sequence is characterized in the shallower layers by silts and sands. These data have been derived from previous corings (Fig. 1).



Figure 1: Local stratigraphic diagram. The installed well point GHEs are all deployed within the first 8 meters from ground level.

With regard to the hydrogeological conditions, the local underground is inserted in the multi-pitch system of the low Venetian plain characterized by an alternation of permeable and impermeable levels. Therefore, there are free and pressurized aquifers. In the area of Padua, the first aquifer has a depth of between 1.0-1.5 m from the ground, with a free water table increase from the North-West to the South-East. The average groundwater oscillations are estimated as ± 1 m during the annual variations. Given the local stratigraphic setting, the same well point technique used in case of fine-grained grounds presence was exploited, hence it is preceded by the construction of a cylindrical, vertical, sand drain. Firstly, a squared excavation is made, in order to lower the surface. After this operation, the vertical hole is drilled; the pipe is placed inside the hole and, at the same time, it is washed with water in order to remove any fine material that may have settled on the walls. Coarse sand is introduced into the hole until it forms a vertical drain. Two different grades of SST (eight SST well point GHEs

in total: 1x AISI 316, 7x AISI 304) and four passive anti-corrosion measures for CS (eight CS well point GHEs in total: 1x sacrificial anode, 2x bitumen, 2x paint, 2x galvanized zinc and 1 bare tube as a reference) have been installed (Table 2). External pipes before installation are shown in Fig. 2.

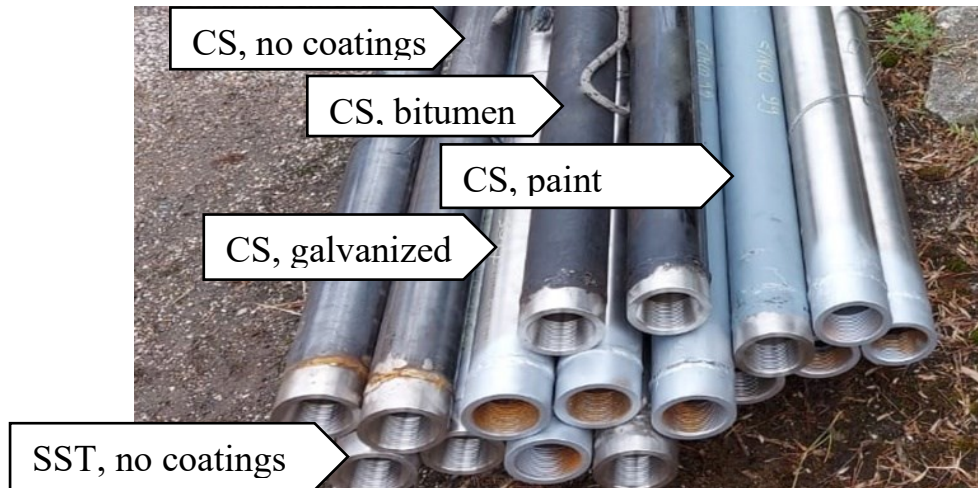


Figure 2: Well point type GHEs before installation.

The actual length of each heat exchanger is substantially less than the entire length of the pipes (i.e. 8 meters). This is because during installation, fine materials happened to pass through the openings (drain filter) at the lower end of the pipes. The openings were subsequently sealed with a filler cement compound. This caused the lower part of the tubes to fill up at different heights, with a consequent decrease in the effectively active part of each GHE. To assess the impact of the pipe alone on the overall thermal resistance of the borehole, a simplified model of heat transfer through the pipe was used to calculate the thermal resistance of the circular geometries [7]. The thermophysical properties necessary for the calculation, both of the materials of the pipes and of the coatings, were taken from the literature [4].

Table 2: Overview of the well point GHEs installed at the Padua case study site.

Well Point ID	Material/anti-corrosion measure	Height from ground level [m]	Actual length [m]	Pipe thermal Resistance [m²·K·W⁻¹] ·10⁻³
1	CS/ bitumen	0.65	6.01	20.91
2	CS/ bitumen	0.72	4.61	20.91
3	CS/ paint (ZINCO99)	0.68	3.67	3.64
4	CS/ paint (ZINCO99)	0.59	3.62	3.64
5	CS/ sacrificial anode in Zn	0.56	4.93	0.29
6	CS/ nothing	0.64	7.05	0.29
7	CS/ galvanized Zn	0.62	5.09	0.29
8	CS/ galvanized Zn	0.66	6.58	0.29
9	SST AISI 304/ nothing	0.51	4.85	0.81
10	SST AISI 304/ nothing	0.52	5.10	0.81
11	SST AISI 304/ nothing	0.87	5.91	0.81
12	SST AISI 316/ nothing	0.95	4.31	0.91
13	SST AISI 304/ nothing	1.07	4.96	0.81
14	SST AISI 304/ nothing	0.53	5.98	0.81
15	SST AISI 304/ nothing	1.18	4.51	0.81
16	SST AISI 304/ nothing	0.75	4.02	0.81

From the hydraulic point of view, the GHEs installed were arranged in two parallel series, counting eight GHEs each. One branch includes only the SST ones, the other the CS ones. Since both series are connected independently to a valved manifold, it is possible to operate both simultaneously, or each independently. The location of the GHEs at the site is shown in Fig. 3, which illustrates the installation phase after the deployment of the horizontal link.

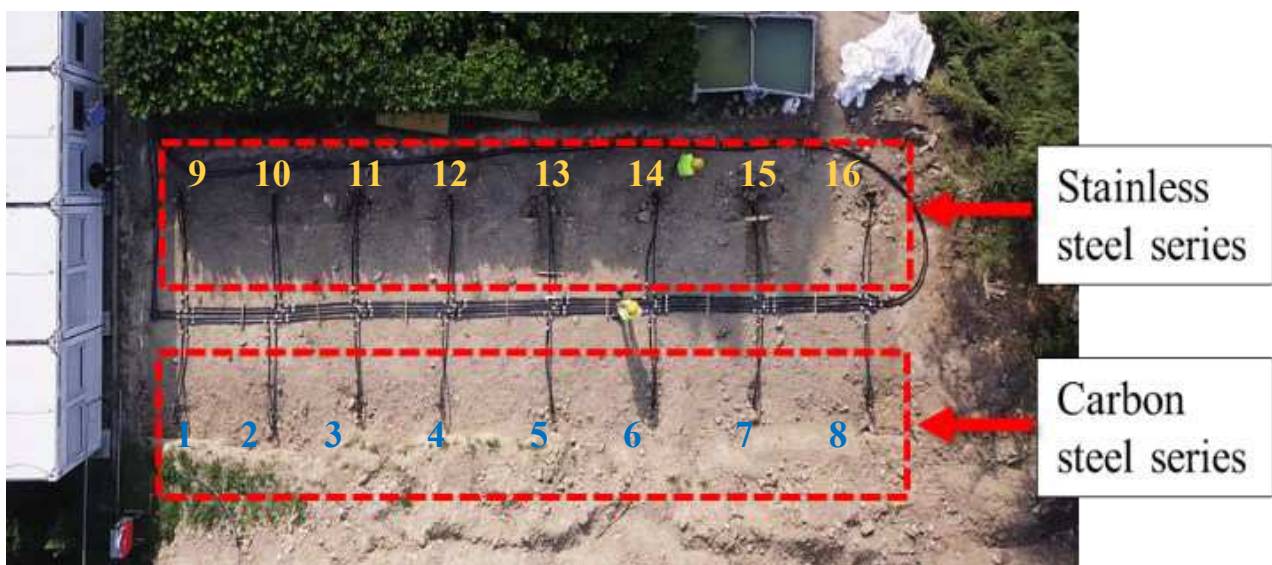


Figure 3: Aerial view of the site. GHEs are numbered according to table 2.

2.1 Ground Response Test

The thermal performance of the installed well point type GHEs have been evaluated by Ground Response Test (GRT). The test system and procedure were established by the American Society of Heating, Refrigerating and Air-Conditioning Engineers (ASHRAE) and it is the most commonly used internationally [5,6]. A GRT apparatus typically consists of a pump, purge valves, an electrical heating element, temperature sensors, a flow meter, and a data logger mounted in a small lorry (Fig. 4).

The test consists in applying a constant thermal load to the completed ground heat exchangers (and therefore to the underground) for a period of time sufficient to allow the system to reach thermal equilibrium. Flow rate, electrical power, inlet and outlet temperatures are measured and recorded. The result of the test allows to obtain the equivalent thermal conductivity and the undisturbed ground temperature.



Figure 4: Ground Response Test rig during measurement campaign at the site.

10.2.4 Results

The test was carried out for each hydraulic circuit, each counting eight GHEs. Fig. 5 shows that GRTs were held under adequate test conditions, with an average ground temperature of 15°C during the test.

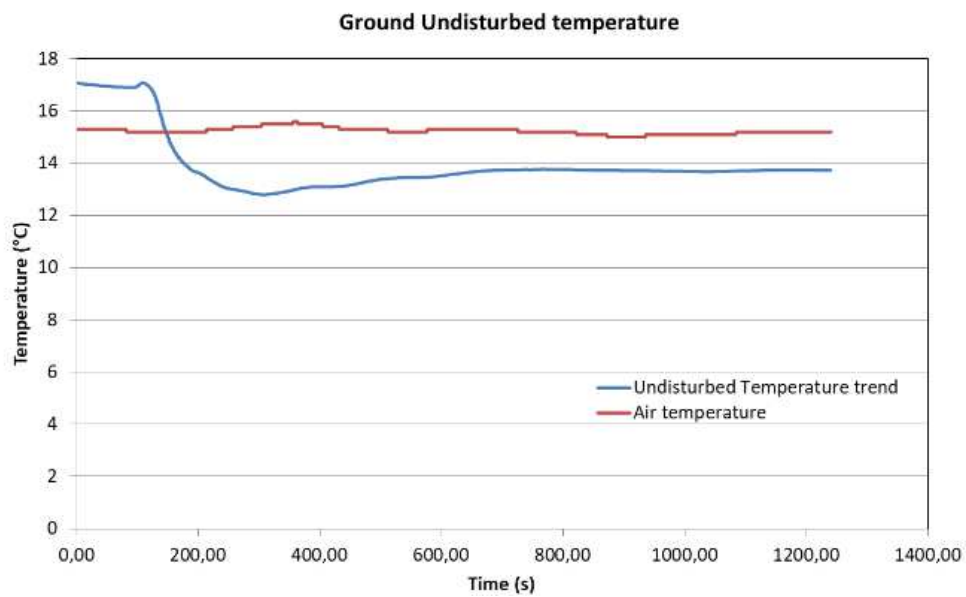


Figure 5: SST circuit, undisturbed ground temperature.

As can be seen in Fig. 5 and 6, the temperature difference is kept almost constant as is the water flow, thus resulting in a constant heat input into the ground for both CS and SST branches test.

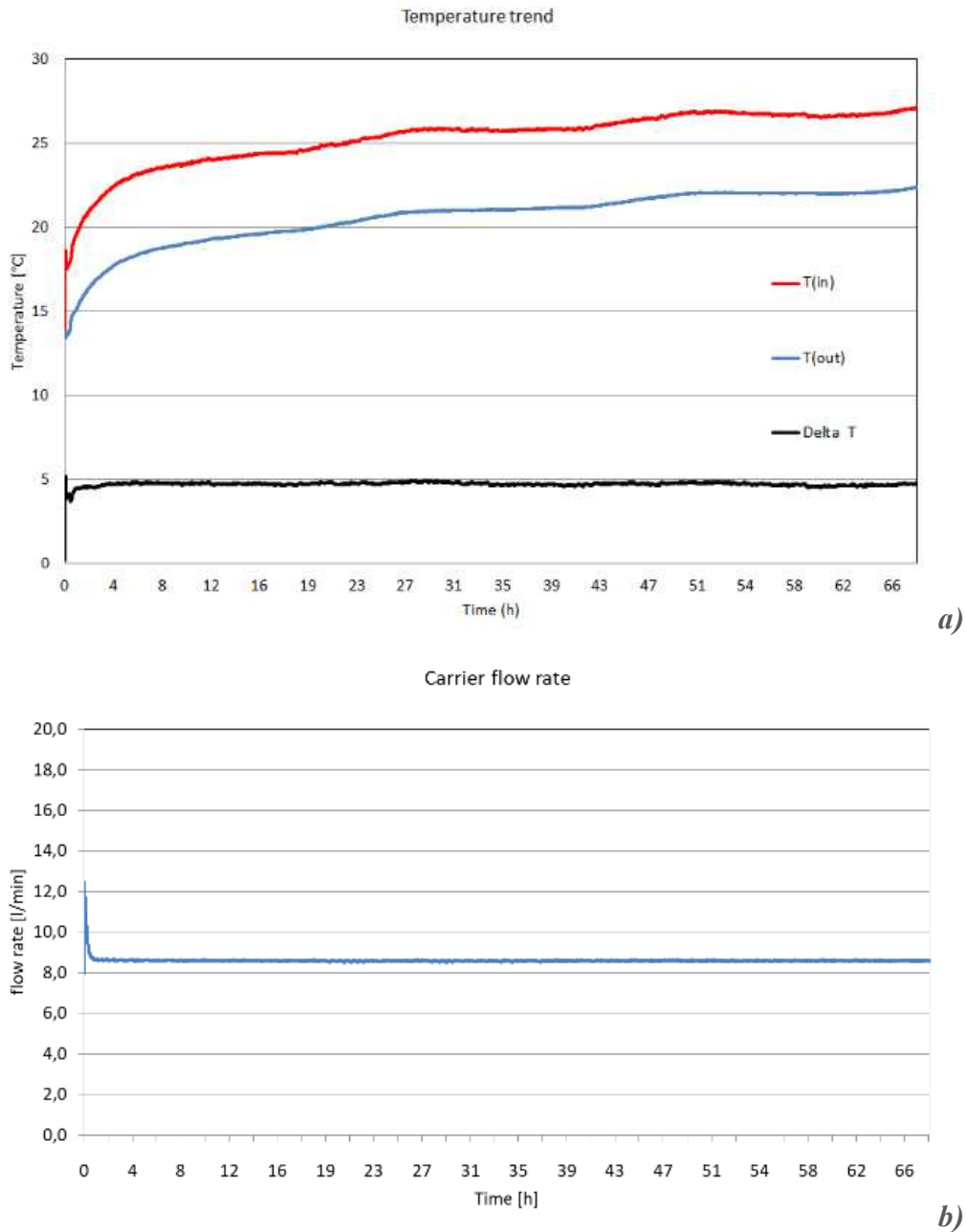


Figure 6: SST circuit, inlet vs outlet water temperature (a), and water flow rate (b).

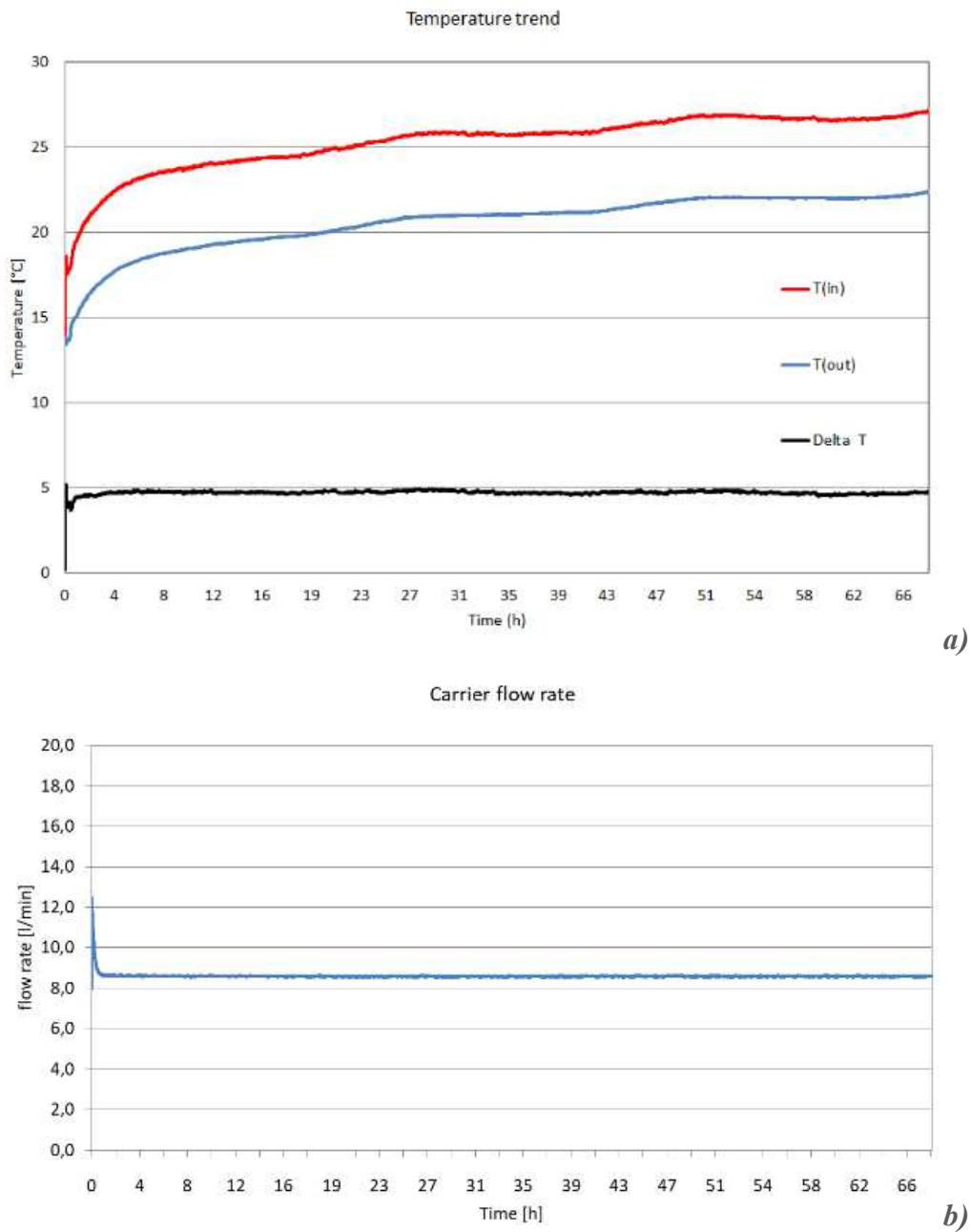


Figure 7: CS circuit, inlet vs outlet water temperature (a), and water flow rate (b).

Temperature as a function of time is presented in Fig. 8 and 9: the heat transfer fluid (water, no anti-icing has been used) is circulating into the heat exchangers and through an external heater until reaching thermal equilibrium with the ground. The temperature is measured every second for a certain amount of time. The average temperature is calculated as the arithmetic average between the inlet and outlet temperatures for each measured step. The thermal power exchanged between the fluid and the ground is calculated (eq. 1) as:

$$Q = m \cdot c_p \cdot \Delta T \quad (1)$$

where m is the mass flow rate in $[\text{kg} \cdot \text{s}^{-1}]$, c_p is the specific heat capacity in $[\text{J} \cdot \text{kg}^{-1} \cdot \text{K}^{-1}]$ and ΔT is the difference between the inlet and outlet temperatures. During the test, mass flow, inlet temperature, and outlet temperature are measured. Specific heat capacity and density of water are standard values taken from literature. The heat flux between the GHE and the ground can be represented as an infinite line source with negligible effect of heat fluxes along the borehole axis. The most widespread and consistent method to date is the continuous line source model, based on a constant heat flux per unit of time. The evaluation of the equivalent thermal conductivity of the ground is possible using the average temperature of the fluid between the inlet and the return. By plotting the average water temperature in the GHE against the natural logarithm of time, a linear relationship can be obtained.

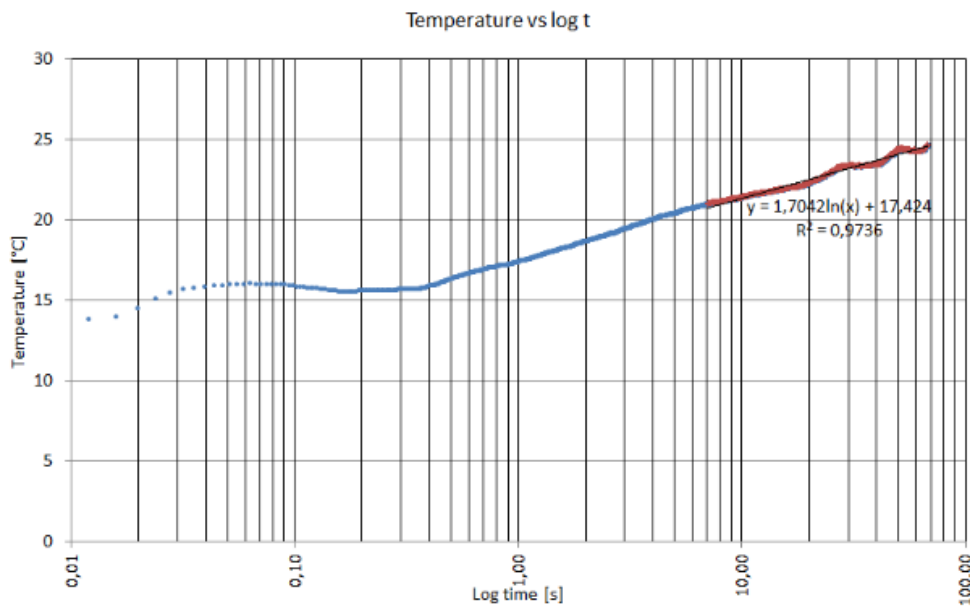


Figure 8: CS circuit, average water temperature, vs logarithm of time.

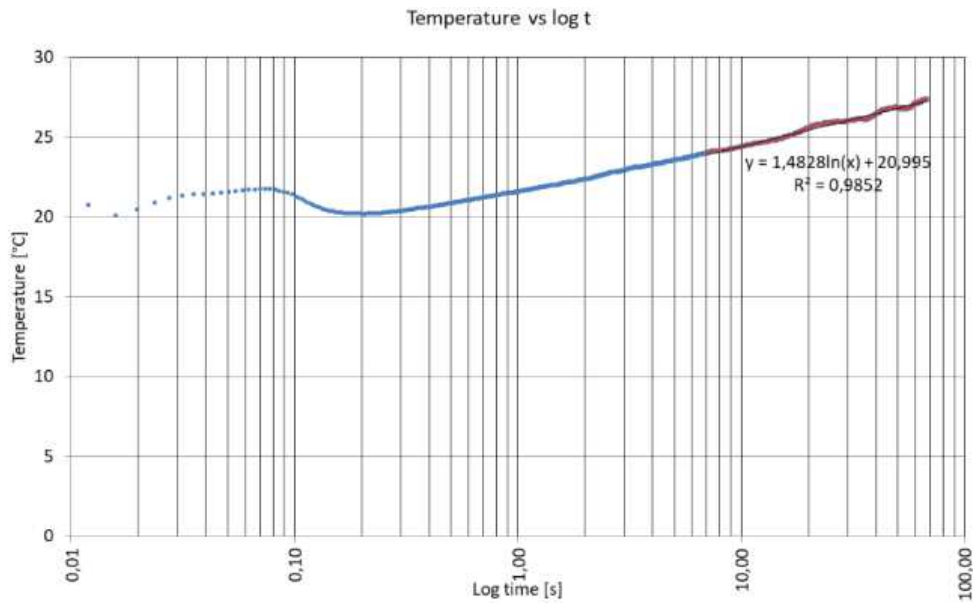


Figure 9: CS circuit, average water temperature, vs logarithm of time.

According to the simplified infinite line source approximation model, using the slope (k) of the linear fittings of plots highlighted in red in Fig. 8 and 9, and the constant power rate per unit of length (q'), thermal conductivity (λ) can be calculated using the following relationship (eq. 2) [7]:

$$k = q' / (4 \cdot \pi \cdot \lambda) \quad (2)$$

Overall results are presented in table 3, where the outcomes of GRT test for each hydraulic circuit are shown. Borehole total depth is the sum of the actual lengths of the individual GHEs of each circuit. The thermal resistance associated with the total boreholes length for both circuits was in turn compared with the average (weighted on the effective heat exchange lengths) thermal resistance of the pipe, calculated from the data in table 2. In addition, an assessment of the cost per meter was presented, taking into account the prices of bulk metals.

Table 3: GRT results comparison between SST and CS circuit.

	Stainless steel well point circuit	Carbon steel overcoat treated well point circuit
Borehole number	8	8
Borehole total depth [m]	39.64	41.56
Specific heat power [W·m⁻¹]	71.26	69.14
Thermal conductivity [W·m⁻¹·K⁻¹]	3.33	3.72
Borehole thermal resistance [m²·K·W⁻¹] ·10⁻³	35	89
Pipe thermal resistance (average) [m²·K·W⁻¹] ·10⁻³	0.81	6.14
Cost per metre (raw material*) [€]	65	20

**Based on stock market prices (source: Milano Finanza), tube manufacturing and anti-corrosion measures excluded.*

Although the thermal resistance of the pipe varies critically depending on the combination of material and possibly the coatings, it does not have a significant impact on the borehole thermal resistance and this is a remarkable benefit of these metal groutless solutions. As a further comparison, the modelled thermal resistance of a hypothetical HDPE pipe with the same geometric characteristics as well point ones would be 0.01 m²·K·W⁻¹. Based on these figures, the selection of CS rather than SST might be negligible in terms of thermal performance. Instead, economic aspects as well as safety should be deeply evaluated. From an economic point of view, Table 3 shows that the CS ones are more affordable than the SST ones. However, as a reference, the cost of raw material per meter of HDPE GHE with the same geometric characteristic would be only around 3 €. On a solely economic basis, the metal solutions to choose from could rule out stainless steel for GHEs in a context such as the one presented in the case study.

10.2.5 Conclusions

A new type of coaxial ground heat exchanger has been proposed by borrowing the technology used for ground drainage. The external pipe is made of metal; therefore, it

is necessary to provide adequate anti-corrosion protection to ensure its safety and reliability over time. Two different solutions were proposed: stainless steel and carbon steel painted over with different coatings or providing other passive anti-corrosion measures. The new GHEs were installed in a real case and their performance tested via GRT. The result does not show significant differences between the two solutions in terms of thermal performance.

10.2.6 References

1. Boban, L.; Miše, D.; Herceg, S.; Soldo, V. Application and Design Aspects of Ground Heat Exchangers. *Energies* 2021, 14, 2134,
2. Pockelé, L.; Mezzasalma, G.; Righini, D.; Vercruyse, J.; Cicolini, F.; Cadelano, G.; Galgaro, A.; Dalla Santa, G.; De Carli, M.; Emmi, G.; et al. Innovative Coaxial Heat Exchangers for Shallow Geothermal. In *World Geothermal Congress*; Elsevier: Reykjavik, Iceland, 2021.
3. Mendrinós, D., Katsantonis S., and Karytsas C. Review of Alternative Pipe Materials for Exploiting Shallow Geothermal Energy.
4. *Innovations in Corrosion and Materials Science*, 2017, 7, 13-29
5. Cadelano G., Bortolin A., Ferrarini G., Bison P., Dalla Santa G., Di Sipio E., Bernardi A. and Galgaro A.: Evaluation of the Effect of Anti-Corrosion Coatings on the Thermal Resistance of Ground Heat Exchangers for Shallow Geothermal Applications. *Energies* 2021, 14, 2586
6. Zarrella, A.; Emmi, G.; Graci, S.; De Carli, M.; Cultrera, M.; Dalla Santa, G.; Galgaro, A.; Bertermann, D.; Muller, J.; Pockelé, L.; Mezzasalma, G.; Righini, D.; Psyk, M.; Bernardi, A. Thermal response testing results of different types of borehole heat exchangers: an analysis and comparison of interpretation methods. *Energies* 2017, 10, 801
7. ISO 17628:2015: Geotechnical investigation and testing — Geothermal testing — Determination of thermal conductivity of ground and rock using a borehole heat exchanger
8. Carslaw, H.S.; Jaeger, J.C. *Conduction of Heat in Solids*; Oxford University Press: Oxford, UK, 1980.

Acknowledgements

The authors thank Terra Geoserv ltd, RED srl and Hiref spa for their support during the design, installation and evaluation of the geothermal plant in Padua.



GEO4CIVHIC project has received funding from the European Union's Horizon 2020 Research and Innovation Programme under grant agreement No 792355.

11 Themed topic chapter: Non-destructive control method for the inspection of metal GHEs based on infrared thermography

This chapter is dedicated at exploring an applicable inspection methodology to improve the safety of metal solutions. Active infrared thermography has been shown to be able to identify internal corrosion and failure of joints in a non-destructive way.

Based on one manuscript:

- G. Cadelano, A. Bortolin, A. Galgaro, P. Bison, G. Ferrarini. **Internal corrosion and joint failure detection for the inspection of vertical geothermal heat exchangers by infrared thermography**, Proc. SPIE 12109, Thermosense: Thermal Infrared Applications XLIV, 121090Q (27 May 2022); <https://doi.org/10.1117/12.2622452>

The manuscript has been published in the proceedings of SPIE Thermosense: Thermal Infrared Applications XLII, Orlando, 2022. GC designed the study; GC, PB and GF developed the methods; GC, AB and GF collected the data; GC, GF and PB developed the numerical model. All the authors discussed the data and agree on their interpretation; GC, AB, PB and GF wrote the manuscript. All the co-authors contributed to the final polishing of the manuscript.

11.1 Internal corrosion and joint failure detection for the inspection of vertical geothermal heat exchangers by infrared thermography

11.1.1 Abstract

The need for greater efficiency in the field of shallow closed-loop geothermal systems has led to the proposal for groutless coaxial geothermal heat exchangers made of steel. In terms of heat transfer performance, they are superior to traditional grouted U-shaped or double-U plastic ones, but they are still not well accepted by the market because there are doubts about their safety in terms of reliability. This work aims to explore the detectability of these defects using active infrared thermography, in order to contribute to the proposal of possible on-site inspection procedures. The experimental work was carried out in the laboratory on a pipe sample that was made of threaded-jointed sections of steel. Defects of various entities have been artificially introduced to simulate internal corrosion, generally related to the presence of chemicals in the heat transfer fluid. Different failures in threaded joints were also simulated and detected after the processing of thermal data.

11.1.2 Introduction

The need for renewable energy production is constantly increasing, as the current standards are designed to promote the use of renewable sources. In this framework, low-enthalpy geothermal energy could give a significant contribution, being a well-developed technology [1]. Ground heat exchangers (GHEs) are pipes that are inserted into the ground. Inside this pipe, a fluid flows to exchange heat between the ground and the pipes. A heat pump could be connected to this piping system, in order to provide heating or cooling to the building. Despite being a known technology, there is still great room for technological improvements in different aspects, such as piping. These energy systems rely on piping to optimize their thermal performances and, in recent times, novel materials [2], such as steel, have been proposed [3] for the heat exchangers. This kind of exchangers could significantly improve the thermal performance of the system, thanks to the high thermal conductivity of the piping [4].

However, this solution poses some challenges in avoiding the risks of internal corrosion and joint failure. The joints that connect each section to the others can be

welds or threads, the latter completed with O-rings to ensure sealing. In both cases, the operation is carried out on-site. While the plastic-based systems are usually supplied in continuous coils, the metallic ones are made up of sections that are assembled on site. Since an unsealed gasket is enough to ruin the entire length of the heat exchanger, they pose a serious safety and financial risk. Moreover, it is feared that the heat transfer fluid flowing inside may cause environmental damage in the event of corrosion leaks. The heat transfer fluid is typically water but the use of additives is very common. The leakage of fluid through corrosion leaks or joint fittings could lead to severe consequences. This is related not only to the malfunctioning of the system, but it could also lead to environmental pollution, as the spill of liquid could contaminate the environment. To detect pipelines and joint failures, several NDT techniques are available[5]. Among them, infrared thermography [6] (IRT) is a well-known method for the inspection of industrial components, ranging from materials characterization [7] to defect detection [8], including also corrosion in pipelines [9]. The wide range of experimental setups and post-processing techniques has been the base of this work, where the test was addressed to two kinds of defects: internal corrosion and joint failure. For the internal corrosion, a setup including a pipe with known defects has been created and a comparison between different image processing technique in different phases of the experiment (heating, steady state, cooling) has been proposed. For joint failures, another pipe mock-up has been designed and investigated with a periodic stimulus.

11.1.3 Internal corrosion

Reference model

Considering the cylindrical symmetry of the system, the problem should be represented in polar coordinates (r, φ) with the origin in the cylinder axis, as shown in the following Figure 1.

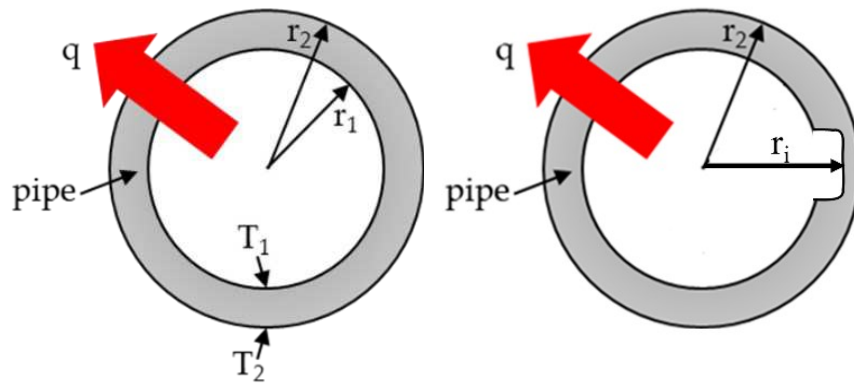


Figure 1. Reference sketch of a pipe without (left side) and with (right side) a thickness reduction due to internal corrosion.

For the one-dimensional case, when the defect is big enough, the temperature is distributed in concentric isotherms so it only depends on the radius r but not on the angle α .

Experimental setup

The experimental activities required the use of a physical model able to simulate corrosion phenomena. The overall aim of the study was to evaluate the effects of the thickness reduction in the pipeline and the presence of water, that is responsible for the most common degradation phenomena. The specimen used, obtained from an element of carbon steel pipe, was chosen to verify the working hypotheses deduced from literature and experience in the field. The specimen was designed to study the effect of corrosion products (mainly Fe_2O_3).

For the analysis of the first situation, four induced defects have been created in the pipe, two of them internal and two external. The defects are obtained decreasing the thickness of the pipe wall manually, through a mechanic process that produces a loss of material between 2 and 5 mm. This removal of the material corresponds to a wall thickness reduction of the 25% and 50% respectively.

All these defects are represented in the following Figure 2. In this representation, the pipe has been cut along a reference line for which is considered $\alpha=0^\circ$, and unrolled clockwise starting from the input water side. The internal defects, in green, are vertically centered in line with the water input ($\alpha=287^\circ$). The larger one goes from the position $x=14\text{cm}$ up to $x=18\text{cm}$ (4cm width) and it is 13 cm height and up to 5 mm deep ($\Delta d=55.5\%$ of lost material). The smaller one goes from the position $x=26.5\text{cm}$ up to $x=29\text{cm}$. It has a circular shape with radius 2.5cm and is up to 2mm deep

($\Delta d=22.2\%$ of lost material). The external defects, in red, are centered in the imaginary line of $\alpha=033^\circ$. The larger one goes from $x=12\text{cm}$ up to $x=19\text{cm}$ and is 5cm width. The smaller one goes from $x=25\text{cm}$ up to $x=32\text{cm}$ and is 3.8cm width. The maximum deep in this case is 5.32mm for the largest ($\Delta d=59.1\%$ of lost material) defect and 3.61mm for the other ($\Delta d=40.1\%$ of lost material).

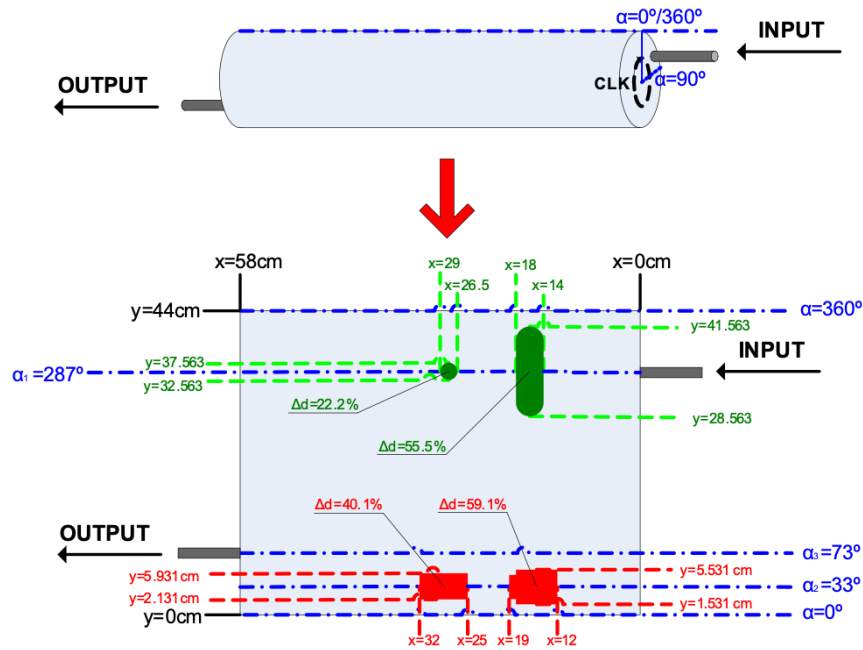


Figure 2: Scheme of the pipe under investigation, including the position and size of the defects.

The thermographic setup included a thermal imaging camera (FLIR SC 660. Uncooled microbolometer / $7.5\text{-}13\ \mu\text{m}$, 640×480 pixels). The camera was placed in such a way to include the lower portion of the pipe in its field of view, thus giving priority to the observation of the most critical area as regards the phenomenon studied. The thermal data were acquired as a sequence of thermographic images with a predetermined sampling rate and then transferred for further processing with a dedicated software developed in Matlab environment.

The curved metal surface of the steel pipe had a very low emissivity in the infrared band. For this reason, the external wall of the pipe was painted with an acrylic-based product, having a high emissivity value ($\epsilon > 0.95$) in the infrared band of the thermal camera. This coating was resembling the optic effect of an anti-corrosion paint layer on the pipeline. Similarly, paper tape, also having a high emissivity value, was used to coat some parts of the specimens in order to facilitate the measurement. In a real application on ground heat exchanger, that commonly use specific anti-corrosion coatings, the varnishing process could be probably omitted. The heating system and its

control units were chosen to simulate a real application. The experimental layout is schematized in the following figure 3.

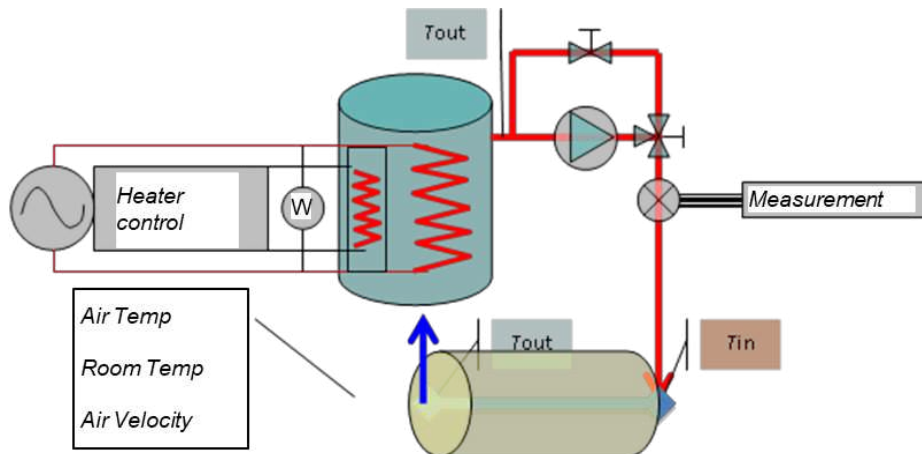


Figure 3: Sketch of the system dedicated to the thermal conditioning of a section of duct, which simulates the effects of corrosion.

Both ends of the specimen have been sealed and equipped with hydraulic fittings to allow the operation of the Haake DC30 thermostatic system, responsible for heating (at a temperature between 65 and 90 ° C) and for the circulation of a liquid (mono ethylene glycol-water solution) inside the pipeline intended to simulate possible real conditions of use.

The pipe segment was placed on insulated stands to allow the maximum visibility of the entire surface and to minimize the thermal contact between the body and the environment, as shown in the following Figure 4.

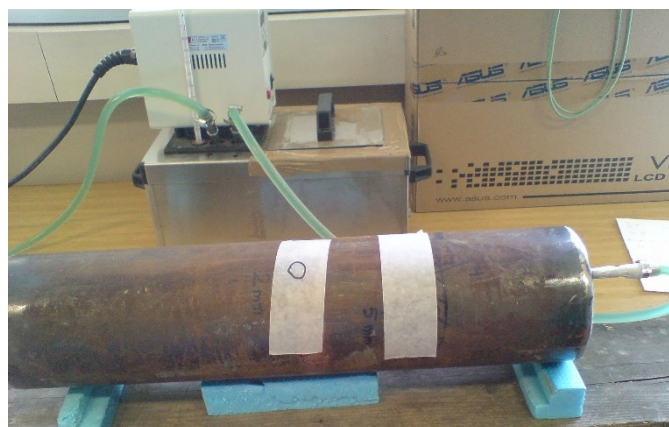


Figure 4: Experimental layout, including the pipe, the heating system, the tape mask used as a reference.

The experimental system was equipped with an apparatus for measuring the operating temperatures, consisting of two type T thermocouples and two Pt100 resistance thermometers, positioned in such a way as to monitor the temperature of the metal surface (also in correspondence of the thinnest region), the temperatures of the liquid entering and leaving the pipe, and the air temperature of the surrounding environment. The signals of the temperature sensors were managed in real time by a computer connected to a National Instrument compact-RIO data logger, using software written in the Labview® environment.

Experimental procedure

The test was performed with the following procedure:

- 1) The thermographic system starts recording the images 5 seconds before the lamps are switched on (thus recording the initial temperature);
- 2) The acquisition frequency of the sequence is set at 0.1 Hz;
- 3) After reaching the steady state, the heater is keeping a stable temperature for 30 minutes. Then, the test ends with the system getting back to the initial room temperature.

The circulation of the liquid inside the pipe and its heating and subsequent cooling allows the distinction of three different stages:

- 1) The heating stage, during which the water reaches the set temperature and consequently the pipe is heated;
- 2) The steady state, which corresponds to the period of time when, after reaching the maximum temperature, the system remains stable;
- 3) The cooling stage, which starts at the time when the thermal source is switched off and the system gets back to the environment temperature.

Data processing

The areas subject to corrosion are identified by a different average surface temperature compared to the reference material, therefore in an optimized procedure an automatic extraction method could be implemented, based on this assumption. In this work the regions have been selected by an operator.

It will be very important to evaluate whether it will be experimentally verified that the thermal effects of the corrosion products will lead to a surface temperature lower than the reference one, as predicted by the model. Otherwise, in the event that the effect of reducing the conductivity of the insulation and the thickness of the pipeline prevails, a higher than undisturbed temperature on the defect must be expected. Measurements under normal conditions are performed in a quasi-stationary thermal regime.

Image processing algorithms

Several techniques are available for post-processing thermographic sequences [10,11]. In this paper, well-known algorithms, such as correlated contrast (CT) [12], Fast Fourier Transform (FFT) [13], principal component thermography (PCT) [14], are compared with less exploited ones, such as multiple sum average filter (MSA) [10], and partial least squares thermography (PLST) [10]. MSA is an algorithm based on sum and filtering, PLST is an adaptation of the partial least squares method to thermography. All data have been imported in the Matlab environment where dedicated routines are available, such as IR view [15].

11.1.4 Results

The sequence of thermographic images was recorded to obtain the surface temperatures of the pipe with the aim of identifying the two internal defects in the field of view of the thermal imaging camera. The heat transfer fluid (ethylene glycol) was heated to 65 ° C. The thermal sequence can be divided into three phases: heating, stationary conditions and cooling, as shown in the following Figure 5.

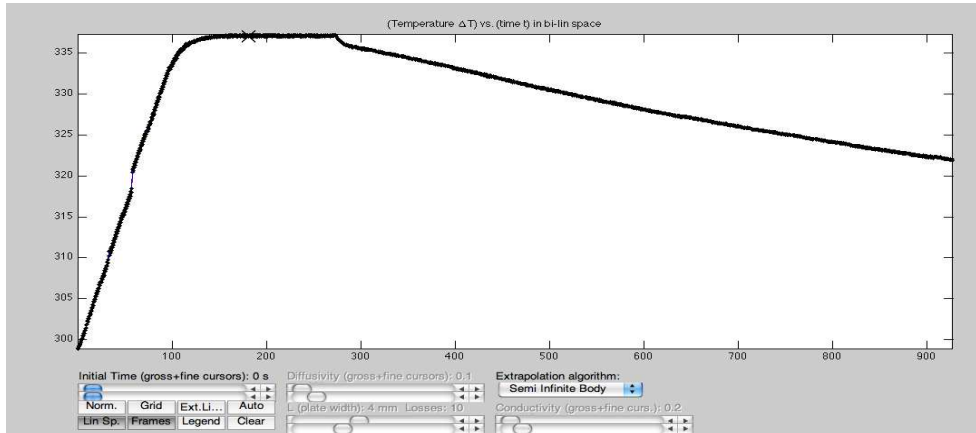


Figure 5: Temporal evolution of the surface temperature of the pipeline during the test. The three phases (heating, steady state, and cooling) are clearly visible.

After the identification, the three phases of the thermal sequence were analyzed separately, applying on each phase all the data processing algorithms. Knowing the location of the defect, it was possible to calculate the value S , that compares the signal on the defect area and on the sound area, using in the following equation:

$$S = \text{mean}_{\text{defect_area}} - \text{mean}_{\text{sound_area}} \quad (4)$$

This value was higher for: PCT during the heating phase, FFT during the steady state phase, PCT during the cooling phase. The best overall value was the PCT during the cooling phase. The best images are shown in the following Figure 6. The most effective phase for the defect detection is cooling: other than the best PCT image, also PLST provided very good results.

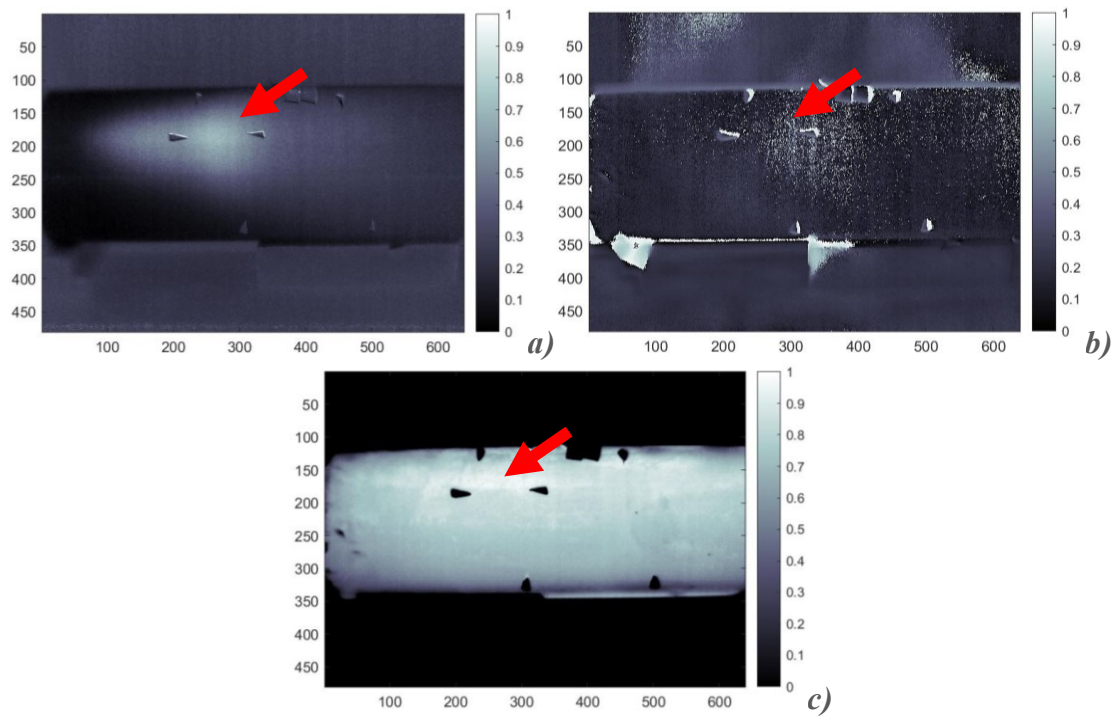


Figure 6: Best images for each of the three phase: heating, steady state, cooling. a) heating phase, best PCT image; b) steady state phase, best FFT image c) cooling phase, best PCT image.

11.1.5 Joint fittings

Experimental setup

The thermal setup for the investigation of joint fittings is based on the same thermal camera of the internal corrosion. The camera is looking at two pipe segments that are connected with a male and female threaded fitting. The stimulus is given by compressed air, that is pushed from an end of a pipe. The complete setup is shown in the following Figure 7.

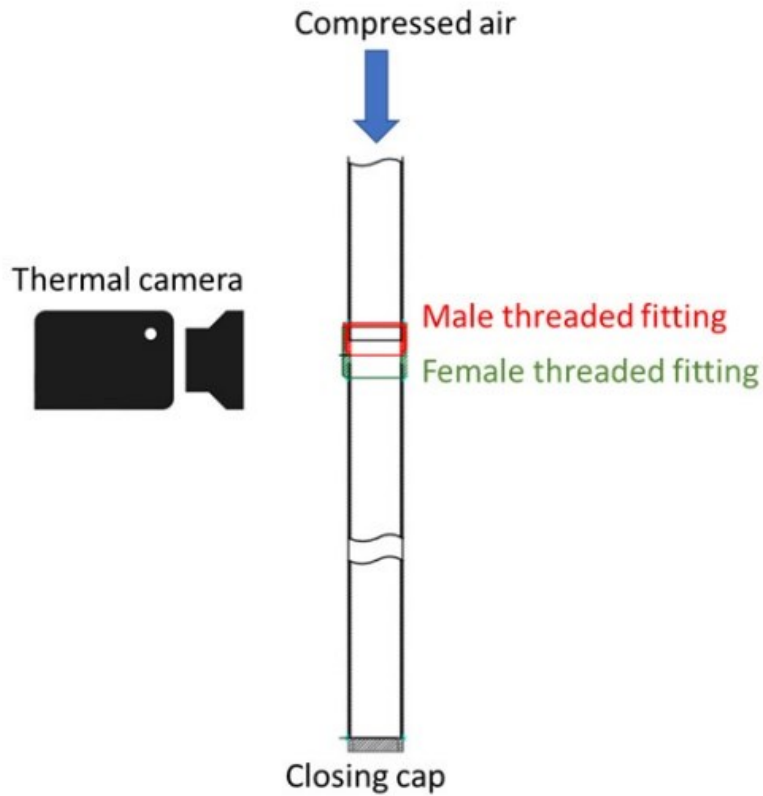


Figure 7: Scheme of the experimental layout. The thermal camera is looking at the region with the connection of the pipes. A stimulus is provided by compressed air pushed at the end of a pipe.

With the same layout, different testing procedures were performed. Data were acquired with two different acquisition frequencies: 5 and 10 Hz. Two types of stimuli were tested: pulsed (1 Hz frequency) and continuous (step mode). Finally, three defects of the fittings were tested: missing O-ring, fitting not completely screwed, fitting not completely screwed and presence of water on the outer pipe surface. In the following Table 1, the different procedures are listed.

Table 1: List of experiments on threaded fittings.

Test Number	Thermal images acquisition frequency [Hz]	Stimulus type (compressed air flow)	Simulated defect
#1	5	Pulsed at 1Hz	O-ring missing
#2	5	Pulsed at 1Hz	Not completely screwed

#3	5	Pulsed at 1Hz	Not completely screwed and presence of water on the outer pipe surface
#4	10	Continuous (step)	O-ring missing
#5	10	Continuous (step)	Not completely screwed
#6	10	Continuous (step)	Not completely screwed and presence of water on the outer pipe surface

11.1.6 Results

All the experiments were analysed with the set of image processing algorithms. The best images, selected after a manual comparison, are shown in the next Figure 8.

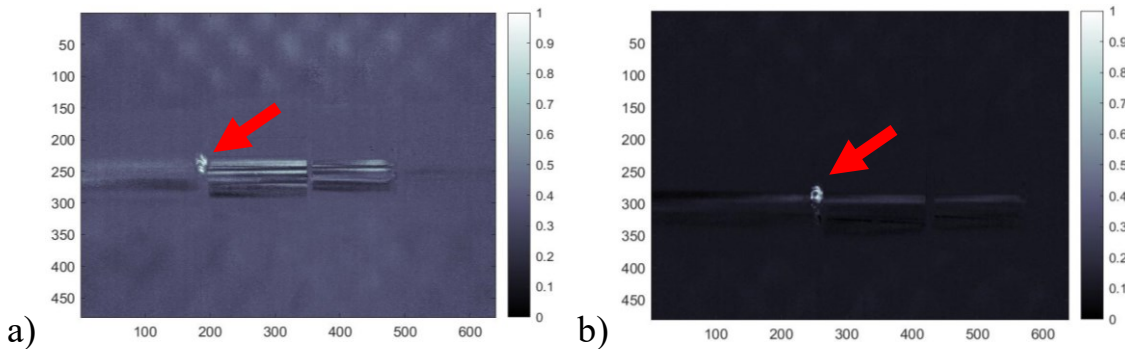


Figure 8: Best images for joint fittings test: a) Test #1, FFT processing b) Test #2, FFT processing

The most effective experiments were with pulsed stimulus, processed with FFT algorithm.

11.1.7 Conclusions

Verifying the quality of pipes is of paramount importance, and thermographic methods could be applied with different methods to define the status of pipes and fittings. In this work, two different thermographic experiments have been performed to investigate the internal corrosion and the fittings, respectively. Both setups showed the feasibility

of the proposed approach, as both kinds of defects were detected successfully. Moreover, the impact of different image processing strategies was investigated. Future work will investigate the applicability of this experimental setups during on-site inspections.

Acknowledgments

This research was funded by H2020 GEO4CIVHIC project, grant number 792355. GEO4CIVHIC project has received funding from the European Union's Horizon 2020 research and innovation program under grant agreement No. 792355.

Author would also like to acknowledge the contribution of RED S.r.l. and HYDRA S.r.l. for providing the pipe samples.

11.1.8 References

1. Boban, L., Miše, D., Herceg, S. and Soldo, V., “Application and Design Aspects of Ground Heat Exchangers,” 8, *Energies* 14(8), 2134 (2021).
2. Mendrinos, D., Katsantonis, S. and Karytsas, C., “Review of Alternative Pipe Materials for Exploiting Shallow Geothermal Energy,” *Innov. Corros. Mater. Sci. Former. Recent Pat. Corros. Sci.* 7(1), 13–29 (2017).
3. Galgaro, A., Santa, G. D., Cultrera, M., Bertermann, D., Mueller, J., De Carli, M., Emmi, G., Zarrella, A., Di Tuccio, M., Pockelé, L., Mezzasalma, G., Psyk, M., Righini, D., Bernini, M. and Bernardi, A., “EU project ‘Cheap-GSHPs’: the geoexchange field laboratory,” *Energy Procedia* 125, 511–519 (2017).
4. Cadelano, G., Bortolin, A., Ferrarini, G., Bison, P., Dalla Santa, G., Di Sipio, E., Bernardi, A. and Galgaro, A., “Evaluation of the Effect of Anti-Corrosion Coatings on the Thermal Resistance of Ground Heat Exchangers for Shallow Geothermal Applications,” 9, *Energies* 14(9), 2586 (2021).
5. Wong, B. and McCann, J. A., “Failure Detection Methods for Pipeline Networks: From Acoustic Sensing to Cyber-Physical Systems,” 15, *Sensors* 21(15), 4959 (2021).
6. Maldague, X., [Theory and practice of infrared technology for nondestructive testing], Wiley (2001).

7. Barizza, A., Bison, P., Boldrini, S., Bortolin, A., Cadelano, G., Colla, L. and Ferrarini, G., “Comparison of the insulation property of an innovative material and a traditional one by infrared thermography,” presented at Proceedings of SPIE - The International Society for Optical Engineering, 2015.
8. Vavilov, V. and Burleigh, D., “Heat Conduction in Structures Containing Defects and the Optimization of TNDT Procedures,” [Infrared Thermography and Thermal Nondestructive Testing], V. Vavilov and D. Burleigh, Eds., Springer International Publishing, Cham, 93–180 (2020).
9. Cadelano, G., Bortolin, A., Ferrarini, G., Molinas, B., Giantin, D., Zonta, P. and Bison, P., “Corrosion Detection in Pipelines Using Infrared Thermography: Experiments and Data Processing Methods,” *J. Nondestruct. Eval.* 35(3) (2016).
10. Bison, P., Bortolin, A., Cadelano, G., Ferrarini, G., López, F. and Maldague, X., “Comparison of image processing techniques for the on-site evaluation of damaged frescoes,” *Thermosense Therm. Infrared Appl.* XXXVI 9105 (2014).
11. Vavilov, V. and Burleigh, D., “Statistical Data Treatment and Decision Making in TNDT,” [Infrared Thermography and Thermal Nondestructive Testing], V. Vavilov and D. Burleigh, Eds., Springer International Publishing, Cham, 397–414 (2020).
12. Klein, M. T., Ibarra-Castanedo, C., Bendada, A. and Maldague, X. P., “Thermographic signal processing through correlation operators in pulsed thermography,” *Proc SPIE 6939 Thermosense XXX 6939* (2008).
13. Maldague, X., Galmiche, F. and Ziadi, A., “Advances in pulsed phase thermography,” *Infrared Phys. Technol.* 43(3–5), 175–181 (2002).
14. Rajic, N., “Principal component thermography for flaw contrast enhancement and flaw depth characterisation in composite structures,” *Compos. Struct.* 58(4), 521–528 (2002).
15. Klein, M. T., Ibarra-Castanedo, C., Maldague, X. P. and Bendada, A., “A straightforward graphical user interface for basic and advanced signal processing of thermographic infrared sequences,” *Proc SPIE 6939 Thermosense XXX 6939* (2008).

12 Conclusions

Currently, most shallow geothermal heat pump systems in Europe use vertical heat exchangers, which are tubes inserted into the ground where a fluid flows allowing heat exchange. Today, it is a well-proven technology that has been used for over 30 years in hundreds of thousands of systems around the world. Nonetheless this renewable energy source is largely underexploited with respect to its potential. The drawbacks are high installation costs and environmental concerns, as pipes often run through sensible geological strata and even drinking water aquifers. In some areas the drilling depth is limited: in the Netherlands, for example, it is not allowed to drill more than 30 m below the ground surface. In the current state of the art, the exchangers are made of a single material. It follows that in the design of the plant it is necessarily forced to seek economy and safety, compromising performance and consequently increasing the length of the exchangers and therefore their depth which, as stated before, it is a not negligible barrier.

In many contexts, shallow geothermal systems are not easily applicable due to the chemical interaction between the subsoil and the materials of the ground heat exchangers, which has an important effect on their durability. The installation of the exchangers involves the alteration of the undisturbed conditions of the subsoil, which could lead to a considerable development of corrosive phenomena, mainly due to the penetration of atmospheric oxygen into the subsoil and to the presence of groundwater in contact with the pipes. There are also particular conditions such as coastal environments with a high chloride and sulphate content, in which the high electrical conductivity of the water increases the corrosion rate. According to the current state of the art, the use of metal exchangers is an imprudent choice if the pipes are not made of corrosion resistant alloys and is mostly not recommended by the regulations.

The efficiency of the heat exchange with the ground therefore depends on the material that makes up the exchanger, while safety is also the result of the correct coupling between the material and the ground. In some deep geological layers the conditions are anoxic and therefore it is not necessary to use stainless steel or HDPE, while in other contexts passive anti-corrosive measures can be proposed, among the already available solutions taken from technical standards not specific for geothermal (e.g. protective coatings - UNI 9099 and UNI 5256).

As part of this research work, several aspects have been addressed that lead to innovative metal GHEs that are safe, efficient and cost effective:

Study of the materials in relation to the possible anti-corrosion measures envisaged by the regulations for underground structures, also considering practical aspects such as durability throughout installation and economic evaluation.

The metals to be considered as the external part of a coaxial exchanger must comply with criteria of economy, sufficient tensile strength to be processed in pipes and machinability, because welding is required to assemble the GHE. These requirements exclude materials such as copper, aluminium, titanium and many grades of stainless steel other than AISI 304 or 316. From an economic standpoint, stainless steel is not competitive against plastic. Carbon steel is promising because the cost of raw material is in the same price range of HDPE.

To make carbon steel viable as a safe solution for GHE, measures must be taken to limit corrosion. Active protections such as impressed current cathodic protection systems are not considered for economically sustainable geothermal plants. In fields other than geothermal there are standards and regulations to protect buried metal items from corrosion, which can be adapted and applied to GHEs. In plumbing and electricity distribution poles, passive protection is used in the form of cladding materials that provide mechanical barriers against oxygen and water.

The most feasible solution was deemed to be overcoating the carbon steel pipes with bitumen (according to UNI 5256) or primer paints. Other passive measures that can be taken into account are sacrificial anode, or zinc plating. It is worth underlining that the latter solution would in any case require the application of primer or bitumen to protect the welded parts, as it is not practically possible to apply galvanization on that spots. Moreover, protruding sacrificial anodes would not comply with some installation methodologies based on piling.

Study of the materials of the outer tube of the coaxial heat exchangers based on the resulting thermal resistance of the outer tube. Thermal performance was evaluated by applying the modified laser flash technique to high conductivity materials and then by modelling the heat transfer both in steady state and in transient condition. The thermal effects of anti-corrosion measures were also identified by measuring their impact on the thermal resistance on the metal samples to which they were applied.

The evaluation of the thermal performance of different GHE solutions was based on the comparison of the thermal resistance values. The values of thermal conductivity, that are necessary for the calculation of the thermal resistance, were obtained starting

from the measurement of the thermal diffusivity using the laser flash method (LFM). LFM was used to measure tube materials (carbon steel, AISI 304, AISI 316 and HDPE) in transmission mode, also implementing a new methodology and apparatus aimed at improving the measurement reliability of high conductivity materials such as metals. The thermal diffusivity of the coatings was also measured by LFM, this time in one-sided mode. To calculate thermal conductivity, starting from thermal diffusivity, density and specific heat are also needed. Therefore, the materials of the tube and coatings were measured by the buoyancy thrust method (density) and differential scanning calorimetry (specific heat). The final results show that the application of low conductivity coatings (primer and bitumen) has the effect of limiting the performance of carbon steel. However, the coated carbon steel solutions are still comparable to AISI 304 and 316. Furthermore, all the metal solutions have been shown to have lower thermal resistance than HDPE pipes. For a 2 mm wall thickness pipe made of coated carbon steel, the resulting thermal resistance would be approximately two times higher than the thermal resistance of an unprotected bare pipe. Stainless steel pipes of the same thickness would be about 3 times higher, while a plastic one would be more than a hundred times higher.

According to this, galvanized carbon steel appears to be the best solution in terms of minimizing the thermal resistance of the pipe. In fact, it allows to maintain the advantage of carbon steel, because the zinc layer is negligible from a thermal point of view. Considering also the cost of the materials, low performance but economical plastic solutions are to be preferred where the drilling depth is not a limiting factor. In sites where the drilling depth is a constrain, coated carbon steel solutions are an interesting option that allows to maintain cost effectiveness and limit pipe length due to their superior thermal performance. The same is true where space for the geothermal field is a constraint, because metal solutions can reduce the number of GHEs needed to cover the building's energy needs. A simplified finite element method (FEM) has been used to compare the heat exchange efficiency of metallic vertical coaxial GHEs against traditional grouted plastic ones, in transient working conditions, thus replicating the actual functioning of a GSHP. The advantages offered by metal solutions are less impactful when the ground is saturated with water, because the thermal inertia of the water acts in a more stringent way than the advantage given by high conductivity metal pipes in transferring heat through the surrounding ground. The advantages of the metallic solution are most evident in dry underground conditions, especially in clayey silty lithologies. One caveat is the risk of damaging the anti-corrosion coating when handling and installing pipes, which can be scratched making it useless against corrosion.

Proposal of a methodology based on laboratory test for the site-specific selection of materials based on compatibility in the main hydrogeological layers found in the field of application.

The laboratory measurement of the corrosion rate allowed a quantitative assessment of the durability of GHEs. A methodology was proposed, that is based on the already established “ASTM G162-Standard Practice for Conducting and evaluating laboratory corrosion tests in grounds”. It allows to determine the expected life of a buried pipe, with a decent estimate because it takes into account the coupling between the materials of the pipes with the lithology and ground characteristics of a site. Furthermore, this methodology can be modified and adapted to the specific conditions of the site. For example, the presence of water of a specific chemistry, and also their variation over time, as in the case of water plumes or precipitation. This methodology would be useful during the design phase of the geothermal plant, both for the selection of GHE materials, and for the economic evaluations based on the calculation of the operating time on the long term. The disadvantage lies in the impossibility of evaluating all the parameters that contribute to corrosion, that is, stray currents and microbial corrosion. The proposed procedure was tested on carbon steel specimens exposed to ground samples collected at the GEO4CIVHIC demonstration site in Padua. The ground samples were wetted at different water contents and presented two levels of density (to simulate a different compactness of the ground). After about three months it was possible to observe the relationship between the calculated corrosion rate and the changed parameters. The water content was the most impacting in the corrosion rate. Subsequently, it was possible to estimate the life span of an unprotected carbon steel pipe in relation to the modelled water content at the actual site.

Inspection protocol on site of the joints through active infrared thermography. The analysis of thermal data through the automation of image processing based on statistical and physical-mathematical algorithms will allow the identification of possible sealing defects and inner corrosion, increasing the general reliability of a geothermal plant.

One of the main reasons why metal GHEs are not allowed by decision makers is the risk of the heat transfer fluid leaking in the event of joint failure. In fact, while the plastic GHEs are continuous because they are supplied in rolls, the metal GHEs are made up of many pieces of pipe stacked one on top of the other and then joined, usually by welding or, as proposed by Hydra and Red companies, with threaded joints. These

are weak points in the pipes and require more stringent quality control to be proposed as a safe solution. Joining operations are always carried out on site, often in unfavourable conditions, such as in the presence of dirt or water. A non-destructive inspection methodology based on active infrared thermography capable of identifying defects was developed and demonstrated. The apparatus consist of a thermal camera observing the allegedly sealed joints, while compressed air is flowing into the pipe. The air pressure represents the thermal stimulus, and it is periodic. The processing of the collected thermal sequence is based on the statistical analysis of thermal images, which allows for the filtering of disturbances. One of the most promising algorithm is based on the use of the Fourier transform and on the isolation of the frequency content equal to that of the imposed thermal stimulus. This operation allows to emphasize the thermal anomalies due to failure of the threaded joint (i.e., components not well screwed) and defects of the O-ring gasket which should guarantee the sealing of the joints.

It has also been shown that the active thermography technique is able to identify internal corrosion on a carbon steel pipe when the corrosive attack penetrates at least 50% of the pipe wall thickness. The test was conducted in the laboratory on a mock-up of tube. The tube was machined to obtain two artificial defects in terms of reduction of the wall equal to 50% and 20% respectively. The pipeline was connected to a water circulator and heating system, which allowed the water temperature flowing inside to be controlled by replicating the operating phases of a geothermal system: heating, steady and cooling. During each phase, an infrared camera recorded the temperature variation on the external surface, thus obtaining three thermal sequences. The sequences have been processed separately with statistical algorithms such as PCT (Principal Components Thermography), Correlation contrast, and a new one that has been developed taking into account the temperature variation of each pixel of the image also with respect to the surrounding areas (e.g. Multiple Average sum , MSA). All algorithms rely on the expected thermal anomaly due to the reduced thermal resistance at the defects, compared to the surrounding sound environment. PCT and MSA made it possible to locate the main of the two machined defects.

Design of experimental metal coaxial GHEs for very shallow applications. Test on real case of the novel GHEs, with experimentation of different passive anti-corrosion measures. Evaluation of the thermal performance of the installed solutions.

The theoretical premises presented in the previous paragraphs were put into practice in a case study located in Padua, Italy. These included the design of a new type of metal

coaxial ground heat exchanger, which concept comes from the “well point” pipe used for the drainage in excavation sites. The developed well point GHEs (Figure 1) have been built using metal pipes (stainless steel and protected carbon steel), and measures meant to overcome the weak points subject to corrosion such as the galvanic chains between components such as the tube, the head of the GHE, the auxiliary metal components present in the GHE, and also the welds. This was achieved by interposing materials such as adapters for plastic and brass pipes.

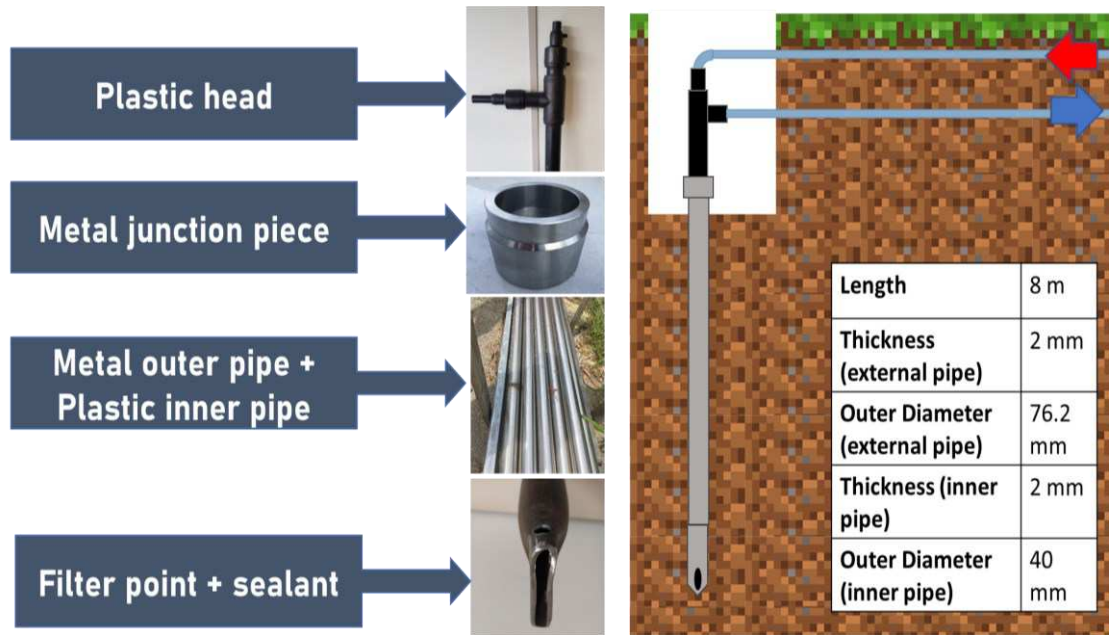


Figure 1: Components and construction scheme of the novel “well point” GHE.

The installation methodology was also implied in the study, and it was designed not only to replicate the traditional use of well point system, but also to avoid risk damage to the coating. It included the pre-drilling of the borehole, the installation of the pipe using pressurized water, and the filling of the annular space with sand. A total of 16 GHEs were installed, subdivided into two branches made of stainless steel (SST) and carbon steel (CS), respectively. The carbon steel GHEs were protected with different anti-corrosion measures, ranging from coatings (bitumen and primer paint), to sacrificial anode, and galvanized zinc. The following table schematize the installed GHE typologies.

Figure 1: Overview of the GHEs installed at the Padua case study site.

GHE No.	Material/anti-corrosion measure
1	CS/ bitumen
2	CS/ bitumen
3	CS/ paint (ZINCO99)
4	CS/ paint (ZINCO99)
5	CS/ sacrificial anode in Zn
6	CS/ nothing
7	CS/ galvanized Zn
8	CS/ galvanized Zn
9	SST AISI 304/ nothing
10	SST AISI 304/ nothing
11	SST AISI 304/ nothing
12	SST AISI 316/ nothing
13	SST AISI 304/ nothing
14	SST AISI 304/ nothing
15	SST AISI 304/ nothing
16	SST AISI 304/ nothing

From a thermal performance point of view, the borehole thermal resistance was measured in both carbon steel and stainless steel branches. Net the contribution of the heat exchange of the fluid and the characteristics of the ground, it allowed to confirm the theoretical evaluation that saw all the metallic solutions comparable. Long-term measurements are currently underway. Based on the first results of the thermal performance monitoring, both metal solutions show a higher specific power than two other grouted coaxial GHEs that have been installed in the premises also in the frame of GEO4CIVHIC project.

12.1.1 Future research developments

This research work paved the path to develop modular geothermal exchangers consisting of alternating sections in carbon steel and plastic aimed at optimizing compatibility with different geological layers in terms of heat exchange performance, cost and safety during the long-term life cycle. A new generation of modular coaxial ground heat exchangers is envisioned and will be used in shallow geothermal applications and will broaden their diffusion because it can be applied to a greater number of geological and hydrogeological contexts.

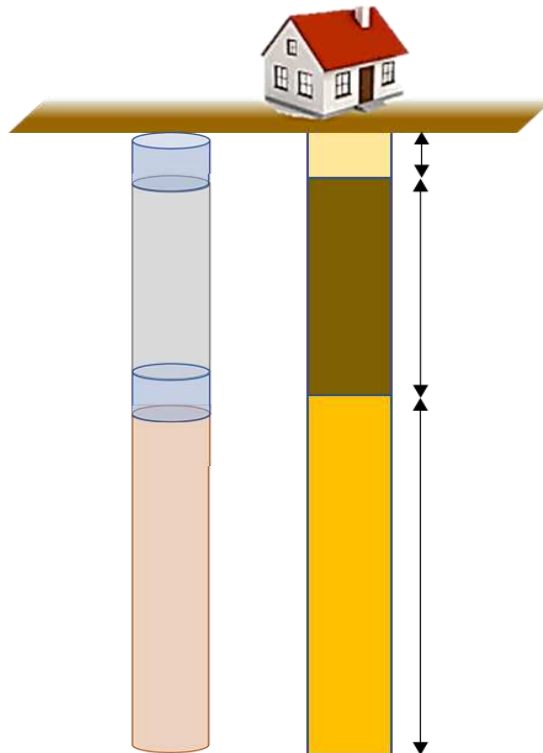


Figure 2: Scheme of the future type of vertical ground heat exchangers based on the results of this study. In this example, the outer tube is made up of sections of different materials selected to ensure optimal coupling with each corresponding geological/hydrogeological layer. Corrosion resistant material (plastic) is used in correspondence to the interfaces between each layer. Carbon steel is preferred for deeper layers where the environment is dry and oxygen-free.

The study allowed a better comprehension of advantages and limits of different material solutions for GHE, that will increase in the field of applicability of ground source heat pump systems. The assessment of corrosion in a more quantitative way will expand the use of this energy source to contexts in which the geological conditions do not make it possible or limit the current state of the art. The compatibility of the materials with respect to each individual hydrogeological layer represents *a sine qua*

non condition for the construction of a geothermal plant compared to traditional exchangers made of a single material. Implementing the selected anti corrosion measures in safe context, will make it possible to use geothermal energy without limitations or performance compromises even in areas where there are aggressive ground conditions. Moreover, the increased thermal performance of GHEs will allow exceeding the limits on the drilling depth. Thanks to the use of materials with high thermal conductivity, a shorter length of pipes will be required, which will allow the installation of geothermal systems even in the presence of aquifers or other conditions that limit their application. A better estimation of the operational life time and the improved reliability will increase the life expectancy beyond the standard operating period. Improved sealing and corrosion prevention will significantly limit the risk of pipe failures. This will be achieved through the use of methodologies for the inspection of welded joints and other junctions that can be applied on site.